UNIVERSITY OF CALIFORNIA SAN DIEGO

The Many Faces of Quantum Matter and Quantum Phase Transitions

A dissertation submitted in partial satisfaction of the
requirements for the degree Doctor of Philosophy

in

Physics

by

Dachuan Lu

Committee in charge:

      Professor Yi-Zhuang You, Chair
      Professor Tarun Grover
      Professor Kenneth Intriligator
      Professor John McGreevy
      Professor Dragos Oprea

2024

The Dissertation of Dachuan Lu is approved, and it is acceptable in quality and form for publication on microfilm and electronically.

University of California San Diego

2024

DEDICATION

To my wife, my parents and my family.

EPIGRAPH

The most beautiful thing we can experience is the mysterious. It is the source of all true art and science.

Albert Einstein

TABLE OF CONTENTS

LIST OF FIGURES

LIST OF TABLES

ACKNOWLEDGEMENTS

their guidance and support during the undergraduate school time.

I would like to thank my parents, family, and especially my wife Hengyu Ai for supporting me in pursuing my Ph.D. degree. I would like to thank my parents for their unconditional support in my education and for encouraging me to pursue my academic dreams. They never push me but let me slow down and they prioritizes my health, sports, life and become a happy human-being. I would like to deeply thank my wife Hengyu Ai for her unwavering support and flexibility in accommodating my academic pursuits. I would like to thank my dog, Miso, for her company and always being a happy dog.

My Ph.D. life is much more enjoyable with the company of my friends. During the years of Ph.D. before Covid, I played a lot of ping-pong and learned the techniques from Meng Zeng, Yi Guo and Yiheng Xu. We had fun time exploring San Diego and food with Taige Wang, Jofan Chien, Wei-Ting Kuo, Yifan Xiang, Jinlong Huang, Yue Liang and Xinyan Tong. We had good days playing basketball and board games with Wenbo Fu, Junyi Cao, Zhehao Zhang, Xiaoyang Huang and Wanda Hou.

In the post Covid-era, I developed the interest in rock climbing after Hengyu introduced me into the climbing gym. We had countless happy days on the rocks or plastic rocks. I would like to thank Hengyu for years' belaying. I would like to thank my climbing friends, Anze Xie, Han Zhang, Chen Chen, Yimu Bao, Ali Lavasani, Shijun Sun, Abbey, Gina, Xiangyu Guo, Davi Costa, with whom the climbing journey is much more fun.

Last but not least, I would thank Doyle park, as shown in Fig. 0.1. Doyle Park has been a witness to the disbanding of the basketball companions and the growing up of Miso. It has also been a constant companion, holding all my sorrows and joys during my many walks through its paths.

Figure 0.1. Doyle park. White dog is Miso, the golden doodle is Pashmak. There is a basketball court in the distance.

Chapter. 2, in full, is a reprint of the material as it appears in Da-Chuan Lu. Nonlinear sigma model description of deconfined quantum criticality in arbitrary dimensions. *SciPost Physics Core*, 6(3):047, July 2023. The dissertation author was the primary investigator and author of this paper.

Chapter. 3, in full, is a reprint of the material as it appears in Da-Chuan Lu, Meng Zeng, Juven Wang, and Yi-Zhuang You. Fermi surface symmetric mass generation. *Physical Review B*, 107(19):195133, May 2023. The dissertation author was the primary investigator and author of this paper.

Chapter. 4, in full, is a reprint of the material as it appears in Da-Chuan Lu, Meng Zeng, and Yi-Zhuang You. Green's function zeros in Fermi surface symmetric mass generation. *Physical Review B*, 108(20):205117, November 2023. The dissertation author was the primary investigator and author of this paper.

Chapter. 5, in full, is a reprint of the material as it appears in Yichul Choi, Da-Chuan Lu, and Zhengdi Sun. Self-duality under gauging a non-invertible symmetry. *Journal of High Energy Physics*, 2024(1):142, January 2024. The dissertation author was one of the primary investigator and author of this paper.

VITA

2018	Bachelor of Science in Physics, Nanjing University
2021	Master of Science in Physics, University of California San Diego
2024	Doctor of Philosophy in Physics, University of California San Diego

PUBLICATIONS

1. Da-Chuan Lu, Juven Wang, and Yi-Zhuang You. Definition and classification of Fermi surface anomalies. *Physical Review B*, 109(4):045123, January 2024

2. Yichul Choi, Da-Chuan Lu, and Zhengdi Sun. Self-duality under gauging a non-invertible symmetry. *Journal of High Energy Physics*, 2024(1):142, January 2024

3. Sheng Yang, Zhiming Pan, Da-Chuan Lu, and Xue-Jia Yu. Emergent self-duality in a long-range critical spin chain: From deconfined criticality to first-order transition. *Physical Review B*, 108(24):245152, December 2023

4. Da-Chuan Lu, Meng Zeng, and Yi-Zhuang You. Green's function zeros in Fermi surface symmetric mass generation. *Physical Review B*, 108(20):205117, November 2023

5. Da-Chuan Lu, Miao Li, Zhao-Yi Zeng, Wanda Hou, Juven Wang, Fan Yang, and Yi-Zhuang You. Superconductivity from Doping Symmetric Mass Generation Insulators: Application to $La_3Ni_2O_7$ under Pressure. August 2023

6. Da-Chuan Lu. Nonlinear sigma model description of deconfined quantum criticality in arbitrary dimensions. *SciPost Physics Core*, 6(3):047, July 2023

7. Da-Chuan Lu, Meng Zeng, Juven Wang, and Yi-Zhuang You. Fermi surface symmetric mass generation. *Physical Review B*, 107(19):195133, May 2023

8. Da-Chuan Lu and Zhengdi Sun. On triality defects in 2d CFT. *Journal of High Energy Physics*, 2023(2):173, March 2023

9. Da-Chuan Lu, Taige Wang, Shubhayu Chatterjee, and Yi-Zhuang You. Correlated metals and unconventional superconductivity in rhombohedral trilayer graphene: A renormalization group analysis. *Physical Review B*, 106(15):155115, October 2022

10. Da-Chuan Lu, Cenke Xu, and Yi-Zhuang You. Self-duality protected multicriticality in deconfined quantum phase transitions. *Physical Review B*, 104(20):205142, November 2021

11. Rui-Zhen Huang, Da-Chuan Lu, Yi-Zhuang You, Zi Yang Meng, and Tao Xiang. Emergent symmetry and conserved current at a one-dimensional incarnation of deconfined quantum critical point. *Physical Review B*, 100(12):125137, September 2019

12. Wei Wang, Da-Chuan Lu, Xiao Yan Xu, Yi-Zhuang You, and Zi Yang Meng. Dynamics of compact quantum electrodynamics at large fermion flavor. *Physical Review B*, 100(8):085123, August 2019

ABSTRACT OF THE DISSERTATION

The Many Faces of Quantum Matter and Quantum Phase Transitions

by

Dachuan Lu

Doctor of Philosophy in Physics

University of California San Diego, 2024

Professor Yi-Zhuang You, Chair

Symmetry, anomaly and duality put strong constraints on the low-energy physics of the quantum field theory. In this dissertation, we used generalized symmetry and symmetry anomaly to investigate the quantum phases of matter and their transitions. In particular, we studied the generalized exact duality in 1+1d systems and infrared duality for 2+1d gauge theories. We investigated the 't Hooft anomaly matching of non-linear sigma model with the Wess-Zumino-Witten term. We focus on the implications of these non-perturbative methods on 1+1d quantum phase transitions, 2+1d deconfined quantum criticality and Fermi surface symmetric mass generation.

Introduction

Symmetry is a crucial concept in physics that has long served as a guiding principle for developing theories and understanding the fundamental nature of the universe [94]. It helps organize and classify the various particles and excitations that emerge in physical systems. By studying the symmetry of a system, physicists can gain deep insights into its properties and behavior.

One of the most remarkable aspects of symmetry is its ability to reveal surprising connections between seemingly unrelated phenomena. It provides a framework for understanding how different parts of the universe are intertwined and how they evolve over time. Symmetry also serves as a roadmap for discovering new theories and predicting the existence of new particles. It's a testament to the power of mathematics in physics, showcasing how abstract mathematical concepts can have profound implications for our understanding of the physical world.

In particular, our universe is composed of elementary particles, like proton, neutron and photons. The kinematic properties of the elementary particles are well described using the representations of Lie group. For example, symmetry yields the selection rule answering which particles can be scattered into each other. The dynamics of particles are studied by the gauge theory that also utilizes the symmetry principle.

In the condensed matter systems, each material could have their own universe, and the collective behaviour of electrons resembles bosons, fermions and even anyons. These collective modes of the electrons are dubbed as quasi-particles. The emergentism in the condensed matter system aligns with Anderson's famous paper "more is different" [9], where the collective behavior of a large number of particles can give rise to novel phenomena that cannot be explained by

1

simply studying the individual components.

The emergentism results in gardens of novel physical phenomena. However, the different systems could behave similarly despite their very distinct natures. For example, both 3-dimensional easy-plane magnets and liquid Helium-4 share the same critical behaviour which is described by the three dimensional XY model. One is then eager to ask what are the universal features of the zoos of different models. It turns out that models with the universal features fall into the *universality class*. What determines the universality class? The answer is still mostly symmetry.

For the classical many-body systems, their phases and phase transitions are classified by symmetry. The classification of phases and phase transitions based on symmetry is rooted in Landau's theory of phase transitions, which provides a phenomenological framework for describing the free energy of the system in terms of the order parameter. In the disordered phase, where the constituents of the system are randomly arranged, the order parameter is zero, reflecting the lack of any preferred direction or spatial arrangement. However, as the system approaches a phase transition, the order parameter acquires non-zero values, signaling the emergence of an ordered phase.

The nature of the ordered phase is determined by the specific symmetry that is broken during the phase transition. For example, in a ferromagnetic system, the order parameter is the magnetization, which measures the degree of alignment of the magnetic moments. Above the critical temperature, the system is in the paramagnetic phase, where the magnetic moments are randomly oriented, and the magnetization is zero. As the temperature is lowered below the critical point, the system undergoes a spontaneous symmetry breaking, and the magnetic moments align, giving rise to a non-zero magnetization and the ferromagnetic phase.

Moreover, the symmetry-based classification of phases and phase transitions has far-reaching consequences in the form of universality. The renormalization group is a powerful tool that connects seemingly distinct theories within the same universality class. It allows us to understand how the macroscopic behavior of a system emerges from its microscopic properties

by systematically coarse-graining the system and studying how the effective interactions change as we move from one length scale to another. Through this process, the renormalization group reveals that systems with different microscopic details can exhibit the same critical behavior, as long as they share the same symmetries and dimensionality. This remarkable insight unifies our understanding of phase transitions and critical phenomena, showing that the essential physics near a critical point is determined not by the specific microscopic model but by the universality class to which it belongs.

The symmetry principle to understanding phases and phase transitions in classical many-body systems has proven to be a powerful tool in condensed matter physics. Such framework is called Landau-Ginzburg-Wilson-Fisher (LGWF) paradigm. The LGWF paradigm successfully applied to a wide range of physical systems, including magnets, superfluids, superconductors, and liquid crystals.

However, the LGWF paradigm will be broken down when quantum physics steps in. Unlike classical phase transitions, which are driven by thermal fluctuations, quantum phase transitions occur at absolute zero temperature and are driven by quantum fluctuations. These transitions arise when the ground state of a quantum system undergoes a fundamental change as a physical parameter, such as magnetic field or pressure, is varied. The competition between different quantum states leads to a non-analytic behavior of the ground state energy and the emergence of novel quantum phases with exotic properties. The exotic quantum phases and their transitions are the main focus of this dissertation.

0.1 Examples of exotic quantum phases and phase transitions

In this dissertation, we will mainly discuss various aspects of deconfined quantum critical point (DQCP) and symmetric mass generation (SMG). Both of them are beyond Landau paradigm. DQCP describes the continuous quantum phase transition (QPT) between two spontaneously

symmetry breaking phases, which would be forbidden in the LGWF paradigm. Fermi surface symmetric mass generation transition describes the continuous QPT between Fermi liquid and symmetric mass generation insulator, which are both symmetric phases.

Deconfined quantum critical point

In 2+1d quantum magnets, each site supports the spin-$\frac{1}{2}$ degree of freedom, there are two interesting phases, one is the Néel phase, where the spins are aligned antiferromagnetically, another one is the valence-bond-solid(VBS) phase, where the spins form singlets with the singlets towards different directions. The Néel phase and the VBS phase breaks different symmetries, in the Néel phase, the spin $SU(2)$ rotation symmetry is spontaneously broken but lattice symmetry is preserved, while in the VBS phase, the lattice symmetry is broken but the spin rotation symmetry is preserved.
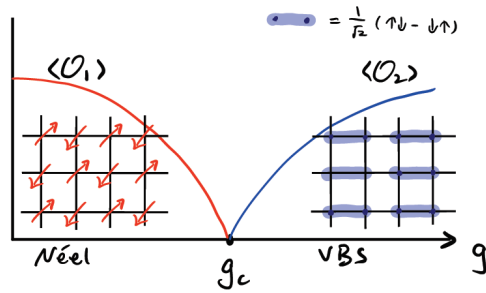
Figure 0.2. Phase diagram of deconfined quantum phase transition, the Néel order parameter gradually becomes smaller and the VBS order parameter becomes larger when tuning the coupling constant *g*.

The deconfined quantum critical point (DQCP) is quantum phase transition between Néel phase and valence-bond-solid phase. Landau paradigm states that this transition would be either first-order transition or phases overlapping. However, it is proposed that the DQCP can be continuous and be described by continuous field theories. Rather interestingly, the transition is driven by proliferating the disorder operator which carries the charge of the other symmetry. For

example, in the VBS phase, the vortex core carries spin-$\frac{1}{2}$ degree of freedom,
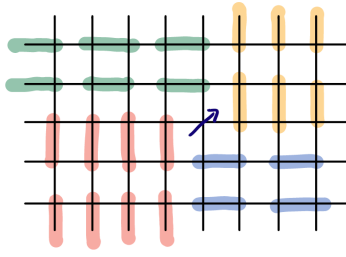
$$\tag{1}$$

This intertwining between different symmetry is a manifestation of *'t Hooft anomaly*. And because of this 't Hooft anomaly, one can think the DQCP as the boundary of certain symmetry protected topological phases (SPT) by anomaly inflow.

In the original proposal, the DQCP is described by the non-compact $\mathbb{C}P^1$ model, which is two bosons coupled to the $U(1)$ gauge field. Later, the DQCP is found to be described by several *dual theories*, namely though they are distinct in the ultraviolet, they will eventually flow the same infrared fixed point and describe the same physics. Those theories are nonlinear σ model with Wess-Zumino-Witten term, $N_f = 2$ QED$_3$ with Gross-Neveu term and noncompact $\mathbb{C}P^1$ model [393].

In the recent Monte Carlo simulations and conformal bootstrap analysis, there are more relevant operators at the critical point [459, 434, 83]. These works provide more evidence that the DQCP is a multicritical point. Besides the Néel and VBS phases, there is a quantum spin liquid phase. When tuning the parameter, the quantum spin liquid phase will end at the multicritical point and connects to the first order transition between the Néel and VBS phases [459, 252, 434, 246, 352]. Another possibility is that the DQCP is a pseudo-criticality which suggests the physical model is close to a second order phase transition point but the fixed points become slightly complex for the physical model [284, 263, 283].

Symmetric mass generation

Symmetric mass generation (SMG) is a fundamental concept in particle physics that explains how particles acquire mass without breaking the underlying symmetries of the theory [403]. The Anderson-Higgs mechanism is the well-known mass generating mechanism, however, it will necessarily break certain symmetry. In the field theory level, the Lagrangian $\mathcal{L}$ has the Yukawa term like,

$$\phi^a \bar{\psi} T^a \psi \subset \mathcal{L} \tag{2}$$

where ϕ^a is the bosonic field and $\bar{\psi}, \psi$ are the fermionic fields. T^a are certain representation of the flavor symmetry. When condensing the boson field ϕ^a, the fermion acquires mass, but the boson condensation will break the flavor symmetry.

It is possible to give the fermion mass without breaking the protected symmetry. The necessary condition for this to happen is 't Hooft anomaly free. For example, if preserving the time reversal symmetry $T^2 = 1$, the edge modes of the majorana chain in 1+1d cannot be gapped out by fermiom bilinear terms. However, for 8 copies of the majorana chain, it is possible to add an 4-fermion interaction term to gap out the edge modes [127, 128].

To simulate the chiral theory on the lattice, there is always the fermion double problem that obstructs it. However, if the anomaly is carefully cancelled, then it is possible to gap them out by multi-fermion term without breaking the chiral symmetry. In particular, the 3-4-5-0 model in 1+1d is proposed and numerically verified [396, 397].

In higher dimension, the SMG transition is more intriguing. Similar to the DQCP transition, the direct transition between the free fermion phase and SMG phase involves gauge field [447, 446]. Using the parton construction, the physical fermion is fractionalized into fermionic and bosonic partons. By tuning the coupling of bosonic partons, it is possible to drive a direct transition between the SMG phase and Dirac semimetal phase [447, 446].

In another direction, it is interesting to study the SMG in the fermion systems with finite density. In this case, we develop the anomaly free condition for the fermion systems [250]. The

stability of the Fermi surface can be viewed as protected by the quantum anomaly of an emergent LU(1) loop group symmetry at low energy. For Fermi surface SMG, it is peculiar that the Fermi surface will be transformed into Luttinger surface which is defined by the zeros of the Green's function as presented in Chapter. 4, instead of poles. This phenomenon resembles the Green's function zero in the relativistic case [450, 443, 433]. The Fermi surface SMG as presented in Chapter. 3 has also been used to study the superconductivity in the nickelate superconductor [248].

0.2 Non-perturbative methods - anomaly and duality

To better understand the exotic quantum phases and their transitions, we need to upgrade the symmetry principle to incorporate new challenges in the quantum world. In this dissertation I will mainly focus on two tools that will constrain the infrared quantum phases and their transitions, the tools are *anomaly* and *duality*.

Anomaly

In quantum many-body system, the local states live in the complex Hilbert space, the symmetry could have more interesting phenomena, such as symmetry fractionalization. Therefore, the symmetry principle needs to be upgraded with additional information of the symmetry anomaly. One particular important notion is the 't Hooft anomaly of the global symmetry. If the global symmetry G has 't Hooft anomaly, then the theory will run into trouble if one try to gauge the symmetry G. The 't Hooft anomaly also constrains that the theory flows in IR to be

1. Gapless

2. G symmetry spontaneously breaking (SSB)

3. Topological order,

but not symmetric trivial gapped phase. The 't Hooft anomaly of theory in d spacetime dimension is classified by $H^{d+1}(G, U(1))$, the $d+1$-th group cohomology of G with coefficient in $U(1)$. The 't Hooft anomaly can be cancelled by attaching the anomalous theory to a $d+1$ bulk with symmetry protected topological phase. More aspects of anomaly matching of the non-linear sigma model with the Wess-Zumino-Witten term is presented in Chapter. 2

Weak (Infrared) Duality

In the context of DQCP, the duality is the so-called weak-duality, i.e. they are distinct in the UV but conjectured to flow to the same IR fixed point. One can match the global symmetry and the anomaly of these theories. In contrast, the strong duality is that one can do exact mapping to get the dual theory, for example, the Kramer-Wannier duality of 2d Ising model is the strong duality.

Duality in general provides a powerful tool in understanding field theories. In 1+1d, the bosonization maps the fermionic model to a bosonic model, the 4 fermion interactions can be mapped to bilinears in the boson model, hence many 1d problems can be solved. In 2+1d, the particle-vortex duality is known for many years, where the XY-model is mapped to an Abelian Higgs model,

$$|D_B \phi|^2 - |\phi|^4 \quad \Longleftrightarrow \quad |D_b \phi|^2 - |\phi|^4 + \frac{1}{2\pi} b d B'. \tag{3}$$

where the particle ϕ is mapped to the vortex $\mathcal{M}_b$ in the dual description. Recently, many 2+1d theories are found to have their dual theories and form a duality web [341], the non-abelian Chern-Simons theories with matter fields are generalized to have the level/rank duality as that in the 2d WZW conformal field theory [177]. The many dualities help us understand more about the phase diagrams of the QCD theories.

The 2+1d duality of the abelian gauge theory has its 3+1d bulk understanding. Consider the 3+1d $U(1)$ gauge theory in the bulk, besides Maxwell term, there is also a θ term with θ

being periodic in 2π (fermionic). It is conventional to write the action as,

$$
\begin{aligned}
I(A) &= \frac{1}{8\pi} \int_X d^4x \sqrt{g} \left(\frac{2\pi}{g^2} F_{mn} F^{mn} + \frac{i\theta}{4\pi} \varepsilon_{mnpq} F^{mn} F^{pq} \right) \\
&= \frac{i}{8\pi} \int_X d^4x \sqrt{g} (\bar\tau F^+_{mn} F^{+mn} - \tau F^-_{mn} F^{-mn})
\end{aligned}
\tag{4}
$$

where $\tau = \frac{\theta}{2\pi} + \frac{2\pi i}{g^2}$. It is interesting that adding $\frac{i}{2\pi} \int G \wedge F$ or $\frac{i}{4\pi} \int F \wedge F$ will not change the partition function, this results in S and T transformation, they generate the $SL(2,\mathbb{Z})$ action [425],

$$
\tau \to \tau' = \frac{a\tau + b}{c\tau + d}, \quad \begin{pmatrix} a & b \\ c & d \end{pmatrix} \in SL(2,\mathbb{Z})
\tag{5}
$$

$$
Z(\tau) = Z(\tau')
\tag{6}
$$

The duality transformation in the 3+1d bulk can also be thought of as transformation on the dyon lattice [273]. these bulk transformations have their corresponding duality transformations at the boundary. S, T duality transformations at the boundary are,

$$
S: \quad \tau \to \tau' = -\frac{1}{\tau}, \quad \begin{pmatrix} 0 & -1 \\ 1 & 0 \end{pmatrix}, J \cdot A \to J \cdot a - \frac{1}{2\pi} a dA'
$$

$$
T: \quad \tau \to \tau' = \tau + 1, \quad \begin{pmatrix} 1 & 1 \\ 0 & 1 \end{pmatrix}, J \cdot A - \frac{1}{4\pi} A dA
$$

where the background gauge field becomes dynamical under the S transformation, and the action is shifted by a Chern-Simons term when doing the T transformation. In the presence of matter fields, charge and spin need to be matched, hence, there are only several dualities in the contrary to the infinite many $SL(2,\mathbb{Z})$ dualities in the pure gauge theory.

These 2+1d dualities have many applications in the condensed matter system, one is the understanding of particle-hole symmetric half filled Landau level [363]. The idea of duality was

also used in the DQCP problems, as mentioned in previous section, the DQCP has many dual descriptions [393], some are even self-dual [432]. The operators may be easily described in the dual theory but hard in the original one, utilizing the duality gives a more complete understanding of the phase diagram as presented in Chapter. 1.

Besides the descriptive power, many dualities make the strong coupling theory dual to a weak coupling one, therefore, the theory can be understood using perturbative calculation. One interesting application is presented in Ref. [111], where they utilize the duality constraind ansatz to extrapolate the scaling dimension of certain operator in the strongly coupled theory from its dual weakly coupled theory. It would be interesting to generalize this idea to more flavors of fermions or bosons, and the bulk would be $U(1) \rightarrow U(1)^n$ gauge theory, because large fermion flavors have more applications in condensed matter system such as DQCP, SMG transition and quantum spin liquid. This duality contrained RG would be an alternative way to calculate the scaling dimension besides the large N calculations, this is also relevant to the understanding of bulk-boundary correspondence.

Strong (Exact) Duality and Non-Invertible Symmetry

As mentioned previously, the Kramers-Wannier duality is the strong or exact duality. The UV lattice model can be mapped to the dual model by an exact mapping between the operators. The 1+1d duality mapping in general can be obtained by orifolding the discrete symmetry. Since the discrete gauge field is not dynamical, gauging the discrete symmetry will not change the central charge of the critical theory, but will permute the different symmetry sectors.

If a theory is invariant under the duality, then it is self-dual. In the generalized symmetry perspective, the self-dual theory admits the non-invertible symmetry associated to the self-duality. For 1+1d system, the 0-form symmetry is generated by line operators. In particular, these line operators commute with the energy-momentum tensor and they are topological defect line (TDL) operators. The TDL associated to the self-duality can be understood as the interface between the original theory and the dual theory. Because the theory is self-dual, the duality TDL can be

moved freely as a consequence of commuting with the Hamiltonian.

Since the duality transformation permutes the gapped phases, it provides the additional data about how one gapped phase relates to the other. The duality puts the constraints on the phase diagram. Therefore, the phase boundary or the critical line is invariant under the duality transformation, and it admits the corresponding non-invertible symmetry. One can then study the dynamical properties of the critical line by tuning the duality invariant operators. In the 1+1d transverse field Ising model $H = \sum_j Z_j Z_{j+1} + g X_j$, the Ising transition at $g = 1$ is invariant under the Kramers-Wannier duality. One can add duality invariant operator $\sum_j X_j Z_{j+1} Z_{j+2} + Z_j Z_{j+1} X_{j+2}$ to drive the Ising transition to first order transition via a multicritical point [296]. This analysis can also be generalized to non-local mapping beyond duality.

Similar to ordinary symmetry, the non-invertible symmetry has anomaly and symmetry protected topological phases, but the precise meaning deviates from those of ordinary symmetry. The anomaly of a non-invertible symmetry is the obstruction to symmetric gapped phase with a unique ground state. If a non-invertible symmetry is anomaly free, then it is possible to have a symmetric gapped phase with a unique ground state, more interestingly, it could have non-invertible symmetry protected topological phases [379, 344]. For example, the self-duality non-invertible symmetry in the Ising transition has anomaly, therefore, the Ising transition cannot be drived to a symmetric gapped phase with unique ground state. Instead, the Ising transition will be drived to a first order transition with 3 degenerate ground states [339]. More details of the non-invertible symmetry and self-duality will be discussed in Chapter. 5.

Chapter 1

Self-duality protected multi-criticality in deconfined quantum phase transitions

1.1 Introduction

Duality plays an important role in relating different phases of matter. One famous example is the Kramers-Wannier duality[223] in (1+1)D transverse field Ising model $H = \sum_i -JZ_iZ_{i+1} - hX_i$, which exchanges J and h and maps the ferromagnetic (Ising symmetry breaking) phase to the paramagnetic (Ising symmetric) phase and vice versa. More generally, two theories are dual to each other when they have different ultraviolet (UV) descriptions but flow to the same infrared (IR) theory. A well-known example in (2+1)D is the particle-vortex duality, which states that the XY model is dual to the Abelian Higgs model [207, 308, 101]. Recent developments further extend this understanding and discover many theories and their dual partners, altogether they form a web of duality[340].

If the theory remains the same under a duality, the duality will be called a self-duality. For example, the Kramers-Wannier duality is a self-duality for the (1+1)D Ising model at the critical point. Recent studies [70, 190, 379, 237] further propose to interpret the self-duality as a categorical symmetry, making connections to the fusion category of anyon excitations in the corresponding bulk topological order in one higher dimension. When the self-duality is imposed as a symmetry, the system is enforced to stay on the phase boundary between the two duality-related phases, leading to the self-duality protected criticality and multi-
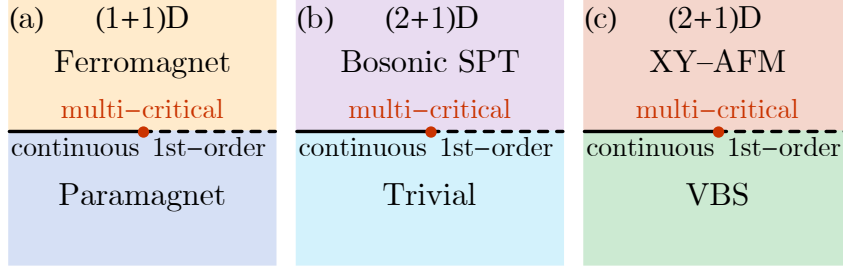
Figure 1.1. Quantum phases related by the duality or emergent symmetry: (a) ferromagnetic (ordered) and the paramagnetic (disordered) phases across the Ising transition are related by the Kramers-Wannier duality, (b) bosonic symmetry protected topological (SPT) and trivial phases are related by the fermionic particle-vortex duality, (c) XY antiferromagnetic (AFM) and valence bond solid (VBS) phases are related by an emergent $\mathbb{Z}_2$ symmetry. In all phase diagrams, the vertical axis is the relevant perturbation that drives the transition between the duality/symmetry-related phases, and the horizontal axis is always taken to be the square of the transition-driving perturbation. In phase diagrams (b,c), the existence of continuous transitions between the adjacent phases is assumed, which corresponds to the $N_f = 2$ QED$_3$ field theory without four-fermion interactions.

criticality[3, 51, 18, 189, 220, 76]. For example, as illustrated in Fig. 1.1(a), in the presence of the Kramers-Wannier duality (enforcing $J = h$), a generic Ising chain (with all additional duality-allowed terms like $-K(X_iX_{i+1} + Z_{i-1}Z_{i+1})$) can either preserve the self-duality and remain gapless along the Ising critical line ($K < K_c$), or spontaneously break the self-duality and becomes gapped along the first-order transition line ($K > K_c$). The continuous and first-order Ising transitions are separated by a multi-critical point ($K = K_c$), i.e. the tricritical Ising point[45, 294]. The multi-critical point can be circumvented if the self-duality is explicitly broken (e.g. by $J \neq h$). In this sense, the multi-criticality is protected by self-duality.

Similar continuous to first-order transition also happens in higher dimensions between the duality-related quantum phases. Here we will explore the (2+1)D example of self-duality-protected multi-criticality. In particular, we will consider the topological transition between the bosonic symmetry protected topological (SPT) phase and the trivial phase, as illustrated in Fig. 1.1(b), where the two phases across the transition are related by the self-duality[432, 340, 177, 81, 29] of the quantum electrodynamics in (2+1)D (QED$_3$) with fermionic

matters at flavor number $N_f = 2$. This theory also describes the deconfined quantum critical point (DQCP)[350, 348, 232] between the XY antiferromagnet (AFM) and the valence bond solid (VBS) in square-lattice quantum magnets with the easy-plane spin anisotropy, as shown in Fig. 1.1(c). In this case, the two phases are related by a $\mathbb{Z}_2$ subgroup of the emergent $O(4)$ symmetry that maps the two-component XY-AFM order parameter to the two-component VBS order parameter. Imposing these emergent symmetries (including the self-duality) essentially promotes the tuning parameters to the fluctuating scalar fields and prohibits the explicit mass terms. This leads to a unified field theory that describes the continuous-to-first-order transition in these systems. Such multi-critical point lies in the universality class described by the QED$_3$-Gross-Neveu[156, 340, 207] (QED$_3$-GN) theory. More generally, the Chern-Simons (CS) term for the gauge fields can be included to describe the multi-critical point of the exotic quantum phase transitions.

To further investigate the stability of this (2+1)D self-duality-protected multi-criticality, we extend the field theory to the large fermion flavor number (large N_f) limit, and use the $1/N_f$ expansion[156, 431, 430, 192, 446, 6, 47] to analyze the renormalization group (RG) flow of the fermion quartic operators, including the mass-mass $(\bar{\psi}M\psi)^2$ and current-current $(\bar{\psi}\gamma^\mu M\psi)^2$ interactions, at the QED$_3$-GN fixed point. Our analysis indicates that the DQCP and the multi-criticality can be driven to the first-order transition by current-current interactions. Such current-current interactions can be realized in the lattice spin model as a staggered dimer-dimer interaction (or stagger-Q) as proposed and observed in the recent quantum Monte Carlo (QMC) studies[459, 460]. Unlike the conventional dimer-dimer interaction that couples the dimers along the vertical or horizontal directions on the square lattice, the stagger-Q interaction couples the dimers along the diagonal direction. The QMC results indicate that such a stagger-Q interaction may be responsible for driving the DQCP between continuous and first-order transitions (see Sec. 1.4.2 for more concrete discussion of the QMC results and our theoretical explanation).

The RG analysis can be further generalized to the QED$_3$-GN theory with additional Chern-Simons (CS) terms for the gauge field. Although there is a lack of known examples

of self-dual theory with a non-zero-level CS term, a similar multi-critical point separating the continuous and first-order transition still exists and can be analyzed. The result can be applied to the direct transition between bosonic fraction quantum Hall (FQH) and superfluid (SF) phases in interacting boson systems[24, 21].

1.2   Self-Duality of $N_f = 2$ QED$_3$

The fermionic particle-vortex duality[363, 273] dualizes a free Dirac fermion theory to $N_f = 1$ QED$_3$ theory with CS terms and the fermion operator is mapped to the fermion operator combined with gauge fluxes. Since CS terms break parity symmetry, the orientation reversed version of the fermionic particle-vortex duality is obtained by changing the sign of the CS terms. By combining the fermion particle-vortex duality and its orientation reversed version, one can obtain a duality between two $N_f = 2$ QED$_3$ theories[432, 29, 177] described by the following Lagrangians,

$$i\bar{\psi}_1 \slashed{D}_{a+X} \psi_1 + i\bar{\psi}_2 \slashed{D}_{a-X} \psi_2 + \frac{1}{4\pi}(a+Y)d(a+Y) + \frac{2}{4\pi}(XdX - YdY) \tag{1.1}$$

$$\Longleftrightarrow i\bar{\chi}_1 \slashed{D}_{\tilde{a}+Y} \chi_1 + i\bar{\chi}_2 \slashed{D}_{\tilde{a}-Y} \chi_2 + \frac{1}{4\pi}(\tilde{a}+X)d(\tilde{a}+X), \tag{1.2}$$

where ψ_i, χ_i are fermion fields, $\slashed{D}_a \equiv \gamma^\mu(\partial_\mu - ia_\mu)$ is the Dirac operator coupled to the $\mathsf{U}(1)$ gauge field a. $ada \equiv \varepsilon_{\mu\nu\rho} a_\mu \partial_\nu a_\rho$ is understood as the exterior product $a \wedge da$, and the same applies for other CS terms. We adopt the convention as the lower case letters $a, \tilde{a}$ represent the dynamical $\mathsf{U}(1)$ gauge fields which will be integrated over in the path integral, and the upper case letters X, Y represent the background gauge fields which are used to keep track of the $\mathsf{U}(1)_X$ and $\mathsf{U}(1)_Y$ global symmetries.

The two theories (at least) have the common UV symmetry $\mathsf{U}(1)_X \times \mathsf{U}(1)_Y$. For the $\mathsf{U}(1)$ gauge theories in 2+1d, they automatically have an emergent global $\mathsf{U}(1)_M$ magnetic symmetry due to the Bianchi identity $\varepsilon^{\mu\nu\lambda} \partial_\mu F_{\nu\lambda} = 0$ where $F_{\nu\lambda}$ is the gauge field strength. The charged operator of this $\mathsf{U}(1)_M$ symmetry is the magnetic monopole operator which creates the gauge

flux and its coupling with the background gauge field are $\frac{1}{2\pi}adY, \frac{1}{2\pi}\tilde{a}dX$ in the both hand sides respectively. The symmetry charges of the operators are,

	$\mathsf{U}(1)_a$	$\mathsf{U}(1)_X$	$\mathsf{U}(1)_Y$		$\mathsf{U}(1)_{\tilde{a}}$	$\mathsf{U}(1)_X$	$\mathsf{U}(1)_Y$
$\mathscr{M}_a$	1	0	1	$\mathscr{M}_{\tilde{a}}$	1	1	0
ψ_1	1	1	0	χ_1	1	0	1
ψ_2	1	-1	0	χ_2	1	0	-1

$$\leftrightarrow \tag{1.3}$$

and the gauge invariant operators are built from these operators.

Renaming the fermion fields $\psi \leftrightarrow \chi$ will exchange $X \leftrightarrow Y$ and add a background term $\frac{2}{4\pi}(XdX - YdY)$ to the Lagrangian, the left-hand-side (LHS) Eq. (1.1) and the right-hand-side (RHS) of Eq. (1.2) of the duality will be swapped, therefore, establishes the self-duality.

This self-duality can also be understood as exchanging the "electric charge" and the "magnetic charge". On the LHS of the duality, the fermion field ψ_i is charged under the $\mathsf{U}(1)_X$ flavor symmetry, and the magnetic monopole operator $\mathscr{M}_a$ which creates 2π-flux for a is charged under the magnetic $\mathsf{U}(1)_Y$ due to the mixed CS term $\frac{1}{2\pi}adY$ (note that $\mathscr{M}_a$ is the bare magnetic monopole operator which is not gauge invariant due to the CS term $\frac{1}{4\pi}ada$, the gauge-invariant operators are the combination of the $\mathscr{M}_a$ and fermion creation operators). However, on the RHS, the fermion field χ_i is charged under $\mathsf{U}(1)_Y$ and the magnetic monopole operator $\mathscr{M}_{\tilde{a}}$ is charged under $\mathsf{U}(1)_X$. This suggests that the fermion creation operators (resp. monopole operators) on the LHS become monopole operators (resp. fermion creation operators) on the RHS. More details of the self-duality are presented in App. A.2

Here is a side-note on the conventions to regularize the fermion path integral:

One convention is that integrating out a single Dirac fermion in (2+1)D will contribute a (-1)-level CS term for the negative fermion mass and a 0-level CS term for the positive fermion mass. Physically, fermions are doubled when putting on the lattice, one Dirac fermion is accompanied by a massive fermionic partner, otherwise, the single Dirac fermion will have parity

anomaly in (2+1)D [420]. This convention assumes that the massive fermionic partner *is not* integrated out beforehand and it is more explicit on the quantization of the level of Chern-Simons term, this is easier to analyze the symmetry charges of the operators since the magnetic monopole operator has charge k if there is a level-k CS term. We will use this convention in discussing the dualities of quantum field theories, such as the self-duality of $N_f = 2$ QED$_3$.

Another convention is that integrating out the fermion will contribute a $\frac{\text{sgn}(m)}{2}$-level CS term, this assumes that the massive fermionic partner has been integrated out beforehand and this is relevant to the analysis of the scaling dimensions of the critical theory since the massive fermionic partner does not involve in the transition. Using the later convention, half level CS term will involve in the massless theory, and now the Chern-Simons level is effectively $-\frac{N_f}{2} + k$ where N_f is the number of fermion flavors. We will adopt this convention in the discussion of renormalization group analysis on the critical behavior of the theory.

Schematically, the fermion theory with the level-k CS term using the first convention is related to that using the second convention by,

$$\underbrace{\mathrm{i}\sum_{i=1}^{N_f} \bar{\psi}_i \slashed{D}_a \psi_i + \frac{k}{4\pi} ada}_{\text{the 1st convention}} \cong \underbrace{\mathrm{i}\sum_{i=1}^{N_f} \bar{\psi}_i \slashed{D}_a \psi_i + \frac{k - N_f/2}{4\pi} ada}_{\text{the 2nd convention}} . \tag{1.4}$$

The duality presented in Eq. (1.1) and (1.2) will be equivalent to the self-dual theory presented in Ref. [432] by converting to the second convention of the fermion path integral regularization. However, both conventions have the same gauge-invariant operators and they yield the same response theories in the gapped phases.

1.2.1 Phase diagram

The $N_f = 2$ QED$_3$ has two relevant fermion mass deformations, the *singlet mass* $m\bar{\psi}\mathbb{1}\psi \equiv m(\bar{\psi}_1\psi_1 + \bar{\psi}_2\psi_2)$ and the *triplet mass* $m'\bar{\psi}\sigma^3\psi \equiv m'(\bar{\psi}_1\psi_1 - \bar{\psi}_2\psi_2)$, where σ^i is the *i*-th Pauli matrix. Under these mass deformations, one can integrate out the fermions and

obtain the following effective theories for the background gauge fields Eq. (1.1)[432, 81],

$$
\begin{cases}
\frac{2}{4\pi}(XdX - YdY) & m > 0,\ m' = 0 \\[2mm]
0 & m < 0,\ m' = 0
\end{cases}
\tag{1.5}
$$

$$
\begin{cases}
\frac{1}{2\pi}ad(Y+X) + \frac{1}{4e^2}f^2 + ... & m' > 0\ m = 0 \\[2mm]
\frac{1}{2\pi}ad(Y-X) + \frac{1}{4e^2}f^2 + ... & m' < 0\ m = 0
\end{cases}
.
\tag{1.6}
$$

where e is the electron charge. The ... represents the gapped degrees of freedom that are not important at low energy since the low-energy physics is dominated by the Maxwell term $\frac{1}{4e^2}f^2$ and the first term which describes the gapless Goldstone boson associated to the broken symmetry $U(1)_{Y+X}$ or $U(1)_{Y-X}$.

When the singlet mass m is non-zero, the two response theories in Eq. (1.5) differ by a $U(1)_{X,2} \times U(1)_{Y,-2}$ CS term, where the number indicates the level of the CS term, i.e. $\frac{2}{4\pi}(XdX - YdY)$, which corresponds to the topological response of a bosonic SPT state with $U(1)_X \times U(1)_Y$ symmetry[1]. Therefore, the $m > 0$ and $m < 0$ phases should be ascribed to the topological and trivial SPT phases respectively[2]. When the triplet mass term m' is non-zero, the effective theories in Eq. (1.6) describe the Goldstone modes in the spontaneous symmetry breaking (SSB) phases with broken symmetries associated to $Y + X$ and $Y - X$ respectively (two different combinations of the generators of $U(1)_X, U(1)_Y$). In the context of square-lattice easy-plane quantum magnets[315, 262], we might interpret $U(1)_{Y+X}$ as the in-plane spin rotation symmetry and $U(1)_{Y-X}$ as the lattice rotation symmetry (ignoring the discrete nature of the actual C_4 rotation), then the $m' > 0$ and $m' < 0$ phases could be identified as the XY-AFM and the VBS phases respectively. Fig. 1.2(a) shows the phase diagram summarizing the above interpretations. Under the duality transformation, the singlet mass is odd ($m \to -m$) while the triplet mass is

---

[1]Since the gauge-invariant operators in UV are all bosonic (no single fermion operators), the resulting gapped phases can possibly connect to the bosonic theory.

[2]Which phase is topological/trivial is only a matter of convention, as the notion of SPT phases is only relative.
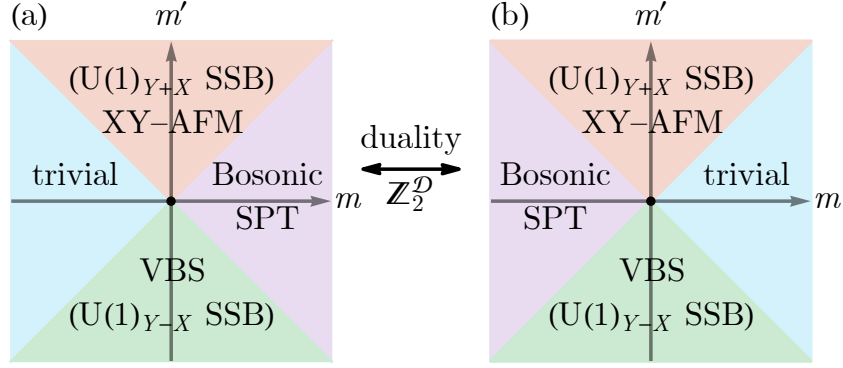
Figure 1.2. The phase diagram of $N_f = 2$ QED$_3$ theory. The singlet mass m drives the SPT transition between two symmetric phases, and the triplet mass m' drives AFM-VBS transition between two symmetry broken phases.

even ($m' \to m'$), which effectively swap the SPT and trivial phases but leaving the AFM and VBS phases unchanged (see Fig. 1.2). To restore the original phase diagram after the duality transformation, one should exchange $\mathsf{U}(1)_X \leftrightarrow \mathsf{U}(1)_Y$ and add a background $\mathsf{U}(1)_{X,2} \times \mathsf{U}(1)_{Y,-2}$ CS term to the Lagrangian.

1.2.2 Self-duality as a symmetry

As pointed out in Ref. [29, 177], the explicit UV symmetry $\mathsf{U}(1)_X \times \mathsf{U}(1)_Y$ in Eq. (1.1) and (1.2) can be enhanced to the emergent symmetry $\frac{\mathsf{SU}(2)_X \times \mathsf{SU}(2)_Y}{\mathbb{Z}_2} \cong \mathsf{SO}(4)$ in the IR. Together with the self-duality $\mathbb{Z}_2^{\mathscr{D}}$ which exchanges $\mathsf{SU}(2)_X \leftrightarrow \mathsf{SU}(2)_Y$ and attaches a $\mathsf{SU}(2)_{X,1} \times \mathsf{SU}(2)_{Y,-1}$ CS term (which falls back to the $\mathsf{U}(1)_{X,2} \times \mathsf{U}(1)_{Y,-2}$ CS term in the UV), the IR symmetry becomes $\mathsf{SO}(4) \rtimes \mathbb{Z}_2^{\mathscr{D}} \cong \mathsf{O}(4)$. However, as the IR theory is shifted by the $\mathsf{SU}(2)_{X,1} \times \mathsf{SU}(2)_{Y,-1}$ background response under the self-duality transformation, the $\mathbb{Z}_2^{\mathscr{D}}$ and the $\mathsf{SO}(4)$ have the mixed 't Hooft anomaly, thus they cannot be simultaneously coupled to the background gauge fields and promoted to the dynamical ones. Nonetheless, it can be viewed as the boundary of a (3+1)D SPT with the full $\mathsf{O}(4)$ symmetry. With appropriate counterterm in the bulk, the whole system can also have time-reversal symmetry $\mathbb{Z}_2^{\mathsf{T}}$, altogether gives $\mathsf{O}(4) \times \mathbb{Z}_2^{\mathsf{T}}$ as suggested in Ref. [393].

Note that the singlet mass m is invariant under $\mathsf{SO}(4)$ but is odd under $\mathbb{Z}_2^{\mathscr{D}}$, while

the triplet mass m' explicitly breaks $\mathsf{SO}(4)$ (as it is in the $(\mathbf{3}, \mathbf{3})$ representation[81, 393] of $\mathsf{SU}(2)_X \times \mathsf{SU}(2)_Y$) but is even under $\mathbb{Z}_2^{\mathscr{D}}$. Hence, if both the emergent $\mathsf{SO}(4)$ and the self-duality $\mathbb{Z}_2^{\mathscr{D}}$ symmetries are imposed, no fermion bilinear mass could be included in the Lagrangian.

1.2.3 Self-duality protected multi-criticality

Although the mass term cannot be added to the Lagrangian, squares of the mass term still can, which may take the form of four-fermion interactions $(\bar{\psi} M^a \psi)^2$, where M^as are mass matrices acting on the flavor indices. Adding these mass-squared deformations to the QED theory Eq. (1.1) could potentially drive the theory to new fixed points[192]. The fate of the self-duality $\mathbb{Z}_2^{\mathscr{D}}$ and the $\mathsf{SO}(4)$ symmetry depends on the RG flow of such mass-squared deformations. If both symmetries are preserved, the theory will remain critical (as no mass deformation is allowed), which describes the continuous transition between AFM and VBS phases (as well as the transition between SPT and trivial phases), which is also known as the $\mathsf{O}(4)$ DQCP. When the self-duality $\mathbb{Z}_2^{\mathscr{D}}$ symmetry is spontaneously broken, the SPT transition becomes first-order. When the emergent $\mathsf{SO}(4)$ symmetry (more specifically the $\mathbb{Z}_2$ subgroup that swaps $\mathsf{U}(1)_{Y+X}$ and $U(1)_{Y-X}$) is spontaneously broken, the AFM-VBS transition becomes first-order. These first-order transitions are separated from the continuous transition by the multi-critical points/lines. We will analyze the RG flow of the generic four-fermion interactions at these multi-critical points, aiming to understand how certain kinds of interactions can drive the DQCP from a continuous transition to a first-order transition.

The multi-critical point happens when Dirac fermion masses change the sign. To analyze the scaling dimensions of the operators at the multi-critical point, we do not need to include the massive fermionic parton which is served to cancel the subtlety in the fermion path integral regularization. We rewrite Eq. (1.1) as

$$ i\bar{\psi}_1 \slashed{D}_{a+X} \psi_1 + i\bar{\psi}_2 \slashed{D}_{a-X} \psi_2 + \frac{1}{2\pi} adY + \frac{1}{4\pi}(XdX - YdY). \tag{1.7} $$

The CS terms look different from Eq. (1.1), because we integrate out the massive fermionic partners beforehand and it corresponds to the second convention as discussed in the last three paragraphs of Sec. 1.2, following from Ref. [432]. Note that the changing of convention will not change the gauge invariant operators as well as the different gapped phases. The background gauge fields X and Y won't affect the dynamics and can be set to zero. Adding the mass-squared deformations amounts to promoting the mass terms m and m' to the dynamic scalar fields ϕ_1 and ϕ_2, that are coupled to the fermions via Yukawa-type couplings $\phi_a \bar{\psi} M^a \psi$, this can also be seen by using the Hubbard–Stratonovich transformation. Together with their own boson mass terms $r_a \phi_a^2$, the action reads as,

$$
\sum_{i=1}^{2} i \bar{\psi}_i \slashed{D}_a \psi_i + \phi_1 \bar{\psi} \mathbb{1} \psi + \phi_2 \bar{\psi} \sigma^3 \psi
$$
$$
+ \sum_{a=1}^{2} \frac{1}{2g^2} \phi_a (r_a - \partial^2) \phi_a + \frac{\lambda}{4} (\phi_a \phi_a)^2. \tag{1.8}
$$

For each scalar field ϕ_a, the boson mass r_a has a corresponding critical value $r_{a,c}$. When $r_a \gg r_{a,c}$, the boson is gapped and $\langle \phi_a \rangle = 0$. When $r_a \ll r_{a,c}$, the boson is condensed, such that $\langle \phi_a \rangle \neq 0$ and the symmetry is spontaneously broken. This will dynamically generate the corresponding fermion mass terms. We may loosely set $r_{a,c} = 0$ and assume the bosons are critical when $r_a = 0$ in the following discussion.

The qualitative phase diagram of Eq. (1.8) is shown in Fig. 1.3, which can be considered as the extension of the Fig. 1.2's origin, since no fermion mass terms m, m' are added in the Eq. (1.8). In the phase diagram, when $r_1, r_2 \gg 0$ (the blue region), both bosons are gapped, leaving Eq. (1.8) to be the $N_f = 2$ QED$_3$ theory at low energy. As discussed previously, this theory has an emergent $O(4)$ symmetry and describes the continuous DQCP transition between the AFM and VBS phases (i.e. between the $U(1)_{Y+X}$ and $U(1)_{Y-X}$ SSB phases) when tuning the triplet fermion mass m' externally. If r_1 is at its critical value and $r_2 \gg 0$ (along the red line), the critical theory becomes $N_f = 2$ QED$_3$-Gross-Neveu model, which describes the continuous
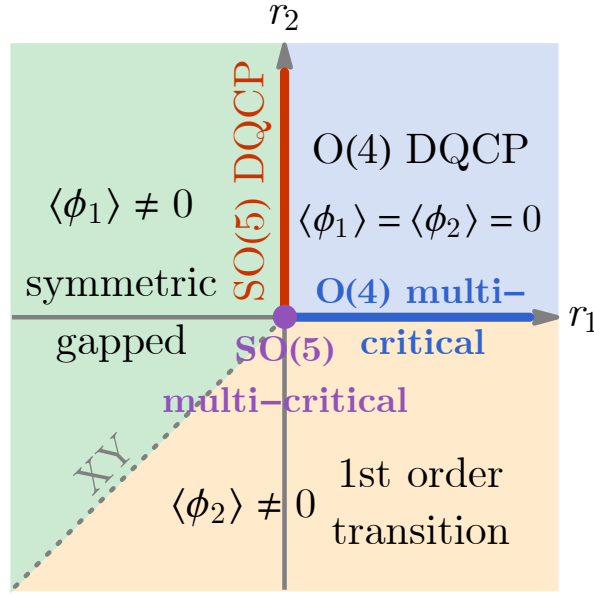
Figure 1.3. Mean-field phase diagram of Eq. (1.8).

DQCP with emergent $\mathsf{SO}(5)$ symmetry as proposed in Ref. [393]. If instead, r_2 is at its critical value and $r_1 \gg 0$ (across the blue line), the theory describes the multi-criticality between the $\mathsf{O}(4)$ DQCP and the first-order AFM-VBS transition. If both r_1 and r_2 are critical (the purple point), the theory describes the multi-criticality between the $\mathsf{SO}(5)$ DQCP and the first-order AFM-VBS transition.

To see that the ϕ_2 condensed phase (the orange region) corresponds to the first-order AFM-VBS transition, we consider driving the AFM-VBS transition by an external triplet mass m'. The actual mass term seen by the fermion will be $(m' + \langle \phi_2 \rangle) \bar{\psi} \sigma^3 \psi$, meaning that the driving parameter m' needs to overcome the expectation value $\langle \phi_2 \rangle$ in order to change the sign of the triplet mass effectively and switch the system from one phase to another. Therefore $\langle \bar{\psi} \sigma^3 \psi \rangle$ will exhibit the hysteresis behavior as m' is tuned back and forth, which manifests the first-order transition. Without the external driving ($m' = 0$), the ground state will be degenerated between AFM and VBS phases.

On the other hand, the ϕ_1 condensed phase (the green region) is a symmetric gapped phase whose ground state is degenerated between topological and trivial SPT phases, which may

as well be interpreted as the 1st-order SPT transition if the singlet mass *m* is tuned externally. The ϕ_1 condensed phase and the ϕ_2 condensed phase do not coexist, because they compete with each other to gap out the fermion, and the ground state is determined by the condensate that has a larger vacuum expectation value $|\langle \phi_a \rangle|$. When the competition reaches a balance at $|\langle \phi_1 \rangle| = |\langle \phi_2 \rangle|$ (along the gray dashed line), it triggers a direct transition between the symmetric and the SSB phases (either the in-plane magnetic order or the VBS order), which is of the 3d XY universality.

The multi-criticality between the continuous and first-order transitions cannot be circumvented in the presence of the anomalous $O(4)$ symmetry. However, it is possible that the protecting symmetry may be broken spontaneously under other potentially relevant perturbations, such that the $O(4)$ DQCP is not stable in general. In the following, we will explore this possibility by analyzing the effect of generic four-fermion interactions in the QED-GN theory using the large-*N* renormalization group (RG) approach.

1.3 Large-*N* Renormalization Group Analysis

1.3.1 QED-Gross-Neveu-Chern-Simons theory

We extend Eq. (1.8) to N_f flavors of Dirac fermions $\psi = (\psi_1, \cdots, \psi_{N_f})^\mathsf{T}$ coupled to the dynamical $U(1)$ gauge field, together with Yukawa-type couplings to N_b flavors of scalar bosons ϕ_a ($a = 1, ..., N_b$). The bosons will have their kinetic terms and can be tuned critical by the r_a parameters. We also add the level-*k* CS term for the dynamical $U(1)$ gauge field (to be general) and consider the QED$_3$-Gross-Neveu-Chern-Simons (QED-GN-CS) theory as follows

$$
\begin{aligned}
\mathscr{L} = {}& \bar{\psi}(\mathbb{1}_{N_f} \otimes \gamma^\mu)(\partial_\mu - \mathrm{i}a_\mu)\psi + \phi_a \bar{\psi}(M^a \otimes \mathbb{1}_2)\psi \\
& + \frac{1}{2g^2}\phi_a(r_a - \partial^2)\phi_a + \frac{\lambda}{4}(\phi_a\phi_a)^2 \\
& + \frac{\mathrm{i}k}{4\pi}\varepsilon^{\mu\nu\lambda}a_\mu\partial_\nu a_\lambda + \frac{1}{4e^2}f_{\mu\nu}f^{\mu\nu}.
\end{aligned}
\tag{1.9}
$$

Here, matrices $\mathbb{1}_{N_f}, M^a$ act on the flavor space, while matrices $\mathbb{1}_2, \gamma^\mu$ act on the spinor space. We take the γ-matrices to be $(\sigma^3, \sigma^1, \sigma^2)$. M^as are vertices of Yukawa couplings associated with fermion bilinear masses, which are assumed to be orthogonal to each other such that $\text{tr}(M^a M^b) = \mathbb{M} \delta_{ab}$. The last term is the Maxwell term, with the gauge curvature defined as $f_{\mu\nu} = \partial_\mu a_\nu - \partial_\nu a_\mu$.

The multi-critical points/lines in the phase diagram Fig. 1.3 correspond to tuning one or more scalar bosons to critical. We assume that all scalar fields in the effective theory Eq. (1.9) correspond to the critical bosons (other gapped bosons will be dropped from the effective theory automatically). The theory is tuned to the QED-GN-CS fixed point. The boson mass term $(r_a - r_{a,c})\phi_a^2$ is a relevant perturbation that drives the system away from the multi-criticality. It also is possible that some types of fermion interactions may flow to the boson mass term ϕ_a^2, as it is equivalent to the mass-mass interaction $(\bar\psi(M^a \otimes \mathbb{1}_2)\psi)^2$ under the Hubbard–Stratonovich transform. Such fermion interactions will appear relevant at the QED-GN-CS fixed point and can drive the system away from multi-criticality as well.

1.3.2 Renormalization of four-fermion interactions

To explore this possibility, we carry out a systematic study of the scaling dimension of four-fermion interactions at the QED-GN-CS fixed point (see App. A.1 for technical details). We will follow the large-N_f expansion approach recently developed for the QED$_3$-GN model in [47], where the scaling dimensions of fermion and boson bilinear operators were analyzed. Here, we will carry over the analysis to four-fermion operators, which has not been presented yet. To be more general, we also include a CS term, such that our result could potentially be applied to other DQCP such as the superfluid to bosonic fractional quantum Hall transition (described by the QED-GN-CS fixed point at level $k = 1$[24]).

In particular, our scheme to extend Eq. (1.8) to large N_f corresponds to generalizing the fermion flavor symmetry group from $\text{SU}(2) \to \text{SU}(2N)$, such that the fermion flavor number

scales as $N_f = 2N$ with $N \to \infty$. The Yukawa vertices are generalized to

$$\{M^a\} = \{\mathbb{1}_2, \sigma^3\} \to \{M_N^a\} = \{\mathbb{1}_2, \sigma^3\} \otimes \mathbb{1}_N. \tag{1.10}$$

where $\{M^a\}$ denotes the set formed by M^as, similar for $\{V^\alpha\}$. The perturbative interactions are,

$$\mathscr{L}_{\text{int}} = u_{\alpha,m}(\bar{\psi} V^\alpha \otimes \mathbb{1}_2 \psi)^2 + u_{\alpha,\mu}(\bar{\psi} V^\alpha \otimes \gamma^\mu \psi)^2 \tag{1.11}$$

where $V^\alpha = \sigma^\alpha \otimes \mathbb{1}_N$ ($\alpha = 0,1,2,3$). $u_{\alpha,m}$, $u_{\alpha,\mu}$ represent the coupling coefficient of the mass-mass interactions and the current-current interactions respectively, which can be combined to a vector $u_{\alpha,i} = (u_{\alpha,m}, u_{\alpha,0}, u_{\alpha,1}, u_{\alpha,2})^\mathsf{T}$ in each α-channel. The RG equations for $u_{\alpha,i}$ takes the following general form,

$$\frac{du_{\alpha,i}}{d\ell} = \left(-1 + \frac{64}{3\pi^2 N_f} \mathbf{M}_{(\alpha,i),(\beta,j)}\right) u_{\beta,j} \tag{1.12}$$

where the repeated indices are summed over and $\mathbf{M}$ is a matrix with entries given by the $\mathcal{O}(1/N_f)$ corrections, the detailed calculations are presented in App. A.1. One can further diagonalize $\mathbf{M}$ to find the eigen-channels. We take $N_f \to 2$ to restore the case of Eq. (1.8). The large-N_f analysis is not well controlled for small N_f, as sub-leading corrections may not be sufficiently small. However, in our case, we assume the $N_f = 2$ QED$_3$ has the IR conformal fixed point which is suggested by the QMC simulation[315] and then perform the analysis on the perturbative four-fermion interactions. It turns out that our large-N_f RG results are consistent with the latest QMC simulation[459, 460, 434].

The first quadrant, $\mathrm{O}(4)$ DQCP: Without the contribution from the critical bosons, there is no relevant channel for $\alpha = 0$. But for $\alpha = 1,2,3$, it has one relevant channel,

$$\frac{du_{\alpha,i}}{d\ell} = 2.24 u_{\alpha,i}, \quad \text{with } u_{\alpha,i} = (3,1,1,1)^\mathsf{T}, \tag{1.13}$$

25

and the spatio-temporal anisotropic channels are irrelevant. Therefore the mass-mass interaction can be generated from the current-current interaction under the RG flow, which could potentially drive the $O(4)$ DQCP to a first-order transition (if the generated mass-squared interaction is strong enough to overcome the bare r_2 term).

With large-N_f, $u_{\alpha,i}$ are independent parameters. But for $N_f = 2$ (i.e. $N = 1$), the Fierz identity demands the uniform combination $\sum_{\alpha=1,2,3} u_{\alpha,i}$ "fuses" into the $\alpha = 0$ channel, which is irrelevant. Additionally, the explicit $U(1)_X \times U(1)_Y$ symmetry guarantees $u_{1,i} = u_{2,i}$, hence for $N_f = 2$, there is only one independent channel of the relevant four-fermion interaction with $\alpha = 3$.

The positive-r_2 axis, $SO(5)$ DQCP: In this case, the scalar boson associated to the singlet mass is critical, $\{M^a\} = \mathbb{1}_2$. There is still no relevant channel for $\alpha = 0$. For $\alpha = 1, 2, 3$, it has the same relevant channel as the previous case,

$$\frac{du_{\alpha,i}}{d\ell} = 1.70 u_{\alpha,i}, \quad \text{with } u_{\alpha,i} = (3, 1, 1, 1)^\mathsf{T}. \tag{1.14}$$

Hence, the stagger-Q term still overlaps with the relevant channel at $SO(5)$ DQCP fixed point. Similarly, as discussed in the last paragraph, for $N_f = 2$, there is only one independent channel of the relevant four-fermion interaction with $\alpha = 3$.

The positive-r_1 axis and the origin: Both cases are more involved. The positive-r_1 axis describes the transition between the $O(4)$ DQCP and first-order transition, and the origin is a multi-critical point where 3 critical lines joins. Both ϕ_1 and ϕ_2 scalar fields are critical at the origin, such that the Yukawa vertices are $\{M^a\} = \{\mathbb{1}_2, \sigma^3\}$. The eigen-channels will have mixture of V^0, V^3 or V^1, V^2, because M^a will mix V^0 with V^3 as well as V^1 with V^2. Considering $\{V^\alpha\} = \{V^0, V^3\}$, there is one relevant channel with $u_{03} \equiv (u_{0,i}; u_{3,i}) = (-0.03, -0.071, -0.071, -0.071; 0.82, 0.32, 0.32, 0.32)^\mathsf{T}$, and the RG

equation reads

$$\frac{du_{03}}{d\ell} = 1.89 u_{03} \quad \text{(positive-}r_1 \text{ axis)},$$
$$\frac{du_{03}}{d\ell} = 1.35 u_{03} \quad \text{(origin)}.$$

(1.15)

The detailed calculation is presented in App. A.1. With one more critical boson at the origin compared to the positive-r_1 axis, the RG eigenvalue of the relevant interaction is smaller at the SO(5) multi-critical point compared to the O(4) multi-critical line.

1.4 Implications of RG Analysis

1.4.1 Consequence of the relevant interactions

The RG analysis suggests that the SO(5) and O(4) DQCP may not be stable against the perturbation of certain Lorentz symmetry breaking four-fermion interactions in the field theory. The interaction is relevant and flows to the following form

$$\mathscr{L}_{\text{int}} = u(3(\bar{\psi}\sigma^3\psi)^2 + (\bar{\psi}\sigma^3\gamma^\mu\psi)^2).$$

(1.16)

Depending on the sign of the coefficient u, the interaction may drive different instabilities of the QED theory. By analyzing all possible Wick decomposition of the interaction term, we found the leading eigen decompositions with both positive and negative interaction strength is $\mathscr{L}_{\text{int}} = u(\bar{\psi}\sigma^3\psi)^2 + \cdots - u(\bar{\psi}\psi)^2$. Therefore, if $u < 0$, the interaction favors the condensation of the triplet mass term $\bar{\psi}\sigma^3\psi$, or equivalently the scalar field ϕ_2 that couples to it. In this case, the emergent SO(4) symmetry is spontaneously broken, and the AFM-VBS transition becomes first-order. On the other hand, if $u > 0$, the interaction favors the condensation of the singlet mass term $\bar{\psi}\psi$, or equivalently the corresponding scalar field ϕ_1, which spontaneously breaks the self-duality and results in the symmetric gapped state. Fig. 1.4 shows the extension of the phase diagram in the presence of four-fermion interaction.

The next leading eigen decompositions of the interaction are the singlet pairing channels $-\frac{2}{3}u|\psi^\mathsf{T}\sigma^2\gamma^0\gamma^x\psi|^2$ and $-\frac{2}{3}u|\psi^\mathsf{T}\sigma^2\gamma^0\gamma^y\psi|^2$ with slightly less interaction strength. When $u > 0$, the system may condense the Cooper pairs $\psi^\mathsf{T}\sigma^2\gamma^0\gamma^{x,y}\psi$, breaking the Lorentz symmetry. Since this term commutes with some of the kinetic terms in the Hamiltonian, it will split the Dirac points in the momentum space but will not gap out the fermions. It will also Higgs the $\mathsf{U}(1)$ gauge group down to $\mathbb{Z}_2$. Therefore, it opens the possibility for the gapless $\mathbb{Z}_2$ spin liquid phase instead of the symmetric gapped phase away from the multicritical point, which provides a candidate scenario for the phase diagram observed in the recent QMC study Ref. [434] where the first-order transition and the gapless $\mathbb{Z}_2$ spin liquid phase are separated by the multicritical point. Another scenario of the gapless $\mathbb{Z}_2$ spin liquid phase near the DQCP is recently proposed in Ref. [352]. The Lorentz symmetry is also broken by the Higgs field. However, the fermion flavors are doubled in that proposal compared to ours, thus it describes a different gapless $\mathbb{Z}_2$ spin liquid phase (see App. A.3 for details). For example, the entanglement entropy contributed from the massless degrees of freedom will be different, which could be distinguished in future numerical studies.
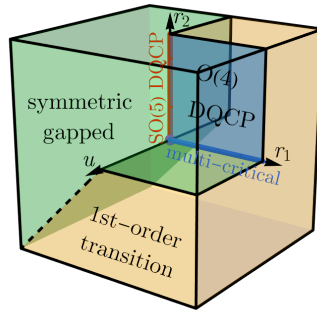
Figure 1.4. Extended phase diagram in the presence of relevant interaction u. The $u = 0$ plane corresponds to the phase diagram in Fig. 1.3.

1.4.2 Role of the stagger-Q perturbation

Recent QMC studies revealed the possibility of tuning the DQCP between continuous and first-order transitions[459, 460]. In particular, the stagger-Q term (denoted by Q_s, or the so-called Z-deformation) was proposed in [459] as a modification of the J-Q model,

$$H = H_{JQ} + H_{Q_s},$$

$$H_{JQ} = -J\sum_i P_i^x - Q\sum_i P_i^x P_{i+\hat{y}}^x + (x \leftrightarrow y),$$

$$H_{Q_s} = -Q_s \sum_i P_i^x P_{i+\hat{x}+\hat{y}}^x + (x \leftrightarrow y),$$

(1.17)

where $P_i^x = 1/4 - \mathbf{S}_i \cdot \mathbf{S}_{i+\hat{x}}$ and $P_i^y = 1/4 - \mathbf{S}_i \cdot \mathbf{S}_{i+\hat{y}}$ are the dimer operators on the x and y bonds respectively. The stagger-Q term Q_s favors a staggered VBS pattern, and hence the name. The illustration of the Q term and the stagger-Q term is shown in Fig. 1.5. Another version of the stagger-Q term that involves three dimers interacting along the diagonal direction is studied in [460]. The three-dimer stagger-Q term has the same symmetry as the two-dimer stagger-Q term, and shares the similar physical effect (both favors the same staggered VBS order). The QMC phase diagram in [460] explicitly shows that the stagger-Q term can drive the DQCP to a first-order transition. We will connect this observation to our field-theory analysis.
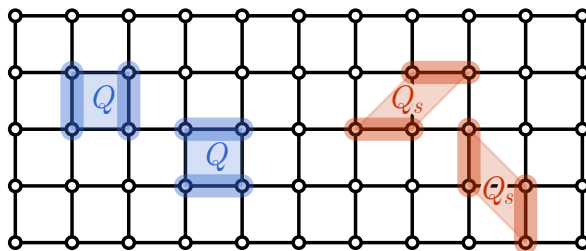
Figure 1.5. Illustration of the (standard) Q term (in blue) and the stagger-Q term (Q_s, in red) on the square lattice. Both are dimer-dimer interactions, but along different directions.

In the momentum space, the stagger-Q term should correspond to the dimer-dimer interaction near momentum (π, π), which can be argued as follows. Let $P_{\mathbf{q}}^{x,y} = \sum_i P_i^{x,y} e^{-i\mathbf{q}\cdot\mathbf{r}_i}$ be

the dimer operator of momentum $\boldsymbol{q}$. A large Q_s term favors the dimer to order in the staggered pattern (along the diagonal direction), which corresponds to the condensation of the dimer order parameter at momentum $\boldsymbol{q} = (\pi, \pi)$, i.e. $\langle P^x_{(\pi,\pi)} \rangle \neq 0$ or $\langle P^y_{(\pi,\pi)} \rangle \neq 0$. Therefore, the effect of the stagger-Q interaction H_{Q_s} can be expressed as

$$H_{Q_s} \sim -Q_s \left((P^x_{(\pi,\pi)})^2 + (P^y_{(\pi,\pi)})^2 \right), \tag{1.18}$$

because a large Q_s in Eq. (1.18) also promotes the ordering of $P^{x,y}_{(\pi,\pi)}$, matching the effect of H_{Q_s} in the real space Eq. (1.17).

At low-energy, the dimer fluctuation near momentum (π, π) should correspond to the spatial component of the Noether current associated with the emergent $\mathsf{U}(1)_{Y-X}$ symmetry that rotates the VBS order parameters:

$$P^x_{(\pi,\pi)} \sim j^y_{\text{VBS}}, P^y_{(\pi,\pi)} \sim j^x_{\text{VBS}}. \tag{1.19}$$

This mapping was derived in Ref. [408] from the fermionic parton construction. A simple symmetry argument is as follows. We first notice that $P^x_{(\pi,0)}$ and $P^y_{(0,\pi)}$ are the VBS order parameters favored by the standard Q term in the J-Q model. They can be combined into a complex order parameter $\Psi_{\text{VBS}} = P^x_{(\pi,0)} + iP^y_{(0,\pi)}$. The $\mathsf{U}(1)_{Y-X}$ rotation corresponds to $\Psi_{\text{VBS}} \to e^{i\theta} \Psi_{\text{VBS}}$, therefore the associated current operator should be

$$\begin{aligned}
j^x_{\text{VBS}} &= i\Psi^\dagger_{\text{VBS}} \partial_x \Psi_{\text{VBS}} + \text{h.c.} \\
&= P^y_{(0,\pi)} \partial_x P^x_{(\pi,0)} - P^x_{(\pi,0)} \partial_x P^y_{(0,\pi)}, \\
j^y_{\text{VBS}} &= i\Psi^\dagger_{\text{VBS}} \partial_y \Psi_{\text{VBS}} + \text{h.c.} \\
&= P^y_{(0,\pi)} \partial_y P^x_{(\pi,0)} - P^x_{(\pi,0)} \partial_y P^y_{(0,\pi)}.
\end{aligned} \tag{1.20}$$

Thus both j^x_{VBS} and j^y_{VBS} carry the total momentum (π, π) (as a summation of $(\pi, 0)$ and $(0, \pi)$). Under the (site-centered) reflection about the y axis, i.e. $(x, y) \to (-x, y)$,

30

we have $(P^x, P^y) \rightarrow (-P^x, P^y)$, $(\partial_x, \partial_y) \rightarrow (-\partial_x, \partial_y)$, thus $(j^x_{\text{VBS}}, j^y_{\text{VBS}}) \rightarrow (j^x_{\text{BVS}}, -j^y_{\text{BVS}})$ transforms as a pseudo-vector. Similarly, under the reflection $(x, y) \rightarrow (x, -y)$, we have $(j^x_{\text{VBS}}, j^y_{\text{VBS}}) \rightarrow (-j^x_{\text{BVS}}, j^y_{\text{BVS}})$. Furthermore, $j^{x,y}_{\text{VBS}}$ does not transform under spin rotation symmetry. All these symmetry properties are precisely matched by Eq. (1.19), which speaks for its validity.

Using the operator correspondence in Eq. (1.19), Eq. (1.18) can be casted into

$$H_{Q_s} \sim -Q_s \left((j^y_{\text{VBS}})^2 + (j^x_{\text{VBS}})^2 \right), \tag{1.21}$$

which identifies the stagger-Q term to the current-current interaction in the spatial channel. We can make further connection to the field theory. Since the $\mathsf{U}(1)_{Y-X}$ symmetry is generated by $\psi_1^\dagger \psi_1 - \psi_2^\dagger \psi_2$ in the $N_f = 2$ QED$_3$ theory, the corresponding Noether current should be $j^\mu_{\text{VBS}} = \bar{\psi} \sigma^3 \gamma^\mu \psi$, therefore the current-current interaction in Eq. (1.21) further translates to the four-fermion interaction in Eq. (1.11) with $u_{3,i} \propto Q_s(0, 0, 1, 1)^\mathsf{T}$. According to the RG analysis above, the current-current interaction will generate the mass-mass interaction and flow towards the combined interaction in Eq. (1.16).

Since the u term in Eq. (1.16) corresponds to the stagger-Q term in the lattice model, the original J-Q model may be very close to $u = 0$, i.e. the QED-GN fixed point in the field theory, though u should never be precisely zero. But the stagger-Q term in the lattice model will turn on a non-negligible u term in the field theory which is relevant at the QED-GN fixed point, therefore render the transition first order, as was observed numerically. In fact, according to Eq. (1.14), our calculation of the scaling dimension of the relevant four fermion term is $1.3 = 3 - 1.7$ at the $\mathsf{SO}(5)$ DQCP, which is close to the observed scaling dimension of the stagger-Q deformation of the J-Q model ($\Delta_Z \sim 1.4$ in Ref. [459]).
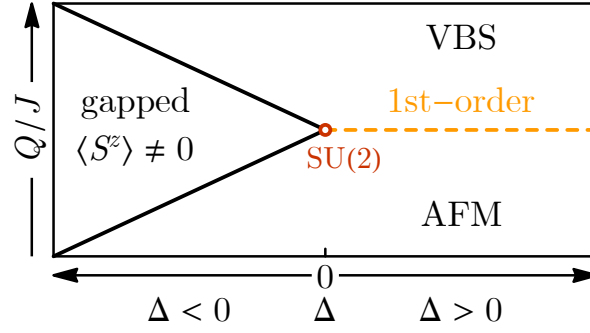
Figure 1.6. Schematic phase diagram of the easy-plane *J-Q* model Eq. (1.22).

The above field theory understanding also applies to the easy-plane *J-Q* model[315, 262],

$$H = H_{JQ} + H_{\Delta},$$

$$H_{\Delta} = -J\Delta \sum_i S_i^z S_{i+\hat{x}}^z + (x \leftrightarrow y), \tag{1.22}$$

where the parameter Δ tunes the easy-plane anisotropy. $\Delta = 0$ is the $\mathsf{SU}(2)$ isotropic limit, and $\Delta = 1$ is the $\mathsf{U}(1) \rtimes \mathbb{Z}_2$ easy-plane limit.

Tuning Δ away from 0 breaks the spin $\mathsf{SU}(2)$ symmetry and the *u* term should in principle also exist for the easy-plane *J-Q* model, but because it is more relevant compared to that in the $\mathsf{SU}(2)$ symmetric case (according to Eq. (1.13) and Eq. (1.14)), the easy-plane *J-Q* model may be a first-order transition more obviously than the isotropic limit. Based on the phase diagram Fig. 1.4, the system will either enter an intermediate symmetric gapped phase or exhibit a first-order AFM-VBS transition, in the presence of spin anisotropy. Given the physical meaning of the anisotropy term Δ, we can identify the symmetry gapped phase to the easy-axis anisotropy ($\Delta < 0$) and the first-order transition to the easy-plane anisotropy ($\Delta > 0$). A schematic phase diagram is presented in Fig. 1.6 for the lattice model Eq. (1.22). The symmetric gapped phase may as well be interpreted as the Ising ordered phase of $\langle S^z \rangle \neq 0$, since the condensation of ϕ_1 field corresponds to the ordering of $\langle S^z \rangle$. The scenario that the AFM-VBS transition becomes first-order as the easy-plane anisotropy is turned on is consistent with the recent QMC study Ref. [108].

1.5 Summary

In this work, we studied the $N_f = 2$ QED$_3$ with self-duality. The $N_f = 2$ QED$_3$ has SO(4) symmetry in the IR, if imposing the self-duality symmetry, it can be enhanced to O(4). The singlet mass is invariant under SO(4) but self-duality odd and the triplet mass is transformed by SO(4) but self-duality even. Requiring the O(4) symmetry, the theory cannot have explicit mass terms, which enables us to treat the mass terms as fluctuation scalar fields and to investigate the continuous-to-first-order transition driven by the mass fluctuations. The multi-critical points (lines) separating the continuous and first-order transitions can be described by the QED-GN theory.

We further analyzed the stability of the theory under the four-fermion interactions. In particular, we focus on the spatial current-current interaction of fermions in the field theory, which corresponds to a class of dimer-dimer interaction (the stagger-Q term) in the lattice spin model[459, 460]. This operator has been shown to drive the continuous DQCP to a first-order transition in recent numerical works. Our analysis indicates that such dimer interaction can be relevant at the O(4) DQCP and adjacent multi-critical lines, which generally destabilize the continuous DQCP to first-order transitions (or intermediate gapped phases). Our finding provides a theoretical understanding of the numerically observed first-order transition driven by the dimer-dimer interaction. Our analysis also suggests a possibility to have $\mathbb{Z}_2$ spin liquid in this model[434].

We provide systematically large-N renormalization group calculation of the general $N_f = 2$ QED$_3$ with Gross-Neveu term in App. A.1. Thanks to viewing the Feynman diagrams as string diagrams of symmetry group representations[100], the complicated diagram at $\mathcal{O}(1/N_f)$ can be expressed by a few group parameters. Scaling dimensions of generic fermion/boson bilinear terms and four-fermion perturbations are presented. We expect these general results will find broader applications in other exotic quantum critical systems.

Chapter. 1, in full, is a reprint of the material as it appears in Da-Chuan Lu, Cenke Xu, and

Yi-Zhuang You. Self-duality protected multicriticality in deconfined quantum phase transitions. *Physical Review B*, 104(20):205142, November 2021. The dissertation author was the primary investigator and author of this paper.

Chapter 2

Nonlinear sigma model description of deconfined quantum criticality in arbitrary dimensions

In this paper, we propose using the nonlinear sigma model (NLSM) with the Wess-Zumino-Witten (WZW) term as a general description of deconfined quantum critical points that separate two spontaneously symmetry-breaking (SSB) phases in arbitrary dimensions. In particular, we discuss the suitable choice of the target space of the NLSM, which is in general the homogeneous space G/K, where G is the UV symmetry and K is generated by $\mathfrak{k} = \mathfrak{h}_1 \cap \mathfrak{h}_2$, and $\mathfrak{h}_i$ is the Lie algebra of the unbroken symmetry in each SSB phase. With this specific target space, the symmetry defects in both SSB phases are on equal footing, and their intertwinement is captured by the WZW term. The DQCP transition is then tuned by proliferating the symmetry defects. By coupling the G/K NLSM with the WZW term to the background gauge field, the 't Hooft anomaly of this theory can be determined. The bulk symmetry-protected topological (SPT) phase that cancels the anomaly is described by the relative Chern-Simons term in odd spacetime dimensions or mixed θ term in even dimensions. We construct and discuss a series of models with Grassmannian symmetry defects in 3+1d. We also provide the fermionic model that reproduces the G/K NLSM with the WZW term.
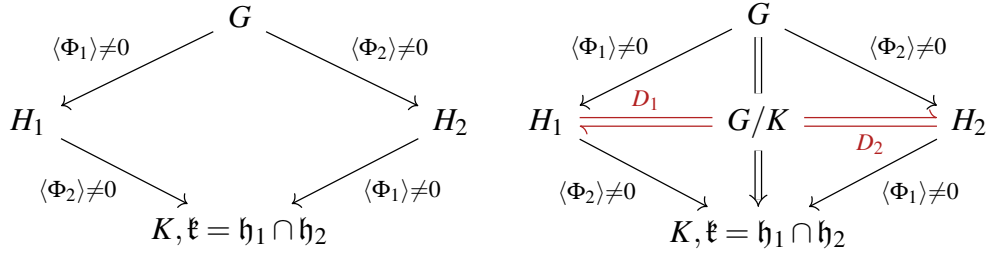
Figure 2.1. G is the UV symmetry and K is generated by the Lie algebra $\mathfrak{k} = \mathfrak{h}_1 \cap \mathfrak{h}_2$, where $\mathfrak{h}_1, \mathfrak{h}_2$ are the Lie algebras of unbroken symmetries H_1, H_2 of SSB phases. The different SSB phases are obtained by condensing order parameters Φ_i as in the left graph. Alternatively, the right graph emphasizes using the symmetry defects in the homogeneous space G/K where the bosonic field lives in. Proliferating symmetry defects D_i will drive the transition from one SSB phase to the other due to the additional charges assigned by WZW term.

2.1 Introduction

The continuous symmetry-breaking transitions are well described within the Landau-Ginzburg-Wilson (LGW) paradigm, the local order parameter acquires a non-zero expectation value in the spontaneous symmetry breaking (SSB) phase, and vanishes continuously when approaching the transition point. However, within the LGW paradigm, two SSB phases cannot be joined by a continuous transition but only first order or level crossing. Quantum effects open the possibility to have a such continuous transition, and the first explicit example is the deconfined quantum critical point (DQCP) between the VBS phase and Néel phase in 2+1d quantum magnet [348, 350, 375, 332].

The ordinary symmetry breaking transition can be alternatively understood by proliferating the symmetry defects in the SSB phase to arrive at the disordered phase. This point of view is particularly useful to understand the DQCP - the symmetry defect in the VBS phase is decorated with the quantum number of the spin $\mathrm{SU}(2)$ symmetry, proliferating which will restore the lattice rotation symmetry but break the spin symmetry, and arrive at the Néel phase [232]. Decorated symmetry defects are also studied in other beyond LGW quantum transitions [328, 281, 366].

Intertwinement of symmetry defects in different SSB phases, i.e. the symmetry defect in

one SSB phase carries the quantum number of the broken symmetry of the other SSB phase, is the prominent and ubiquitous feature of the DQCP theories. To properly describe the symmetry defects and their intertwinement, we consider the following generic symmetry breaking pattern of DQCP theory as shown in Fig. 2.1. Once condensing the order parameter Φ_i, one arrives at different SSB phases with unbroken symmetry H_i. Further condensing the other order parameter, one arrives at the minimal symmetry K. We will show that the symmetry defects in G/K incorporate all the symmetry defects in both SSB phases Sec. 2.5. The reason is based on that the codimension-$(q+1)$ symmetry defect in each SSB phase is classified by $\pi_q(G/H_i)$ [270], and $\pi_\star(G/K)$ contains roughly the generators of these homotopy groups. Moreover, the generators of the homotopy group are related to the differential forms via the Hurewicz theorem, then these symmetry defects are described by the differential form in the Lagrangian, and this term corresponds to the charge operator of symmetry defect. Technically, we use de Rham cohomology to find the generators of the cohomology group of G/K. The intertwinement of symmetry defects is essentially captured by the linking number of their corresponding charge operators, and the Wess-Zumino-Witten term in the action assigns phase to the linking number. Therefore, we propose using the nonlinear sigma model (NLSM) with the target space G/K to describe the DQCP between two SSB phases with unbroken symmetry H_1, H_2, and the intertwinement of symmetry defects is described by the Wess-Zumino-Witten (WZW) term. We also use G/K NLSM in short. The DQCP transition is driven by proliferating symmetry defects D_i in G/K along the red arrows in the right graph of Fig. 2.1. We will provide details and examples in the Sec. 2.5.

Intertwinement of symmetry defects in different SSB phases is also the manifestation of the (mixed) 't Hooft anomaly of the global symmetry. When global symmetry has 't Hooft anomaly, the theory is still well-defined unless the symmetry is gauged. The 't Hooft anomaly of global symmetry constrains the infrared phases not being trivial gapped phases but either SSB phase, gapless or topological order. The phase diagram of DQCP theory, namely two SSB phases connected by a gapless phase, agrees with the consequence of the 't Hooft anomaly.

37

The anomaly of 1+1d, 2+1d DQCP theories have been carefully analyzed in [272, 219, 393]. However, previous anomaly analysis is based on gauge theories, we focus on the anomaly analysis of NLSM description in terms of coupling the theory to background gauge fields. Since G is anomalous but K is non-anomalous, the NLSM with target space G/K saturates the anomaly of G. We provide a detailed calculation of coupling the WZW term to the background gauge field and show the gauged WZW term gives the 't Hooft anomaly [185, 110, 48]. By anomaly inflow, the 't Hooft anomaly in even spacetime dimensions is canceled by one higher dimensional bulk (relative) Chern-Simons term [279, 97, 440] and discussed in Sec. 2.4, while in odd spacetime dimension, the 't Hooft anomaly is canceled by bulk mixed θ term [185, 110, 48]. The lattice models that describe DQCP do not need additional higher dimensional bulk, it is because some of the global symmetries are acting in the *non-onsite* way, when it flows to IR, the field theory description requires these symmetries to be internal but with the 't Hooft anomaly [86, 193]. We should point out that the NLSM has long been used to describe the Goldstone mode in the SSB phase [413, 95, 59], and the additional Wess-Zumino-Witten term is used to match the anomaly in the ultraviolet [422]. Recently, the gauge theory and its dual NLSM with Stiefel manifold or Grassmannian manifold as the target space have been studied in the context of spin liquid and quantum critical point beyond the LGW paradigm [465, 439, 427]. In current paper, we present a general construction of NLSM with WZW that describes any given DQCP with continuous symmetry breaking. In the following, we explore its connection to the mixed 't Hooft anomaly, relative Chern-Simons term, and the intertwinement of different symmetry defects.

Inspired by recent work on deconfined quantum criticality (which can be critical point or critical phase depending on the model details) among grand unified theories [402, 401, 449], we apply our framework to construct the theory of 3+1d deconfined quantum critical phase (DQCPh) with global symmetry $G = \mathsf{SO}(2n)$ that separates two SSB phases with unbroken symmetries $H_1 = \mathsf{U}(n), H_2 = \mathsf{SO}(2n-2m) \times \mathsf{SO}(2m)$, and $K = \mathsf{SU}(n-m) \times \mathsf{U}(1) \times \mathsf{SU}(m) \times \mathsf{U}(1)$. The symmetry defects are then described by $\pi_2(G/K) = \ker(\pi_1(K) \to \pi_1(G)) = \mathbb{Z} \oplus \mathbb{Z}$. This is particularly interesting since the symmetry defect in the SSB phase with unbroken symmetry H_2

is Grassmannian manifold and has topological charge $\pi_2(G/H_2) = \mathbb{Z}_2$, which cannot be captured by de Rham cohomology, but once embedding into the larger space G/K, the topological charge becomes integer, and it has corresponding differential form via de Rham cohomology. This manifests the similar way that the non-perturbative $\mathsf{SU}(2)$ anomaly (due to $\pi_4(\mathsf{SU}(2)) = \mathbb{Z}_2$) can be perturbatively found by embedding $\mathsf{SU}(2) \hookrightarrow \mathsf{SU}(3)$ [120, 422, 421], and here we embed $G/H_2 \hookrightarrow G/K$. This series of 3+1d DQCPh theories has "new $\mathsf{SU}(2)$ anomaly" of the global symmetry $\mathsf{SO}(2n)$ [400], and it is matched by symmetry-protected topological phase in 5d bulk described by $w_2 w_3(\mathsf{SO}(2n))$ [402, 401, 449]. The mixed anomaly is obtained by pull-back via the embedding map of the subgroup into G. Recently, this embedding procedure is rigorously analyzed using bordism theory [103, 104].

We then present the alternative fermionic model that reproduces the G/K NLSM with WZW term. The fermions are coupled to the fluctuating bosonic fields which live in the homogeneous space, the bosonic fields parameterize the mass manifold of the fermions. We dub such fermionic construction of the nonlinear sigma model as fermionic sigma model [4]. When integrating out the massive fermions, the effective action is the nonlinear sigma model with level-1 WZW term [4, 182]. For generic homogeneous space G/K, the fermion mass manifold needs to be properly chosen. This fermionic model also implies that the nonlinear sigma model with level-1 WZW term needs a spin structure which is used to define the parallel transport of spinor fields, though the Goldstone boson fields are bosonic [231]. We then construct the fermionic sigma model of the 4d DQCPh theories and explicitly show the charge operators of two symmetry defects in different SSB phases link together.

The paper is structured as follows, we review the essential ingredients of the nonlinear sigma model and Wess-Zumino-Witten term as well as Lie group cohomology in Sec. 2.2. Then we review the 't Hooft anomaly and anomaly matching by WZW term in Sec. 2.3. Readers who are familiar with these can safely skip Sec. 2.2 and Sec. 2.3 but skimming through the notations would be helpful. We present the gauged WZW term and its anomaly matching with the bulk (relative) Chern-Simons term for generic spontaneously symmetry breaking in Sec. 2.4. We

construct specific DQCP theories in Sec. 2.5 and present the fermionic sigma model description in Sec. 2.6. We summarize our results and list further directions in Sec. 2.7. Finally, there are two appendices about de Rham cohomology of Lie group in App. B.1 and Cartan homotopy method in App. B.2 that are used to derive an explicit formula for the various WZW terms and Chern-Simons terms.

2.2 Review of nonlinear sigma model and Wess-Zumino-Witten term for general homogeneous space G/H

2.2.1 The Lagrangian of NLSM and WZW term

Supposing the UV theory has global symmetry G, which can contain spacetime symmetry as well as internal symmetry. In the IR, the symmetry is spontaneously broken down to H, then the IR theory contains the part with unbroken global symmetry H and the gapless Goldstone mode lives on the coset G/H. For example, the 3+1d N_f flavors fermion couples to $\mathsf{SU}(n)$ gauge field, the global symmetry $\mathsf{SU}(N)_L \times \mathsf{SU}(N_f)_R$ is spontaneously broken down to $\mathsf{SU}(N)_{\text{diag}}$, the coset where the Goldstone boson lives in is simply the Lie group $\mathsf{SU}(N)$ [422]. Or the Heisenberg spin in 2+1d, the spin rotation symmetry $\mathsf{SO}(3)_S$ is spontaneously broken down to $\mathsf{SO}(2)_S$, and the Goldstone mode lives in the coset $\mathbb{S}^2_S = \frac{\mathsf{SO}(3)_S}{\mathsf{SO}(2)_S}$ [411]. Before parametrizing the coset G/H, let's take the Goldstone boson lives in an arbitrary closed manifold M.

The Goldstone bosons are described by the nonlinear sigma model, where the scalar field takes value in the target manifold M. The field configuration is represented by a map from d-dimensional spacetime manifold X to the target manifold M,

$$U(x^\mu) : X \to M, \tag{2.1}$$

where x^μ is the coordinate of X and U lives in M. The kinetic term is,

$$S_0 = \frac{1}{2} \int_X d^d x \, \text{tr}\{(U^{-1}\partial_\mu U U^{-1}\partial^\mu U)\}. \tag{2.2}$$

where repeated indices mean summation. Besides the kinetic term, one can define the WZW term by pull-back the closed form $\Gamma^{(d+1)}$ on M. It seems the WZW term depends on the additional dimension, however, since the variation of the closed $(d+1)$-form yields the exact form, $\delta\Gamma^{(d+1)} = d\eta^{(d)}$, according to the Stokes' theorem, the equation of motion is indeed in d-dimension and does not rely on the fictitious extra dimension. We may view the spacetime manifold X as the boundary of a certain bulk manifold Y, such that $\partial Y = X$, and extend the map $\tilde{U} : Y \to M$, the WZW action is,

$$S_{\text{WZW}} = 2\pi k \mathrm{i} \int_Y \tilde{U}^*(\Gamma^{(d+1)}), \tag{2.3}$$

where $\tilde{U}^*$ is the pull-back map, k is the quantized level which is important for the theory to be well-defined and not depend on an extension to the bulk Y. Suppose we have another extension $\bar{Y}$ which is the orientation reverse of Y, and $Y \cup \bar{Y}$ is a closed manifold, then the integral over this combined manifold should be $2k\pi\mathrm{i}$, $k \in \mathbb{Z}$, such that the WZW term does not depend on the extension, otherwise, there is a phase ambiguity for different extensions. $\Gamma^{(d+1)}$ is actually the generator of integral cohomology of M, $\Gamma^{(d+1)} \in H^{(d+1)}(M, \mathbb{Z})$. If the closed form is also exact, then the WZW term is a term expressed in the d-dimensional spacetime.

Apart from the closed $(d+1)$-form which can be used to define the WZW term, other closed q-form with $q < d$ can be used to represent the charge operators of the possible topological defects. The topological defects are classified by the homotopy group [270], and the qth homotopy group of M is isomorphic to the homology group of M via the Hurewicz theorem if M is $(q-1)$-connected. Therefore, the charge operator of possible codimension-$(q+1)$ topological defect is given by the generator of $H^q(M, \mathbb{Z})$. This charge operator is like a counter, if the defect matches, then yield 1, and 0 otherwise. For example, the baryon in 4d $\mathsf{SU}(N)$ gauge theory is classified by $\pi_3(SU(N_f)) = \mathbb{Z}$, the charge operator or the baryon number current is

$\Gamma^{(3)} \in H^3(\mathsf{SU}(N_f), \mathbb{Z})$, and it couples to the $\mathsf{U}(1)$ background gauge field A as,

$$\exp\left(i \int_{X^4} A \wedge \Gamma^{(3)}\right) \tag{2.4}$$

This reproduces the Goldstone-Wilczek current [154, 93].

To sum up, the WZW term and the charge operators of the topological defects in SSB phases are given by the generators of the integer coefficient cohomology group of the target space with a certain degree. In the following, we are using de Rham cohomology to find these generators. Since the coefficient of de Rham cohomology is $\mathbb{R}$, one needs to normalize these generators such that the integral on the generator of the corresponding homotopy group yields 1 [231]. After normalization, this gives the generators of the cohomology group with $\mathbb{Z}$ coefficient and can be used to define the WZW term and charge operators of the topological defects.

2.2.2 Construction of the coset

The Goldstone boson field U lives in the coset G/H, meaning that the Goldstone boson fields are equivalent under the right multiplication of the elements in H, $U \sim U'h$, $h \in H$. We need the following parametrization of the coset G/H [413]. We denote the generators of compact Lie group G as $T^A, A = 1, ..., \dim G$, and the subgroup H has generators $T^\alpha, \alpha = \dim G - \dim H + 1, ..., \dim G$. The orthogonal part of the $\mathfrak{h}$ in $\mathfrak{g}$ is $\mathfrak{f} = \mathfrak{g} - \mathfrak{h}$, denoted as $T^a, a = 1, ..., \dim G - \dim H$ (capital letters are for generators in $\mathfrak{g}$, greek letters are for those in $\mathfrak{h}$ and lower case letters are for $\mathfrak{f}$). We have grouped the indices such that $\mathfrak{g} = \mathfrak{f} \oplus \mathfrak{h}$. These generators in general satisfy the algebraic relation $[\mathfrak{h}, \mathfrak{h}] \subset \mathfrak{h}$, $[\mathfrak{h}, \mathfrak{f}] \subset \mathfrak{f}$, $[\mathfrak{f}, \mathfrak{f}] \subset \mathfrak{g}$. We often encounter that the coset G/H is a symmetric space, in this case, the relation is, $[\mathfrak{h}, \mathfrak{h}] \subset \mathfrak{h}$, $[\mathfrak{h}, \mathfrak{f}] \subset \mathfrak{f}$, $[\mathfrak{f}, \mathfrak{f}] \subset \mathfrak{h}$. For $\mathfrak{h} = \varnothing$, the coset is simply G. The Goldstone boson field $U(\pi(x))$ is parametrized by the Nambu-Goldstone boson $\pi^a(x)$ as [95, 59, 413],

$$U(\pi) = e^{i\pi^a(x)T^a}, \quad T^a \in \mathfrak{f}. \tag{2.5}$$

A general element g in G acting on the coset $U(\pi)$ gives,

$$g^{-1}U(\pi) = e^{i\pi'^a(\pi,g)T^a}e^{i\lambda_\alpha(\pi,g)T^\alpha} = U(\pi')h^{-1}(\pi,g) \tag{2.6}$$

the group transformation is equivalent to $g : U(\pi) \to U(\pi') = g^{-1}U(\pi)h(\pi,g)$, where $h(\pi,g)$ as well as π depend on the spacetime coordinate. $\pi(x)$ is in general transformed in a complicated nonlinear way. But when restricted to H, one can always choose the Goldstone boson $\pi(x)$ transformed in a linear way.

2.2.3 Cohomology of the homogeneous space

The generators of the cohomology group are particularly relevant to the terms that describe the symmetry defects and the WZW term. The cohomology of homogeneous space G/H is given by the closed G-invariant forms on G/H modulo exact G-invariant forms. We first discuss differential forms on G and then restrict them on G/H. These differential forms are constructed by the basis of left-invariant 1-forms, the Maurer–Cartan 1-form on G [1],

$$\theta \equiv U^{-1}(\pi)\mathrm{d}U(\pi) = \theta^A T^A. \tag{2.7}$$

where T^A is the Lie algebra generator and θ^A is the component. The Maurer-Cartan 1-form is Lie-algebra valued 1-form on G, and its component satisfies the Maurer-Cartan equations,

$$\mathrm{d}\theta^C = -\frac{1}{2}f^{ABC}\theta^A \wedge \theta^B, \tag{2.8}$$

where f^{ABC} is the structure constant of the Lie group. Then the general left-invariant n-form on G is given by, $\Omega_G^{(n)} = \frac{1}{n!}(\Omega_G)_{A_1,...,A_n}\theta^{A_1} \wedge ... \wedge \theta^{A_n}$. If the left-invariant n-form on G is closed, $d\Omega_G^{(n)} = 0$, but non-exact, $\Omega_G^{(n)} \neq d\eta_G^{(n-1)}$, then it gives the generator of the cohomology groups

---

[1]The Maurer–Cartan 1-form is on G instead of G/H, additional conditions need specifying as discussed later. More details can be found in, for example, [110]

43

of G.

On the other hand, the invariant n-form on G/H should satisfy, a) the indices vanish on $\mathfrak{h}$, and b) invariant under the adjoint action of $\mathfrak{h}$. These two conditions can be explicitly expressed using the component of Maurer-Cartan 1-form, namely,

$$\Omega^{(n)} = \frac{1}{n!}\Omega_{a_1,\ldots,a_n}\theta^{a_1} \wedge \ldots \wedge \theta^{a_n}, \tag{2.9}$$

$$\mathscr{L}_\alpha\Omega^{(n)} = -\sum_{i=1}^{n}\frac{1}{n!}\Omega_{a_1,\ldots,a_n}f^{b_j,\alpha,a_j}\theta^{a_1} \wedge \ldots \wedge \theta^{b_j} \wedge \ldots \wedge \theta^{a_n} = 0. \tag{2.10}$$

Then the cohomology of G/H is given by,

$$H^*(G/H,\mathbb{R}) = \frac{\text{invariant closed } n\text{-form on } G/H}{\text{invariant exact } n\text{-form on } G/H}. \tag{2.11}$$

Note that the de Rham cohomology of G/H is isomorphic to the relative Lie algebra cohomology, $H^*(G/H,\mathbb{R}) = H^*(\mathfrak{g},\mathfrak{h};\mathbb{R})$, therefore, we use de Rham cohomology of G/H and relative Lie algebra cohomology interchangeably.

It is convenient to decompose the $\mathfrak{g}$-valued 1-form θ into $\mathfrak{h}$-valued and $\mathfrak{f}$-valued parts,

$$\theta = U^{-1}dU = (U^{-1}dU)|_\mathfrak{f} + (U^{-1}dU)|_\mathfrak{h} \equiv \phi + V, \tag{2.12}$$

and in the component form, $\theta = \theta^A T^A = \theta^a T^a + \theta^\alpha T^\alpha = \phi + V$. The above conditions can be intuitively understood by doing the group action on the 1-forms according to Eq. (2.6),

$$\theta \to h^{-1}\theta h + h^{-1}dh, \tag{2.13}$$

$$V \to h^{-1}Vh + h^{-1}dh, \quad \phi \to h^{-1}\phi h, \tag{2.14}$$

therefore, $\phi = \theta^a T^a$ transforms under the adjoint action of $\mathfrak{h}$, while $V = \theta^\alpha T^\alpha$ transforms as the $\mathfrak{h}$-valued connection. The invariant n-form on G/H is then given by the combination of ϕ

and curvature $W = dV + V \wedge V$ or using the component form under the condition Eq. (2.9).

2.2.4 Generators of cohomology group on G/H

Among these invariant n-forms on G/H, the cohomology on G/H is obtained by closed invariant n-form modulo invariant exact n-form. We postpone the detailed algorithm that finds the generators of the cohomology group to App. B.1. For physical relevance, we are interested in the generator with a degree less than 6, for example, the degree 5 generator may correspond to the 4d WZW term, and the degree 3 generator corresponds to 2d WZW term.

Compact Lie group G

For $H = \varnothing$, the cohomology group of G has degree 3 generator for all compact Lie group (SU, SO, Sp), and degree 5 generator only for SU group [274]. The generators are given by,

$$x^{(3)} = \frac{1}{3} \operatorname{tr}(U^{-1} dU)^3 = \frac{1}{3} \operatorname{tr} \theta^3, \quad x^{(5)} = \frac{1}{10} \operatorname{tr}(U^{-1} dU)^5 = \frac{1}{10} \operatorname{tr} \theta^5. \tag{2.15}$$

These generators are of cohomology group with $\mathbb{R}$ coefficient, and they need to be normalized such that the integral over the generator of $\pi_3(G) = \mathbb{Z}$, $\pi_5(SU) = \mathbb{Z}$ equal to 1 [46, 231]. The normalized forms are the generators of $H^3(G, \mathbb{Z}), H^5(SU, \mathbb{Z})$. These generators can be written in the component form as,

$$x^{(3)} = \frac{1}{6} f_{ABC} \theta^A \wedge \theta^B \wedge \theta^C, \tag{2.16}$$

$$x^{(5)} = \frac{1}{40} d_{A_1 BC} f_{BA_2 A_3} f_{CA_4 A_5} \theta^{A_1} \wedge \theta^{A_2} \wedge \theta^{A_3} \wedge \theta^{A_4} \wedge \theta^{A_5} \tag{2.17}$$

where $f_{ABC} = \operatorname{tr}(T^A [T^B, T^C])$ is the structure constant, $d_{ABC} = \operatorname{tr}(T^A \{T^B, T^C\})$ is the totally symmetric rank 3 tensor. The totally symmetric rank 3 tensors are non-zero for $SU(N)$ group with $N > 2$.

Homogeneous space G/H

The cohomology of homogeneous space is much richer, the generators in general should satisfy Eq. (2.9). Before case-by-case discussion of the homogeneous spaces, the non-trivial generators of $H^3(G/H,\mathbb{Z}), H^5(G/H,\mathbb{Z})$ that may correspond to 2d and 4d WZW terms or codimension-4, 6 symmetry defects are given by,

$$y^{(3)} = \frac{1}{3}\operatorname{tr}\left(3\phi W + \phi^3\right), \quad y^{(5)} = \frac{1}{5}\operatorname{tr}\left(\phi^5 + \frac{10}{3}W\phi^3 + 5\phi W^2\right), \tag{2.18}$$

where $W = dV + V \wedge V$ is the curvature of V. Since V transforms as $\mathfrak{h}$-valued connection based on Eq. (2.13), its curvature will transform as adjoint action under H as well as ϕ. The generators $y^{(3)}, y^{(5)}$ are invariant under G. One can express these generators in terms of Goldstone boson field by $\phi = (U^{-1}dU)|_{\mathfrak{f}}, V = (U^{-1}dU)|_{\mathfrak{h}}$. We postpone the derivation of these generators to the discussion of its corresponding anomaly.

Similarly, we can express these generators in terms of components,

$$y^{(3)} = \frac{1}{6}(d_{ad}f_{dbc}\theta^a \wedge \theta^b \wedge \theta^c - 2d_{a\beta}f_{\beta bc})\theta^a \wedge \theta^b \wedge \theta^c \tag{2.19}$$

$$y^{(5)} = \frac{1}{60}(3d_{a_1 bc}f_{ba_2 a_3}f_{ca_4 a_5} - 4d_{a_1 b\gamma}f_{ba_2 a_3}f_{\gamma a_4 a_5}$$

$$+ 8d_{a_1 \beta\gamma}f_{\beta a_2 a_3}f_{\gamma a_4 a_5})\theta^{a_1} \wedge \theta^{a_2} \wedge \theta^{a_3} \wedge \theta^{a_4} \wedge \theta^{a_5} \tag{2.20}$$

where the lower case letters are for $\mathfrak{f}$ part, and the Greek letters are for $\mathfrak{h}$ part. $d_{ab} = \operatorname{tr}\left(\{T^a, T^b\}\right)$ is the totally symmetric rank-2 tensor, which is proportional to Kronecker delta for the most cases.

The 5th cohomology groups are non-vanishing for $\mathsf{SU}(n)/\mathsf{SO}(n)$, $n \geq 3$ and $\mathsf{SU}(2n)/\mathsf{Sp}(n)$, $n \geq 2$ which are relevant to the spontaneous symmetry breaking of QCD with SO gauge group and Sp gauge group. More details can be found in App. B.1.3.

Besides the generators that correspond to WZW terms, there are low degree cohomology generators corresponding to the charge operators of topological defects. The second cohomology

group is of particular interest in the following specific models since the generators of it correspond to the charge operators of codimension 3 topological defects, they are particle-like in 3d and string-like in 4d. The second cohomology on G/H is related to the first Chern class, evaluated on $\mathfrak{h}$-valued gauge field on G/H [110]. In terms of the 1-forms, the generator of $y^{(2)} = H^2(G/H, \mathbb{R})$ is given by,

$$y^{(2)} = m_{\alpha_0} W^{\alpha_0} = \frac{1}{2} m_{\alpha_0} f^{\alpha_0 bc} \theta^b \wedge \theta^c \qquad (2.21)$$

where α_0 is the index for the $\mathsf{U}(1)$ factor in $\mathfrak{h}$, if $\mathfrak{h}$ has the decomposition $\mathfrak{h} = \mathfrak{h}_1 + ... + \mathfrak{u}(1) + ...$. The elements in $\mathfrak{h}_i$ vanish similar to that the first Chern class of non-abelian gauge field vanishes. We will demonstrate this explicitly in the following specific models.

The 4th cohomology is constructed in a similar way by using the symmetric tensor $m_{\alpha,\beta}$ that is invariant under the adjoint transformation of H,

$$y^{(4)} = m_{\alpha,\beta} W^\alpha \wedge W^\beta \qquad (2.22)$$

The non-vanishing 2nd and 4th cohomology of some homogeneous spaces G/H are listed in the App. B.1.3 [274].

2.3 Review of 't Hooft anomaly and anomaly matching by WZW term

2.3.1 't Hooft anomaly and anomaly inflow

The theory with global symmetry that has 't Hooft anomaly is still well-defined but the anomalous symmetry cannot be gauged, otherwise, the anomaly is lifted to gauge anomaly and the theory is inconsistent. Recent understanding of symmetry-protected topological (SPT) phases gives a general picture of anomaly matching, the anomalous theory in d-dimension can be viewed as the boundary of $d+1$-dimension SPT (or invertible phase), and the anomaly is canceled by the bulk, therefore, the bulk-boundary combined system is non-anomalous [380, 97, 440].

The 't Hooft anomaly for global symmetry G of a quantum field theory constrains the infrared phases to be

- gapless with G symmetry
- spontaneously symmetry breaking
- topological order

but never a trivial gapped phase. The theory with 't Hooft anomaly is dubbed as "anomalous theory $\mathscr{T}$". The 't Hooft anomaly of the global symmetry in a theory can be found by coupling the theory to the background gauge field associated with its global symmetry. When performing a gauge transformation on the background gauge field, the partition function of the anomalous theory on spacetime manifold X instead of being invariant becomes,

$$\mathscr{Z}_{\mathscr{T}}[A + \delta_\lambda A] \to \mathscr{Z}_{\mathscr{T}}[A] e^{i \int_X \alpha(\lambda, A)}. \tag{2.23}$$

where λ is some gauge parameter. The partition function suffered from the ambiguity that different regularization yields different results. Some ambiguity can be cured by adding local counterterms, but for anomalous theory, the phase remains.

However, one can eliminate the ambiguity by viewing the anomalous theory $\mathscr{T}$ as the boundary of certain SPT phase $\mathscr{I}$. We can extend the background gauge field to the bulk Y, $\partial Y = X$, the partition function of the SPT phase under the gauge transformation is,

$$\mathscr{Z}_{\mathscr{I}}[A] = e^{-i \int_Y \omega(A)} \to \mathscr{Z}_{\mathscr{I}}[A + \delta_\lambda A] = e^{-i \int_Y \omega(A) - i \int_X \alpha(\lambda, A)}. \tag{2.24}$$

Therefore, the bulk-boundary combined system is invariant under the gauge transformation,

$$\mathscr{Z}_{\mathscr{T}}[A] \mathscr{Z}_{\mathscr{I}}[A] \to \mathscr{Z}_{\mathscr{T}}[A + \delta_\lambda A] \mathscr{Z}_{\mathscr{I}}[A + \delta_\lambda A] = \mathscr{Z}_{\mathscr{T}}[A] \mathscr{Z}_{\mathscr{I}}[A] \tag{2.25}$$

The pictorial description is shown in Fig. 2.2. Using the bulk SPT to cancel the 't Hooft anomaly of the boundary theory is called anomaly inflow. On the other hand, the bulk SPT determines the

't Hooft anomaly of the boundary theory.
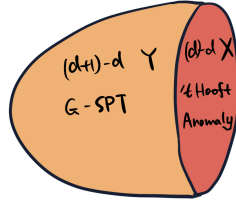
Figure 2.2. Bulk-boundary combined system is invariant under the gauge transformation.

2.3.2   Anomaly matching by Wess-Zumino-Witten term

The 't Hooft anomaly is a property of the Hilbert space, therefore, it should be matched in the ultraviolet and the infrared theory. From UV to IR, a common scenario is that the theory has spontaneously symmetry breaking. Suppose the UV theory $\mathscr{T}_{UV}$ has the global symmetry G, and it is spontaneously broken down to H in the IR, the IR theory contains the $\mathscr{T}_{IR}$ with the unbroken H symmetry and Goldstone bosons U lives in the coset G/H. If the UV theory $\mathscr{T}_{UV}$ has an anomaly, then the IR theory $\mathscr{T}_{IR}$ together with the Goldstone boson U should match the anomaly in $\mathscr{T}_{UV}$. We can break the sufficient symmetry such that $\mathscr{T}_{IR}$ does not suffer from the anomaly and all the UV anomaly is matched by the Goldstone boson that lives in the homogeneous space G/H.

The chiral anomaly is an example that the local (perturbative) anomaly which can be seen from the triangle diagram is known to be matched by the Goldstone boson with WZW term [266, 423]. However, the global (non-perturbative) anomaly is more subtle and needs a proper definition for the WZW term [231, 214, 134]. In some cases, the non-perturbative anomaly can be found perturbatively by embedding the group into a larger group [422].

Coupling the WZW term to gauge field and constructing gauge invariant gauged WZW term has been extensively studied over the three decades [184, 185, 265, 129], and it has very rich mathematical structures [424, 133, 102]. The gauged WZW term for general coset was studied in Ref. [91, 48].

In the following, we discuss a bulk-boundary combined construction of the gauged WZW term that could match general 't Hooft anomaly [440]. More specifically, assuming the d-dimensional UV theory has an anomaly described by $d+1$-dimension SPT phase $\mathscr{I}$, and the anomalous symmetry G is spontaneously broken down to (anomalous or not) H in the IR. Ref. [440] defines the general WZW term associated with $\mathscr{I}$ so that the anomalies of UV and IR are matched.

As presented in Sec. 2.2.2, the Goldstone boson lives in the coset G/H, where G can contain both spacetime and internal symmetries. Another view of the coset G/H is that the Goldstone boson locally takes value in G and has gauge symmetry H, or cover of H. The Goldstone boson transforms under G as Eq. (2.6). Consider the connection A on the principal G-bundle, A is the background gauge field associated with the global symmetry G, the gauge transformation of A is given by,

$$A \to A^g = g^{-1}Ag + g^{-1}dg. \tag{2.26}$$

We can use the Goldstone boson field as the transition function to define the new connection,

$$A^U \equiv U^{-1}AU + U^{-1}dU \tag{2.27}$$

which transforms as H connection under G action according to Eq. (2.6),

$$A^U \to h^{-1}A^U h + h^{-1}dh. \tag{2.28}$$

Therefore, A^U is the connection of the principal H-bundle. Note that the Lie algebra valued 1-form $\theta = U^{-1}dU$ is precisely $A^U|_{A=0}$. Similarly, we can decompose the connection into $\mathfrak{h}$ and $\mathfrak{f}$ part, they transform under G action as,

$$A^U = A^U_{\mathfrak{h}} + A^U_{\mathfrak{f}} \to (h^{-1}A^U_{\mathfrak{h}}h + h^{-1}dh) + (h^{-1}A^U_{\mathfrak{f}}h) \tag{2.29}$$

where $A_{\mathfrak{h}}^U$ is the connection of H-bundle and $A_{\mathfrak{f}}^U$ transforms under the adjoint action of H. Since A^U and $A_{\mathfrak{h}}^U$ are the connections of the same bundle, we can consider the interpolation of these connections,

$$A^U(t) = A_{\mathfrak{h}}^U + (1-t)A_{\mathfrak{f}}^U = \begin{cases} A^U & t = 0 \\ \\ A_{\mathfrak{h}}^U & t = 1 \end{cases} \tag{2.30}$$

As shown in Fig. 2.3, one can imagine a cylinder where the leftmost is the connection A^U, and the rightmost is the connection $A_{\mathfrak{h}}^U$. The leftmost gauge field A^U is extended to the bulk SPT with anomalous symmetry G via the transition function U, while the rightmost gauge field $A_{\mathfrak{h}}^U$ is extended to the bulk with anomalous symmetry H (if H is non-anomalous, then the extension is not needed).
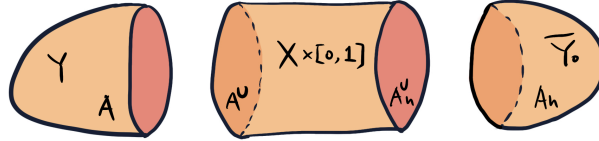
Figure 2.3. Pictorial description of the construction of WZW term. The left manifold Y describes the SPT with symmetry G whose connection is the background gauge field A. With the transition function U, the left manifold Y can be glued with the middle cylinder $[0,1] \times X$, where the WZW term lives in. The path $[0,1]$ connects the connection A^U and $A_{\mathfrak{h}}^U$, where the background gauge field $A_{\mathfrak{h}}^U$ can be extended to the right manifold $\bar{Y}$ with global symmetry H. The WZW term on the cylinder then describes the Goldstone boson in the symmetry breaking phase with $G \to H$.

The general gauged WZW term in [440] is defined by taking the partition function of the invertible theory on the total manifold $Y_{\text{total}} = Y \cup (X \times [0,1]) \cup \bar{Y}_0$. The resulting partition function is gauge invariant. The Goldstone boson field U is defined on the cylinder $X \times [0,1]$, therefore, the WZW term actually only depends on the dynamics of U on d-dimensional manifold X. The connection A^U at the left-most of the cylinder is extended to Y by transition function U, $A_{\mathfrak{h}}^U$ is extended to $\bar{Y}_0$.

However, this construction is slightly different from the ordinary understanding of the WZW term, namely the WZW term only depends on the spacetime manifold X, though it is written in one higher dimension. In the following section, we provide an alternative construction

of the gauged WZW term that is in accordance with the pictorial understanding of anomaly inflow in Fig. 2.2

2.4 (Relative) Chern-Simons functional, gauged WZW term and its anomaly

We first recall the setup of our system - given an anomalous UV global symmetry G, and it is spontaneously broken down to anomalous or not symmetry H in the IR, then the UV anomaly is matched by the Goldstone boson in G/H and IR theory with unbroken symmetry H. Instead of the construction in Sec. 2.3.2, we give an alternative construction of gauged WZW term that agrees with the anomaly inflow picture in Fig. 2.2, however, as shown in Fig. 2.4, the price is that the bulk SPT is described by the more complicated relative Chern-Simons functional (for $H = \varnothing$, the relative Chern-Simons term reduces to the Chern-Simons term) in the odd spacetime dimensions. For the even spacetime dimensional bulk, the bulk SPT is described by the mixed θ term, i.e. wedge product of various curvature tensor, and the gauged WZW term can be written as the derivative of a lower degree form [185, 110, 48]. For our purpose, we will only consider odd spacetime dimensional bulk in the following, which is relevant to the DQCP of GUTs in Sec. 2.5.2, and mention the even dimensional case in Sec. 2.5.1.

For two connections A, A' on the principle H-bundle, and a path of connection that interpolates these two, the *relative* Chern-Simons term is defined by the form that trivializes the difference between the curvature characteristic forms of different connections [279],

$$d\mathsf{CS}^{(2n+1)}(A, A') = \mathsf{ch}^{(2n+2)}(A) - \mathsf{ch}^{(2n+2)}(A') \tag{2.31}$$

where $\mathsf{ch}^{(2n)}(A) = \frac{1}{n!} \mathrm{tr}(\mathrm{i}F/(2\pi))^n$, $F = dA + A \wedge A$ is the curvature of the connection A. The Chern-Simons form is then the special case of the relative Chern-Simons form with $A' = 0$, $d\mathsf{CS}^{(2n+1)}(A) = \mathsf{ch}^{(2n+2)}(A)$.

As reviewed in the previous section, the theory with the 't Hooft anomaly needs to be

52
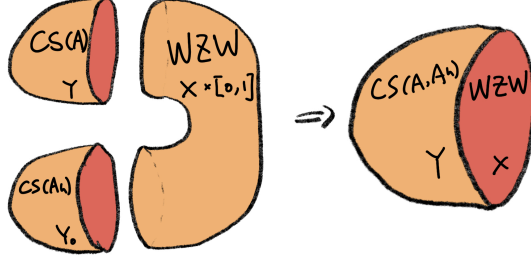
Figure 2.4. Instead of defining WZW term on a cylinder as discussed in Fig. 2.3, we bend the cylinder such that the anomaly matching agrees with the gauge invariant bulk-boundary combined system in Fig. 2.2, and the WZW term only depends on spacetime manifold $X = \partial Y$. However, the bulk SPT is now described by relative Chern-Simons term in odd spacetime dimensions and mixed θ term in even spacetime dimensions.

matched with bulk SPT. The SPT $\mathscr{I}$ with U or SU symmetry can be expressed as Chern-Simons functional, and many other SPTs can be obtained by higgsing the gauge field, for example, discrete gauge theories can be obtained from the Chern-Simons functional [20, 343]. We take the SPT $\mathscr{I}$ to be described by the Chern-Simons functional or more general the relative Chern-Simons functional [372, 440],

$$\mathscr{Z}_{\mathscr{I}}[A] = \exp\left(ik \int_Y \mathsf{CS}(A)\right), \quad \mathscr{Z}_{\mathscr{I}}[A,A'] = \exp\left(ik \int_Y \mathsf{CS}(A,A')\right). \tag{2.32}$$

where $k \in \mathbb{Z}$ is the level, $k = 1$ for SPTs. The anomaly associated with these SPTs is matched by the gauged WZW term in the following form,

$$\underline{\Gamma}^{(d+1)}(U,A,A_\mathfrak{h}) \equiv \mathsf{CS}(A^U,A_\mathfrak{h}^U) - \mathsf{CS}(A,A_\mathfrak{h}) = \Gamma^{(d+1)}(U) + d\alpha^{(d)}(U,A,A_\mathfrak{h}), \tag{2.33}$$

where $\alpha^{(d)}(U,A,A_\mathfrak{h})$ is a d-form, and it is clear that the gauged WZW term does not depend on the extra dimension, since the first term is a closed $(d+1)$ form whose variation depends on the d-dimensional boundary X and the second term only depends on the boundary X by the Stokes' theorem. The relative Chern-Simons form $\mathsf{CS}(A,A')$ manifests the gauge invariance under H

53

transformation, and the gauged WZW term is invariant under $U \rightarrow Uh$ without any counterterms. If $\mathfrak{h} = \varnothing$, then the gauged WZW term is given by the Chern-Simons form,

$$\underline{\Gamma}^{(d+1)}(U,A) \equiv \mathsf{CS}(A^U) - \mathsf{CS}(A) = \Gamma^{(d+1)}(U) + d\alpha^{(d)}(U,A). \qquad (2.34)$$

We note that the gauged WZW term in Eq. (2.33) indeed reproduces the 't Hooft anomaly under the global symmetry G. Let's first focus on the case when $\mathfrak{h} = \varnothing$, the connection $A \rightarrow g^{-1}Ag + g^{-1}dg$ and Goldstone boson field $U \rightarrow g^{-1}U$ under the G transformation. A^U is then invariant under this transformation, therefore, the first term $\mathsf{CS}(A^U)$ is invariant under the gauge transformation of G. However, the second term $-\mathsf{CS}(A)$ contributes to the anomalous phase under the transformation of G by the descent equation argument.

For the case when $\mathfrak{h} \neq \varnothing$, under the G transformation, the connection transforms as $A \rightarrow g^{-1}Ag + g^{-1}dg$ and Goldstone boson goes as $U \rightarrow g^{-1}Uh$, both A^U and $A^U_{\mathfrak{h}}$ transform as the connection on H according to Eq. (2.29). The $\mathsf{CS}^{(2n+1)}(A^U, A^U_{\mathfrak{h}})$ is invariant under the gauge transformation, this can be explicitly checked. But the second term $-\mathsf{CS}^{(2n+1)}(A, A_{\mathfrak{h}})$ part will give the anomaly associated with the symmetry G and H which needs to be canceled by the SPT in the bulk, this mechanism is called anomaly inflow [97], and the bulk boundary combined system is non-anomalous. In short, the gauged WZW term Eq. (2.33) has the anomaly associated with the bulk SPT which is described by $\mathsf{CS}^{(2n+1)}(A, A_{\mathfrak{h}})$. If we assume there is no anomaly associated to the symmetry H, then the gauged WZW term matches with the anomaly of the bulk SPT described by $\mathsf{CS}^{(2n+1)}(A, A_{\mathfrak{h}})$ and $d\mathsf{CS}^{(2n+1)}(A, A_{\mathfrak{h}}) = \mathsf{ch}^{(2n+2)}(A)$.

We summarize the anomaly matching by WZW term in the following, given the WZW term $\Gamma^{(d+1)}(U)$ with field U lives in G/H, couple it to the background gauge fields A, A' associated with global symmetry G, H and get $\underline{\Gamma}^{(d+1)}(U, A, A')$. Under the gauge transformation, the anomalous phase of the gauged WZW term is canceled by the bulk SPT described by the (relative) Chern-Simons term.

Another way to see the necessity of relative Chern-Simons term is as follows, supposing

the UV symmetry G has 't Hooft anomaly and it is matched by $CS^{(2n+1)}(A)$, the IR symmetry H also has the 't Hooft anomaly and matched by $CS^{(2n+1)}(A_\mathfrak{h})$. The gauged WZW term together with the IR anomaly should match the UV anomaly, in other word, the gauged WZW term should yields the same anomalous phase as $CS^{(2n+1)}(A) - CS^{(2n+1)}(A_\mathfrak{h})$ which is roughly the relative Chern-Simons term $CS^{(2n+1)}(A, A_\mathfrak{h}) = CS^{(2n+1)}(A) - CS^{(2n+1)}(A_\mathfrak{h}) + d\beta^{(2n)}(A, A_\mathfrak{h})$, where $\beta^{(2n)}(A, A_\mathfrak{h})$ is some $2n$-form depending on $A, A_\mathfrak{h}$.

In the following, we will use the Cartan homotopy method to find the explicit form of $CS(A^U, A_\mathfrak{h}^U)$, $\alpha^{(d)}(U, A, A_\mathfrak{h})$, and compare them with the simple case when $\mathfrak{h} = \varnothing$.

2.4.1 Cartan's homotopy method and relative Chern-Simons term

We postpone the detailed review of Cartan's homotopy method to App. B.2 [286]. For any invariant polynomial $S(A, F)$ of connection A and curvature $F = dA + A \wedge A$, (dA can be substituted by $F - A^2$ and dF is substituted by $-[A, F]$), we have the following formula,

$$(d\ell_t + \ell_t d)S(A_t, F_t) = \delta t \frac{\partial}{\partial t} S(A_t, F_t), \tag{2.35}$$

where the operator ℓ_t is an anti-derivative operator,

$$\ell_t(\eta^{(p)} \wedge \omega^{(q)}) = (\ell_t \eta^{(p)}) \wedge \omega^{(q)} + (-1)^p \eta^{(p)} \wedge (\ell_t \omega^{(q)}). \tag{2.36}$$

If A_0, A_1 both are connections on the same bundle, one can define a one-parameter family, $A_t = A_0 + t(A_1 - A_0)$, and the curvature is given by $F_t = dA_t + A_t \wedge A_t$. The operator ℓ_t acts on A_t, F_t as,

$$\ell_t A_t = 0, \quad \ell_t F_t = \delta t (A_1 - A_0). \tag{2.37}$$

Integrating over t from 0 to 1 on both sides of Eq. (2.35), we have,

$$S(A_1, F_1) - S(A_0, F_0) = \left(d \int_t \ell_t + \int_t \ell_t d \right) S(A_t, F_t). \tag{2.38}$$

Relative Chern-Simons form

Since the Chern class is even degree closed form $\mathsf{ch}^{(2n)} = \frac{1}{n!}\,\mathrm{tr}\big(\frac{\mathrm{i}F}{2\pi}\big)^n$, it can be locally written as an exact form, $\mathsf{ch}^{(2n+2)}(F) = d\mathsf{CS}^{(2n+1)}(A)$. But this is not globally true, if true then the integral of Chern class on any closed manifold would yield 0. From Eq. (2.32), the difference of two Chern classes with curvature F, F' can be written as the relative Chern-Simons term. And according to Cartan's homotopy formula,

$$\mathsf{ch}^{(2n+2)}(F) - \mathsf{ch}^{(2n+2)}(F_\mathfrak{h}) = \left(d\int_t \ell_t + \int_t \ell_t d \right) \mathsf{ch}^{(2n+2)}(F_t) \tag{2.39}$$
$$= d\int_t \ell_t \mathsf{ch}^{(2n+2)}(F_t) \equiv d\mathsf{CS}^{(2n+1)}(A, A_\mathfrak{h}),$$

where $F_t = dA_t + A_t^2$, and $A_t = A_\mathfrak{h} + tA_\mathfrak{f}$ as discussed around Eq. (2.30). The relative Chern-Simons term is given by,

$$\mathsf{CS}^{(2n+1)}(A, A_\mathfrak{h}) = \int_t \ell_t \mathsf{ch}^{(2n+2)}(F_t) = \frac{1}{n!}\left(\frac{\mathrm{i}}{2\pi}\right)^{n+1}\int dt\ \mathrm{tr}\big(A_\mathfrak{f}F_t^n\big). \tag{2.40}$$

More explicitly, we have

$$\mathsf{CS}^{(2n+1)}(A, A_\mathfrak{h}) = \frac{1}{n!}\left(\frac{\mathrm{i}}{2\pi}\right)^{n+1}\int dt\ \mathrm{tr}\big(A_\mathfrak{f}(F_\mathfrak{h} + t\mathscr{D}_\mathfrak{h}A_\mathfrak{f} + t^2 A_\mathfrak{f}^2)^n\big), \tag{2.41}$$

where $\mathscr{D}_\mathfrak{h}$ is the covariant derivative with respect to $\mathfrak{h}$-connection, $\mathscr{D}_\mathfrak{h}A_\mathfrak{f} = dA_\mathfrak{f} + \{A_\mathfrak{h}, A_\mathfrak{f}\}$. The relative Chern-Simons terms with degrees 3 and 5 are,

$$\mathsf{CS}^{(3)}(A, A_\mathfrak{h}) = -\frac{1}{4\pi^2}\,\mathrm{tr}\left(A_\mathfrak{f}F_\mathfrak{h} + \frac{1}{2}A_\mathfrak{f}\mathscr{D}_\mathfrak{h}A_\mathfrak{f} + \frac{1}{3}A_\mathfrak{f}A_\mathfrak{f}A_\mathfrak{f} \right), \tag{2.42}$$

$$\mathsf{CS}^{(5)}(A, A_\mathfrak{h}) = -\frac{\mathrm{i}}{16\pi^3}\,\mathrm{tr}\left(A_\mathfrak{f}F_\mathfrak{h}^2 + \frac{1}{2}A_\mathfrak{f}\{F_\mathfrak{h}, \mathscr{D}_\mathfrak{h}A_\mathfrak{f}\} + \frac{2}{3}F_\mathfrak{h}A_\mathfrak{f}^3 \right.$$
$$\left. + \frac{1}{3}A_\mathfrak{f}(\mathscr{D}_\mathfrak{h}A_\mathfrak{f})^2 + \frac{1}{2}A_\mathfrak{f}^3\mathscr{D}_\mathfrak{h}A_\mathfrak{f} + \frac{1}{5}A_\mathfrak{f}^5 \right). \tag{2.43}$$

Since $A_{\mathfrak{f}}$, the curvature of $A_{\mathfrak{h}}$ and the covariant derivative with respect to $A_{\mathfrak{h}}$ are all transformed under adjoint action of H, the relative Chern-Simons term is manifestly invariant under the H transformation as well as G transformation. If $H = \varnothing$, $A_{\mathfrak{f}}$ is identified with the G-connection A, the curvature $F_{\mathfrak{h}} = 0$ and $\mathscr{D}_{\mathfrak{h}} A_{\mathfrak{f}} = dA$, then,

$$\mathsf{CS}^{(3)}(A) = -\frac{1}{8\pi^2}\, \mathrm{tr}\left(AdA + \frac{2}{3}A^3\right), \tag{2.44}$$

$$\mathsf{CS}^{(5)}(A) = -\frac{\mathrm{i}}{48\pi^3}\, \mathrm{tr}\left(A(dA)^2 + \frac{3}{2}A^3 dA + \frac{3}{5}A^5\right), \tag{2.45}$$

which reproduce the Chern-Simons forms with only the background field associated with the global symmetry G.

Explicit form of gauged WZW term

According to the definition of gauged WZW term $\underline{\Gamma}^{(d+1)}(U, A, A_{\mathfrak{h}})$ in Eq. (2.33), the gauged WZW term is obtained by the difference of relative Chern-Simons terms with connection A^U and A which result in a closed $d+1$-form $\Gamma^{(d+1)}(U)$ only depending on the Goldstone boson configuration U and an exact $d+1$-form expressed as $d\alpha^{(d)}(U, A)$ which depends on the configuration U as well as the gauge field A. We will use Cartan's homotopy formula to obtain the explicit form of the d-form $\alpha^{(d)}$ and give the explicit form of the gauged WZW term.

The closed $d+1$-form $\Gamma^{(d+1)}(U)$ is easily obtained by turning off the background gauge field A in the relative Chern-Simons forms Eq. (2.42) and Eq. (2.43). The connection A^U defined in Eq. (2.27) and Eq. (2.29) can be decomposed as,

$$A^U = A_{\mathfrak{h}}^U + A_{\mathfrak{f}}^U = (U^{-1}A_{\mathfrak{h}}U + V) + (U^{-1}A_{\mathfrak{f}}U + \phi). \tag{2.46}$$

Once turning off the background gauge field, $A_{\mathfrak{h}}^U = V, A_{\mathfrak{f}}^U = \phi$ and the curvature of $A_{\mathfrak{h}}$ becomes

$W = dV + V^2$, then $\Gamma^{(d+1)}(U)$ becomes,

$$\Gamma^{(3)}(U) = \mathsf{CS}^{(3)}(\theta, V) = -\frac{1}{4\pi^2} \operatorname{tr}\left(\phi W + \frac{1}{2}\phi \mathscr{D}_V \phi + \frac{1}{3}\phi^3\right) \quad \in H^3(G/H, \mathbb{R}), \qquad (2.47)$$

$$\Gamma^{(5)}(U) = \mathsf{CS}^{(5)}(\theta, V) = -\frac{i}{16\pi^3} \operatorname{tr}\left(\phi W^2 + \frac{1}{2}\phi\{W, \mathscr{D}_V \phi\} + \frac{2}{3}W\phi^3\right.$$

$$\left. + \frac{1}{3}\phi(\mathscr{D}_V \phi)^2 + \frac{1}{2}\phi^3 \mathscr{D}_V \phi + \frac{1}{5}\phi^5\right) \quad \in H^5(G/H, \mathbb{R}), \qquad (2.48)$$

where $\mathscr{D}_V \phi = d\phi + \{V, \phi\} = 0$. One can check when $H = \varnothing$, ϕ is identified with θ, the curvature W vanishes and the covariant derivative $\mathscr{D}_V \phi = d\theta = -\theta \wedge \theta$, the WZW terms become,

$$\Gamma_G^{(3)}(U) = -\frac{1}{24\pi^3} \operatorname{tr}\theta^3 = -\frac{1}{24\pi^3} \operatorname{tr}\left(U^{-1}dU\right)^3 \quad \in H^3(G, \mathbb{R}), \qquad (2.49)$$

$$\Gamma_G^{(5)}(U) = -\frac{i}{480\pi^3} \operatorname{tr}\theta^5 = -\frac{i}{480\pi^3} \operatorname{tr}\left(U^{-1}dU\right)^5 \quad \in H^5(G, \mathbb{R}). \qquad (2.50)$$

These match with the standard WZW term for WZW conformal field theory in 2d and chiral symmetry breaking in 4d. The WZW terms for G and G/H obtained by the Cartan homotopy method reproduce those in Sec. 2.2.

The gauged WZW defined in Eq. (2.33) can be obtained by considering the interpolation $A_t = tU^{-1}AU + \theta, A_{\mathfrak{h},t} = tU^{-1}A_{\mathfrak{h}}U + V$, in this case the Cartan homotopy formula becomes,

$$\mathsf{CS}^{(2n+1)}(A^U, A_{\mathfrak{h}}^U) - \mathsf{CS}^{(2n+1)}(\theta, V) = \left(d\int_t \ell_t + \int_t \ell_t d\right) \mathsf{CS}^{(2n+1)}(A_t, A_{\mathfrak{h},t})$$

$$= d\alpha^{(2n)} + \int_t \ell_t (\mathsf{ch}^{(2n+2)}(F_t) - \mathsf{ch}^{(2n+2)}(F_{t\mathfrak{h}})) = d\beta^{(2n)} + \mathsf{CS}^{(2n+1)}(A) - \mathsf{CS}^{(2n+1)}(A_{\mathfrak{h}}).$$

$$(2.51)$$

Since there is no anomaly for H, the Chern-Simons term for gauge field $A_{\mathfrak{h}}$ vanishes. The Chern-Simons term $\mathsf{CS}^{(2n+1)}(A)$ differs from the relative Chern-Simons term $\mathsf{CS}^{(2n+1)}(A, A_{\mathfrak{h}})$

by a total derivative $d\beta^{(2n)}$, therefore, the gauged WZW term is,

$$\underline{\Gamma}^{(2n+1)}(U,A) \equiv \mathsf{CS}^{(2n+1)}(A^U, A_{\mathfrak{h}}^U) - \mathsf{CS}^{(2n+1)}(A, A_{\mathfrak{h}}) = \Gamma^{(2n+1)}(U) + d(\alpha^{(2n)} + \beta^{(2n)}), \quad (2.52)$$

where the $2n$-form α depends on $U, A, A_{\mathfrak{h}}$ while β depends only on the background gauge fields. For example, $\beta^{(2)} = \mathrm{tr}(A \wedge A_{\mathfrak{h}}), \alpha^{(2)} = \mathrm{tr}(\phi U^{-1}(A + A_{\mathfrak{h}})U)$. If $H = \varnothing$, $\beta^{(2n)}$ vanishes, and $\alpha^{(2n)}$ is obtained by,

$$\int_t \ell_t \, \mathrm{tr}\left(\mathsf{CS}^{(2n+1)}(tA + dUU^{-1})\right). \quad (2.53)$$

This gives, for example, $\alpha^{(2)} = \frac{1}{2}\mathrm{tr}(dUU^{-1}A)$. More details can be found in App. B.2.

2.5 Nonlinear sigma model of DQCP theories

With the gears presented in the previous sections, we will show that the WZW term captures the intertwinement of the topological defects and matches with the 't Hooft anomaly in the anomalous theory. We use the charge operators of topological defects to construct the WZW term and use the gauged WZW term to match the mixed anomaly in the theory.

We are interested in the critical points or phases between spontaneously symmetry-breaking phases in the presence of the 't Hooft anomaly, and the manifestation of the 't Hooft anomaly in different symmetry-breaking phases. This situation is along with many deconfined quantum critical point theories. We begin by revisiting the intertwinement in the DQCP theory of the 3d quantum magnet [393, 272], and then construct a series of 4d DQCP theories which is motivated by recent work on DQCP among grand unified theories [402, 401, 449]. The new set of 4d deconfined quantum criticality theories is the higher dimensional generalization of 3d DQCP theories, and the new 4d DQCP (DQCPh) theories are governed by 't Hooft anomaly of global $\mathsf{SO}(2n)$ symmetry which turns out to be a variation of the new $\mathsf{SU}(2)$ anomaly [402, 401, 400, 449].

2.5.1 Revisiting deconfined quantum critical point in 3d quantum magnet

As mentioned in the introduction, the continuous global symmetry of the 3d quantum magnet is $G = \mathsf{SO}(3)_S \times \mathsf{SO}(2)_R$, which corresponds to spin and lattice rotation symmetry. The Néel phase in this system is the antiferromagnetic phase, with spins pointing up or down. This phase has $H_{\text{Néel}} = \mathsf{SO}(2)_S \times \mathsf{SO}(2)_R$ symmetry, broken by the easy-axis spin configuration. The Goldstone boson in the Néel phase lives in the coset $G/H_{\text{Néel}} \cong \mathsf{SO}(3)_S/\mathsf{SO}(2)_S \cong \mathbb{S}_S^2$. The possible topological defect is classified by $\pi_2(\mathbb{S}_S^2) = \mathbb{Z}$, corresponding to codimension 3 integer-valued defect, which is the hedgehog defect in the Néel phase. On the other hand, the lattice rotation symmetry is broken in the VBS phase, $H_{\text{VBS}} = \mathsf{SO}(3)_S$. The corresponding Goldstone boson lives in the coset $G/H_{\text{VBS}} = \mathsf{SO}(2)_R \cong \mathbb{S}_R^1$. The possible topological defect is classified by $\pi_1(\mathbb{S}_R^1) = \mathbb{Z}$, which corresponds to codimension 2 integer-valued defects, this is the vortex line in the VBS phase.

It is very interesting that the vortex core in the VBS phase carries spin-$\frac{1}{2}$ degree of freedom [232]. When proliferating the vortices in the VBS phase, the defects will destroy the VBS ordered phase, but due to the additional spin-$\frac{1}{2}$ degree of freedom at the vortex core, the system will become the ordered Néel phase. In other words, the disorder operator of lattice rotation symmetry carries the symmetry charge of the spin rotation symmetry, which is reminiscent of the mixed 't Hooft anomaly of these two symmetries.

The 't Hooft anomaly should match along the renormalization group flow, meaning that all possible phases should have such an anomaly. In the ordered phases, although some defects may be suppressed by energy, their intertwined feature should manifest thanks to the anomaly. We can deform the theory by tuning the relevant operators such that the theory flow to the IR phase with the smallest symmetry K and there is no anomaly with K, hence, the anomaly in the UV is matched by the Goldstone boson in the coset G/K.

Theories with the same symmetry properties and anomaly will be dual to each other, in

the sense that they describe the same IR phase with different UV details [340]. We consider the deformation of the theory to the spontaneous symmetry breaking phase with unbroken symmetry $K = H_{\text{Néel}} \cap H_{\text{VBS}} = \text{SO}(2)_S$. Then the gapless theory of the Goldstone boson living in the coset $G/K = \mathbb{S}^2_S \times \mathbb{S}^1_R$ with WZW term would be a suitable dual description of the DQCP theory. Indeed, we will show this construction is related to the $\text{O}(5)$ nonlinear sigma model that served as the dual theory of various gauge theory descriptions of 3d DQCP [393]. Both topological defects in Néel and VBS phase are present in this Goldstone boson theory, since $\pi_k(\mathbb{S}^2_S \times \mathbb{S}^1_R) = \pi_k(\mathbb{S}^2_S) \times \pi_k(\mathbb{S}^1_R)$. The symmetry-breaking routes are summarized as follows,

$$
\begin{array}{c}
G = \text{SO}(3)_S \times \text{SO}(2)_R \\[2em]
\end{array}
$$

$\langle \Phi_N \rangle \neq 0$ $\langle \Phi_V \rangle \neq 0$

$H_{\text{Néel}} = \text{SO}(2)_S \times \text{SO}(2)_R$ $H_{\text{VBS}} = \text{SO}(3)_S$

$\langle \Phi_V \rangle \neq 0$ $\langle \Phi_N \rangle \neq 0$

$$K = H_{\text{Néel}} \cap H_{\text{VBS}} = \text{SO}(2)_S$$

$$\tag{2.54}$$

We denote the generators of $\text{SO}(3)_S$ as $\{T^1, T^2, T^3\}$ and $\text{SO}(2)_R$ as $\{T^4\}$. Supposing the generators of $H_{\text{Néel}}$ are $\{T^3, T^4\}$, then the charge operators of the topological defects in the Néel and VBS phase are represented by,

$$\tilde{\eta}^{(1)} = \theta^4 \in H^1(G/H_{\text{VBS}}, \mathbb{R}), \quad \tilde{\xi}^{(2)} = \theta^1 \wedge \theta^2 \in H^2(G/H_{\text{Néel}}, \mathbb{R}). \tag{2.55}$$

In the ordered phase with global symmetry $K = H_{\text{Néel}} \cap H_{\text{VBS}} = \text{SO}(2)_S$, the generator is $\{T^3\}$, and the cohomology generators are,

$$\eta^{(1)} = \theta^4 \in H^1(G/K, \mathbb{R}), \quad \xi^{(2)} = \theta^1 \wedge \theta^2 \in H^2(G/K, \mathbb{R}). \tag{2.56}$$

In this case, $\tilde{\eta}^{(1)} = \eta^{(1)}$ and $\tilde{\xi}^{(2)} = \xi^{(2)}$ since the global symmetry G is the tensor product of two subgroups. Wedge product of the two generators yields *a* generator of the higher degree

cohomology group, $\eta^{(1)} \wedge \xi^{(2)} = \theta^4 \wedge \theta^1 \wedge \theta^2 \in H^3(G/K, \mathbb{R})$.

The WZW term in the 2+1d DQCP assigns a phase to the linking between the VBS vortex and hedgehog defect or the linking between $\mathbb{S}_S^2$ and $\mathbb{S}_R^1$ in $\mathbb{S}^4$ [324]. The way to define the linking is to find the surface D_R^2 that is bounded by the circle $\mathbb{S}_R^1$ and the intersection with $\mathbb{S}_S^2$ gives the linking number. The form on D_R^2 is denoted by $\hat{\eta}^{(1)}$ and the WZW term is,

$$\Gamma^{(4)} = \xi^{(2)} \wedge d\hat{\eta}^{(1)}. \tag{2.57}$$

More explicitly, we can parameterize $\mathbb{S}_S^2$ and $\mathbb{S}_R^1$ by 3-component unit-vector $\boldsymbol{n}_S$ and 2-component unit-vector $\boldsymbol{n}_R$, then $\xi^{(2)} = \varepsilon_{abc} n_S^a dn_S^b \wedge dn_S^c$, $\eta^{(1)} = n_R^1 dn_R^2$. The 1-form is closed when restricting on the circle, but not closed on the disk, $d\hat{\eta}^{(1)} = dn_R^1 dn_R^2$. Therefore, the WZW term is given by $\Gamma^{(4)} = \varepsilon_{abcde} n_S^a dn_S^b dn_S^c dn_R^d dn_R^e$, which appears in the SO(5) NLSM of DQCP [157, 393, 235, 285, 410].

When coupled to the background gauge field the anomaly of the gauged WZW term comes from the mixed θ term in 4d which matches the anomaly in the bulk SPT phase with global symmetry $\mathsf{SO}(3)_S \times \mathsf{SO}(2)_R$. We can further embed $\mathsf{SO}(3)_S \times \mathsf{SO}(2)_R \hookrightarrow \mathsf{SO}(5)$, the corresponding anomaly is described by $\frac{1}{2} w_4 \in H^4(B\mathsf{SO}(5), U(1))$, upon pull-back to $\mathsf{SO}(3)_S \times \mathsf{SO}(2)_R$, the anomaly becomes,

$$\frac{1}{2} w_4(A_S \oplus A_R) = \frac{1}{2} w_2(A_S) w_2(A_R) = \frac{1}{2} \frac{F_R}{2\pi} w_2(A_S), \tag{2.58}$$

where $F_R = dA_R$ and w_2 is the second Stiefel Whitney class of $SO(3)$ bundle. This anomaly also matches with that in 3d $\mathbb{C}P^1$ model in [219, 272]. The same anomaly in WZW theory and 3d $\mathbb{C}P^1$ model is also a check of the infrared duality of the different theories [393, 340]. Recent works on quantum spin liquid have examined related gauge theories and their corresponding NLSM with WZW term, and the target spaces of the NLSM are Stiefel manifold or Grassmannian manifold [465, 439, 427]. It would also be interesting to construct other 2+1d DQCP theories that saturate

the anomaly discussed in [214, 134]. Similar construction and anomaly matching can be applied to 1+1d system [178, 194, 323, 281, 428].

2.5.2   Deconfined quantum critical point and intertwinement of topological defects in 4d

In contrast to the extensive theoretical and numerical studies of deconfined quantum critical points in 2d and 3d, the 4d generalization of DQCP is rarely explored. One difficulty is that the gauge fields tend to be deconfined in higher dimensions and many gauge theories then describe the deconfined quantum critical phases instead of critical points. Nevertheless, previous works focus on the gauge theory description and find interesting examples of deconfined quantum critical point with mixed 't Hooft anomaly that implies the intertwinement of symmetries [42].

Regardless of the specific models and their critical behaviors, it is interesting to study the intertwinement of topological defects in 4d which manifests the 't Hooft anomaly in the UV theory, since there are more types of topological defects in higher dimensions. This also offers a way to understand the higher dimensional SPTs, since the WZW term essentially describes the linking between extended operators in the bulk where the SPT lives in.

We construct the nonlinear sigma model with WZW term to describe this phenomenon in the following subsections and construct the corresponding fermionic parton theories in Sec. 2.6. Our construction turns out to describe the deconfined quantum critical phase (DQCPh), since the minimal fermionic parton theory contains $U(1)$ gauge field, which is deconfined in the 3+1d [402, 401, 449]. Because the inputs of our construction are the global symmetries and corresponding mixed 't Hooft anomaly, it may have different gauge theory descriptions with the same global symmetry and anomaly. It is interesting to find specific gauge theory description that realizes the deconfined quantum critical point.

From the previous discussion, the DQCP theory is anomalous and can be thought of as the boundary of one higher dimensional SPT. The 4d DQCPh theory can serve as the boundary of 5d SPT. The 5d SPT with only $\mathbb{Z}_2^T$ symmetry is $\mathbb{Z}_2$ classified, this SPT is described by $\int_{Y5} w_2 w_3$

[203, 202] and recently studied in [78, 77, 126], where $w_i \in H^i(Y^5, \mathbb{Z}_2)$ is the ith Stiefel-Whitney class. In the presence of symmetry, similar topological terms are possible for the all-fermion electrodynamics [224] and the new $\mathsf{SU}(2)$ anomaly [400]. Hence, it is possible to have an anomalous theory at the boundary of the nontrivial SPT with the anomaly described in the above mentioned examples. In the following, we will discuss a series of models with the new $\mathsf{SU}(2)$ anomaly, these models describe the gapless theories between two spontaneously symmetry-breaking phases.

Symmetry breaking and topological defects

Recent work shows that the DQCP (or DQCPh, depending on the model details) can present among the Grand Unified Theories (GUTs) in which the standard model with global symmetry generated by $\mathfrak{k}_{\text{SM}} = \mathfrak{su}(3) \oplus \mathfrak{su}(2)_L \oplus \mathfrak{u}(1)_Y \oplus \mathfrak{u}(1)_X$ can be embedded, the three GUTs are $\mathsf{SO}(10)$ GUT with $\mathfrak{g}_{\mathsf{SO}(10)} = \mathfrak{so}(10)$, Pati-Salam (PS) model with $\mathfrak{h}_{\text{PS}} = \mathfrak{so}(6) \oplus \mathfrak{so}(4) = \mathfrak{su}(4) \oplus \mathfrak{su}(2)_L \oplus \mathfrak{su}(2)_R$ and Georgi-Glashow (GG) model with $\mathfrak{h}_{\text{GG}} = \mathfrak{su}(5) \oplus \mathfrak{u}(1)_X$ [402, 401, 449]. The gauge symmetry is "ungauging" such that they can be viewed as global symmetries. In other words, the dynamical gauge fields in the original theories are background gauge fields in these alternative theories. Therefore, the Higgs phases and transitions become symmetry-breaking phases and transitions. When condensing the symmetric $\Phi_{\mathbf{54}}$ or antisymmetric $\Phi_{\mathbf{45}}$ scalar fields charged under $\mathsf{SO}(10)$ in the $\mathsf{SO}(10)$ GUT described in [449], one can get the symmetry breaking phases with unbroken symmetry $\mathfrak{h}_{\text{PS}}$ or $\mathfrak{h}_{\text{GG}}$ respectively, these symmetries can be further broken down to $\mathfrak{k}_{SM}$. The symmetry-breaking pattern is summarized as follows.

$$
\begin{array}{ccc}
& \mathfrak{g}_{\mathsf{SO}(10)} & \\
{\scriptstyle \langle \Phi_{\mathbf{54}} \rangle \neq 0} \swarrow & & \searrow {\scriptstyle \langle \Phi_{\mathbf{45}} \rangle \neq 0} \\
\mathfrak{h}_{\text{PS}} & & \mathfrak{h}_{\text{GG}} \\
{\scriptstyle \langle \Phi_{\mathbf{45}} \rangle \neq 0} \searrow & & \swarrow {\scriptstyle \langle \Phi_{\mathbf{54}} \rangle \neq 0} \\
& \mathfrak{k}_{\text{SM}} = \mathfrak{h}_{\text{PS}} \cap \mathfrak{h}_{\text{GG}} &
\end{array}
\tag{2.59}
$$

where Φ_{45}, Φ_{54} are traceless symmetric and antisymmetric higgs fields of $\mathsf{SO}(10)$. The possible topological defects in the PS and GG phases are classified by,

$$\pi_2 \left(\frac{\mathsf{SO}(10)}{\mathsf{SO}(6) \times \mathsf{SO}(4)} \right) = \mathbb{Z}_2, \quad \pi_2 \left(\frac{\mathsf{SO}(10)}{\mathsf{U}(5)} \right) = \mathbb{Z}. \tag{2.60}$$

The topological defects in the symmetry breaking phases are codimension 3 defects corresponding to the line operators in 4d. The topological defects in the PS phase are Grassmannian manifold and $\mathbb{Z}_2$ classified, meaning that two of such defects can be deformed to nothing.

As discussed around Eq. (2.4) and Sec. 2.5.1, since the coset $\mathsf{SO}(2n)/(\mathsf{SO}(2m) \times \mathsf{SO}(2n-2m))$ and $\mathsf{SO}(2n)/\mathsf{U}(n)$ have vanishing π_1 and π_0, the 2nd homotopy group is isomorphic to the 2nd homology group. We can use the corresponding cohomology generators as the charge operators of these topological defects. However, it is impossible to directly express the charge operator of $\mathbb{Z}_2$ classified topological defect of $\mathsf{SO}(2n)/(\mathsf{SO}(2m) \times \mathsf{SO}(2n-2m))$ within the de Rham cohomology, more generally it is impossible for the $\mathbb{Z}_n$ classified topological defects, since the normalized generator of de Rham cohomology yields $\mathbb{Z}$-valued closed form. Mathematically, one may consider   mod n reduction of the cohomology group or using the Cech cohomology. But the current situation is reminiscent of the non-perturbative $\mathsf{SU}(2)$ anomaly which is characterized by $\pi_4(\mathsf{SU}(2)) = \mathbb{Z}_2$ [421], the way to reproduce the non-perturbative anomaly perturbatively is by embedding $\mathsf{SU}(2) \hookrightarrow \mathsf{SU}(3)$, and the non-perturbative $\mathsf{SU}(2)$ anomaly is seen by the WZW term of $\mathsf{SU}(3)$ group [422]. As in Sec. 2.5.1, we attempt to embed the space $\mathsf{SO}(2n)/(\mathsf{SO}(2m) \times \mathsf{SO}(2n-2m))$ into a larger space, the natural choice is the Goldstone boson in the SM phase with both order parameters condensed and the unbroken symmetry is K. Indeed, we find that the embedding into G/K can capture both topological defects even this $\mathbb{Z}_2$ classified topological defects in the PS phase with target space $\mathsf{SO}(2n)/(\mathsf{SO}(2m) \times \mathsf{SO}(2n-2m))$.

The above statement can be seen by examining the homotopy group of the target

space G/K.   The short exact sequence of the global symmetry G, K and coset is $0 \to K \to G \to G/K \to 0$, this induces the long exact sequence for the homotopy group, and the relevant part is,

$$... \to \pi_2(G) \to \pi_2(G/K) \to \pi_1(K) \to \pi_1(G) \to \pi_1(G/K) \to ... \tag{2.61}$$

The homotopy groups of $G = \mathsf{SO}(n)$ is known, $\pi_2(\mathsf{SO}(n)) = 0, \pi_1(\mathsf{SO}(n)) = \mathbb{Z}_2, n \geq 3$ and G/K is contractible $\pi_1(G/K) = 0$, the long exact sequence becomes,

$$0 \to \pi_2(G/K) \to \pi_1(K) \to \mathbb{Z}_2 \to 0 \tag{2.62}$$

Therefore $\pi_2(G/K) = \pi_1(K) = \pi_1(\mathsf{SU}(3) \times \mathsf{SU}(2) \times \mathsf{U}(1) \times \mathsf{U}(1)) = \mathbb{Z} \oplus \mathbb{Z}$ quotient by $\mathbb{Z}_2$, where the two $\mathbb{Z}$s correspond to the topological defects in PS and GG phase respectively. This construction is valid for a series of theories with $G = \mathsf{SO}(2n), n \geq 2$.

Construction of Lie algebras

In this subsection, we describe the embedding of $\mathfrak{so}(2m) \oplus \mathfrak{so}(2n-2m)$ and $\mathfrak{u}(n)$ into the $\mathfrak{so}(2n)$ Lie algebra. The $\mathfrak{so}(2n)$ Lie algebra is represented by $n(2n-1)$ $2n \times 2n$ anitsymmetric real matrices, which generate the rotation of a $2n$-vector. $\mathfrak{so}(2m) \oplus \mathfrak{so}(2n-2m)$ consists of the $2n \times 2n$ anitsymmetric real matrices that rotate within the first $2m$ elements, or within the last $2(n-m)$ elements in the $2n$-vector. The $\mathfrak{u}(n)$ is embedded in the $\mathfrak{so}(2n)$ by Kronecker producting the symmetric generators of $\mathfrak{u}(n)$ with $i\sigma^2$ and antisymmetric generators of $\mathfrak{u}(n)$ with $i\sigma^0$.

In our case, $m = 2\lfloor n/2 \rfloor$ in $\mathfrak{so}(2m) \oplus \mathfrak{so}(2n-2m)$, where m is taking the floor of $n/2$. The intersection of $\mathfrak{u}(n)$ and $\mathfrak{so}(2m) \oplus \mathfrak{so}(2n-2m)$ is isomorphic to $\mathfrak{u}(m) \oplus \mathfrak{u}(n-m)$ and always contain two $\mathfrak{u}(1)$s, in the upper-left block $\mathfrak{u}(1)_+$ and lower-right block $\mathfrak{u}(1)_-$ of the original $\mathfrak{so}(2n)$ respectively. Hence, $\mathfrak{u}(1)_+ + \mathfrak{u}(1)_- \subset \mathfrak{u}(n)$ rotates the upper and lower block with the same phase, while $\mathfrak{u}(1)_+ - \mathfrak{u}(1)_- \subset \mathfrak{so}(2m) \oplus \mathfrak{so}(2n-2m)$ rotates the upper and lower block

with the opposite phase.

Since the intersection of Lie algebras is $\mathfrak{u}(m) \oplus \mathfrak{u}(n-m)$, the symmetry K generated by this Lie algebra contains two $\mathsf{U}(1)$ factors, $\pi_2(G/K) = \pi_1(K) = \mathbb{Z} \oplus \mathbb{Z}$ due to Eq. (2.62). We have identified that one of the $\mathsf{U}(1)$ factors is in $\mathsf{U}(n)$, the other relates to $\mathsf{SO}(2m) \times \mathsf{SO}(2n-2m)$. Hence, the topological defects in G/K correspond to those in symmetry breaking phases with only unbroken $\mathsf{U}(n)$ or $\mathsf{SO}(2m) \times \mathsf{SO}(2n-2m)$. Since they are $\mathbb{Z}$ classified, we can find the de Rham cohomology expressions of the charge operators corresponding to the topological defects,

$$\eta^{(2)} \in H^2(G/K, \mathbb{R}), \quad \xi^{(2)} \in H^2(G/K, \mathbb{R}), \tag{2.63}$$

where $\eta^{(2)} = \tilde{\eta}^{(2)} \in H^2(G/U(n), \mathbb{R})$ corresponds to the charge operator of topological defect in G breaking down to $H_{\mathsf{U}} = \mathsf{U}(n)$ phase, and $\xi^{(2)}$ should relate to $\tilde{\xi}^{(2)} \in H^2(G/\mathsf{SO}(2m)\mathsf{SO}(2n-2m), \mathbb{Z}_2)$ which corresponds to the charge operator of topological defect in G breaks down to $H_{\mathsf{SO}} = \mathsf{SO}(2m) \times \mathsf{SO}(2n-2m)$ phase.

For $\mathsf{SO}(8)$, these generators of the cohomology group is given by,

$$\eta_{\mathsf{U}}^{(2)} = \theta^1 \wedge \theta^7 + \theta^6 \wedge \theta^{12} + \theta^2 \wedge \theta^8 + \theta^3 \wedge \theta^9 + \theta^4 \wedge \theta^{10} + \theta^5 \wedge \theta^{11} \in H^2(G/K, \mathbb{R}), \tag{2.64}$$

$$\xi_{\mathsf{SO}}^{(2)} = -\theta^1 \wedge \theta^7 + \theta^6 \wedge \theta^{12} + \theta^{14} \wedge \theta^{20} + \theta^{15} \wedge \theta^{21} + \theta^{16} \wedge \theta^{22} + \theta^{17} \wedge \theta^{23} \in H^2(G/K, \mathbb{R}), \tag{2.65}$$

where the indices $1 \sim 12$ are the generators of the coset $\mathfrak{so}(8)/\mathfrak{u}(4)$, while

$$\{2, 3, 4, 5, 8, 9, 10, 11, 14, 15, 16, 17, 20, 21, 22, 23\} \tag{2.66}$$

are the generators of the coset $\mathfrak{so}(8)/\mathfrak{so}(4) \oplus \mathfrak{so}(4)$. The $\eta_{\mathsf{U}}^{(2)} \in H^2(G/K, \mathbb{R})$ coincides with the nontrivial generator in $H^2(\mathsf{SO}(8)/\mathsf{U}(4), \mathbb{R})$. And it is worth mentioning that the first two terms in $\xi_{\mathsf{SO}}^{(2)}$ will cancel each other when pull-back to $\mathbb{S}^2$, the remain terms are all in $\mathfrak{so}(8)/\mathfrak{so}(4) \oplus \mathfrak{so}(4)$, this further supports that $\xi_{\mathsf{SO}}^{(2)}$ relates to the generator in $H^2(\mathsf{SO}(8)/\mathsf{SO}(4)\mathsf{SO}(4), \mathbb{Z}_2)$.

Wess-Zumino-Witten term

As illustrated in Sec. 2.5.1, one can construct *a* WZW term by wedge product of the charge operators,

$$\eta_{\mathsf{U}}^{(2)} \wedge \xi_{\mathsf{SO}}^{(2)} \in H^4(G/K, \mathbb{R}). \tag{2.67}$$

However, to properly include the linking information, an additional degree of freedom should be included. Intuitively, two 2-spheres can link with each other in $\mathbb{S}^5$ but cannot be properly described in 4-dimension, this is similar to the lower dimension example that the linking of two circles needs to be embedded in $\mathbb{S}^3$ and the linking is essentially the intersection between one circle and the disk that is bounded by the other circle. Following this procedure, one needs to find the 3-disk D^3 that is bounded by one of the 2-spheres, say corresponding to $\xi_{\mathsf{SO}}^{(2)}$, then $\xi_{\mathsf{SO}}^{(2)}$ is no longer closed, and the WZW term that encodes the linking of two topological defects is,

$$\Gamma^{(5)} = \eta_{\mathsf{U}}^{(2)} \wedge d\xi_{\mathsf{SO}}^{(2)} \in H^5(\widehat{G/K}, \mathbb{R}), \tag{2.68}$$

where $\widehat{G/K}$ is the extension of G/K such that it contains a 3-disk which is bounded by a 2-sphere. This term corresponds to $\phi W_1 W_2$ in Eq. (2.48). As mentioned in [402], the mixed anomaly of $\mathsf{U}(n)$ and $\mathsf{SO}(2m) \times \mathsf{SO}(2n - 2m)$ is contained in $\mathsf{SO}(2n)$. The gauged WZW term then matches with the anomaly from the Chern-Simons term, for the $\mathsf{SO}(2n)$ global symmetry, $d\mathsf{CS}^{(5)} = W_3(\mathsf{SO}(2n))^2 \in H^6(BSO(2n), \mathbb{Z})$, whose mod 2 reduction is $w_3(\mathsf{SO}(2n))^2 \in H^6(BSO(2n), \mathbb{Z}_2)$ corresponding to the image of $w_2 w_3(\mathsf{SO}(2n))$ [231]. This model is akin to the Stiefel liquid in 2+1d, where the target space is Stiefel manifold, and the anomaly is carefully studied in [465, 439].

Intertwinement of the topological defects and higher linking number

Since both topological defects are codimension 3 and $\mathbb{Z}$ classified, their charge operators are represented by the generators of the second cohomology of G/K, $H^2(G/K, \mathbb{Z}) = \mathbb{Z} \oplus \mathbb{Z}$.

As discussed previously, the two $\mathbb{Z}$s correspond to the two $\mathfrak{u}(1)$ factors in K and one is in the $\mathfrak{u}(n)$, another is in the $\mathfrak{so}(2m) \oplus \mathfrak{so}(2n-2m)$. To illustrate the intertwinement of the topological defects, we consider two 2-spheres embedded in the target space G/K,

$$\mathbb{S}^2_{\mathsf{U}} \sqcup \mathbb{S}^2_{\mathsf{SO}} \xrightarrow{f} G/K. \tag{2.69}$$

where $\sqcup$ is the disjoint union of two manifolds. Intuitively, we are considering the mapping that sends two disjoint 2-spheres into the homogeneous space G/K, such that the second cohomology of G/K is pull-back via f^* to the second cohomology of each sphere, $f^* \eta_{\mathsf{U}}^{(2)} = \omega_{\mathsf{U}}^{(2)} \in H^2(\mathbb{S}^2_{\mathsf{U}}, \mathbb{R})$ and $f^* \xi_{\mathsf{SO}}^{(2)} = \omega^{(2)}\mathsf{SO} \in H^2(\mathbb{S}^2_{\mathsf{SO}}, \mathbb{R})$. The two different topological defects are then simply understood by these two spheres. The linking of the two spheres is characterized by the degree of the map that sends the disjoint spheres into $\mathbb{S}^5$ [109]. We can further embed $\mathbb{S}^5 \overset{h}{\hookrightarrow} \widehat{G/K}$, then the map is summarized as,

$$\mathbb{S}^2_{\mathsf{U}} \sqcup \mathbb{S}^2_{\mathsf{SO}} \xrightarrow{g} \mathbb{S}^5 \overset{h}{\hookrightarrow} \widehat{G/K}. \tag{2.70}$$

Hence, the WZW term $\Gamma^{(5)}$ in Eq. (2.68) is pull-back via h^* to the non-trivial element of $H^5(\mathbb{S}^5, \mathbb{R})$, and $\deg(g) = -\mathsf{Lk}(\mathbb{S}^2_{\mathsf{U}}, \mathbb{S}^2_{\mathsf{SO}})$ is the linking number of $\mathbb{S}^2_{\mathsf{U}}$ and $\mathbb{S}^2_{\mathsf{SO}}$ in $\mathbb{S}^5$ [109]. The WZW term on $\mathbb{S}^5$ captures the essential intertwinement of the different topological defects in G/K.

Explicit construction for $G = \mathsf{SO}(2n), n \geq 4$

In the following example, we are focusing on global symmetry $\mathsf{SO}(8)$, and the subgroups are $H_{\mathsf{SO}} = \mathsf{SO}(4) \times \mathsf{SO}(4)$ and $H_{\mathsf{U}} = \mathsf{U}(4)$. This construction also applies to $G = \mathsf{SO}(2n), n \geq 4$.

We first construct the map from $\mathbb{S}^2_{\mathsf{U}} \sqcup \mathbb{S}^2_{\mathsf{SO}} \to G/K$, the two spheres are related to the two $\mathfrak{u}(1)$ factors in K. The 2-sphere can be viewed as the homogeneous space $\mathbb{S}^2 = \frac{\mathsf{SO}(3)}{\mathsf{SO}(2)}$, thus, we take the generators of $\mathsf{SO}(3) \subset G$ and modulo the subgroup $\mathsf{SO}(2) \subset G$. Since the two $\mathbb{S}^2$s do

not intersect with each other, we take two commuting $\mathfrak{so}(3)$ to construct $\mathbb{S}^2$s, the starting point is,

$$T^A = \{\sigma^{20}, \sigma^{12}, \sigma^{32}\}, \quad \tilde{T}^A = \{\sigma^{02}, \sigma^{21}, \sigma^{23}\}. \tag{2.71}$$

We choose one element of each set as the generator of $\mathsf{SO}(2)$, then the Goldstone boson field for each $\mathbb{S}^2$ is given by, for example,

$$(\theta_1, \phi_1) \in \mathbb{S}^2_{\mathsf{U}} \to U_1 = e^{\mathrm{i}(\theta_1 \sin\phi_1, \theta_1 \cos\phi_1) \cdot (T^1, T^2)^\intercal} \in \mathsf{SO}(3)/\mathsf{SO}(2)$$

$$(\theta_2, \phi_2) \in \mathbb{S}^2_{\mathsf{SO}} \to U_2 = e^{\mathrm{i}(\theta_2 \sin\phi_2, \theta_2 \cos\phi_2) \cdot (\tilde{T}^1, \tilde{T}^2)^\intercal} \in \mathsf{SO}(3)/\mathsf{SO}(2) \tag{2.72}$$

It is easy to show that $(U_i dU_i)^2$ corresponds to the generator of $H^2(\mathbb{S}^2_i, \mathbb{R})$. The Goldstone boson fields are equivalent under the right multiplication of $h \in H$, therefore, we have

$$U_1 = \mathbf{n}_1 \cdot (T^A)^\intercal, \quad U_2 = \mathbf{n}_2 \cdot (\tilde{T}^A)^\intercal \tag{2.73}$$

where $\mathbf{n}_i = (\sin\theta_i \cos\phi_i, \sin\theta_i \sin\phi_i, \cos\theta_i)$ is the 3-vector on the 2-sphere, and generator of the second cohomology is given by $\det(\mathbf{n}_i, d\mathbf{n}_i, d\mathbf{n}_i)$. Moreover, one can construct the 6-vector on 5-sphere by interpolating the $\mathbf{n}_i$ vector, the 6-vector is given by $\mathbf{n} = (\cos\psi\mathbf{n}_1, \sin\psi\mathbf{n}_2)$, $\psi \in (0, \pi]$. The corresponding Goldstone boson field is $\cos\psi(\sigma^1 \otimes U_1) + \sin\psi(\sigma^3 \otimes U_2)$. The 5-form is given by $\omega^{(5)} = \det(\mathbf{n}, d\mathbf{n}, d\mathbf{n}, d\mathbf{n}, d\mathbf{n}, d\mathbf{n})$ which is the volume form of $\mathbb{S}^5$, when pull back to $\mathbb{S}^2_{\mathsf{U}} \sqcup \mathbb{S}^2_{\mathsf{SO}}$, the integral on $\mathbb{S}^5$ gives the linking number of $\mathbb{S}^2_{\mathsf{U}}$ and $\mathbb{S}^2_{\mathsf{SO}}$ in $\mathbb{S}^5$ [109].

The skeleton theory of the Eq. (2.68) together with the kinetic term is given by the $\mathsf{O}(6)$ nonlinear sigma model with WZW term,

$$\int_X \frac{1}{2g} (\partial_\mu \mathbf{n})^2 + \frac{2\pi\mathrm{i}}{\Omega_5} \int_Y \varepsilon_{abcdef} n^a dn^b \wedge dn^c \wedge dn^d \wedge dn^e \wedge dn^f \tag{2.74}$$

where $\Omega_5 = \pi^3$ is the area of 5-sphere. Similar action appears in Ref. [183] and previously in Ref. [43]. The Eq. (2.74) can be viewed as the boundary of the bulk SPT with $\mathsf{SO}(6)$ symmetry

which is described by the nonlinear sigma model with θ-term [41, 445]. With this skeleton theory Eq. (2.74), one can see that the charge operators of the topological defects are given by $\omega_U^{(2)} = \varepsilon_{abc} n^a dn^b \wedge dn^c$ and $\omega_{SO}^{(2)} = \varepsilon_{def} n^d dn^e \wedge dn^f$ where a, b, c are in $\{1, 2, 3\}$ and d, e, f are in $\{4, 5, 6\}$. The WZW term in Eq. (2.74) calculates the linking number between the two charge operators,

$$\frac{2\pi i}{\Omega_5} \int_Y \varepsilon_{abcdef} n^a dn^b \wedge dn^c \wedge dn^d \wedge dn^e \wedge dn^f = 2\pi i \int_Y \omega_U^{(2)} \wedge d\omega_{SO}^{(2)} = 2\pi i \mathrm{Lk}(\mathbb{S}_U^2, \mathbb{S}_{SO}^2). \quad (2.75)$$

If fixing the position of one charge operator $\omega_U^{(2)}$, and move the other charge operator $\omega_{SO}^{(2)}$ around the fixed position one $\omega_U^{(2)}$, then the WZW term describes that the worldsheet of the moving monopole $\omega_{SO}^{(2)}$ detects the flux of $\omega_U^{(2)}$. And the WZW term assigns phase to their linking number, this demonstrates essentially the intertwinement of charge operators of topological defects.

Since the nonlinear sigma model with the WZW term can be viewed as the boundary theory of the bulk SPT, one can instead see the intertwinement in the bulk SPT. Once coupling the charge operators of the defects to 2-form background gauge fields $B^{(2)}, C^{(2)}$, the bulk SPT is described by, $\frac{1}{\pi} \int_Y B^{(2)} \wedge dC^{(2)}$. The linking between the surface operators $e^{i \oint B}, e^{i \oint C}$ is also given by the above linking number [174].

These bosonic fields can be further embedded into G/K by embedding the generators $T^A, \tilde{T}^A$ into the generators of G/K. In the following section Sec. 2.6.3, we will couple these Goldstone boson fields to the fermionic field and construct the fermionic sigma model. The fermionic sigma model also shows the intertwinement of the charge operators is related to the higher linking number of two $\mathbb{S}^2$s in $\mathbb{S}^5$.

2.6 Fermionic sigma model and WZW term

In this section, we construct the fermion model that reproduces NLSM with WZW for general homogeneous space G/H. The fermions are coupled to the fluctuating bosonic fields

living in G/H. After integrating out the fermion fields [4, 182], the resulting effective action is the NLSM with WZW given in Sec. 2.5. We call such models as fermionic sigma model and they provide an alternative insight into the intertwinement of symmetry defects in higher dimensions.

2.6.1 General G-symmetric action and fermionic sigma model

The bosonic fields introduced in Sec. 2.2.2 transforms nonlinearly under the global symmetry G as in Eq. (2.6). We can consider a field χ that transforms under G as,

$$\chi \xrightarrow{g} \chi' = D(h^{-1}(g, \pi))\chi, \tag{2.76}$$

with some representation D. The χ field is like a representative point on the coset, and it can be rotated to the general one by the Goldstone boson field. The χ field can be converted into the field $\psi = U(\pi)\chi$ that transforms as an ordinary linear transformation under G,

$$\psi(x) \xrightarrow{g} \psi'(x) = D(U(\pi'))\chi'(x)$$
$$= D(g^{-1}U(\pi)h(g,\pi))D(h^{-1}(g,\pi))\chi(x) = D(g^{-1})D(U(\pi))\chi(x) = D(g^{-1})\psi(x) \tag{2.77}$$

We can also introduce the covariant derivative, $\mathscr{D}_V \chi$. Under the G transformation it becomes,

$$\mathscr{D}_V \chi = (\partial_\mu + V)\chi \xrightarrow{g} \partial_\mu (h^{-1}(\pi,g)\chi) + (V + h^{-1}dh)h^{-1}(\pi,g)\chi = h^{-1}(\pi,g)\mathscr{D}_V\chi. \tag{2.78}$$

Meanwhile, as in Eq. (2.13), $\phi \xrightarrow{g} h^{-1}\phi h$. Therefore, the general G invariant action can be constructed by $\chi, \mathscr{D}_V \chi, \phi$, which is also invariant under the unbroken symmetry H [413, 95, 59].

To construct the fermionic sigma model, we introduce a mass matrix M_0 as a reference point, and it satisfies,

$$hM_0h^{-1} = M_0. \tag{2.79}$$

For example, $M_0 = \mathrm{diag}(1,..,1,-1,...,-1)$ with n times +1, m times -1, is the matrix that breaks

$SO(n+m) \rightarrow SO(n) \times SO(m)$. The $\bar{\chi} M_0 \chi$ is then G-symmetric,

$$g : \bar{\chi} M_0 \chi \rightarrow \bar{\chi} D(h^{-1})^{-1} M_0 D(h^{-1}) \chi = \bar{\chi} M_0 \chi \tag{2.80}$$

Upon rewriting the term in the ψ basis, the G-symmetric action is,

$$\bar{\psi} i \gamma^\mu \partial_\mu \psi + \bar{\psi} U(\pi) M_0 U(\pi)^{-1} \psi. \tag{2.81}$$

where ψ is the complex fermion that transforms linearly under G. Eq. (2.81) is the general fermionic sigma model where the fermion mass manifold G/H is parameterized by the bosonic field U.

2.6.2   Reproducing the WZW term from the fermionic sigma model

We follow the Ref. [4] and recent presentation in Ref. [182] to derive the Wess-Zumino-Witten term by integrating out the fermion, the partition function of the anomalous theory depends on the Goldstone boson field is,

$$\mathscr{Z}_{\mathscr{F}}[U] = \int \mathscr{D}\bar{\psi} \mathscr{D}\psi e^{-\mathscr{S}[\bar{\psi}, \psi, U]}, \tag{2.82}$$

$$\mathscr{S}[\bar{\psi}, \psi, U] = \int d^n x \, \bar{\psi}(i\gamma^\mu \partial_\mu + imU(\pi) M_0 U(\pi)^\dagger) \psi$$

$$\equiv \int d^n x \, \bar{\psi}(i\slashed{\partial} + imM^U) \psi \equiv \int d^n x \, \bar{\psi} \hat{\mathscr{D}} \psi, \tag{2.83}$$

where $M^U \equiv U(\pi) M_0 U(\pi)^{-1}$ and $\mathscr{Z}_{\mathscr{F}}[U]$ contains the kinetic term and possible Wess-Zumino-Witten term of the Goldstone boson. Following the standard derivation, the WZW action is,

$$S_{\text{WZW}} = -\frac{1}{2\pi} \frac{1}{(4\pi)^{d/2}} \frac{\Gamma(\frac{d}{2}+1)}{\Gamma(d+1)} \int_Y du d^n x \, \text{tr}\left\{ \left(\prod_{i=1}^n (\gamma^{\mu_a} \partial_{\mu_a} M^U) M^{U\dagger} \partial_u M^U \right) \right\} \tag{2.84}$$

where u is the extra coordinate on Y, $\partial Y = X$, $\Gamma(z)$ is the Gamma function $\Gamma(n+1) = n!$ for integer n. Since the WZW term is written locally in 1 higher dimension than the spacetime

manifold, we have extended M^U as the map from Y to the mass manifold. After straightforward calculation, the WZW term for G/H is in general given by,

$$\Gamma^{(d+1)}(U) = -\frac{1}{2\pi} \frac{2^{\lfloor d/2 \rfloor}}{(4\pi)^{d/2}} \frac{\Gamma(\frac{d}{2}+1)}{\Gamma(d+2)} \, \mathrm{tr}\left\{ \left([M_0, U^{-1}dU]^{d+1} M_0^\dagger \right) \right\} \tag{2.85}$$

where $\lfloor x \rfloor$ is the floor function. Recalling that $U^{-1}dU$ can be decomposed into $\mathfrak{h}$ and $\mathfrak{f}$ parts, $U^{-1}dU = V + \phi$, and $[M_0, T^\alpha] = 0, T^\alpha \in \mathfrak{h}$, we have,

$$[M_0, U^{-1}dU] = [M_0, \phi] = [M_0, \theta^a T^a], a \in \mathfrak{f} \tag{2.86}$$

It turns out, for example,

$$\Gamma^{(5)} = -\frac{1}{480\pi^3} \, \mathrm{tr}\left\{ \left([M_0, U^{-1}dU]^5 M_0^\dagger \right) \right\} \quad \in H^5(G/H, \mathbb{R}) \tag{2.87}$$

$$= -\frac{i}{16\pi^3} \, \mathrm{tr}\left(\phi W^2 + \frac{1}{2}\phi\{W, \mathscr{D}_V \phi\} + \frac{2}{3}W\phi^3 + \frac{1}{3}\phi(\mathscr{D}_V \phi)^2 + \frac{1}{2}\phi^3 \mathscr{D}_V \phi + \frac{1}{5}\phi^5 \right) \tag{2.88}$$

This shows that the fermionic sigma model in Eq. (2.81) reproduces the WZW term for G/H homogeneous space.

2.6.3 Fermionic sigma model and intertwinement of mass manifolds

In this section, we present the construction of a fermionic sigma model that could reproduce the WZW term in Sec. 2.5.2. There are two types of topological defects in the symmetry breaking phases, both of them are characterized by the charge operators as the generators of the second cohomology $H^2(G/K)$. We then consider embedding two $\mathbb{S}^2$s into G/K, the linking number of these two spheres is the degree of the mapping from two $\mathbb{S}^2$ to $\mathbb{S}^5$. More explicitly, to illustrate the intertwinement of the topological defects, we consider the mapping in Eq. (2.70), $\mathbb{S}_U^2 \sqcup \mathbb{S}_{SO}^2 \xrightarrow{g} \mathbb{S}^5 \xrightarrow{h} \widehat{G/K}$.

We are focusing on the case where the global symmetry is $SO(8)$, the generalization of

this construction to $SO(2n)$ can be obtained by embedding $SO(8) \hookrightarrow SO(2n)$. The embedding of two disjoint $\mathbb{S}^2$s into G/K is obtained by considering two commuting $\mathfrak{so}(3)$s and modulo the $\mathfrak{so}(2)$ subalgebra.

The Goldstone boson fields in Eq. (2.72) can be used to rotate the mass matrix and coupled to the fermions. Therefore, we can construct the fermionic sigma model that reproduces the WZW term, or the charge operators of the topological defects. Here we consider the fermions that are transformed under vector representation of the global flavor symmetry $SO(2n)$ and the mass matrix can be an antisymmetric or symmetric representation of $SO(2n)$.

As noted in Sec. 2.5.2 and [402, 401, 449], the higgs fields $\Phi_{\mathbf{45}}, \Phi_{\mathbf{54}}$ which are used to approach GG and PS phase have different symmetry properties, they are symmetric and antisymmetric respectively. The mass matrix of the fermion model can be chosen in a way that aligns with the symmetry properties, once integrating out the fermion fields, the corresponding charge operators of the topological defects could match with the symmetry constraints of the higgs fields $\Phi_{\mathbf{45}}, \Phi_{\mathbf{54}}$. We are considering this symmetry constraint also applies to the $SO(2n), n \geq 4$ model.

However, the $\mathfrak{so}(3)$ matrices considering in Eq. (2.71) are all antisymmetric. The way to render the antisymmetric matrix to a symmetric one is to Kronecker product additional σ^2 to the antisymmetric matrices, to preserve the antisymmetry, one needs to Kronecker product additional σ^0 to the antisymmetric matrices. Due to the symmetry constraint [402, 401, 449], we would like to construct one set with all symmetric matrices and the other set with all antisymmetric matrices.

$$Sym : \{\sigma^{220}, \sigma^{212}, \sigma^{232}\}, \quad Asym : \{\sigma^{002}, \sigma^{021}, \sigma^{023}\}. \tag{2.89}$$

Hence, the first set of $SU(2)$ matrices is symmetric, the second set is antisymmetric. The above matrices are ready to couple to complex fermions. In the Majorana basis, the mass matrix should

be antisymmetric, and the general form of the mass matrices in $4d$ is,

$$M = \sigma^{21} \otimes S_1 + \sigma^{23} \otimes S_2, \tag{2.90}$$

where S_i are the symmetric matrices, σ^{21}, σ^{23} are the γ matrices. We need further add indices to the two sets of matrices and make them symmetric,

$$Sym : \{\sigma^{0220}, \sigma^{0212}, \sigma^{0232}\}, \quad Sym : \{\sigma^{2002}, \sigma^{2021}, \sigma^{2023}\}. \tag{2.91}$$

It is convenient to block diagonalize the matrices by doing the unitary transformation $e^{i\frac{\pi}{4}\sigma^{1200}}$,

$$M \to e^{i\frac{\pi}{4}\sigma^{1332}} M e^{-i\frac{\pi}{4}\sigma^{1332}} : Sym : \{\sigma^{0220}, \sigma^{0212}, \sigma^{0232}\}, \quad Sym : \{\sigma^{3202}, \sigma^{3221}, \sigma^{3223}\}. \tag{2.92}$$

One can freely choose the representative matrix in each set, and the other matrices can be obtained by doing the $\mathsf{SU}(2)$ transformation,

$$M_0^{\mathsf{SO}} = \sigma^{0220}, T^a = \{\sigma^{0012}, \sigma^{0032}\}, \tag{2.93}$$

$$M_0^{\mathsf{U}} = \sigma^{3202}, \tilde{T}^a = \{\sigma^{0021}, \sigma^{0023}\}. \tag{2.94}$$

Since the mass matrices are block-diagonal, one can rotate the upper block or the lower block separately by

$$M_0^{\mathsf{SO}} = \sigma^{0220}, T_\pm^a = \{\frac{\sigma^{0012} \pm \sigma^{3012}}{2}, \frac{\sigma^{0032} \pm \sigma^{3032}}{2}\} \tag{2.95}$$

$$M_0^{\mathsf{U}} = \sigma^{3202}, \tilde{T}_\pm^a = \{\frac{\sigma^{0021} \pm \sigma^{3021}}{2}, \frac{\sigma^{0023} \pm \sigma^{3023}}{2}\}. \tag{2.96}$$

Hence, we obtain the map from S^2 to the SU(2) mass matrices,

$$(\theta_1, \phi_1) \in S^2 \to M_\pm^{\mathsf{SO}} = U_1 M_0^{\mathsf{SO}} U_1^{-1} \in \mathsf{SU}(2), \quad U_1 = e^{\mathrm{i}(\theta_1 \sin \phi_1, \theta_1 \cos \phi_1) \cdot (T_\pm^1, T_\pm^2)^\mathsf{T}} \tag{2.97}$$

$$(\theta_2, \phi_2) \in S^2 \to M_\pm^{\mathsf{U}} = U_2 M_0^{\mathsf{U}} U_2^{-1} \in \mathsf{SU}(2), \quad U_2 = e^{\mathrm{i}(\theta_2 \sin \phi_2, \theta_2 \cos \phi_2) \cdot (\tilde{T}_\pm^1, \tilde{T}_\pm^2)^\mathsf{T}} \tag{2.98}$$

where $M_\pm^{\mathsf{SO}}, M_\pm^{\mathsf{U}}$ satisfy $[M_\pm^{\mathsf{SO}}, M_\pm^{\mathsf{U}}] = 0$. We first find that the charge operators of the topological defects can be reproduced by the fermions coupled to the mass manifolds and evaluated on a submanifold,

$$M_\pm^{\mathsf{SO}} dM_\pm^{\mathsf{SO}} dM_\pm^{\mathsf{SO}} = vol_{S^2} \sigma_\pm^{200}, \quad M_\pm^{\mathsf{U}} dM_\pm^{\mathsf{U}} dM_\pm^{\mathsf{U}} = vol_{S^2} \sigma_\pm^{200} \tag{2.99}$$

where $vol_{S^2} = \sin \theta_i d\theta_i d\phi_i$ is the volume form of the S^2. More interestingly, if we interpolate the mass matrix in Eq. (2.90) by,

$$\mathsf{SU} \ni M(u, \theta_1, \phi_1, \theta_2, \phi_2) = \sigma^{21} \otimes u M^{\mathsf{SO}} + \sigma^{23} \otimes \sqrt{1 - u^2} M^{\mathsf{U}}, \tag{2.100}$$

such that $M(0) = \sigma^{23} \otimes M^{\mathsf{U}}, M(1) = \sigma^{21} \otimes M^{\mathsf{SO}}$. Note that the two mass matrices play different roles, one is the identity mass, and the other one relates to the chiral mass. When integrating out the fermion fields, the WZW term is,

$$\begin{aligned} S_{\mathrm{WZW}} &= \frac{2\pi}{960\pi^3} \int_{S^2 \times S^2 \times I} \mathrm{tr}\big(M^{-1} dM\big)^5 \\ &= \frac{2\pi}{960\pi^3} \int_{S^2 \times S^2 \times I} 120 \, \mathrm{tr}\big(\sigma^{000}\big) u^2 \sqrt{1 - u^2} \sin \theta_1 \sin \theta_2 d\theta_1 d\phi_1 d\theta_1 d\phi_1 du. \end{aligned} \tag{2.101}$$

When evaluating the WZW term on an interval $u \in [0,1]$,

$$S_{\text{WZW}} = \frac{2\pi}{960\pi^3} \int_0^1 \int_{S^2} \int_{S^2} 120 \, \text{tr}(\sigma^{000}) u^2 \sqrt{1-u^2} \sin\theta_1 \sin\theta_2 d\theta_1 d\phi_1 d\theta_1 d\phi_1 du \quad (2.102)$$

$$= \int_{S^2 \times S^2} \frac{-i \sin\theta_1 \sin\theta_2}{8\pi} d\theta_1 d\phi_1 d\theta_2 d\phi_2 \quad (2.103)$$

$$= 2\pi i = 2\pi i \text{Lk}(\mathbb{S}^2, \mathbb{S}^2), \quad (2.104)$$

where $\text{Lk}(\mathbb{S}^2, \mathbb{S}^2)$ is the linking number of two $\mathbb{S}^2$ in $\mathbb{S}^5$ [174, 109]. This WZW term corresponds to $\phi W_1 W_2$ in the previous section, where W_1, W_2 are the curvature of the two 2-spheres corresponds to the generator of $H^2(G/H_i, \mathbb{R})$ and ϕ is $\mathfrak{f}$-valued 1-form, but interestingly, ϕ relates to the chiral rotation $U(1)$ in the global symmetry of the fermionic sigma model, which corresponds to the exchange of two symmetry defects in the G/K NLSM in Eq. (2.68).

2.7 Summary and comments

Summary

We propose the nonlinear sigma model with target space G/K and Wess-Zumino-Witten term as the general description of deconfined quantum critical point theory, based on the very important features of the symmetry defects and their intertwinement in the DQCP theories. We show the topological defects in G/K precisely correspond to the symmetry defects in each spontaneous symmetry breaking phase in the DQCP phase diagram. The WZW term decorates the symmetry defects in one SSB phase with the charge of the broken symmetry of the other SSB phase. By proliferating the symmetry defects, the broken symmetry of one SSB phase is restored but the additional charge breaks the symmetry, leading to the other SSB phase.

We connect this NLSM description with the ordinary 't Hooft anomaly matching argument by explicitly calculating the gauged WZW term and its corresponding bulk SPT. When the anomalous UV symmetry G is spontaneously broken to non-zero subgroup H (which can be anomalous or non-anomalous), the odd spacetime dimensional bulk SPT is in general

described by relative Chern-Simons term and mixed θ term for even dimensional bulk. We provide an alternative fermionic sigma model that reproduces the NLSM with the WZW term. This alternative fermionic model gives insight into the detailed global symmetry actions.

We apply our framework to several examples - first revisit the ordinary 2+1d DQCP between Néel and VBS phases. Then motivated by recent works on deconfined quantum criticality among different grand unified theories [402, 401, 449], we studied the deconfined quantum critical theories between two SSB phases with unbroken symmetries $H_{\mathsf{SO}} = \mathsf{SO}(2m) \times \mathsf{SO}(2n-2m)$ and $H_{\mathsf{U}} = \mathsf{U}(n)$, and they come from the theory with $G = \mathsf{SO}(2n)$ global symmetry by condensing the order parameters. Applying the G/K NLSM description ($K = \mathsf{U}(m) \times \mathsf{U}(n-m)$), we are able to find operators that correspond to the symmetry defects in both SSB phases, due to $\pi_2(\frac{G}{\mathsf{U}(m) \times \mathsf{U}(n-m)}) = \mathbb{Z} \oplus \mathbb{Z}$. It is interesting because the symmetry defect in the SSB phase with unbroken symmetry H_{SO} is Grassmannian manifold and has $\mathbb{Z}_2$ valued topological charge, which does not have a corresponding de Rham cohomology description. Embedding G/H_{SO} into larger space G/K is reminiscent of finding non-perturbative $\mathsf{SU}(2)$ anomaly by embedding $\mathsf{SU}(2) \hookrightarrow \mathsf{SU}(3)$, and the non-perturbative anomaly associated with $\pi_4(\mathsf{SU}(2)) = \mathbb{Z}_2$ can be seen from $\mathsf{SU}(3)$ WZW term via perturbative calculation. Then we construct the WZW term and examine the corresponding anomaly which descends from the $\mathsf{SO}(2n)$ anomaly [400, 402, 401, 449].

Furthermore, the symmetry defects in this complicated homogeneous space can be understood by examining the embedding $\mathbb{S}^2 \times \mathbb{S}^2 \xrightarrow{f} G/K$. Hence, the G/K NLSM becomes the ordinary $\mathsf{O}(6)$ nonlinear sigma model with the WZW term. The first and last three components of the $\mathsf{O}(6)$ vector describe the 2-spheres corresponding to different symmetry defects. The WZW term then assigns the phase to the linking of the two 2-spheres in $\mathbb{S}^5$.

We provide an alternative fermionic sigma model to reproduce the NLSM. The fermions are coupled to the fluctuating bosonic fields living in the homogeneous space G/K, when integrating out the fermions, the resulting effective action is the G/K NLSM with level-1 WZW term. As an example, we embed the two 3-component unit vectors into G/K and construct the

fermionic model of O(6) NLSM. We should point out that since the SO(6) is explicitly broken down to SO(3) × SO(3), the chiral U(1) rotation in the fermion model is crucial to get the correct linking between symmetry defects in different SSB phases. This rotation is in SO(6) but not in SO(3) × SO(3).

Comments

The G/K NLSM with WZW description discussed in this paper is applicable to any dimensions and different continuous symmetries of DQCP theory. However, this description focuses on the kinematics of the DQCP theory, namely the symmetry defects, their intertwinement, and 't Hooft anomaly. The dynamics of the DQCP theory is much more complicated - the operator contents and their scaling dimensions are not universal, and the renormalization group schemes vary from different dimensions and different models. Nevertheless, the symmetry of the G/K NLSM would imply infrared duality of gauge theories, for example, the discrete symmetry that exchanges two types of symmetry defects becomes particle-vortex like duality of gauge theories [393, 340, 253]. Furthermore, the duality between different quantum field theories relates the operator contents and set the constraints on the scaling dimensions which reveals information on dynamics [393, 315, 187].

Despite the difficulty in extracting specific dynamical information, our proposal captures the essential features for which the DQCP is beyond ordinary symmetry-breaking transition. In this point of view, the DQCP is not rare, and it can be more ubiquitous if incorporating higher-form symmetry [145, 268, 227, 105, 461], categorical symmetry [190, 72], and loop group symmetry for the system with a fermi surface [122, 392, 106]. The ongoing exploration of non-invertible symmetries should also have their corresponding DQCP theory provided the symmetries have mixed anomaly [70, 378, 88]. One can also apply the current approach to understand multicritical point joined by several SSB phases. This formalism can also be used to construct DQCP models involving average symmetries [264, 456, 229].

Chapter. 2, in full, is a reprint of the material as it appears in Da-Chuan Lu. Nonlinear

sigma model description of deconfined quantum criticality in arbitrary dimensions. *SciPost Physics Core*, 6(3):047, July 2023. The dissertation author was the primary investigator and author of this paper.

Chapter 3

Fermi Surface Symmetric Mass Generation

Symmetric mass generation is a novel mechanism to give gapless fermions a mass gap by non-perturbative interactions without generating any fermion bilinear condensation. The previous studies of symmetric mass generation have been limited to Dirac/Weyl/Majorana fermions with zero Fermi volume in the free fermion limit. In this work, we generalize the concept of symmetric mass generation to Fermi liquid with a finite Fermi volume and discuss how to gap out the Fermi surfaces by interactions without breaking the U(1) loop group symmetry or developing topological orders. We provide examples of Fermi surface symmetric mass generation in both (1+1)D and (2+1)D Fermi liquid systems when several Fermi surfaces together cancel the Fermi surface anomaly. However, the U(1) loop group symmetry in these cases is still restrictive enough to rule out all possible fermion bilinear gapping terms, such that a non-perturbative interaction mechanism is the only way to gap out the Fermi surfaces. This *symmetric Fermi surface reconstruction* is in contrast to the conventional symmetry-breaking gapping mechanism in the Fermi liquid. As a side product, our model provides a pristine 1D lattice regularization for the (1+1)D U(1) symmetric chiral fermion model (e.g., the 3-4-5-0 model) by utilizing a lattice translation symmetry as an emergent U(1) symmetry at low energy. This opens up the opportunity for efficient numerical simulations of chiral fermions in their own dimensions *without* introducing mirror fermions under the domain wall fermion construction.

3.1 Introduction

Fermi liquids are gapless quantum many-body systems of fermions that possess Fermi surfaces and well-defined quasi-particle excitations at low energy. They are the models for the most commonly-seen metallic materials in nature. They are probably also one of the most studied quantum phases of matter in condensed matter physics since Landau [228, 239]. However, there are still many novel aspects of Fermi liquids that might not have been well recognized. This article explores one such aspect: the phenomenon of *symmetric mass generation* (SMG, see a recent overview [403] and references therein) in Fermi liquids.

One intriguing property of the Fermi liquid is the surprising stability of the Fermi surface under generic local interactions of fermions. Although the system is gapless with vastly degenerated ground states, local interactions often do not immediately lift the ground state degeneracy and destabilize the Fermi liquid towards gapped phases. Early understandings of this property came from the perturbative renormalization group (RG) analysis, as the Fermi liquid theory can emerge as a stable RG fix-point of interacting fermion systems [353, 354, 169, 84, 117, 85, 317].

Recently, a modern understanding arose under the name of *Fermi surface anomaly* [122, 121, 250], which states that the stability of the Fermi surface can be viewed as protected by the quantum anomaly of an emergent $LU(1)$ loop group symmetry at low energy, extending and unifying many related discussions [302, 297, 298, 275, 305, 165, 166, 412, 82, 257, 86, 191, 272, 53, 365, 437] about Luttinger's theorem [259] and Lieb-Schultz-Mattis theorem [238] in fermionic systems. Loosely speaking, the $LU(1)$ symmetry corresponds to the fermion number $n_{\boldsymbol{k}}$ conservation at each momentum point $\boldsymbol{k}$ on the Fermi surface (FS), which is preserved by the Landau Fermi liquid Hamiltonian $H_{\text{FL}} = \sum_{\boldsymbol{k} \in \text{FS}} \varepsilon_{\boldsymbol{k}} n_{\boldsymbol{k}} + \sum_{\boldsymbol{k}, \boldsymbol{k}' \in \text{FS}} f_{\boldsymbol{k}\boldsymbol{k}'} n_{\boldsymbol{k}} n_{\boldsymbol{k}'} + \cdots$. In the presence of the Fermi surface anomaly, the Fermi liquid can only be gapped by either (i) spontaneously breaking the $LU(1)$ symmetry or (ii) spontaneously developing anomalous topological orders (or other non-Fermi liquid exotic states) that saturate the Fermi surface

anomaly. The anomaly matching is a kinematic constraint, which is non-perturbative and more robust than the perturbative RG analysis of the Fermi liquid low-energy dynamics.

Over the past decade, the quantum anomaly [327, 415, 204, 404] has been realized as an important theoretical tool in analyzing the protected gapless boundary states of interacting topological insulators/superconductors, which belong to symmetry-protected topological (SPT) phases in a grand scope (see overviews [347, 426, 416] and references therein). An interesting phenomenon, known as symmetric mass generation (SMG) [127, 128, 326, 314, 436, 159, 414, 396, 359, 15, 61, 14, 397], was discovered in the study of interacting fermionic SPT states. It was realized that certain SPT states might look non-trivial at the free-fermion (non-interacting) level but can be smoothly deformed into a trivial gapped phase with a unique ground state by fermion interactions. This implies some integer $\mathbb{Z}$ classification of non-interacting SPT states can be reduced to a finite abelian elementary order-n group $\mathbb{Z}_n$ classification for some interacting SPT states, first emphasized by Fidkowski-Kitaev [127, 128]. Correspondingly, their gapless boundary states can be gapped out by (and only by) interaction without breaking the symmetry or developing the topological order (breaking emergent higher-form symmetry). This provides a novel mechanism to generate a mass for zero-density relativistic gapless fermions (e.g., Dirac/Weyl/Majorana fermions occupying only Fermi points with zero Fermi volumes at the Fermi level, colloquially known as Dirac/Weyl/Majorana cones) without symmetry breaking, which has been proposed to provide lattice regularization for the Standard Model and Grand Unified Theories [414, 442, 444, 211, 398, 321]. This mechanism is called SMG, or "mass without mass term"[30, 31], which is distinct from the conventional Higgs mechanism that relies on symmetry breaking for fermion mass generation.

However, as far as we are aware of the existing literature, the SMG mechanism has not yet been extended to fermion systems at a finite filling (with a finite density). The Fermi liquid is one most notable examples of such, which possesses a Fermi surface enclosing a finite Fermi volume. It is natural to ask: can SMG happen on the Fermi surface as well, gapping out the Fermi surface by interaction without breaking the loop group symmetry of interest? As we will

demonstrate in this article, the answer is yes.

Given the spacetime-internal symmetry G of a fermion system, the conditions [403] for SMG to happen are: (i) the system must be free from G-anomaly such that symmetric gapping (without topological order) becomes possible, and (ii) the symmetry G must be restricted enough to rule out any symmetric fermion bilinear gapping term such that the gapping can only be achieved by interaction. These defining conditions of SMG can be applied to the Fermi liquid system by considering G as the emergent loop group symmetry on the Fermi surface. Based on this understanding, we will investigate the Fermi surface SMG in the presence of the LU(1) symmetry. The general feature is that even though a single Fermi surface is anomalous, it is possible to cancel the Fermi surface anomaly among multiple Fermi surfaces (or Fermi surfaces with multiple fermion flavors), such that interactions can drive the transition from the Fermi liquid phase to a symmetric gapped phase. We shall name this phenomenon as the "Fermi surface Symmetric Mass Generation".

The Fermi surface SMG provides us a different possibility to create a gap to all excitations on the Fermi surface without condensing any fermion bilinear order parameter, which makes it distinct from the superconducting gap (i.e., condensing Cooper pairs) or the density wave gap (i.e., condensing excitons) that are more familiar in condensed matter physics. Nevertheless, it does involve condensing some multi-fermion bound states that transform trivially under the symmetry transformation. One simplest example is the charge-4e superconductor [213, 200, 35, 318, 34, 168, 277, 195], which condenses fermion quartets (four-fermion bound states) that preserves at least the $\mathbb{Z}_4$ subgroup of the charge U(1) symmetry. In this work, we will provide more carefully designed examples preserving the full U(1) symmetry (and other lattice symmetries), but the essential idea of condensing symmetric multi-fermion operators to generate a many-body excitation gap is the same. Therefore, the Fermi surface SMG is intrinsically a strong non-perturbative interaction effect of fermions. The interaction may look irrelevant at the free-fermion (or the Fermi liquid) fixed-point. However, strong enough interaction can still drive the gap-opening transition through non-perturbative effects.

The article will be organized as follows. In Sec. 3.2, we will present a lattice model of Fermi surface SMG in (1+1)D, as the pristine lattice regularization of the 3-4-5-0 chiral fermion model, whose phase diagram can be reliably analyzed by RG approach. In Sec. 3.3, we will extend the discussion of Fermi surface SMG to (2+1)D in a concrete lattice model, which can be exactly solved in both the weak and strong interaction limits. Through these examples, we establish the Fermi surface SMG as a general mechanism to gap out anomaly-free Fermi surfaces in different dimensions. We summarize our result and discuss its connection to future directions in Sec. 3.4.

3.2 Fermi Surface SMG in (1+1)D

3.2.1 (1+1)D Fermi Liquid and Fermi Surface Anomaly

In the free-fermion limit, the (1+1)D Fermi liquid can be realized as a system of fermions occupying a segment of single-particle momentum eigenstates in the 1D momentum space (or Brillouin zone), which can be described by a Hamiltonian $H = \sum_k c_k^\dagger \varepsilon_k c_k$, where c_k (or $c_k^\dagger$) is the fermion annihilation (or creation) operator of the single-particle mode at momentum k. For now, we only consider spinless fermions, such that the c_k operator does not carry spin (or any other internal degrees of freedom). As an example, suppose the band structure is described by $\varepsilon_k = (k^2 - k_F^2)/(2m)$ for non-relativistic fermions with a finite chemical potential $\mu = k_F^2/(2m)$. The ground state of the Hamiltonian H will have fermions occupying the momentum segment $k \in [-k_F, k_F]$ bounded by the Fermi momentum k_F, as illustrated in Fig. 3.1(a).

The low-energy degrees of freedom in the (1+1)D Fermi liquids can be modeled by the chiral fermions near the 0D Fermi surfaces (namely, Fermi points) at $\pm k_F$, which are described by the following Lagrangian density

$$\mathcal{L} = c_L^\dagger(\mathrm{i}\partial_t - v_F \mathrm{i}\partial_x)c_L + c_R^\dagger(\mathrm{i}\partial_t + v_F \mathrm{i}\partial_x)c_R, \tag{3.1}$$

where $v_F = k_F/m$ is the Fermi velocity. The operator c_L (or c_R) annihilates the left (or right)
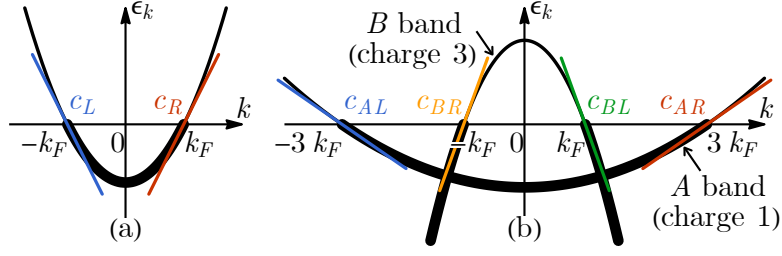
Figure 3.1. (a) A typical single-band Fermi liquid with Fermi surface anomaly. (b) Two-band model of a Fermi liquid with the Fermi surface anomaly canceled. Chiral fermions with linearized dispersions around different Fermi points emerge at low energy.

moving fermion modes, defined as

$$c_{R/L}(x) = \int_{-\Lambda}^{\Lambda} d\kappa \, c_{\pm k_F + \kappa} e^{i(\pm k_F + \kappa)x} \tag{3.2}$$

around the Fermi points within a small momentum cutoff $\Lambda \ll k_F$. The low-energy effective theory $\mathscr{L}$ in Eq. (3.1) has an emergent $\mathsf{U}(1)_L \times \mathsf{U}(1)_R$ symmetry (more precisely as an *emanant symmetry* [80], since the translation and charge conservation symmetry are not the subgroup of $\mathsf{U}(1)_L \times \mathsf{U}(1)_R$ symmetry), corresponding to the separate charge conservation of the left- and right-moving chiral fermions. Under the symmetry transformation with the periodic ϕ_L and ϕ_R in $[0, 2\pi)$,

$$\mathsf{U}(1)_L : c_L \to e^{i\phi_L} c_L, c_R \to c_R;$$
$$\mathsf{U}(1)_R : c_L \to c_L, c_R \to e^{i\phi_R} c_R. \tag{3.3}$$

They can be as well understood as a recombination of the vector $\mathsf{U}(1)_V$ and axial $\mathsf{U}(1)_A$

symmetries, by rewriting $\phi_L = \phi - k_F \, \delta x$ and $\phi_R = \phi + k_F \, \delta x$,

$$
\begin{aligned}
\mathsf{U}(1)_V : c_k \to \mathrm{e}^{\mathrm{i}\phi} c_k \Rightarrow & \begin{cases} c_L \to \mathrm{e}^{\mathrm{i}\phi} c_L, \\[6pt] c_R \to \mathrm{e}^{\mathrm{i}\phi} c_R; \end{cases} \\[12pt]
\mathsf{U}(1)_A : c_k \to \mathrm{e}^{\mathrm{i}k\,\delta x} c_k \Rightarrow & \begin{cases} c_L \to \mathrm{e}^{-\mathrm{i}k_F \, \delta x} c_L, \\[6pt] c_R \to \mathrm{e}^{+\mathrm{i}k_F \, \delta x} c_R. \end{cases}
\end{aligned}
\tag{3.4}
$$

More precisely, the combined symmetry group should be denoted as $\mathsf{U}(1)_V \times_{\mathbb{Z}_2^F} \mathsf{U}(1)_A \equiv \frac{\mathsf{U}(1)_V \times \mathsf{U}(1)_A}{\mathbb{Z}_2^F}$, because the $\mathsf{U}(1)_V$ and $\mathsf{U}(1)_A$ symmetries share the fermion parity $\mathbb{Z}_2^F$ subgroup (under which $c_{L,R} \to -c_{L,R}$). The physical meaning of the vector $\mathsf{U}(1)_V$ symmetry is the total $\mathsf{U}(1)$ charge conservation of the fermions, and the axial $\mathsf{U}(1)_A$ symmetry can be considered an effective representation of the *translation symmetry* in the infrared (IR) limit (that translates all fermions by displacement δx along the 1D system). Although translation symmetry is described by a *non-compact* symmetry group $\mathbb{Z}$ at the lattice scale, its action on the low-energy chiral fermion fields c_L, c_R behaves as a *compact* $\mathsf{U}(1)_A$ emergent symmetry [272, 356].

The stability of the Fermi liquid is protected by the Fermi surface anomaly, which can be viewed as the mixed anomaly between the $\mathsf{U}(1)_V$ and $\mathsf{U}(1)_A$ symmetries. The anomaly index is given by [259, 238, 86]

$$
1 \times k_F - 1 \times (-k_F) = 2k_F = 2\pi\nu,
\tag{3.5}
$$

which can be related to the fermion filling fraction ν. The system is anomalous if the filling ν is not an integer. Without breaking the charge $\mathsf{U}(1)$ and translation symmetries, it is impossible to drive the Fermi liquid to a trivial gap phase due to the non-vanishing Fermi surface anomaly. This can be viewed as a consequence of the Lieb-Schultz-Mattis (LSM) theorem [238]. The situation is also similar to the chiral fermion edge states on the (1+1)D boundary of a (2+1)D quantum Hall insulator.

3.2.2 Two-Band Model and Anomaly Cancellation

To generate a gap for these low-energy fermions in (1+1)D Fermi liquids, the Fermi surface anomaly must be canceled. Here we present a two-band toy model that achieves anomaly cancellation and enables gapping out the Fermi surface without breaking the charge $\mathsf{U}(1)$ and translation symmetries and without generating any Fermi bilinear condensation. It will provide a concrete example of SMG in (1+1)D Fermi liquids.

Consider a 1D lattice (a chain of sites) with two types of fermions c_{iA} and c_{iB} per site. The A-type fermion c_{iA} carries charge q_A under a global $\mathsf{U}(1)$ symmetry, and the B-type fermion c_{iB} carries charge q_B under the same $\mathsf{U}(1)$ symmetry. The Hamiltonian takes the general form of

$$H = -\sum_{ij}(t_{ij}^A c_{iA}^\dagger c_{jA} + t_{ij}^B c_{iB}^\dagger c_{jB} + \text{h.c.}) - \sum_i (\mu_A c_{iA}^\dagger c_{iA} + \mu_B c_{iB}^\dagger c_{iB}) + H_{\text{int}} \tag{3.6}$$

with H_{int} being some fermion interactions to be specified later in Eq. (3.16). The specific details of the hopping coefficients t_{ij}^A and t_{ij}^B are not important to our discussion as long as they produce a band structure that looks like Fig. 3.1(b) in the Brillouin zone. The A-type fermion forms an electron-like band, and the B-type fermion forms a hole-like band. The two bands overlap in the energy spectrum. This will realize a two-band Fermi liquid in general. The Hamiltonian H in Eq. (3.6) has a $\mathsf{U}(1) \times (\mathbb{Z} \rtimes \mathbb{Z}_2)$ symmetry (parameterized by a periodic angle $\phi \in [0, 2\pi)$ and an integer $n \in \mathbb{Z}$ as follows)

$$\begin{aligned}
\mathsf{U}(1) &: c_{iA} \to e^{iq_A\phi} c_{iA}, \quad c_{iB} \to e^{iq_B\phi} c_{iB}; \\
\mathbb{Z} &: c_{iA} \to c_{(i+n)A}, \quad c_{iB} \to c_{(i+n)B}; \\
\mathbb{Z}_2 &: c_{iA} \to c_{(-i)A}, \quad c_{iB} \to c_{(-i)B}.
\end{aligned} \tag{3.7}$$

They correspond to the total charge conservation symmetry $\mathsf{U}(1)$, the lattice translation symmetry $\mathbb{Z}$, and the lattice reflection symmetry $\mathbb{Z}_2$. The question is whether we can gap the Fermi liquid without breaking all these symmetries in (1+1)D.

One significant obstruction towards gapping is the Fermi surface anomaly, which can also be interpreted as a mixed anomaly between the charge $U(1)$ and (the IR correspondence of) the translation symmetry. To cancel the Fermi surface anomaly, we need to fine-tune the chemical potentials μ_A and μ_B such that the anomaly index vanishes

$$q_A \nu_A + q_B \nu_B = 0 \mod 1, \tag{3.8}$$

where ν_A and ν_B are the filling fractions of the A and B bands (for the hole-like B band, we may assign $\nu_B < 0$ such that $|\nu_B|$ corresponds to the hole-filling). This is also known as the *charge compensation* condition in semiconductor physics.

If the A-type and B-type fermions carry the same charge as $q_A = q_B = 1$, the anomaly cancellation condition Eq. (3.8) simply requires $\nu_A = -\nu_B$. In this case, the electron-like Fermi surface of the A-type fermion and the hole-like Fermi surface of the B-type fermion are perfectly nested (with zero nesting momentum). A gap can be opened simply by tuning on a fermion bilinear term $\sum_i (c_{iA}^\dagger c_{iB} + \text{h.c.})$ in the Hamiltonian, which preserves the full $U(1) \times (\mathbb{Z} \rtimes \mathbb{Z}_2)$ symmetry. This is the familiar band hybridization mechanism to open a band gap in a charge-compensated Fermi liquid, which drives a metal to a band insulator without breaking symmetry.

However, we are more interested in the non-trivial case when the fermions carry different charges $q_A \neq q_B$. For example, let us consider the case of $q_A = 1$ and $q_B = 3$, then the anomaly cancellation condition Eq. (3.8) requires $\nu_A = -3\nu_B$, i.e. the electron-like Fermi volume in the A band must be *three times* as large as the hole-like Fermi volume in the B band to cancel the Fermi surface anomaly. Defining the fermion operators c_{kA}, c_{kB} in the momentum space by the Fourier transformation

$$c_{kA} = \sum_i c_{iA} e^{-iki}, \quad c_{kB} = \sum_i c_{iB} e^{-iki}, \tag{3.9}$$

the desired band structure can be effectively described by the following band Hamiltonian

(suppressing the interaction for now)

$$H = \sum_k (c_{kA}^\dagger \varepsilon_{kA} c_{kA} + c_{kB}^\dagger \varepsilon_{kB} c_{kB}), \qquad (3.10)$$

with the band dispersions (see Fig. 3.1(b))

$$\varepsilon_{kA} = \frac{k^2 - (3k_F)^2}{2m_A}, \quad \varepsilon_{kB} = -\frac{k^2 - k_F^2}{2m_B}. \qquad (3.11)$$

Here we assume $m_A, m_B > 0$. The Fermi momentum $k_F = |\nu_B|\pi$ is set by the filling $|\nu_B|$ which is typically an *irrational* number (without fine-tuning). The key feature is that the Fermi momenta of the A and B energy bands must have a $3 : 1$ ratio that matches the inverse charge ratio $(q_A/q_B)^{-1}$ precisely. In this case, the energy band hybridization is forbidden by the charge $U(1)$ symmetry as the two bands now carry different charges. Even if the band hybridization is spontaneously generated at the price of breaking the $U(1)$ symmetry, it does not gap the Fermi liquid because the Fermi surfaces of the two bands are no longer nested at the Fermi level, such that the band hybridization will only create some avoided energy band crossing below the Fermi level. Then the system remains metallic because the (upper) hybridized band still crosses the Fermi level.

One can show that it is impossible to symmetrically gap the Fermi liquid by any fermion *bilinear* terms in this charge-compensated two-band system with $q_A = 1$ and $q_B = 3$, even if the Fermi surface anomaly has already been canceled by the charge-compensated filling $\nu_A = -3\nu_B$. Although the anomaly vanishes (i.e. there is no obstruction towards gapping in principle), the symmetry is still restrictive enough to forbid any fermion bilinear gapping term, such that the only possible gapping mechanism rests on non-perturbative fermion interaction effects.

To see this, we can single out the low-energy chiral fermions near the four Fermi points:

$$c_{AR} = c_{(3k_F)A}, \quad c_{BR} = c_{(-k_F)B},$$

$$c_{BL} = c_{(k_F)B}, \quad c_{AL} = c_{(-3k_F)A}, \tag{3.12}$$

where A, B label the bands that they originated from and L, R label their chiralities (i.e. left- or right-moving), according to Fig. 3.1(b). Similar to Eq. (3.1), the low-energy effective Lagrangian density reads

$$\mathscr{L} = \sum_a c_a^\dagger (i\partial_t + v_a i\partial_x) c_a, \tag{3.13}$$

where the index a sums over the four Fermi point labels AR, BR, BL, AL. Here v_a denotes the Fermi velocity near the Fermi point a.

The original $\mathsf{U}(1) \times \mathbb{Z}$ symmetry at the lattice fermion level reduces to the emergent $\mathsf{U}(1)_V \times_{\mathbb{Z}_2^F} \mathsf{U}(1)_A$ symmetry for the low-energy chiral fermions c_a (see App. C.1 for more explanations)

$$\mathsf{U}(1) \Rightarrow \mathsf{U}(1)_V : c_a \to e^{iq_a^V \phi_V} c_a,$$

$$\mathbb{Z} \Rightarrow \mathsf{U}(1)_A : c_a \to e^{iq_a^A \phi_A} c_a. \tag{3.14}$$

Tab. 3.1 summarizes their charge assignment under $\mathsf{U}(1)_V$ and $\mathsf{U}(1)_A$, where the vector $\mathsf{U}(1)_V$ symmetry is just the charge $\mathsf{U}(1)$ symmetry and the axial $\mathsf{U}(1)_A$ symmetry is an emergent symmetry corresponding to the lattice translation symmetry $\mathbb{Z}$. Alternatively, they can be recombined into the $\mathsf{U}(1)_{\frac{3V+A}{2}} \times \mathsf{U}(1)_{\frac{3V-A}{2}}$ symmetry, such that it becomes obvious that all fermion bilinear back-scattering terms (either the Dirac mass $c_a^\dagger c_b$ or the Majorana mass $c_a c_b$ for $a \neq b$ and $a, b \in \{AR, BR, BL, AL\}$) are forbidden by the symmetry because they are all charged non-trivially under the $\mathsf{U}(1)_{\frac{3V+A}{2}} \times \mathsf{U}(1)_{\frac{3V-A}{2}}$ symmetry due to the distinct charge assignment to every chiral fermion. Given this situation, the only hope to gap the Fermi liquid is to evoke the SMG mechanism that generates the mass for all chiral fermions by non-perturbative multi-

fermion interactions.

Table 3.1. Charge assignments of low-energy fermions. See also the model in [394] on the same charge assignments.

fermion	chirality	$\mathsf{U}(1)_V$	$\mathsf{U}(1)_A$	$\mathsf{U}(1)_{\frac{3V+A}{2}}$	$\mathsf{U}(1)_{\frac{3V-A}{2}}$
c_a	$\operatorname{sgn} v_a$	q_a^V	q_a^A	$\frac{1}{2}(3q_a^V + q_a^A)$	$\frac{1}{2}(3q_a^V - q_a^A)$
c_{AR}	-1 (left)	1	3	3	0
c_{BR}	-1 (left)	3	-1	4	5
c_{BL}	$+1$ (right)	3	1	5	4
c_{AL}	$+1$ (right)	1	-3	0	3

3.2.3   SMG Interaction and RG Analysis

It is worth mentioning that the charge-compensated two-band model with $q_A = 1$ and $q_B = 3$ essentially regularizes the 3-4-5-0 chiral fermion model [40, 148] on a pristine 1D lattice (without introducing any compact extra dimensions). The emergent $\mathsf{U}(1)_{\frac{3V\pm A}{2}}$ symmetries act as the lattice translations decorated by appropriate internal $\mathsf{U}(1)$ rotations, described by the following $\mathbb{Z}$ symmetry groups (parameterized by integer $n \in \mathbb{Z}$) at the lattice level: (see App. C.1 for derivation)

$$\mathbb{Z} \text{ (for } \tfrac{3V\pm A}{2}) : \begin{cases} c_{iA} \to e^{\pm i3k_F n} c_{(i+n)A}, \\ c_{iB} \to e^{\pm i9k_F n} c_{(i+n)B}. \end{cases} \tag{3.15}$$

The 3-4-5-0 model is a toy model for studying the long-standing problem: the lattice regularization of the chiral fermion theory in high-energy physics [292, 293, 291, 369, 119, 201, 19, 276, 398]. Many variants of the model are studied in the lattice community (see references therein [310, 73]). This model is anomaly-free — perturbative local gauge anomaly free within any linear combination of the $\mathsf{U}(1)_V \times_{\mathbb{Z}_2^F} \mathsf{U}(1)_A$ checked by the Adler-Bell-Jackiw method [5, 28], perturbative local gravitational anomaly free because of the zero chiral central charge $c_L - c_R = 0$, also nonperturbative global anomaly free from any gauge or gravitational fields checked by the cobordism [390]. However, it is known much later that symmetric gapping

can only be achieved by minimally six-fermion interactions among the four flavors of 3-4-5-0 fermions. The SMG interaction was first proposed by Wang and Wen [396, 397], which was later discussed by Tong [381] and only recently verified by the density matrix renormalization group (DMRG) [419, 338] numerical simulation in Ref. [452].

Given the existing knowledge about the SMG interaction in the 3-4-5-0 chiral fermion model, we can map the Wang-Wen interaction [396, 397] back to our lattice model following the correspondence listed in Tab. 3.1, which gives us the following SMG interaction (see App. C.2 for more details)

$$H_{\text{int}} = g \sum_i c^\dagger_{(i-1)B} c_{(i-1)A} c_{iB} c_{iA} c^\dagger_{(i+1)B} c_{(i+1)A} + \text{h.c..} \tag{3.16}$$

This is a six-fermion interaction across three adjacent sites on the 1D lattice. It describes the process that first annihilates both A- and B-type fermions on the center site (which annihilates four units of charges on the site i) and then separately converts A-type fermions to B-type fermions on the two adjacent sites (which creates two units of charges on each of the site $i-1$ and $i+1$), such that the $\mathsf{U}(1)_V$ charge is conserved. The interaction is also manifestly translation and reflection symmetric, so the full $\mathsf{U}(1)_V \times (\mathbb{Z} \rtimes \mathbb{Z}_2)$ symmetry is preserved by the interaction as expected. With this interaction, we claim that the lattice model Eq. (3.6) will exhibit an (ersatz) Fermi liquid to SMG insulator transition when the interaction strength g exceeds a finite critical value g_c.

To show that the proposed interaction Eq. (3.16) indeed drives the Fermi liquid to a gapped interacting insulator, we bosonize [261, 130] the fermion operator $c_a \sim \, :\text{e}^{\text{i}\varphi_a}:$ (with $a \in \{AR, BR, BL, AL\}$) and cast the lattice model to an effective Luttinger liquid theory, described by the following Lagrangian density

$$
\begin{aligned}
\mathscr{L} = &\frac{1}{4\pi} (\partial_t \varphi^\mathsf{T} K \partial_x \varphi - \partial_x \varphi^\mathsf{T} V \partial_x \varphi) \\
&+ \sum_{\alpha=1,2} g_\alpha \cos(l_\alpha^\mathsf{T} \varphi),
\end{aligned} \tag{3.17}
$$

where $\varphi = (\varphi_{AR}, \varphi_{BR}, \varphi_{BL}, \varphi_{AL})^\mathsf{T}$ are compact scalar bosons. The K matrix and the l_α vectors are given by

$$K = \begin{bmatrix} 1 & 0 & 0 & 0 \\ 0 & 1 & 0 & 0 \\ 0 & 0 & -1 & 0 \\ 0 & 0 & 0 & -1 \end{bmatrix}, \quad l_1 = \begin{bmatrix} 1 \\ -2 \\ 1 \\ 2 \end{bmatrix}, \quad l_2 = \begin{bmatrix} 2 \\ 1 \\ -2 \\ 1 \end{bmatrix}. \tag{3.18}$$

As shown in App. C.2, the six-fermion interaction H_{int} in Eq. (3.16) translates to the cosine terms g_1 and g_2 in the Luttinger liquid theory in Eq. (3.17), with $g_1 = g_2 = g$ enforced by the $\mathbb{Z}_2$ reflection symmetry (as the $\mathbb{Z}_2$ transformation exchanges the g_1 and g_2 terms). The RG flow in the log energy scale $\ell = -\ln\Lambda$ is given by [221, 196]

$$\frac{\mathrm{d}g}{\mathrm{d}\ell} = (2 - \Delta_{\text{int}})g, \quad \frac{\mathrm{d}\Delta_{\text{int}}^{-1}}{\mathrm{d}\ell} = \pi^2 g^2, \tag{3.19}$$

where Δ_{int} is the scaling dimension of the SMG interaction. The RG flow diagram is shown in Fig. 3.2.
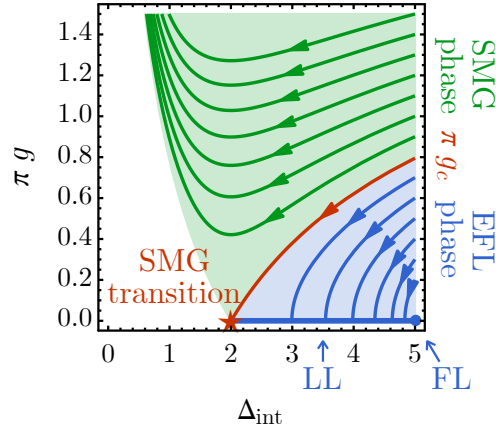
Figure 3.2. The RG flow of the coupling g and the scaling dimension Δ_{int} of the SMG interaction. The abbreviations stand for the following terminology: SMG for symmetric mass generation, FL for Fermi liquid, EFL for ersatz Fermi liquid, LL for Luttinger liquid.

At the Fermi liquid (FL) fixed-point, we have $\Delta_{\text{int}} = \frac{1}{2}l_\alpha^\mathsf{T} l_\alpha = 5 > 2$, meaning that the SMG interaction is perturbatively irrelevant. If the bare coupling g (the interaction strength at the lattice scale) is weak ($g < g_c$), it will just flow to zero and disappear in the IR theory. However, the scaling dimensions of all operators will be renormalized as the coupling g flows toward

zero. Therefore, the FL fixed-point will be deformed into the Luttinger liquid (LL) fixed-line, along which the fermion quasi-particle is no longer well-defined, but the system remains gapless. Despite the different dynamical properties, the LL still preserves all the kinematic properties (e.g. emergent symmetries and anomalies) as the FL, which can be unified under the concept of *ersatz Fermi liquid* (EFL) [122].

If the bare coupling g is strong enough ($g > g_c$), the scaling dimension Δ_{int} can be reduced to $\Delta_{\text{int}} < 2$ such that the SMG interaction becomes relevant and flows strong. As the cosine term in Eq. (3.17) gets strong, the corresponding vertex operators $e^{i l_\alpha^\intercal \varphi}$ ($\alpha = 1, 2$) condense. Any other operators that braid non-trivially with the condensed operators will be gapped, which includes all the fermion operators. Therefore the system enters the SMG insulating phase with all fermion excitations gapped without breaking the $\mathsf{U}(1) \times (\mathbb{Z} \rtimes \mathbb{Z}_2)$ symmetry. This has been confirmed by the DMRG simulation in Ref. [452] for a related model using the domain wall fermion construction, where it has been verified that the fermion two-point function indeed decays exponentially in the SMG phase — a direct piece of evidence for the gap generation. On the lattice level, this corresponds to condensing the six-fermion bound state by developing the ground state expectation value of $\langle c_{(i-1)B}^\dagger c_{(i-1)A} c_{iB} c_{iA} c_{(i+1)B}^\dagger c_{(i+1)A} \rangle \neq 0$. So the gapping is achieved by the multi-fermion condensation (involving more than two fermions), which is distinct from the fermion bilinear condensation in the conventional gapping mechanisms of Fermi liquids (such as the band hybridization or Cooper pairing mechanisms).

The RG analysis also indicates that the ersatz Fermi liquid to SMG insulator transition (at $g = g_c$) is of the Berezinskii-Kosterlitz-Thouless (BKT) [32, 33, 222] transition universality in (1+1)D.

The above analysis established the Fermi surface SMG phenomenon in the lattice model Eq. (3.6) (equipped with the gapping interaction Eq. (3.16)). The significance of this lattice model is that it provides a pristine 1D lattice regularization of the 3-4-5-0 chiral fermion model by using lattice translation to realize the axial $\mathsf{U}(1)_A$ symmetry at low energy. In contrast to the domain wall fermion constructions [397, 398, 452], our construction does not require the

introduction of a (2+1)D bulk to realize the chiral fermions as boundary modes. Such pristine 1D lattice regularization is advantageous for the numerical simulation of chiral fermions, as the model contains no redundant bulk (or mirror) fermions, such that the computational resources can be used more efficiently. We will leave the numerical exploration of this model to future research.

3.3 Fermi Surface SMG in (2+1)D

3.3.1 (2+1)D Fermi Liquid and Fermi Surface Anomaly

Given the example of Fermi surface SMG in (1+1)D, we would like to further explore similar physics in higher dimensions. The most important low-energy features of a (2+1)D Fermi liquid are the gapless fermions on its 1D Fermi surface. Suppose we parameterize the 1D Fermi surface $\boldsymbol{k}_F(\theta) \in \partial \mathcal{V}_F$ by a continuous and periodic parameter θ, such that $\boldsymbol{k}_F(\theta + 2\pi) = \boldsymbol{k}_F(\theta)$ (where we do not require θ to literally represent the geometrical angle, as the Fermi surface may not be a perfect circle in general). The fermions c_θ on the Fermi surface have an emergent symmetry described by the loop group of $\mathsf{U}(1)$ [122, 121], denoted as $\mathrm{L}\mathsf{U}(1)$, under which

$$\mathrm{L}\mathsf{U}(1) : c_\theta \to \mathrm{e}^{\mathrm{i}\phi(\theta)} c_\theta, \tag{3.20}$$

where the $\mathsf{U}(1)$ phase factor $\mathrm{e}^{\mathrm{i}\phi(\theta)}$ is a smooth function of θ with the periodicity $\mathrm{e}^{\mathrm{i}\phi(\theta+2\pi)} = \mathrm{e}^{\mathrm{i}\phi(\theta)}$. Both the (global) charge $\mathsf{U}(1)$ and the translation symmetries $\mathbb{R}^2$ are subgroups of $\mathrm{L}\mathsf{U}(1)$:

$$\mathsf{U}(1) : c_\theta \to \mathrm{e}^{\mathrm{i}q\phi} c_\theta, \quad \mathbb{R}^2 : c_\theta \to \mathrm{e}^{\mathrm{i}\delta\boldsymbol{x}\cdot\boldsymbol{k}_F(\theta)} c_\theta, \tag{3.21}$$

assuming the fermions c_θ carry charge q under the global $\mathsf{U}(1)$ symmetry and are translated by the vector $\delta\boldsymbol{x} \in \mathbb{R}^2$.

The presence of the Fermi surface causes a mixed anomaly between the $\mathsf{U}(1)$ and

translation symmetries [417], which is characterized by the anomaly index

$$\frac{q}{2(2\pi)^2} \oint d\theta (\boldsymbol{k}_F \times \partial_\theta \boldsymbol{k}_F)_3 = \frac{q\mathcal{V}_F}{(2\pi)^2} = q\nu, \tag{3.22}$$

where $\mathcal{V}_F$ stands for the Fermi volume in the momentum space, and ν is the filling factor. If the Fermi surface anomaly is non-vanishing, it is impossible to trivially gap out the Fermi liquid without breaking any symmetry or developing any topological order. The Fermi surface SMG is only possible if the Fermi liquid system contains multiple Fermi surfaces of opposite anomaly indices, such that their anomalies cancel as a whole.

3.3.2 Kagome-Triangular Lattice Model

We present a concrete lattice model to demonstrate the Fermi surface SMG in (2+1)D. Consider two types of *spinless* fermions labeled by A and B that are charged under a global U(1) symmetry with charges $q_A = 1$ and $q_B = 3$, respectively. The A-type (or B-type) fermion is defined on a Kagome (or triangular) lattice. As depicted in Fig. 3.3(a), the Kagome and the triangular lattices lie on top of each other, with the site I of the triangular lattice aligned with the upper triangle $\triangle_I$ on the Kagome lattice. We will use the lower-case letters i, j (or the upper-case letters I, J) to label the Kagome (or the triangular) lattice sites.

The lattice model is described by the following Hamiltonian

$$\begin{aligned} H &= H_A + H_B + H_{\text{int, CF}}, \\ H_A &= -t_A \sum_{\langle ij \rangle} (c_i^\dagger c_j + \text{h.c.}) - \mu_A \sum_i c_i^\dagger c_i, \\ H_B &= -t_B \sum_{\langle IJ \rangle} (c_I^\dagger c_J + \text{h.c.}) - \mu_B \sum_I c_I^\dagger c_I, \\ H_{\text{int, CF}} &= -g \sum_I \sum_{ijk \in \triangle_I} (c_I^\dagger c_i c_j c_k + \text{h.c.}), \end{aligned} \tag{3.23}$$

where $\langle ij \rangle$ (or $\langle IJ \rangle$) denotes the nearest neighboring link on the A (or B) lattices and $ijk \in \triangle_I$
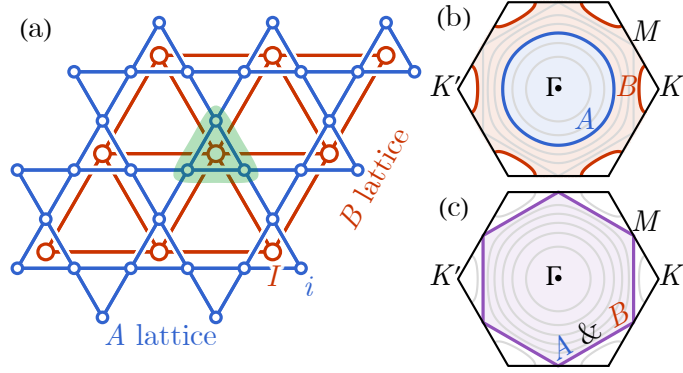
Figure 3.3. (a) In the real space, we design the overlapping Kagome (A) and triangular (B) lattices. The green triangle marks out the unit cell. In the momentum k space, we draw many contours to represent various equal energy curves of the energy band, at different filling levels (equally spaced by 1/8 filling fraction). We illustrate the A-type (in blue) and B-type (in red) Fermi surfaces (b) at a general filling such as $v_A = 3/8$ and $v_B = 7/8 (= -1/8)$, or (c) at a special filling $v_A = v_B = 3/4 (= -1/4)$ where the Fermi surfaces coincide.

stands for the three A-sites i, j, k at the vertices of the upper triangle surrounding the B-site labeled by I. The model has a $\mathsf{U}(1)$ symmetry that acts as

$$\mathsf{U}(1) : c_i \to e^{i\phi} c_i, \quad c_I \to e^{i3\phi} c_I. \tag{3.24}$$

The Hamiltonian in Eq. (3.23) preserves the internal $\mathsf{U}(1)$ symmetry and all symmetries of the Kagome-triangular lattice (most importantly, the lattice translation symmetry).

The model Eq. (3.23) describes the two types of fermions hopping separately on their corresponding lattices. Because every unit cell contains four sites (three from the Kagome lattice and one from the triangle lattice), the hopping model will give rise to four energy bands (three bands for A-type fermions and one band for B-type fermions). The chemical potentials μ_A and μ_B are adjusted to ensure the desired filling of these fermions. We will focus on a simple case when only the *lowest* A-type (Kagome lattice) bands and the *single* B-type (triangular lattice) bands are filled by filling fractions v_A and v_B respectively, such that the Fermi surface only involves *two* of the four bands.

99

The A-type and B-type fermions are coupled together only through a four-fermion interaction $H_{\text{int, CF}}$ in Eq. (3.23) that fuses three A-type (charge-1) fermions to one B-type (charge-3) fermions (and vice versa) within each unit cell. We will call it a *charge fusion* (CF) interaction. The CF interaction breaks the separate $U(1)$ charge conservation laws for A-type and B-type fermions in the hopping model to a joint $\mathsf{U}(1)$ charge conservation, associated with the symmetry action in Eq. (3.24). Similar interactions also appear in a recent study [236] of quantum breakdown.

Without interaction ($g = 0$), the system is in a Fermi liquid phase. According to Eq. (3.22), the Fermi surface anomaly cancellation condition requires

$$q_A \nu_A + q_B \nu_B = 0 \quad \text{mod } 1. \tag{3.25}$$

Given the charge assignment of $q_A = 1$ and $q_B = 3$, it requires $\nu_A = -3\nu_B$. There is no further requirement on the choice of ν_A itself. With a generic choice of filling (assuming $\nu_A < 3/4$) as in Fig. 3.3(b), the A-type fermions (on the Kagome lattice) will form an electron-like Fermi surface, whose Fermi volume is three times as large as that of the hole-like Fermi surfaces formed by the B-type fermions (on the triangular lattice). Although the Fermi liquid has a vanishing Fermi surface anomaly, the charge $\mathsf{U}(1)$ and the lattice translation symmetries are still restrictive enough to forbid any gap opening on the free-fermion level. For example, any pairing (charge-2e superconducting) gap will break the $\mathsf{U}(1)$ symmetry. The only possibility to gap the Fermi liquid relies on the multi-fermion interaction.

We claim that the charge fusion interaction $H_{\text{int, CF}}$ in Eq. (3.23) is a valid SMG interaction that drives the Fermi liquid into a trivially gaped insulator without breaking symmetry (or developing any topological order). To see this, we go to the strong coupling limit by taking $g \to \infty$. Of course, the chemical potentials μ_A, μ_B must increase correspondingly to keep the fermion fillings fixed. The model Hamiltonian decouples to each unit cell in the strong coupling

limit

$$H = \sum_{I|ijk\in\triangle_I} -\mu_A(n_i + n_j + n_k) - \mu_B n_I - g(c_I^\dagger c_i c_j c_k + \text{h.c.}), \tag{3.26}$$

where $n_i = c_i^\dagger c_i$ (and $n_I = c_I^\dagger c_I$) denotes the fermion number operator. Within each unit cell, there are only two relevant states $|1110\rangle$ and $|0001\rangle$ (in the Fock state basis $|n_i n_j n_k n_I\rangle$) acted by the Hamiltonian. Their hybridization will produce the ground state in each unit cell. The full-system ground state will be the following direct product state

$$|\text{SMG}\rangle = \bigotimes_I \left(\sqrt{p}|1110\rangle + \sqrt{1-p}|0001\rangle\right)_I, \tag{3.27}$$

where $p = \frac{1}{2}\left(1 + \frac{-3\mu_A + \mu_B}{\sqrt{(-3\mu_A + \mu_B)^2 + 4g^2}}\right)$ is the probability to observe the $|1110\rangle$ state in the unit cell, which is tunable by adjusting μ_A, μ_B relative to g. The fermion fillings (per unit cell) in the ground state $|\text{SMG}\rangle$ will be

$$\nu_A = 3p, \quad \nu_B = 1 - p = -p \mod 1, \tag{3.28}$$

which automatically satisfies the anomaly cancellation condition $\nu_A = -3\nu_B$ (as it should be). The ground state $|\text{SMG}\rangle$ is non-degenerated and gapped from all excited states (with a gap of the order g). It also preserves the charge $\text{U}(1)$ and all the lattice symmetries and does not have topological order. Therefore, we have explicitly shown that the system ends up in the SMG insulator phase as $g \to \infty$. As a gapped phase, we expect it to be stable against perturbations (such as the hopping terms t_A, t_B) over a finite region in the parameter space. The SMG phase is a strongly interacting insulating phase, which has no correspondence in the free-fermion picture.

Established the Fermi liquid (metallic) phase at $g = 0$ and the SMG insulator phase at $g \to \infty$, there must be an SMG transition (an interaction-driven metal-insulator transition) at some intermediate coupling strength g_c. However, the nature of the transition is still an open question,

which we will leave for future numerical study. In the following, we will only analyze the SMG transition at a special filling: $v_A = v_B = 3/4$, where the Fermi surfaces coincide precisely and take the perfect hexagon shapes as shown in Fig. 3.3(c). This allows us to gain some analytic control of the problem.

3.3.3 RG Analysis of the SMG Transition

In this subsection, we analyze the interaction effect in Eq. (3.23) when the filling is $v_A = v_B = 3/4$. In this case, the Fermi surface of the system contains three Van Hove singularities (VHSs), also known as hot spots, located at three distinct M points as shown in Fig. 3.3(c). This allows us to study the interaction effects using the hot-spot renormalization group (RG) method at the one-loop level [144, 319, 289, 186, 244, 245, 306, 448]. The hot-spot RG approach assumes that the low-energy physics emerges from the correlated effects of fermions near the VHSs, where the density of states diverges. This divergence leads to the a high instability towards gap opening.

Under RG, the charge fusion interaction $H_{\text{int, CF}}$ will generate two types of density-density interactions at the one-loop level, namely, $H_{\text{int, AA}} = \sum_{i,j} n_i n_j$ and $H_{\text{int, AB}} = \sum_{i,I} n_i n_I$ as well as other (less important) exchange interactions. These density-density interactions are more important in the sense that they will in turn contribute to the correction of $H_{\text{int, CF}}$. Therefore, we should include $H_{\text{int, CF}}, H_{\text{int, AA}}, H_{\text{int, AB}}$ altogether in the RG analysis and study the RG flow jointly.

To proceed, we transform the interactions into the momentum space. The fermion operators are labeled by the flavor index $S = A, B$ and the hot-spot index $\alpha, \beta \in \{1, 2, 3\}$ (referring to the three different VHSs). We note that $H_{\text{int, CF}}$ would vanish if it is naively restricted to the hot spots because the momentum conservation requires multiple A-type fermion operators to appear on the same hot spot, which violates the Pauli exclusion principle of fermions. So we need to introduce point splitting in the momentum space around each hot spot. Our strategy is to further split the A-type fermion into three modes A_s labeled by $s = 1, 2, 3$, and define the

interaction,

$$H_{\text{int, CF}} = g_{\text{rs}} \sum_{\alpha} \varepsilon^{ijk} c_{B\alpha}^{\dagger} c_{A_i\alpha} c_{A_j\alpha} c_{A_k\alpha}$$

$$+ g_{\text{rt}} \sum_{\alpha \neq \beta} \varepsilon^{ijk} c_{B\alpha}^{\dagger} c_{A_i\alpha} c_{A_j\beta} c_{A_k\beta} + \text{h.c.} \tag{3.29}$$

g_{rs} and g_{rt} are the CF interaction decomposed into different momentum transfer channels: the intra-hot-spot scattering g_{rs} and the inter-hot-spot scattering g_{rt}.

These CF interactions receive corrections from the following density-density interactions at the one-loop level,

$$H_{\text{int, AA}} + H_{\text{int, AB}} = g_{\text{as}} \sum_{\alpha, st} n_{A_s\alpha} n_{A_t\alpha} + (A_s \leftrightarrow A_t)$$

$$+ g_{\text{bt}} \sum_{\alpha \neq \beta, s} n_{B\alpha} n_{A_s\beta} + (A_s \leftrightarrow B) + \text{h.c.} + ... \tag{3.30}$$

where ... refers to the other interactions that are decoupled from $g_{\text{rs}}, g_{\text{rt}}, g_{\text{as}}, g_{\text{bt}}$ in the RG equations. The scattering processes of these four important interactions are illustrated in Fig. 3.4. The complete set of all possible interactions is presented in App. C.3.

We derive the RG equations based on the systematic approach developed in Ref. [251]. Since we are interested in the flow of $H_{\text{int, CF}}$, the relevant part of the RG equations reads,

$$\frac{dg_{\text{bt}}}{d\ell} = 2d_0 d_{\text{AB}} g_{\text{bt}}^2, \quad \frac{dg_{\text{as}}}{d\ell} = -2g_{\text{as}}^2, \tag{3.31}$$

$$\frac{dg_{\text{rs}}}{d\ell} = -6g_{\text{as}} g_{\text{rs}}, \quad \frac{dg_{\text{rt}}}{d\ell} = 4d_0 d_{\text{AB}} g_{\text{bt}} g_{\text{rt}} - 2g_{\text{as}} g_{\text{rt}}.$$

where the RG parameter is defined by the Cooper-pairing susceptibility of A-type fermions $\ell = \chi_{pp,\text{AA}}(\boldsymbol{k} = 0, E) \sim v_0 \log^2(\Lambda/E)$, in which $v_0 \log(\Lambda/E)$ is the diverging density of states at the VHS, E is the running energy scale and Λ is the high energy cutoff. $d_0 = d\chi_{ph,\text{AA}}(\boldsymbol{Q})/d\ell \leq 1$ is the nesting parameter of A-type fermions, which saturates to one in the perfectly nested limit

($d_0 \to 1$). In our case, different VHSs are half-nested (only one of the two crossing Fermi surfaces is perfectly nested between every pair of different VHSs), so $d_0 = 1/2$ is a suitable estimation. Similarly, we define $d_{AB} = d\chi_{pp,AB}(\mathbf{0})/d\ell$, which depends on the energies of A and B-type fermions near the VHS. The full RG equations and details are listed in App. C.3.
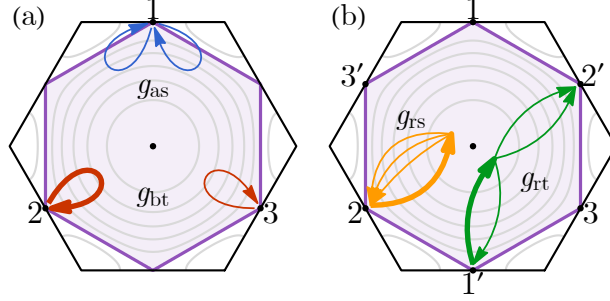
Figure 3.4. Scattering of fermions between Van Hove singularities (VHSs) by (a) density-density interactions g_{bt} (red), g_{as} (blue) and (b) non-vanishing processes g_{rs} (yellow), g_{rt} (green) of $H_{int, CF}$. Thin (or thick) arrows correspond to A-type (or B-type) fermions.

According to the one-loop RG equations, if the density-density interactions g_{bt}, g_{as} are initially zero, then the CF interactions g_{rs}, g_{rt} remain marginal along the RG flow. However, if we turn on small density-density interactions g_{bt}, g_{as} with correct signs ($g_{bt} > 0$ or $g_{as} < 0$), the charge fusion interactions g_{rs}, g_{rt} will be marginally relevant. The solutions of RG equations Eq. (3.31) are

$$
g_{bt}(\ell) = \frac{g_{bt}(0)}{1 - 2d_0 d_{AB} g_{bt}(0)\ell}, \quad g_{as}(\ell) = \frac{g_{as}(0)}{1 + 2g_{as}(0)\ell},
$$
$$
g_{rs}(\ell) = \frac{g_{rs}(0)}{(1 + 2g_{as}(0)\ell)^3},
$$
$$
g_{rt}(\ell) = \frac{g_{rt}(0)}{(1 + 2g_{as}(0)\ell)(1 - 2d_0 d_{AB} g_{bt}(0)\ell)^2}. \tag{3.32}
$$

As the RG parameter ℓ increases under the RG flow, the coupling strengths can diverge at some critical scale ℓ_c, when any of the denominators in Eq. (3.32) vanish. The critical scale is set by the bare density-density interaction strengths $g_{bt}(0)$ and $g_{as}(0)$, but the CF interaction strengths g_{rs}, g_{rt} diverge faster than the density-density interactions as the critical scale is approached.

Therefore, the RG fixed points are characterized by the behavior of g_{rs}, g_{rt}.
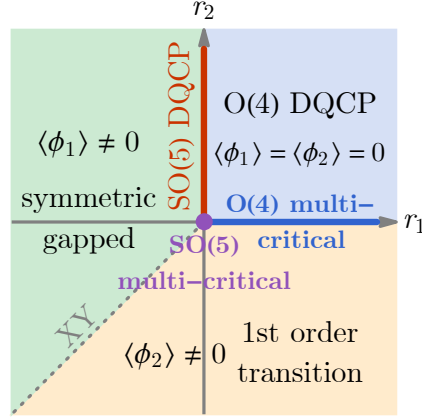
Figure 3.5. The RG phase diagram with respect to the density-density interactions g_{as}, g_{bt}. In the Fermi liquid (FL) phase, the gapping interaction flows to zero. In the symmetric mass generation (SMG) phase, the gapping interaction flows to infinity.

Depending on the bare density-density interaction strengths $g_{as}(0)$ and $g_{bt}(0)$, the system can flow towards different RG fixed points as shown Fig. 3.5. When $g_{as}(0) > 0$ and $g_{bt}(0) < 0$, all interactions flow to zero, which corresponds to the Fermi liquid fixed point. When $g_{as}(0) < \min(0, -d_0 d_{AB} g_{bt}(0))$, both charge fusion interactions g_{rs}, g_{rt} flow to infinity, which should correspond to the SMG phase according to the previous lattice model analysis. However, we also find a region in the phase diagram, described by $g_{bt} > \max(0, -g_{as}/d_0 d_{AB})$, where $g_{rs} \to 0$ and $g_{rt} \to \infty$, i.e. flowing towards different limits. We are not sure how to interpret the physical meaning of this RG fixed point. It might still be in the SMG phase as one interaction still flows strong. But it could as well end up in a spontaneous symmetry breaking (SSB) phase that breaks the $LU(1)$ symmetry since the A-type and B-type Fermi surfaces have pretty strong nesting instability. This might also be an artifact of the hot-spot RG method, as it does not fully capture all low-energy fermionic degrees of freedom of the Fermi surface.

Admittedly, it is not possible to determine whether the full Fermi surface is gapped using the hot-spot RG analysis alone. This is because the hot-spot RG approach only takes into account the fermions near the VHSs, and does not consider the Fermi surface freedom away from the VHSs. In order to determine whether the strong coupling fixed point is a fully gapped state,

we have to rely on lattice model analysis in the strong coupling limit. The exact ground state solution Eq. (3.27) provides evidence to support the argument that the strong coupling fixed point is indeed a fully gapped state.

To improve, functional RG [418, 331, 116, 407] might provide a better resolution of the Fermi surface and remove the uncertainty in the phase diagram Fig. 3.5. A recent study [151] has demonstrated the functional RG method in a triangle lattice model with spinless fermions. The same technique might apply to our model as well. However, we will leave such study for future research.

By tuning $g_{as}(0)$ across zero on the $g_{bt}(0) < 0$ side, one can drive a FL to SMG transition. The gapping interaction is marginally relevant at the transition point. According to the solution of the RG equations in Eq. (3.32), the coupling diverges at the critical scale $\ell_c \sim v_0 \log^2(\Lambda/\Delta_{SMG})$ when the denominator $(1 + 2g_{as}(0)l_c)$ vanishes. This implies that the SMG gap Δ_{SMG} (the energy gap between the ground state and the first excited state) opens up as [362, 278]

$$\Delta_{SMG} \sim \Lambda \exp\left(-c/\sqrt{g_{as}(0)v_0}\right), \tag{3.33}$$

where Λ is the UV cutoff energy scale, v_0 is the coefficient in front of the diverging density of state at the VHS, and c is some non-universal constant.

3.4 Summary and Discussion

In this work, we propose the concept of Fermi surface SMG: a mechanism to gap out Fermi surfaces by non-perturbative interaction effects without breaking the LU(1) symmetry. This phenomenon can only happen when the Fermi surface anomaly is canceled out in the fermion system. We present (1+1)D and (2+1)D examples of Fermi surface SMG. We expect that the mechanism can generally occur in all dimensions.

Fermi surface SMG belongs to a broader class of phenomena, called the symmetric Fermi surface reconstruction (SFSR), as summarised in Fig. 3.6. The SFSR is in contrast to the

more conventional symmetry-breaking Fermi surface reconstruction, where the Fermi surface is reconstructed (or gapped) by developing spontaneous symmetry-breaking orders. Depending on the cancellation of the Fermi surface anomaly, the SFSR further splits into two classes: the Fermi surface symmetric mass generation (SMG) if the anomaly vanishes, or the Fermi surface topological mass generation (TMG) if the anomaly does not vanish. The former class, the Fermi surface SMG, is the focus of this work. The latter class, the Fermi surface TMG, is also discussed in the literature, where the non-vanishing Fermi surface anomaly is absorbed by an anomalous topological quantum field theory (TQFT), such that the SFSR is achieved by developing the corresponding topological order. This gives rise to deconfined/fractionalized Fermi liquid (FL*) [349, 351, 147] or orthogonal metal [290, 173, 74]. *Symmetry extension* [399] has provided a unified framework, to understand TMG and SMG for bosons or fermions of zero Fermi volume [371, 395, 160, 215, 313, 312], where the symmetric gapping can be achieved by extending the symmetry group to lift any gapping obstruction that was otherwise imposed by the symmetry. Similar constructions can be applied to understand SFSR more generally.
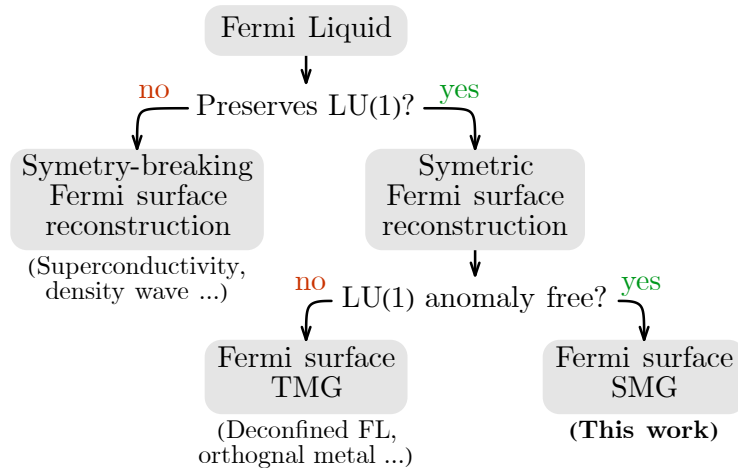
Figure 3.6. Classification of Fermi surface reconstruction mechanisms, based on the LU(1) loop group symmetry. Symmetric Fermi surface reconstruction (SFSR) contains two broad classes: (1) Fermi surface symmetric mass generation (SMG) if the total Fermi surface anomaly is canceled. (2) Fermi surface topological mass generation (TMG) if the total Fermi surface anomaly is matched by topological order with low energy topological field theory.

Fermi surface SMG deforms an anomaly-free (charge-compensated) Fermi liquid state to

a fully gapped product state. Although the resulting SMG gapped state does not have non-trivial features like topological order, the SMG transition from the Fermi liquid phase to the SMG phase can still be quite exotic. The SMG transition of relativistic fermions has been proposed to be a deconfined quantum critical point [447, 446], where the physical fermion fractionalizes to bosonic and fermionic partons with emergent gauge fluctuations at and only at the critical point. It is conceivable that similar scenarios might apply to the Fermi surface SMG transition as well, where deconfined Fermi liquid (orthogonal metal) could emerge at the critical point. The lattice models presented in this study lay the ground for future theoretical and numerical studies of the exotic SMG transition in these models.

It is also known that the fermion single-particle Green's function has symmetry-protected zeros at zero frequency in the SMG phase [443, 62, 65, 433]. It will be interesting to investigate further the Green's function structure in the Fermi surface SMG phase. Whether or not the SMG interaction will replace the original Fermi surface (a loop of poles) with a loop of zeros in the Green's function is still an open question to explore.

Another potential experimental connection is to apply the Fermi surface SMG to understand the nature of pseudo-gap phases, which is an exotic state of electrons where the Fermi surface is partially gapped without obvious symmetry breaking. It has been observed in many correlated materials. The recent proposal of the ancilla qubit approach [458, 457] for pseudo-gap physics draws a connection between the pseudo-gap metal to Fermi liquid transition with the Fermi surface SMG transition in the ancilla layers, as both transitions are described by field theories of fermionic deconfined quantum critical points [447, 446, 464, 463, 176]. The Fermi surface anomaly constrains the dynamical behavior of such field theories and can potentially shed light on the open problem of pseudo-gap transition in correlated materials.

Chapter. 3, in full, is a reprint of the material as it appears in Da-Chuan Lu, Meng Zeng, Juven Wang, and Yi-Zhuang You. Fermi surface symmetric mass generation. *Physical Review B*, 107(19):195133, May 2023. The dissertation author was the primary investigator and author of this paper.

Chapter 4

Green's Function Zeros in Fermi Surface Symmetric Mass Generation

The Fermi surface symmetric mass generation (SMG) is an intrinsically interaction-driven mechanism that opens an excitation gap on the Fermi surface without invoking symmetry-breaking or topological order. We explore this phenomenon within a bilayer square lattice model of spin-1/2 fermions, where the system can be tuned from a metallic Fermi liquid phase to a strongly-interacting SMG insulator phase by an inter-layer spin-spin interaction. The SMG insulator preserves all symmetries and has no mean-field interpretation at the single-particle level. It is characterized by zeros in the fermion Green's function, which encapsulate the same Fermi volume in momentum space as the original Fermi surface, a feature mandated by the Luttinger theorem. Utilizing both numerical and field-theoretical methods, we provide compelling evidence for these Green's function zeros across both strong and weak coupling regimes of the SMG phase. Our findings highlight the robustness of the zero Fermi surface, which offers promising avenues for experimental identification of SMG insulators through spectroscopy experiments despite potential spectral broadening from noise or dissipation.

4.1 Introduction

Symmetric mass generation (SMG) [127, 128, 396, 359, 15, 61, 381, 403] is an interaction-driven mechanism that creates many-body excitation gaps in anomaly-free fermion

109

systems *without* condensing any fermion bilinear operator or developing topological orders. It has emerged as a alternative symmetry-preserving approach for mass generation in relativistic fermion systems, which is distinct from the traditional symmetry-breaking Higgs mechanism [288, 287, 153, 8, 123, 170]. The prospect of SMG offering a potential solution to the long-standing fermion doubling problem [293, 292, 291, 369, 119, 360, 201] has sparked significant interest in the lattice gauge theory community [414, 442, 444, 30, 14, 13, 12, 107, 16, 336, 55, 57, 211, 210, 397, 398, 66, 321, 63, 56, 58, 452, 67, 64, 161]. In condensed matter physics, SMG was initially explored within the framework of the interaction-reduced classification of fermionic symmetry protected topological (SPT) states [127, 128, 383, 326, 314, 436, 159, 391, 271, 206, 451, 79, 441, 158, 364, 316, 420, 405, 205, 395, 406, 160, 1, 23], and has been recently extended to systems with Fermi surfaces [463, 458, 464, 457, 295, 254], given the growing understanding that Fermi liquids can be perceived as fermionic SPT states within the phase space [52, 250].

One important feature of the SMG gapped state lies in the zeros of fermion Green's function [162, 450, 62, 447, 65, 433] at low-energy. Investigations reveal that the poles of the fermion Green's function in the pristine gapless fermion state will be replaced by zeros in the gapped SMG state as the fermion system goes across the SMG transition upon increasing the interaction strength. This pole-to-zero transition was postulated [450] as a direct indicator of the SMG transition [447, 446] that can be probed by spectroscopy experiments. However, the presence of similar zeros in the Green's function within Fermi surface SMG states has not been investigated yet, and it is the focus of our present research.

Fermi surface SMG [254] refers to the occurrence of SMG phenomena on Fermi surfaces with non-zero Fermi volumes. It describes scenarios where the fermion interaction transforms a gapless Fermi liquid state (metal) into a non-degenerate, gapped, direct product state (trivial insulator), without breaking any symmetry (for example, without invoking Cooper pairing or density wave orders). Such a metal-insulator transition is viable when Fermi surfaces collaboratively cancel the Fermi surface anomaly [392, 417, 254]. This anomaly can be perceived as a mixed anomaly between the translation symmetry and the charge conservation

U(1) symmetry on the lattice [82, 86, 53, 377, 417, 392, 80], or as an anomaly of an emergent

loop LU(1) symmetry [122, 121, 356] in the infrared theory.

In this work, we present evidence of robust Green's function zeros in Fermi surface SMG

states. Let t be the energy scale of band dispersion and J be the energy scale of SMG gapping

interaction, we investigate the problem from two parameter regimes:

- Deep in the SMG phase ($J/t \gg 1$), we start with an exact-solvable SMG product state in a

  lattice model and calculate the fermion Green's function by treating the fermion hopping

  as perturbation [345]. We find that the Green's function $G_{\mathrm{SMG}}(\omega, \boldsymbol{k})$ deep in the SMG

  phase takes the following form

$$G_{\mathrm{SMG}}(\omega, \boldsymbol{k}) = \frac{\omega + \alpha \varepsilon_{\boldsymbol{k}}/J^2}{(\omega - \varepsilon_{\boldsymbol{k}}/2)^2 - J^2}, \tag{4.1}$$

  where $(\omega, \boldsymbol{k})$ labels the frequency-momentum of the the fermion. $\varepsilon_{\boldsymbol{k}}$ is the energy dispersion

  of the original band structure in the free-fermion limit, and α is an order-one number

  depending on other details of the system. One salient feature of G_{SMG} is that it has a

  series of zeros at $\omega = -\alpha \varepsilon_{\boldsymbol{k}}/J^2$ in the frequency-momentum space. At $\omega = 0$, the Green's

  function zeros form a zero Fermi surface that replaces the original Fermi surface.

- If the SMG phase is adjacent to a spontaneous symmetry breaking (SSB) phase, we use

  perturbative field theory to argue that the Green's function in the SMG phase near the

  symmetry-breaking transition ($J/t \gtrsim 1$) should take the form of [388, 118, 409]

$$G'_{\mathrm{SMG}}(\omega, \boldsymbol{k}) = \frac{\omega + \varepsilon_{\boldsymbol{k}}}{\omega^2 - \varepsilon_{\boldsymbol{k}}^2 - \Delta_0^2} \tag{4.2}$$

  where we assume that the SSB order parameter retains a finite amplitude Δ_0 in the SMG

  phase, but its phase is randomly fluctuating [409]. Again, G'_{SMG} features a series of zeros

  at $\omega = -\varepsilon_{\boldsymbol{k}}$, with the same zero Fermi surface.

Many previous works [7, 298, 118, 152] suggest that the Luttinger theorem [259] will

not be violated in the presence of the interaction that preserves the translation and charge conservation symmetry. However, quasi-particles (poles of Green's function) may not exist in the strongly correlated systems, the Fermi surface is instead defined by the surface of Green's function zeros at zero frequency, i.e., $G(0, \boldsymbol{k}) = 0$, and the Green's function changes sign on the two sides of the *zero Fermi surface*, or the so-called Luttinger surface [367, 118, 122, 337, 429]. This can be regarded as the remnant of the conventional Fermi surface in the strongly interacting gapped phase. Our analysis shows that the volume enclosed by the zeros of the Green's function in the SMG phase is the same as the Fermi volume in the Fermi liquid phase, which agrees with the Luttinger theorem.

The paper will be structured as follows. We start by introducing a concrete lattice model for Fermi surface SMG in Sec. 4.2.1 and briefly discussing its phase diagram. We give theoretical arguments for Green's function zeros in the SMG phase from the Luttinger theorem in Sec. 4.2.2 (general), and the particle-hole symmetry in Sec. 4.2.3 (specific). We provide numerical and field theoretical evidence of Green's function zeros from both the strong coupling Sec. 4.3.1 and the weak coupling Sec. 4.3.2 perspectives. We comment on the robustness of probing the zero structure in spectroscopy experiments in Sec. 4.4. We conclude in Sec. 4.5 with a discussion of the relevance of our model to the nickelate superconductor $La_3Ni_2O_7$.

4.2   Argument For Green's Function Zeros

4.2.1   Lattice Model and Phase Diagram

As a specific example of Fermi surface SMG, we consider a bilayer square lattice [453, 325, 322] model of spin-1/2 fermions, as illustrated in Fig. 4.1(a). Let $c_{il\sigma}$ be the fermion annihilation operator on site-i layer-l ($l = 1, 2$) and spin-σ ($\sigma = \uparrow, \downarrow$). The model is described by the following Hamiltonian

$$H = -t \sum_{\langle ij \rangle, l, \sigma} (c_{il\sigma}^\dagger c_{jl\sigma} + \text{h.c.}) + J \sum_i \boldsymbol{S}_{i1} \cdot \boldsymbol{S}_{i2}, \tag{4.3}$$

where $\boldsymbol{S}_{il} := \frac{1}{2}c^{\dagger}_{il\sigma}\boldsymbol{\sigma}_{\sigma\sigma'}c_{il\sigma'}$ denotes the spin operator with $\boldsymbol{\sigma} := (\sigma^1, \sigma^2, \sigma^3)$ being the Pauli matrices. The Hamiltonian H contains a nearest-neighbor hopping t of the fermions within each layer and an inter-layer Heisenberg spin-spin interaction with antiferromagnetic coupling $J > 0$. The Heisenberg interaction should be understood as a four-fermion interaction, that there is no explicitly formed local moment degrees of freedom. Unlike the standard t-J model [71], we do *not* impose any on-site single-occupancy constraint [163] here. We assume that the fermions are half-filled in each layer.
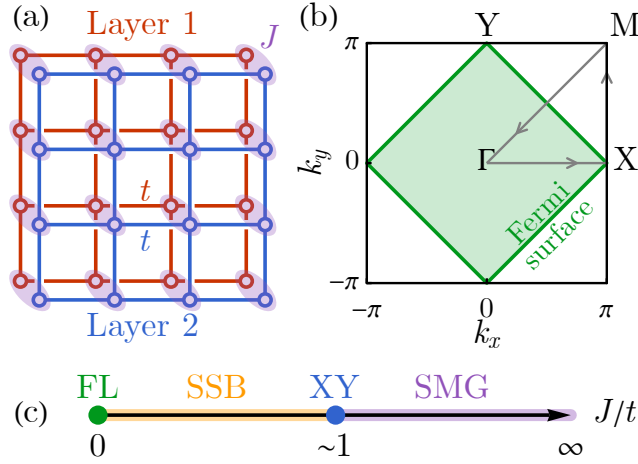
Figure 4.1. (a) Bilayer square lattice model with intra-layer hopping and inter-layer spin interaction. (b) Fermi sea and Fermi surface at $J = 0$ in the Brillouin zone. A high-symmetry path is traced out in gray. (c) A conjectured phase diagram consist of a Fermi liquid (FL) fixed point, a spontaneous symmetry breaking (SSB) phase, a XY transition, and a SMG insulating phase.

In the non-interacting limit ($J/t \rightarrow 0$), the ground state of the tight-binding Hamiltonian in Eq. (4.3) is a Fermi liquid with a four-fold degenerated (two layers and two spins) square-shaped Fermi surface in the Brillouin zone, as shown in Fig. 4.1(b). The fermion system is gapless in this limit. However, given that the fermion carries one unit charge under the $\mathsf{U}(1)$ symmetry, the Fermi surface anomaly vanishes due to [86, 250]

$$\sum_{a=1}^{4} q_a \nu_a = 4 \times 1 \times \frac{1}{2} = 0 \quad \text{mod } 1, \tag{4.4}$$

where a indexes the four-fold degenerated Fermi surface with $q_a = 1$ being the $U(1)$ charge carried by the fermion and $\nu_a = 1/2$ being the filling fraction. This implies there must be a way to gap out the Fermi surface into a trivial insulator while preserving both the translation and the $U(1)$ charge conservation symmetries. Nevertheless, these symmetry requirements are restrictive enough to rule out all possible fermion bilinear gapping mechanisms, leaving Fermi surface SMG the only available option.

One possible SMG gapping interaction is the interlayer Heisenberg spin-spin interaction J in Eq. (4.3). In the strong interaction limit ($J/t \to \infty$), the system has a unique ground state, given by

$$|0\rangle = \bigotimes_i (c_{i1\uparrow}^\dagger c_{i2\downarrow}^\dagger - c_{i1\downarrow}^\dagger c_{i2\uparrow}^\dagger) |\text{vac}\rangle, \tag{4.5}$$

which is a direct product of the inter-layer spin-singlet state on every site. $|\text{vac}\rangle$ stands for the vacuum state of fermions (i.e. $c_{il\sigma} |\text{vac}\rangle = 0$). The SMG ground state $|0\rangle$ does not break any symmetry and does not have topological order. All excitations are gapped by an energy of the order J from the ground state. Any local perturbation far below the energy scale J can not close this excitation gap, so the SMG phase is expected to be stable in a large parameter regime as long as $J \gg t$.

Given the distinct ground states in the two limits of J/t, we anticipate at least one quantum phase transition separating the Fermi liquid and the SMG insulator. However, due to the perfect nesting of the Fermi surface, the Fermi liquid state is unstable towards spontaneous symmetry breaking (SSB) upon infinitesimal interaction, so a more plausible phase diagram should look like Fig. 4.1(c), where an intermediate SSB phase sets in. A mean-field analysis based on the Fermi liquid fixed point shows that there are two degenerated leading instabilities: (i) the inter-layer exciton condensation (EC) and (ii) the inter-layer superconductivity (SC). They are respectively described by the following order parameters

$$\phi_{\text{EC}} = \sum_{i,\sigma} (-)^i c_{i1\sigma}^\dagger c_{i2\sigma}, \quad \phi_{\text{SC}} = \sum_{i,\sigma} (-)^\sigma c_{i1\sigma}^\dagger c_{i2\bar{\sigma}}^\dagger. \tag{4.6}$$

114

Here, $(-)^i$ denotes the stagger sign on the square lattice of lattice momentum (π, π). $(-)^\sigma = +1$ for $\sigma = \uparrow$ and -1 for $\sigma = \downarrow$. $\bar{\sigma}$ stands for the opposite spin of σ.

The energetic degeneracy of these two SSB orders can be explained by the fact that their order parameters ϕ_{EC} and ϕ_{SC} are related by a particle-hole transformation $c_{i2\sigma} \to (-)^i(-)^\sigma c_{i2\bar{\sigma}}^\dagger$ in the second layer only, which is a symmetry of the model Hamiltonian in Eq. (4.3). The EC $\langle \phi_{EC} \rangle \neq 0$ spontaneously breaks the translation and interlayer $U(1)$ symmetry, and the SC $\langle \phi_{SC} \rangle \neq 0$ spontaneously breaks the total $U(1)$ symmetry. Both of them gap out the Fermi surfaces fully, leading to an SSB insulator (or superconductor). The SSB and SMG phases are likely separated by an XY transition, at which the symmetry gets restored. We will leave the numerical verification of the proposed phase diagram Fig. 4.1(c) for future study, as the main focus of this research is to investigate the structure of fermion Green's function in the SMG insulating phase.

We note that the model Eq. (4.3) was also introduced as the "coupled ancilla qubit" model to describe the pseudo-gap physics in the recent literature [458, 457, 295]. Its honeycomb lattice version has been investigated in recent numerical simulations [176], where a direct quantum phase transition between semimetal and insulator phases was observed.

4.2.2 Luttinger Theorem and Green's Function Zeros

The Luttinger theorem [260, 259] asserts that in a fermion many-body system with lattice translation and charge $U(1)$ symmetries, the ground state charge density $\langle N \rangle / V$ (i.e., the $U(1)$ charge per unit cell) is tied to the momentum space volume in which the real part of the zero-frequency fermion Green's function is positive $\mathrm{Re}\, G(0, \boldsymbol{k}) > 0$. This can be formally expressed as

$$\frac{\langle N \rangle}{V} = N_f \int_{\mathrm{Re}\, G(0,\boldsymbol{k})>0} \frac{\mathrm{d}^2 \boldsymbol{k}}{(2\pi)^2}. \tag{4.7}$$

Here, the $U(1)$ symmetry generator $N = \sum_{i,l,\sigma} c_{il\sigma}^\dagger c_{il\sigma}$ measures the total charge, and the volume $V = \sum_i 1$ is defined as the number of unit cells in the lattice system. $N_f = 4$ counts the fermion

flavor number (or the Fermi surface degeneracy), including two layers and two spins. The Green's function $G(\omega, \boldsymbol{k})$ in Eq. (4.7) is defined by the fermion two-point correlation as

$$\langle c_{l\sigma}(\omega, \boldsymbol{k}) c_{l'\sigma'}(\omega, \boldsymbol{k})^{\dagger} \rangle = G(\omega, \boldsymbol{k}) \delta_{ll'} \delta_{\sigma\sigma'}. \tag{4.8}$$

The correlation function is proportional to an identity matrix in the flavor (layer-spin) space because of the layer $U(1): c_{l\sigma} \to e^{(-)^l i\theta} c_{l\sigma}$, the layer interchange $\mathbb{Z}_2 : c_{1\sigma} \leftrightarrow c_{2\sigma}$, and the spin $SU(2): c_{l\sigma} \to (e^{i\boldsymbol{\theta} \cdot \boldsymbol{\sigma}/2})_{\sigma\sigma'} c_{l\sigma'}$ symmetries.

The Luttinger theorem applies to the Fermi liquid and SMG states in the bilayer square lattice model Eq. (4.3), as both states preserve the translation and charge $U(1)$ symmetries. Given that the fermions are half-filled ($\nu = 1/2$) in the system, the Fermi volume should be

$$\int_{\mathrm{Re}\, G(0,\boldsymbol{k})>0} \frac{\mathrm{d}^2 \boldsymbol{k}}{(2\pi)^2} = \frac{\langle N \rangle}{V N_f} = \nu = \frac{1}{2}. \tag{4.9}$$

The Fermi volume is enclosed by the Fermi surface, across which $\mathrm{Re}\, G(0, \boldsymbol{k})$ changes sign. The sign change can be achieved either by poles or zeros in the Green's function.

In the Fermi liquid state, the required Fermi volume is satisfied via Green's function poles along the Fermi surface, as pictured in Fig. 4.1(b). However, the SMG insulator is a fully gapped state of fermions that has no low-energy quasi-particles (below the energy scale J). Consequently, the Green's function $G(\omega, \boldsymbol{k})$ cannot develop poles at $\omega = 0$, meaning the required Fermi volume can only be satisfied by Green's function zeros. Therefore, the Lutinger theorem implies that there must be robust Green's function zeros at low energy in the SMG phase, and the zero Fermi surface must enclose half of the Brillouin zone volume in place of the original pole Fermi surface.

It is known that the Luttinger theorem can be violated in the presence of topological order [349, 351, 305, 301, 290, 82, 337, 329, 53, 358]. However, this concern does not affect our discussion in the SMG phase, because the SMG insulator is a trivial insulator without topological

order.

4.2.3 Particle-Hole Symmetry and Zero Fermi Surface

The Luttinger theorem only constrains the Fermi volume but does not impose requirements on the shape of the Fermi surface. However, in this particular example of the bilayer square lattice model Eq. (4.3), the system has sufficient symmetries to determine even the shape of the Fermi surface.

The key symmetry here is a particle-hole symmetry $\mathbb{Z}_2^C$, which acts as

$$c_{il\sigma} \to (-)^i(-)^\sigma c_{il\bar{\sigma}}^\dagger. \tag{4.10}$$

The Hamiltonian H in Eq. (4.3) is invariant under this transformation. Since the Green's function is an identity matrix in the flavor space Eq. (4.8) which is invariant under any flavor basis transformation, we can omit the flavor indices and focus on the frequency-momentum dependence of the Green's function, written as

$$G(\omega, \mathbf{k}) = \sum_{t,\mathbf{x},t',\mathbf{x}'} \langle c(t,\mathbf{x})c(t',\mathbf{x}')^\dagger \rangle e^{i(\omega(t-t') - \mathbf{k}\cdot(\mathbf{x}-\mathbf{x}'))}. \tag{4.11}$$

Given Eq. (4.10), the fermion field $c(t,\mathbf{x})$ transforms under the $\mathbb{Z}_2^C$ symmetry as

$$c(t,\mathbf{x}) \to c(t,\mathbf{x})^\dagger e^{i\mathbf{Q}\cdot\mathbf{x}}, \quad c(t,\mathbf{x})^\dagger \to c(t,\mathbf{x})e^{-i\mathbf{Q}\cdot\mathbf{x}}, \tag{4.12}$$

where $\mathbf{Q} = (\pi, \pi)$ is the momentum associated with the stagger sign factor $(-)^i$ on the square lattice. As a consequence, the Green's function transforms as

$$G(\omega, \mathbf{k}) \to -G(-\omega, \mathbf{Q} - \mathbf{k}). \tag{4.13}$$

Furthermore, there are also two diagonal reflection symmetries on the square lattice, which maps

$\boldsymbol{k} = (k_x, k_y)$ to (k_y, k_x) or $(-k_y, -k_x)$ in the momentum space.

Both the Fermi liquid and the SMG states preserve the particle-hole symmetry $\mathbb{Z}_2^C$ and the lattice reflection symmetry, which requires the Green's function to be invariant under the combined symmetry transformations. So the zero-frequency Green's function must satisfy

$$G(0, k_x, k_y) = -G(0, \pi \pm k_y, \pi \pm k_x), \qquad (4.14)$$

meaning that the sign change of $G(0, \boldsymbol{k})$ should happen along $k_x \pm k_y = \pi \mod 2\pi$, which precisely describes the shape of the Fermi surface. The Fermi surface is pole-like in the Fermi liquid state and becomes zero-like in the SMG state, but its shape and volume remain the same.

However, it should be noted that the precise overlap of the zero Fermi surface in the SMG insulator and the pole Fermi surface in the Fermi liquid is a fine-tuned feature of the bilayer square lattice model Eq. (4.3). In more general cases, such as including further neighbor hopping in the model, the particle-hole symmetry would cease to exist, thus the invariance in the shape of the Fermi surface is no longer guaranteed. Nevertheless, the Luttinger theorem can still ensure the invariance in the Fermi volume, thereby providing the SMG insulator with robust Green's function zeros.

To verify this proposition, we will analyze the behavior of the Green's function in the SMG phase from both strong and weak coupling perspectives in Sec. 4.3. Our calculations suggest that, for this specific model, the SMG state indeed possesses a Fermi surface (of Green's function zeros) that is identical in shape to that in the Fermi liquid state.

4.3 Evidence of Green's Function Zeros

4.3.1 Strong Coupling Analysis

We will first focus on the strong interaction limit ($J/t \to \infty$), where the system is deep in the SMG phase and the exact ground state is known (see Eq. (4.5)). We start from this limit and turn on the hopping term as a perturbation. We employ exact diagonalization and

cluster perturbation theory (CPT) [345, 346] to compute the Green's function in the SMG phase. The details of our method are described in Appendix D.1. It is valid to use a small cluster to reconstruct the Green's function in the SMG phase since the ground state is close to a product state that does not have long-range correlation or long-range quantum entanglement. This is quite different from the Hubbard model, where the Fermi surface anomaly is non-vanishing, and the infrared phase must be either SSB order or topological order [349, 301, 290, 82]. In either case, the ground state wave functions cannot be reconstructed from the small clusters due to the long-range correlation/entanglement. This argument has been noted in the original paper on the CPT method [345].
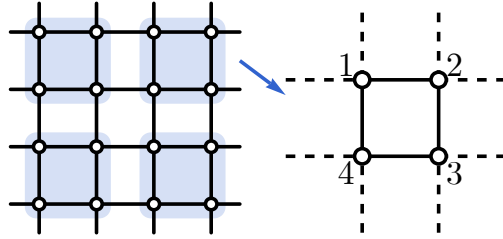
Figure 4.2. Partition the square lattice into 2×2 clusters. The many-body Hamiltonian is exactly diagonalized within each cluster. The effect of inter-cluster hopping is included in an RPA-like approach.

To be specific, we first partition the square lattice (including both layers) into 2×2 square clusters as shown in Fig. 4.2. Let us first ignore the inter-cluster hopping. Within each cluster, we represent the Hamiltonian in the many-body Hilbert space and use the Lanczos method to obtain the lowest ~ 2000 eigenvalues and eigenvectors. The Green's function in the cluster can then be obtained by the Källén–Lehmann representation

$$G_0(\omega)_{ij} = \sum_{m>0} \frac{\langle 0| c_i |m\rangle \langle m| c_j^\dagger |0\rangle}{\omega - (E_m - E_0)} + \frac{\langle m| c_i |0\rangle \langle 0| c_j^\dagger |m\rangle}{\omega + (E_m - E_0)}, \tag{4.15}$$

where $|m\rangle$ is the mth excited state with energy E_m, and $|0\rangle$ is the ground state with energy E_0, whose wave function was previously given in Eq. (4.5). Since the four fermion flavors (two spins

and two layers) are identical under the internal flavor symmetry, we can drop the flavor index in the Green's function and only focus on one particular flavor with the site indices i, j, where $i, j = 1, 2, 3, 4$ as indicated in Fig. 4.2. The convergence of the Green's function can be verified by including more eigenstates from the Lanczos method. We checked that increasing the number of eigenpairs to ~ 8000 will not change the result significantly, indicating that the result with ~ 2000 eigenpairs has already converged.

Now we restore the inter-cluster hoping to extend the Green's function from small clusters to the infinite lattice. The Green's function of super-lattice momentum $\boldsymbol{k}$ can be obtained from the random phase approximation (RPA) approach [345],

$$G(\omega, \boldsymbol{k})_{ij} = \left(\frac{G_0(\omega)}{1 - T(\boldsymbol{k}) G_0(\omega)} \right)_{ij}, \tag{4.16}$$

where the $T(\boldsymbol{k})$ matrix

$$T(\boldsymbol{k}) = -t \begin{pmatrix} 0 & e^{-i2k_x} & 0 & e^{i2k_y} \\ e^{i2k_x} & 0 & e^{i2k_y} & 0 \\ 0 & e^{-i2k_y} & 0 & e^{i2k_x} \\ e^{-i2k_y} & 0 & e^{-i2k_x} & 0 \end{pmatrix} \tag{4.17}$$

describes the inter-cluster fermion hopping. The resulting Green's function $G(\omega, \boldsymbol{k})_{ij}$ is defined in the folded Brillouin zone $\boldsymbol{k} \in (-\pi/2, \pi/2]^{\times 2}$ with sub-lattice indices i, j. To unfold the Green's function to the original Brillouin zone $\boldsymbol{k} \in (-\pi, \pi]^{\times 2}$, we perform the following (partial) Fourier transform

$$G(\omega, \boldsymbol{k}) = \frac{1}{L} \sum_{i,j} e^{-i\boldsymbol{k} \cdot (\boldsymbol{r}_i - \boldsymbol{r}_j)} G(\omega, \boldsymbol{k})_{ij}. \tag{4.18}$$

We numerically calculated the unfolded Green's function $G(\omega, \boldsymbol{k})$ using the above-mentioned cluster perturbation method. We take a large interaction strength $J/t = 8$ deep in the SMG phase and present the resulting Green's function in Fig. 4.3. From Fig. 4.3(a), the poles of
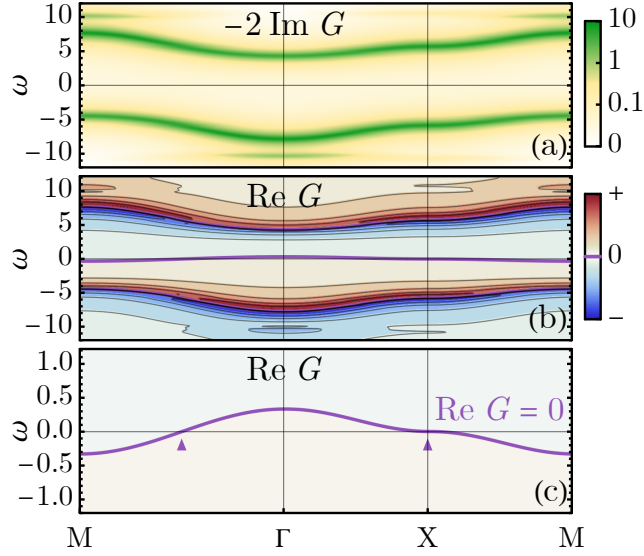
Figure 4.3. Fermion Green's function Eq. (4.18) deep in the SMG insulator phase, at $J = 8t$. (a) The imaginary part (spectral function) $-2\,\mathrm{Im}\,G(\omega + \mathrm{i}0_+, \boldsymbol{k})$ shows the pole (spectral peak) structure. (b) The real part $\mathrm{Re}\,G(\omega, \boldsymbol{k})$ shows the pole (divergence) and zero (purple contour) structures. (c) Same as (b) but zoomed in near $\omega = 0$ to show the dispersion of Green's function zeros.

the Green's function form two dispersing bands around $\omega = \pm J$, which resembles the upper and lower Hubbard bands in the Hubbard model. This indicates the quasi-particles are fully gapped in the SMG phase. Meanwhile, from Fig. 4.3(b,c), the zeros of the Green's function appear around $\omega = -\alpha\varepsilon_{\boldsymbol{k}}/J^2$ with some non-universal but positive coefficient $\alpha > 0$. We find that the "dispersion" of zeros is reversed compared to the original band dispersion $\varepsilon_{\boldsymbol{k}}$. In Fig. 4.4, we also numerically confirmed that the "bandwidth" w_{zero} of zeros is suppressed by the interaction J as $w_{\mathrm{zero}} \sim J^{-2}$ as $J \to \infty$.

Building upon the above observation of the poles and zeros of the Green's function, we put forth the following empirical formula:

$$G_{\mathrm{SMG}}(\omega, \boldsymbol{k}) = \frac{\omega + \alpha\varepsilon_{\boldsymbol{k}}/J^2}{(\omega - \varepsilon_{\boldsymbol{k}}/2)^2 - J^2}, \tag{4.19}$$

as an approximate description of our numerical result Eq. (4.18). An important aspect of this
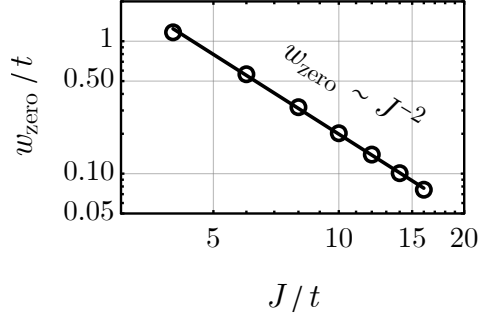
Figure 4.4. Scaling of the Green's function zero "bandwidth" w_{zero} with the interaction strength J. Circles represent the numerically calculated w_{text} at different J, and the line is a fit to the data.

formula is the positioning of the Green's function zeros precisely around the initial Fermi surface (where $\varepsilon_{\boldsymbol{k}} = 0$) at $\omega = 0$. This is indicated by the small arrows in Fig. 4.3(c).

Assuming $\text{Re}\,G_{\text{SMG}}(0, \boldsymbol{k}) = 0$ as the definition of the zero Fermi surface in the SMG phase, it would encompass the same Fermi volume as the pole Fermi surface in the Fermi liquid phase. As both translation and charge conservation symmetries remain unbroken in the SMG phase, the Luttinger theorem mandates the preservation of the Fermi volume. Given that the SMG state is a fully gapped trivial insulator, there is no pole (no quasi-particle) at low energy, thus the Green's function can only rely on zeros to fulfill the Fermi volume required by the Luttinger theorem, which is explicitly demonstrated by Eq. (4.19).

4.3.2 Weak Coupling Analysis

Nevertheless, SMG is not the sole mechanism for gapping out the Fermi surface. SSB might also open a full gap on the Fermi surface, which corresponds to the Higgs mechanism for fermion mass generation. Specifically, in the bilayer square lattice model Eq. (4.3), due to the perfect nesting of the Fermi surface, the Fermi liquid exhibits strong instability toward SSB orders. Without loss of generality, we will focus on the inter-layer exciton condensation in the weak coupling limit. The corresponding order parameter ϕ_{EC} was introduced in Eq. (4.6), which carries momentum $\boldsymbol{Q} = (\pi, \pi)$. The exciton condensation leads to an SSB insulating phase, as noted in the phase diagram Fig. 4.1(c). However, there are significant differences between the

SMG insulator and the SSB insulator, especially in terms of the structure of Green's function zeros.
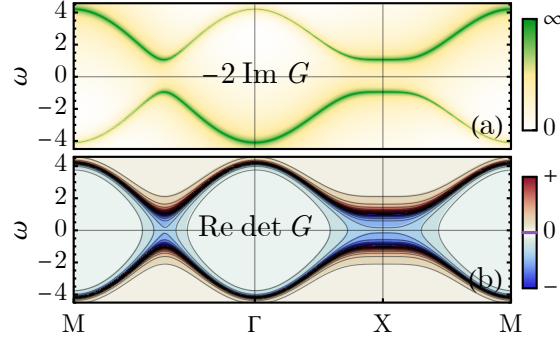
Figure 4.5. Fermion Green's function Eq. (4.20) G_{SSB} in the SSB insulator phase, assuming a gap size of $|\Delta| = t$. (a) The imaginary part $-2\,\mathrm{Im}\,G(\omega + \mathrm{i}0_+, \boldsymbol{k})_{11}$ in the $\langle c_{\boldsymbol{k}}^\dagger c_{\boldsymbol{k}} \rangle$ channel, showing the pole (quasi-particle peak) along gapped bands. (b) The real part of the determinant $\mathrm{Re}\det G(\omega, \boldsymbol{k})$. No zero within the gap. In both plots, the frequency is shifted by a small imaginary part $\omega \to \omega + 0.01\mathrm{i}t$ for better visualization of spectral features.

In the SSB insulator phase, the Brillouin zone folds by the nesting vector $\boldsymbol{Q} = (\pi, \pi)$. The fermion Green's function can be written in the $(c_{\boldsymbol{k}}, c_{\boldsymbol{k}+\boldsymbol{Q}})^\mathsf{T}$ basis (omitting layers and spins freedom) as

$$G_{SSB}(\omega, \boldsymbol{k}) = \frac{\omega\sigma^0 + \varepsilon_{\boldsymbol{k}}\sigma^3 + \mathrm{Re}\,\Delta\sigma^1 + \mathrm{Im}\,\Delta\sigma^2}{\omega^2 - \varepsilon_{\boldsymbol{k}}^2 - |\Delta|^2}, \tag{4.20}$$

where $\Delta = J\langle\phi_{EC}\rangle$ denotes the exciton gap induced by the exciton condensation $\langle\phi_{EC}\rangle \neq 0$. The properties of G_{SSB} are illustrated in Fig. 4.5. The spectral function in Fig. 4.5(a) depicts the quasi-particle peak along the band dispersion, reflecting a gapped (insulating) band structure.

Since G_{SSB} is a matrix, its zero structure should be defined by its determinant being zero, i.e., $\det G_{SSB}(\omega, \boldsymbol{k}) = 0$, which is the only way to define the zero structure in a basis independent manner. Fig. 4.5(b) indicates the determinant of G_{SSB} remains the same sign within the band gap induced by the exciton condensation. Since G_{SSB} does not preserve the translation symmetry (as $\Delta \to -\Delta$ is translation-odd), and Δ is non-zero, $\det G_{SSB}$ does not have zeros crossing $\omega = 0$ at the original Fermi surface. These two observations are linked: the absence of translation symmetry makes the Luttinger theorem ineffective, hence there is no expectation for the zero

Fermi surface in the SSB insulator.

As the interaction J intensifies, the SSB insulator ultimately transitions into the SMG insulator, as depicted in the phase diagram Fig. 4.1(c). During this transition, the broken symmetry is restored, yet the fermion excitation gap remains intact, similar to the pseudo-gap phenomenon seen in correlated materials [230, 209]. In the context of modeling fermion spectral functions, the pseudo-gap phenomenon can be interpreted as a consequence of the phase (or orientation) fluctuations of fermion bilinear order parameters [131, 225, 226, 132, 99, 233, 234, 438]. In this picture, the order parameter $\Delta = \Delta_0 e^{i\theta}$ maintains a finite amplitude Δ_0 as we enter the SMG phase from the adjacent SSB phase, but its phase θ is disordered by long-wavelength random fluctuations. Consequently, on the large scale, Δ cannot condense to form long-range order; but on a smaller scale, Δ_0 still provides a local excitation gap everywhere for fermions.

Based on this picture of the SMG state, the simplest treatment is to focus on the long wavelength fluctuation of Δ and estimate its self-energy correction for the fermion by

$$\Sigma(\omega, \mathbf{k}) = \overset{\frown}{\bullet\!\!-\!\!\bullet} = \underset{\Delta}{\mathbb{E}} \hat{\Delta}^\dagger G_0(\omega, \mathbf{k}) \hat{\Delta} = \frac{\Delta_0^2}{\omega \sigma^0 + \varepsilon_{\mathbf{k}} \sigma^3}, \tag{4.21}$$

where the vertex operator is $\hat{\Delta} := \mathrm{Re}\Delta \sigma^1 + \mathrm{Im}\Delta \sigma^2$ and the bare Green's function is $G_0(\omega, \mathbf{k}) = (\omega \sigma^0 - \varepsilon_{\mathbf{k}} \sigma^3)^{-1}$. Here we have assumed that the correlation length ξ of the bosonic field Δ is long enough that its momentum is negligible for fermions. This assumption is valid near the transition to the SSB phase, as the correlation length diverges ($\xi \to \infty$) at the transition.

Using this self-energy to correct the bare Green's function, we obtain

$$\begin{aligned} G(\omega, \mathbf{k}) &= (G_0(\omega, \mathbf{k})^{-1} - \Sigma(\omega, \mathbf{k}))^{-1} \\ &= \frac{\omega \sigma^0 + \varepsilon_{\mathbf{k}} \sigma^3}{\omega^2 - \varepsilon_{\mathbf{k}}^2 - \Delta_0^2}. \end{aligned} \tag{4.22}$$

Since the translation symmetry has been restored in the SMG phase, we can unfold the Green's

function back to the original Brillouin zone (by taking the $G(\omega, \boldsymbol{k})_{11}$ component), which leads to a weak coupling description of the Green's function in the shallow SMG phase near the transition to the SSB phase

$$G'_{\text{SMG}}(\omega, \boldsymbol{k}) = \frac{\omega + \varepsilon_{\boldsymbol{k}}}{\omega^2 - \varepsilon_{\boldsymbol{k}}^2 - \Delta_0^2}. \tag{4.23}$$

A more rigorous treatment of a similar problem can be found in Ref. [409], which includes finite momentum fluctuations of Δ. The major effect of these fluctuations is to introduce a spectral broadening for the fermion Green's function as if replacing $\omega \to \omega + i\delta$ in Eq. (4.23). It was also found that the broadening $\delta \sim \xi^{-1}$ scales inversely with the correlation length ξ of the order parameter, which justifies our simple treatment in the large-ξ regime. Similar Green's functions as Eq. (4.23) was previously constructed to describe non-Fermi liquid [118] statisfying the Luttinger theorem. However, its physical meaning is now clarified as Green's function in the SMG phase.
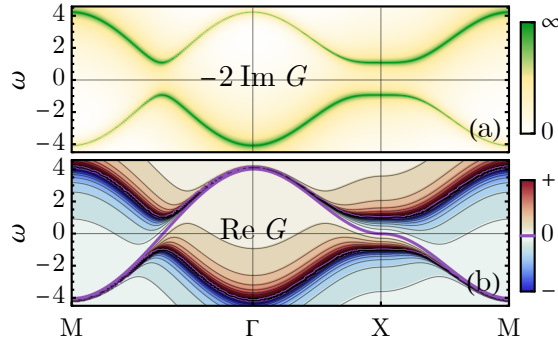
Figure 4.6. Fermion Green's function Eq. (4.23) G'_{SMG} in the SMG insulator phase near the phase transition to an adjacent SSB phase, assuming a local gap size of $\Delta_0 = t$. (a) The imaginary part (spectral function) $-2\operatorname{Im} G(\omega + i0_+, \boldsymbol{k})$ shows the pole (quasi-particle peak) along gapped bands. (b) The real part $\operatorname{Re} G(\omega, \boldsymbol{k})$ exhibits the zero (purple contour) crossing $\omega = 0$ at the original Fermi surface. In both plots, the frequency is shifted by a small imaginary part $\omega \to \omega + 0.01 it$ for better visualization of spectral features.

The features of G'_{SMG} in Eq. (4.23) are presented in Fig. 4.6. When comparing Fig. 4.6(a) and Fig. 4.5(a), we can observe that the pole structure of G'_{SMG} is identical to that of G_{SSB} (in the diagonal component), both showcasing a gapped spectrum. However, they significantly

differ in their zero structures, as seen by comparing Fig. 4.6(b) and Fig. 4.5(b). Due to the restoration of symmetry, the low-energy zeros reemerge in the Green's function in the SMG phase. Additionally, its zero Fermi surface perfectly aligns with the original pole Fermi surface, fulfilling the Luttinger theorem's requirement for the Fermi volume.

Comparing the Green's function in the SMG phase derived from the strong coupling analysis Eq. (4.19) and the weak coupling analysis Eq. (4.23) (see also Fig. 4.3 and Fig. 4.6), we find that despite the apparent difference in high-energy spectral features, the zero Fermi surface defined by $G(0, \boldsymbol{k}) = 0$ remains a resilient low-energy feature. The persistent zero Fermi surface in the SMG phase is a consequence of the Luttinger theorem.

Nonetheless, besides the low-energy zero structure, it is also intriguing to understand how the high-energy spectral feature deforms from the weak coupling case to the strong coupling case. However, this problem requires non-perturbative numerical simulations. Fortunately, the bilayer square lattice model Eq. (4.3) admits a sign-problem-free [382] quantum Monte Carlo [142, 334, 44, 172, 171] simulation. We will leave this interesting direction for future research.

4.4   Probing Green's Function Zeros

While Green's function zeros are an important feature of the SMG insulator, they are not directly observable in experiments. Spectroscopy experiments, such as angle-resolved photoemission spectroscopy (ARPES), can directly probe the fermion's spectral function $A(\omega, \boldsymbol{k}) = -2 \operatorname{Im} G(\omega + \mathrm{i}0_+, \boldsymbol{k})$, which is the imaginary part of Green's function. By employing the Kramers-Kronig (KK) relation to recover the real part of Green's function from the spectral function,

$$\operatorname{Re} G(\omega, \boldsymbol{k}) = \frac{1}{2\pi} \mathscr{P} \int d\omega' \frac{A(\omega', \boldsymbol{k})}{\omega' - \omega}, \tag{4.24}$$

we can indirectly study the zero structure of the Green's function.

However, the spectral function might be broadened in experimental data due to noise or dissipation. We are interested in studying how sensitive the reconstructed Green's function

126
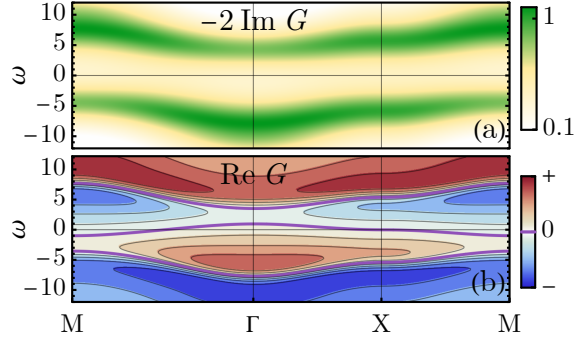
Figure 4.7. (a) Broadened spectral function from the one in Fig. 4.3. (b) Reconstructed Green's function real part by the KK relation, showing robust Green's function zeros (purple contour) crossing $\omega = 0$.

zero is to these disturbances, in order to understand the stability of the method. Following Sec. 4.3.1, we start from the strong coupling limit and use the CPT approach to calculate Green's function. To account for the spectral broadening effect, we replace ω with $\omega + i\delta$, where δ is relatively large, say, about the order of the hopping t. Based on the broadened spectral function in Fig. 4.7(a), we use the KK relation to reconstruct the real part, as shown in Fig. 4.7(b). We find that the zero Fermi surface maintains the same shape, but the zero "dispersion" bandwidth gets larger.

The increase in bandwidth can be understood by taking the SMG Green's function $G_{\mathrm{SMG}}(\omega, \boldsymbol{k})$ in Eq. (4.19), and solving for its zeros $\mathrm{Re}\,G(\omega + i\delta, \boldsymbol{k}) = 0$. To the leading order of $1/J$ and δ, the solution is given by

$$\omega(\boldsymbol{k}) = -\left(1 + \frac{\delta^2}{\alpha}\right)\frac{\alpha\varepsilon_{\boldsymbol{k}}}{J^2} + \cdots,\tag{4.25}$$

meaning that the bandwidth of Green's function zero dispersion will increase by δ^2/α, but the corresponding Luttinger surface remains unchanged. Therefore, the Green's function zero in the SMG phase is a robust feature that can be potentially identified from spectroscopy measurements, even in the presence of noises or dissipations.

4.5 Summary and Discussions

In this paper, we investigated the Fermi surface SMG in a bilayer square lattice model. A crucial finding of this study lies in the robust Green's function zero in the SMG phase. Traditionally, a Fermi liquid state is characterized by poles in the Green's function along the Fermi surface. However, as the fermion system is driven into the SMG state by interaction effects, these poles are replaced by zeros. This is a robust phenomenon underlined by the constraints of the Luttinger theorem.

Our exploration is not limited to theoretical assertions. We also offer a tangible demonstration of this occurrence in the bilayer square lattice model. By applying both strong and weak coupling analyses, we provide a comprehensive portrayal of the fermion Green's function across different interaction regimes. We highlight that the emergence of the zero Fermi surface is not an ephemeral or fine-tuned phenomenon, but rather a robust and enduring feature of the SMG phase. We show that even when the system is subjected to spectral broadening, the zero Fermi surface persists, retaining the Fermi volume.

The results of this study confirm the robustness of the zero Fermi surface and underscore the possibility of observing it in experimental setups, such as through ARPES. Despite not being directly observable, the zero structure of the Green's function could be inferred indirectly via the KK relation.

The bilayer square lattice model may be relevant to the nickelate superconductor recently discovered in pressurized $La_3Ni_2O_7$ [368, 175], which is a layered two-dimensional material where each layer consists of nickel atoms arranged in a bilayer square lattice. The Fermi surface is dominated by d_{z^2} and $d_{x^2-y^2}$ electrons of Ni. The d_{z^2} electron has a relatively small intra-layer hopping t due to the rather localized d_{z^2} orbital wave function in the xy-plane but enjoys a large interlayer antiferromagnetic Heisenberg interaction J due to the super-exchange mechanism mediated by the apical oxygen. This likely puts the d_{z^2} electrons in an SMG insulator phase in the bilayer square lattice model and opens up opportunities to investigate the proposed Green's

function zeros in real materials. The potential implication of SMG physics on the nickelate high-T_c superconductor still requires further theoretical research in the future.

Chapter. 4, in full, is a reprint of the material as it appears in Da-Chuan Lu, Meng Zeng, and Yi-Zhuang You. Green's function zeros in Fermi surface symmetric mass generation. *Physical Review B*, 108(20):205117, November 2023. The dissertation author was the primary investigator and author of this paper.

Chapter 5

Self-duality under gauging a non-invertible symmetry

We discuss two-dimensional conformal field theories (CFTs) which are invariant under gauging a non-invertible global symmetry. At every point on the orbifold branch of $c = 1$ CFTs, it is known that the theory is self-dual under gauging a $\mathbb{Z}_2 \times \mathbb{Z}_2$ symmetry, and has $\mathrm{Rep}(H_8)$ and $\mathrm{Rep}(D_8)$ fusion category symmetries as a result. We find that gauging the entire $\mathrm{Rep}(H_8)$ fusion category symmetry maps the orbifold theory at radius R to that at radius $2/R$. At $R = \sqrt{2}$, which corresponds to two decoupled Ising CFTs (Ising^2 in short), the theory is self-dual under gauging the $\mathrm{Rep}(H_8)$ symmetry. This implies the existence of a topological defect line in the Ising^2 CFT obtained from half-space gauging of the $\mathrm{Rep}(H_8)$ symmetry, which commutes with the $c = 1$ Virasoro algebra but does not preserve the fully extended chiral algebra. We bootstrap its action on the $c = 1$ Virasoro primary operators, and find that there are no relevant or marginal operators preserving it. Mathematically, the new topological line combines with the $\mathrm{Rep}(H_8)$ symmetry to form a bigger fusion category which is a $\mathbb{Z}_2$-extension of $\mathrm{Rep}(H_8)$. We solve the pentagon equations including the additional topological line and find 8 solutions, where two of them are realized in the Ising^2 CFT. Finally, we show that the torus partition functions of the Monster^2 CFT and Ising$\times$Monster CFT are also invariant under gauging the $\mathrm{Rep}(H_8)$ symmetry.

5.1   Introduction

Given a quantum field theory (QFT), it is a useful strategy to first analyze in detail its global symmetries and 't Hooft anomalies, before one asks more difficult dynamical questions (for instance, its long-distance behavior). The understanding of the former can drastically constrain the possible answers to the latter [370]. The advent of generalized global symmetries [145] has increased the power of symmetries and one's ability to constrain possible answers to the dynamical questions in QFTs. At the same time, a new challenging quest emerges, which is to effectively discover new generalized symmetries in familiar and important classes of QFTs. The task of finding all the generalized global symmetries of a given QFT turns out to be a difficult one, and to date there is no systematic way to achieve such a goal for generic QFTs. See [268, 96, 155, 49, 258, 335, 36, 355] for recent reviews on generalized global symmetries.

This paper focuses on finite generalized symmetries in 1+1d CFTs described by fusion categories [39, 70].[1] Such symmetries are generated by topological defect lines, which commute with both the left- and right-moving Virasoro algebras (also known as totally transmissive defects). Topological defect lines in 1+1d CFTs have been studied extensively, with various applications and perspectives. See, for instance, [39, 70, 386, 299, 300, 309, 137, 138, 139, 3, 2, 280, 141, 60, 50, 379, 98, 241, 304, 218, 69, 378, 181, 54, 199, 240, 68, 249, 197, 454, 243, 320, 90, 26, 164, 385, 115, 75, 282, 38, 37, 180, 357].

Other than topological quantum field theories (TQFTs), the only QFTs for which the full set of generalized symmetries is known are the Virasoro minimal model CFTs, whose central charge $c < 1$. Perhaps the next simplest class of QFTs for which one may hope to classify all the generalized symmetries would be the $c = 1$ CFTs [150], which includes free compact boson and its orbifold. They play an important role both in condensed matter physics and in string theory. For instance, the orbifold branch of $c = 1$ describes the critical line on the phase diagram

---

[1]We focus on internal symmetries, and do not consider spacetime symmetries such as time-reversal. Also, we always work with unitary, compact, bosonic CFTs with a unique vacuum.

of the Ashkin-Teller model on the lattice [11, 216, 330, 149]. The Ashkin-Teller model is widely used to describe 1+1d deconfined quantum critical points [194, 179, 455], SPT transitions [387, 376, 311] and edges of 2+1d gauge theories [333, 462, 361].

Many topological defect lines are known for $c = 1$ CFTs [378, 140, 17, 27, 188], and in particular, [378] provides a zoo of fusion category symmetries at $c = 1$. However, the full classification of topological defect lines at $c = 1$ is not yet accomplished. It is interesting to study the origin and physical consequences of these topological defect lines in concrete models, and also to discover new ones.

Below, we find a new topological defect line at $c = 1$, at a point on the orbifold branch of the moduli space of $c = 1$ CFTs where the theory is described by two decoupled Ising CFTs (Ising^2 in short). Our finding is based on a generalized version of the "half-space gauging," discussed in [378, 88, 87] (see also [217, 198]). Given a QFT in arbitrary spacetime dimensions which is self-dual under gauging a discrete symmetry, which we may call the "parent" symmetry, one can construct a codimension-1 topological defect by gauging the parent symmetry in only half of spacetime. The resulting codimension-1 topological defect obeys a universal non-invertible fusion algebra, generating a "child" non-invertible symmetry. The most standard example of such a construction is in the 1+1d Ising CFT, where the parent symmetry is the $\mathbb{Z}_2$ spin-flip symmetry, and the child non-invertible symmetry is generated by the Kramers-Wannier duality defect line [299, 300, 309, 137, 138, 139, 3, 2, 342].

In the known examples of half-space gauging, the parent symmetry is generally a discrete, invertible (higher-form) symmetry, whereas the child symmetry is non-invertible. Below, we discuss a generalization of this, where the parent symmetry is also non-invertible, and described by a fusion category $\mathscr{C}$. Given a 1+1d QFT which is self-dual under gauging a fusion category symmetry $\mathscr{C}$, we claim that one can construct a new topological defect line obtained by gauging $\mathscr{C}$ in only half of spacetime. We elaborate on this more in Section 5.3, and briefly summarize it below.

Let $\{\mathscr{L}_i\}$ be the set of simple topological lines in $\mathscr{C}$. By "gauging $\mathscr{C}$," we always mean

132

that we gauge an algebra object of the form

$$\mathscr{A} = \bigoplus_i \langle \mathscr{L}_i \rangle \mathscr{L}_i. \tag{5.1}$$

where $\langle \mathscr{L}_i \rangle$ is the quantum dimension of the line $\mathscr{L}_i$. There exists an algebra object of the form (5.1) which can be gauged if and only if the fusion category symmetry $\mathscr{C}$ can be realized in a trivially gapped phase, namely if $\mathscr{C}$ is anomaly-free [90]. This is a generalization of the familiar fact that 't Hooft anomalies are obstruction to gauging a global symmetry, to the case of fusion category symmetries. For instance, recall that a necessary condition for the fusion category $\mathscr{C}$ to be anomaly-free is that all the quantum dimensions $\langle \mathscr{L}_i \rangle$ are non-negative integers [70], and notice that (5.1) is a well-defined object in $\mathscr{C}$ only when such a condition is satisfied. Given an anomaly-free fusion category, there may exist more than one algebra object of the form (5.1) which can be gauged, and this generalizes the choice of discrete torsion.

Now, let $\mathscr{T}$ be a 1+1d QFT with a non-anomalous fusion category symmetry $\mathscr{C}$ and an algebra object $\mathscr{A}$ of the form (5.1) which can be gauged. The partition function of the gauged theory, denoted as $\mathscr{T}/\mathscr{C}$, is obtained from that of $\mathscr{T}$ by inserting a fine mesh of the algebra object $\mathscr{A}$ across the dual triangulation of the spacetime manifold [141, 39].

Instead of gauging $\mathscr{C}$ everywhere on the spacetime manifold, we may gauge it in only half of spacetime, i.e. by inserting a mesh of the algebra object $\mathscr{A}$ in half of spacetime. This "half-space gauging" of $\mathscr{C}$ produces a topological interface between the two theories $\mathscr{T}$ and $\mathscr{T}/\mathscr{C}$.

If the theory $\mathscr{T}$ is self-dual under gauging $\mathscr{C}$, then the half-space gauging results in a topological defect line of $\mathscr{T}$, which we denote as $\mathscr{D}$. Such a topological line $\mathscr{D}$ obeys a fusion

algebra:

$$\mathscr{D} \otimes \overline{\mathscr{D}} = \mathscr{A} = \bigoplus_i \langle \mathscr{L}_i \rangle \mathscr{L}_i = \mathbb{1} \oplus \cdots , \tag{5.2}$$

$$\mathscr{D} \otimes \mathscr{L}_i = \mathscr{L}_i \otimes \mathscr{D} = \langle \mathscr{L}_i \rangle \mathscr{D} .$$

Here, $\overline{\mathscr{D}}$ is the orientation-reversal of $\mathscr{D}$. We note that the resulting line $\mathscr{D}$ is non-invertible. The quantum dimension of the line $\mathscr{D}$ is determined by the total dimension of the parent fusion category $\mathscr{C}$, namely

$$\langle \mathscr{D} \rangle = \sqrt{\sum_i \langle \mathscr{L}_i \rangle^2} . \tag{5.3}$$

As a concrete example, we discuss $c = 1$ CFTs as mentioned above. In particular, we take the CFTs on the orbifold branch of the $c = 1$ moduli space, and the "parent" fusion category symmetry to be the $\mathsf{Rep}(H_8)$ symmetry which was discussed in [378]. Here, $\mathsf{Rep}(H_8)$ denotes the representation category of a 8-dimensional Hopf algebra constructed by Kac and Paljutkin. It is also one of the Tambara-Yamagami categories based on $\mathbb{Z}_2 \times \mathbb{Z}_2$. The $\mathsf{Rep}(H_8)$ symmetry, which exists everywhere on the orbifold branch of $c = 1$, is free of an anomaly, and admits a unique algebra object of the form (5.1) which can be gauged. The simple lines of $\mathsf{Rep}(H_8)$ consist of four invertible lines $\mathbb{1}$, a, b, ab, generating a $\mathbb{Z}_2 \times \mathbb{Z}_2$ symmetry, and one non-invertible line $\mathscr{N}$, satisfying $\mathscr{N} \otimes \mathscr{N} = \mathbb{1} \oplus a \oplus b \oplus ab$.

We find that gauging the algebra object $\mathscr{A} = \mathbb{1} \oplus a \oplus b \oplus ab \oplus 2\mathscr{N}$ on the orbifold branch of $c = 1$ maps the theory at radius R to that at $2/R$, and vice versa (our convention is such that the T-duality acts as $R \leftrightarrow 1/R$). Thus, at a generic point, the orbifold CFT is not self-dual under gauging $\mathsf{Rep}(H_8)$, and instead such a gauging defines an order 2 operation on the orbfold branch. However, the special point $R = \sqrt{2}$, namely the Ising^2 CFT, remains invariant under gauging $\mathsf{Rep}(H_8)$. See Figure 5.1.

This implies the existence of a new topological defect line $\mathscr{D}$ in the Ising^2 CFT, coming
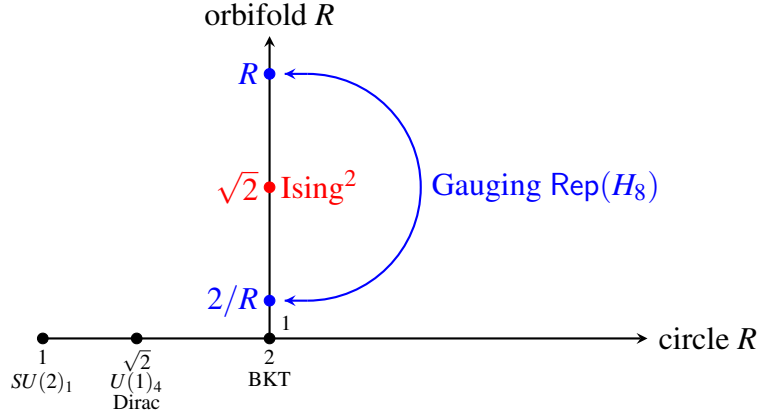
Figure 5.1. Moduli space of $c = 1$ CFTs [150]. The horizontal line is the circle branch consisting of free compact boson CFTs with radius R, and the vertical line is the orbifold branch obtained from gauging the charge conjugation symmetry of the circle branch theories. In addition, there are 3 isolated points (not shown). Along the orbifold branch, two theories at radii R and $2/R$ are related by gauging the $\mathrm{Rep}(H_8)$ symmetry, and $R = \sqrt{2}$, corresponding to the Ising^2 CFT, is a fixed point under this gauging.

from the half-space gauging of $\mathrm{Rep}(H_8)$.[2] Since gauging $\mathrm{Rep}(H_8)$ is an order 2 operation, we propose that $\mathscr{D}$ is a self-dual line, namely $\overline{\mathscr{D}} = \mathscr{D}$. This new topological line then obeys the following fusion algebra:

$$\mathscr{D} \otimes \mathscr{D} = \mathbb{1} \oplus a \oplus b \oplus ab \oplus 2\mathscr{N} \,,$$

$$\mathscr{D} \otimes g = g \otimes \mathscr{D} = \mathscr{D} \,, \tag{5.4}$$

$$\mathscr{D} \otimes \mathscr{N} = \mathscr{N} \otimes \mathscr{D} = 2\mathscr{D} \,,$$

where $g \in \{\mathbb{1}, a, b, ab\}$. In particular, $\langle \mathscr{D} \rangle = \sqrt{8} \notin \mathbb{Z}_{>0}$, implying a nontrivial anomaly of the fusion category symmetry.

The Ising^2 CFT is rational with respect to the fully extended chiral algebra, namely two copies of the Ising chiral algebra. The new topological defect line $\mathscr{D}$ does not preserve this extended chiral algebra, and only a subalgebra of it (which includes the $c = 1$ Virasoro algebra)

---

[2]This topological defect line $\mathscr{D}$ of the Ising^2 CFT can be shown to be the product of a "cosine" line [69, 378] with a Kramers-Wannier duality line from one of the Ising factors [112]. A similar comment applies to the topological line $\mathscr{D}'$ in Section 5.5 which obeys the same fusion algebra as $\mathscr{D}$. We thank Yifan Wang for discussions on this point.

is preserved.

We carefully analyze the action of this new topological line $\mathscr{D}$ on the $c = 1$ Virasoro primary operators of the Ising^2 CFT, by imposing several consistency conditions. We find that there are no relevant or marginal operators preserving $\mathscr{D}$. Furthermore, by examining the spin selection rules derived from the explicit solutions to the pentagon identities based on the fusion algebra (5.4), we determine the full fusion category structure formed by the line $\mathscr{D}$ and the original Rep(H_8) symmetry. Mathematically, the resulting fusion category is a $\mathbb{Z}_2$-extension of Rep(H_8). We find that there are 8 such $\mathbb{Z}_2$-extensions satisfying the fusion algebra (5.4), denoted as $\underline{\mathscr{E}}_{\mathbb{Z}_2}^{(i,\kappa_\mathscr{D},\varepsilon_\mathscr{D})}$Rep($H_8$) with $i, \kappa_\mathscr{D}, \varepsilon_\mathscr{D} = \pm$. Among these, the ones corresponding to $\kappa_\mathscr{D} = \varepsilon_\mathscr{D} = +$ and $i = \pm$ are physically realized in the Ising^2 CFT (related by the $\mathbb{Z}_2$ symmetry that exchanges the two Ising factors). Here, $\varepsilon_\mathscr{D}$ is the Frobenius-Schur indicator of $\mathscr{D}$.

Finally, at the level of torus partition functions, we find that the Monster^2 and Ising$\times$Monster CFTs are also self-dual under gauging Rep(H_8). The Monster CFT is a $c = 24$ holomorphic CFT with an extremely rich global symmetry group, the Monster group [136]. Similar to the Ising CFT, the Monster CFT is self-dual under gauging a $\mathbb{Z}_2$ symmetry, and has the corresponding Kramers-Wannier-like duality defect line [241]. We leave for the future more detailed studies of potential new topological defect lines coming from half-space gauging of Rep(H_8) in these additional examples.

The rest of the paper is organized as follows. In Section 5.2, we begin by reviewing several properties of topological defect lines in 1+1d, finite invertible symmetries and their (half-space) gauging, as well as group extensions of fusion categories. In Section 5.3, we generalize the half-space gauging to the case where the parent symmetry is already non-invertible. We also explain how to explicitly gauge the Rep(H_8) symmetry and compute the torus partition function of the gauged theory. In Section 5.4, we gauge the Rep(H_8) symmetry along the orbifold branch of $c = 1$, and find that the Ising^2 CFT is self-dual under this gauging. In Section 5.5, we discuss in more detail several properties of the new topological defect line in the Ising^2 CFT, including its action on the Virasoro primary operators. In Section 5.6, we discuss various other 1+1d

CFTs with the Rep(H_8) symmetry. We find that the Monster[2] and Ising×Monster CFTs are also self-dual at the level of torus partition functions. We also provide non-examples, namely theories with the Rep(H_8) symmetry which are not self-dual under gauging. Finally, in Section 5.7, we explicitly solve the pentagon identities based on the fusion algebra (5.4), and find 8 solutions. We derive the spin selection rules, which allow us to physically distinguish the 8 fusion categories. Two of them are realized in the Ising[2] CFT.

5.2 Review

We first briefly review several defining properties of topological defect lines in 1+1d CFTs [141, 39, 70] to set up the notations, as well as the half-space gauging for the case where the parent symmetry is an invertible symmetry. Finally, group extension of fusion categories [125] is also reviewed.

5.2.1 Topological defect lines in 1+1d

Topological defect lines (denoted as $\mathscr{L}$) are line operators which commute with the stress-energy tensor, and various correlation functions are invariant under local deformations of them. We focus on topological defect lines which satisfy the mathematical axioms of (unitary) fusion categories [141, 39, 70]. Such topological lines generate finite (generalized) symmetries in 1+1d.[3] For instance, we can fuse two topological lines $\mathscr{L}_a$ and $\mathscr{L}_b$ by putting them close to each other and generate a new topological line, which then in general decomposes into a finite sum of other topological lines,

$$\mathscr{L}_a \otimes \mathscr{L}_b = \bigoplus_c N_{ab}^c \mathscr{L}_c, \quad N_{ab}^c \in \mathbb{Z}_{\geq 0}. \tag{5.5}$$

The *simple* topological lines are those that cannot be written as a sum of at least two other lines. We denote the trivial topological line as $\mathbb{1}$.

---

[3]There are topological defect lines which go beyond the mathematical definition of fusion categories [69, 378], the simplest example being just an ordinary continuous symmetry in 1+1d.

When $N_{ab}^c \neq 0$, two topological lines $\mathscr{L}_a$ and $\mathscr{L}_b$ can join each other locally and become the line $\mathscr{L}_c$ at a trivalent junction. The set of topological junction operators form a vector space whose complex dimension is given by N_{ab}^c. We always fix a basis of the junction vector space and use the Greek letters $\mu, \nu, \cdots = 1, 2, \cdots, N_{ab}^c$ to denote the corresponding basis vectors.[4]

$$
\begin{array}{c}
\mathscr{L}_c \\
\mu \\
\mathscr{L}_a \qquad \mathscr{L}_b
\end{array}
\qquad , \qquad \mu = 1, 2, \cdots, N_{ab}^c .
\tag{5.6}
$$

Given three topological defect lines, there are two possible ways they can fuse together. They are related by the so-called associativity map. In the explicitly chosen basis, the associativity map is characterized by the F-symbols,

$$
\begin{array}{c}
\mathscr{L}_d \\
\nu \\
\mu \quad \mathscr{L}_e \\
\mathscr{L}_a \quad \mathscr{L}_b \quad \mathscr{L}_c
\end{array}
= \sum_{f,\rho,\sigma} \left[F_d^{abc} \right]_{(e,\mu,\nu),(f,\rho,\sigma)}
\begin{array}{c}
\mathscr{L}_d \\
\sigma \quad \mathscr{L}_f \\
\rho \\
\mathscr{L}_a \quad \mathscr{L}_b \quad \mathscr{L}_c
\end{array} .
\tag{5.7}
$$

The F-symbols satisfy the consistent conditions known as pentagon equations (our conventions follow [22]),

$$
\sum_{\delta} \left[F_e^{fcd} \right]_{(g,\beta,\gamma)(l,\nu,\delta)} \left[F_e^{abl} \right]_{(f,\alpha,\delta)(k,\mu,\lambda)}
$$
$$
= \sum_{h,\sigma,\psi,\rho} \left[F_g^{abc} \right]_{(f,\alpha,\beta)(h,\psi,\sigma)} \left[F_e^{ahd} \right]_{(g,\sigma,\gamma)(k,\rho,\lambda)} \left[F_k^{bcd} \right]_{(h,\psi,\rho)(l,\nu,\mu)} .
\tag{5.8}
$$

Fusion category symmetries are ubiquitous in 1+1d. For instance, the category Vec_G^ω describes an ordinary finite 0-form symmetry G with an 't Hooft anomaly $[\omega] \in H^3(G, U(1))$. The simple lines are labeled by group elements, $\mathscr{L}_g$ with $g \in G$, and their fusion rules are

---

[4]Later we will also use μ (and μ only) to denote the multiplication junction of an algebra object. The reader should be able to distinguish the two based on the context.
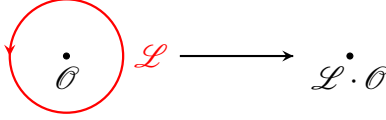
Figure 5.2. Action of a topological defect line $\mathscr{L}$ on a local operator $\mathcal{O}$. We start with the line $\mathscr{L}$ wrapping around the local operator $\mathcal{O}$. After shrinking $\mathscr{L}$, $\mathcal{O}$ is transformed by $\mathscr{L}$ to another local operator $\mathscr{L} \cdot \mathcal{O}$.
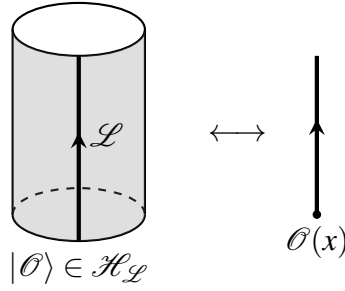
Figure 5.3. Under the state-operator correspondence, a state in the defect Hilbert space $\mathscr{H}_{\mathscr{L}}$ is mapped to a non-local operator $\mathcal{O}$ which is attached to $\mathscr{L}$.

governed by the group multiplication law, $\mathscr{L}_g \otimes \mathscr{L}_h = \mathscr{L}_{gh}$. Below, we denote the line $\mathscr{L}_g$ by the corresponding group element g for simplicity. Then, the F-symbols are given by

$$\left[F_{ghk}^{g,h,k} \right]_{gh,hk} = \omega(g,h,k). \tag{5.9}$$

The action of G on a local operator is obtained by encircling the local operator with a closed loop of g. Similarly, an arbitrary topological defect line $\mathscr{L}$ can act on a local operator $\mathcal{O}$, as shown in Figure 5.2. We denote such an action of a topological line $\mathscr{L}$ on a local operator $\mathcal{O}$ as $\mathscr{L} \cdot \mathcal{O}$.

A topological defect line $\mathscr{L}$ may end on a (non-local) operator $\mathcal{O}$, and under the state-operator map, such a non-local operator $\mathcal{O}$ is mapped to a state in the Hilbert space $\mathscr{H}_{\mathscr{L}}$ quantized on S^1 but with the boundary condition twisted by $\mathscr{L}$, see Figure 5.3. $\mathscr{H}_{\mathscr{L}}$ is known as the defect (or twisted) Hilbert space.

Topological defect lines can also act on non-local operators, via the *lasso* diagram [70, 240] in Figure 5.4. To define the action of $\mathscr{L}_2$ on a non-local operator $\mathcal{O}$ attached to
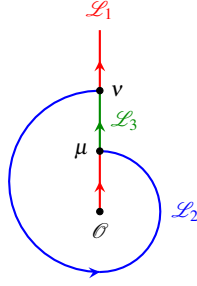
Figure 5.4. The lasso diagram describing the action of a topological defect line $\mathscr{L}_2$ on a non-local operator $\mathscr{O}$ attached to $\mathscr{L}_1$. To fully determine the action, we need to also specify the line $\mathscr{L}_3$ as well as two junctions μ, ν.

$\mathscr{L}_1$, we must additionally specify a line $\mathscr{L}_3$ and two junctions μ, ν. Under the state-operator correspondence, this defines an operator $\widehat{\mathscr{L}}_{2(\mathscr{L}_3, \mu, \nu)}$ acting on the defect Hilbert space $\mathscr{H}_{\mathscr{L}_1}$.[5]

The twisted partition function $\text{Tr}_{\mathscr{H}_{\mathscr{L}_1}}\left(\widehat{\mathscr{L}}_{2(\mathscr{L}_3, \mu, \nu)} q^{L_0 - c/24} \bar{q}^{\bar{L}_0 - c/24}\right)$ is an important observable of the 1+1d CFT. From the state-operator map applied to Figure 5.4, we see that this twisted partition function corresponds to the torus partition function with the following network of topological defect lines inserted:

$$\text{Tr}_{\mathscr{H}_{\mathscr{L}_1}}\left(\widehat{\mathscr{L}}_{2(\mathscr{L}_3, \mu, \nu)} q^{L_0 - c/24} \bar{q}^{\bar{L}_0 - c/24}\right) \equiv Z[\mathscr{L}_1, \mathscr{L}_2, \mathscr{L}_3; \mu, \nu](\tau) = \quad \text{} \quad . \quad (5.10)$$

When every fusion coefficient $N_{ab}^c = 0, 1$, we will simply drop the μ, ν indices, and write $Z[\mathscr{L}_1, \mathscr{L}_2, \mathscr{L}_3]$. These twisted torus partition functions are constrained by the covariance under the modular transformations. For instance, under the S-transformation, we find
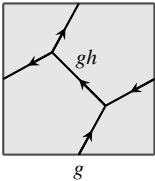
$$Z[\mathscr{L}_1, \mathscr{L}_2, \mathscr{L}_3]\left(-\frac{1}{\tau}\right) = \sum_{\mathscr{L}_k} \left[F_{\mathscr{L}_2}^{\mathscr{L}_1, \mathscr{L}_2, \overline{\mathscr{L}_1}}\right]_{\mathscr{L}_3 \mathscr{L}_k} Z[\mathscr{L}_2, \overline{\mathscr{L}_1}, \mathscr{L}_k](\tau). \quad (5.11)$$

[5]One may also define a more general map from $\mathscr{H}_{\mathscr{L}_1}$ to a different defect Hilbert space $\mathscr{H}_{\mathscr{L}_4}$, by a similar diagram as in Figure 5.4, with the topmost topological line replaced by $\mathscr{L}_4$.

140
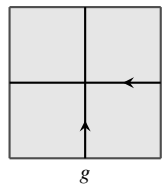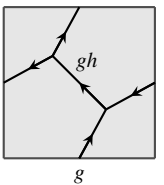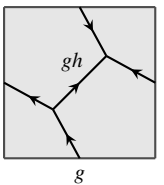
5.2.2 Invertible symmetries and gauging

Here, we review and rephrase the gauging of an anomaly-free finite group symmetry G in terms of an algebra object $\mathscr{A}$, which generalizes naturally to the case of general non-invertible symmetries [141, 39]. For an ordinary global symmetry, an 't Hooft anomaly is characterized as an obstruction to gauge the symmetry, and its nontriviality implies that the low-energy phase cannot be trivially gapped while preserving the symmetry. For a (bosonic) theory in d spacetime dimensions with a finite, internal 0-form symmetry G, possible 't Hooft anomalies are classified by the elements of $H^{d+1}(G, U(1))$. In particular, the 't Hooft anomaly associated to a non-trivial class $[\omega(g, h, k)] \in H^3(G, U(1))$ obstructs orbifolding a 1+1d CFT with the 0-form symmetry G. When the obstruction vanishes, $H^2(G, U(1))$ then parameterizes inequivalent ways of gauging G, known as the discrete torsion.

Let $\mathscr{C} = \mathrm{Vec}_G^\omega$ below, where we keep ω to be arbitrary for now. We will see that ω must be trivial for it to be possible to gauge G consistently. To gauge G in a CFT $\mathscr{T}$ and to compute the corresponding orbifold partition function on a torus, we consider

$$Z_{\mathscr{T}/G} = \frac{1}{|G|} \sum_{\substack{g,h \in G \\ gh=hg}} \frac{\varphi(g,h)}{\varphi(h,g)} Z_{\mathscr{T}}[g,h,gh] = \frac{1}{|G|} \sum_{\substack{g,h \in G \\ gh=hg}} \frac{\varphi(g,h)}{\varphi(h,g)} \quad \text{} \quad , \qquad (5.12)$$

where $[\varphi] \in H^2(G, U(1))$ is a choice of the discrete torsion. Each diagram with non-trivial g and h is a choice of a resolution of the 4-way junction diagram, and there exists another resolution

$$\text{} \qquad (5.13)$$

The two resolutions represent two different local trivializations of the same G-bundle, and they must agree in order for the gauging to be consistent. The 't Hooft anomaly ω exactly measures

the ambiguity in the resolution of the twisted partition function.

Alternatively, we can also obtain the orbifold partition function (5.12) by inserting a single mesh of the non-simple topological defect line $\mathscr{A} = \bigoplus\limits_{g \in G} g$:

$$\mathscr{L}_{\mathscr{T}/G} = \quad \quad . \tag{5.14}$$

The consistency of the gauging requires the line $\mathscr{A}$ to be an *algebra object* in $\mathscr{C}$ (with a few additional conditions) [141, 39]. First, it requires the data of a fusion junction (multiplication) $\mu \in \mathrm{Hom}_{\mathscr{C}}(\mathscr{A} \otimes \mathscr{A}, \mathscr{A})$ and a splitting junction (comultiplication) $\mu^{\vee} \in \mathrm{Hom}_{\mathscr{C}}(\mathscr{A}, \mathscr{A} \otimes \mathscr{A})$. In our case, they are given by
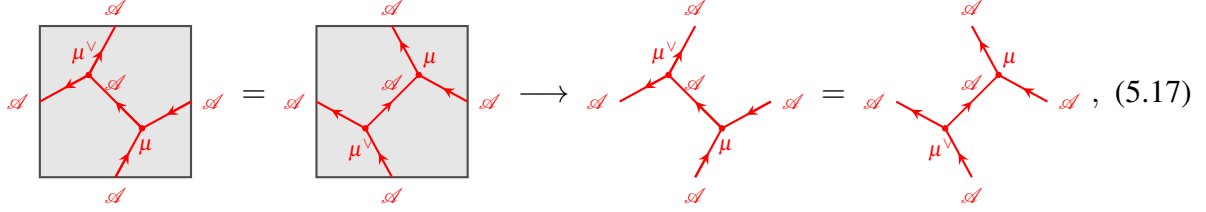
$$ = \frac{1}{\sqrt{|G|}} \sum_{g,h \in G} \varphi(g,h) \quad \quad , \quad = \frac{1}{\sqrt{|G|}} \sum_{g,h \in G} \varphi^{\vee}(g,h) \quad \quad , \tag{5.15}$$

where $\varphi^{\vee}(g,h) = \frac{1}{\varphi(g,h)}$. Expanding (5.14) using (5.15), we indeed recover (5.12):
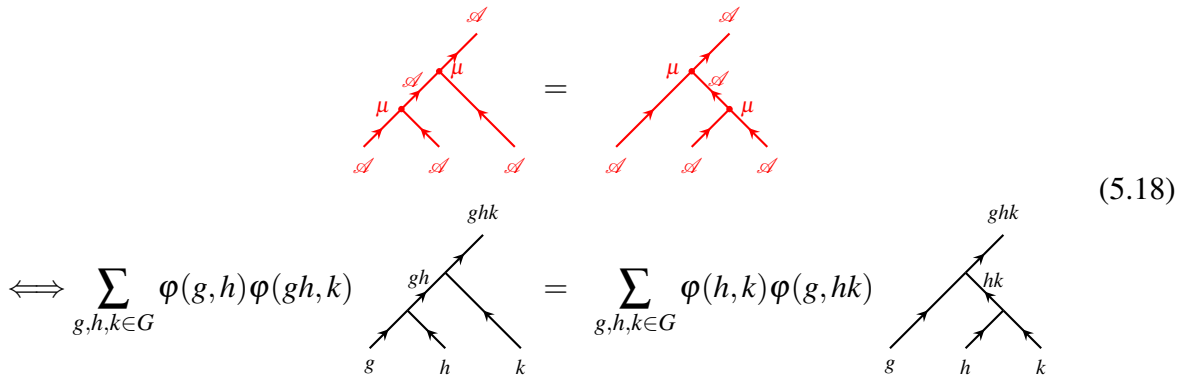
$$ = \frac{1}{|G|} \sum_{g,g',h,h' \in G} \delta_{g,g'} \delta_{h,h'} \delta_{gh,h'g'} \varphi(g,h) \varphi^{\vee}(h',g') \quad $$

$$= \frac{1}{|G|} \sum_{\substack{g,h \in G \\ gh=hg}} \frac{\varphi(g,h)}{\varphi(h,g)} \quad \quad . \tag{5.16}$$

The partition function (5.14) admits an alternative resolution, similarly to (5.13), and the

different resolutions should agree with each other in order for the orbifold partition function to be well-defined. This requires the following condition on the junctions μ, $\mu^\vee$:

$$\tag{5.17}$$

which requires $\varphi^\vee(g,h) = \frac{1}{\varphi(g,h)}$ for the anomaly free ordinary symmetry. This is called the Frobenius condition. The multiplication μ must satisfy the associativity condition (and there is a similar coassociativity condition on $\mu^\vee$):

$$\tag{5.18}$$

$$\iff \sum_{g,h,k\in G} \varphi(g,h)\varphi(gh,k) \quad \text{(diagram)} \quad = \sum_{g,h,k\in G} \varphi(h,k)\varphi(g,hk) \quad \text{(diagram)}$$

which in components reads

$$\frac{\varphi(g,h)\varphi(gh,k)}{\varphi(h,k)\varphi(g,hk)} = \omega(g,h,k). \tag{5.19}$$

The equation (5.19) can be solved if and only if ω is cohomologically trivial in $H^3(G,U(1))$, i.e. the symmetry G is anomaly-free. When $[\omega]$ is trivial, the inequivalent solutions are classified by $H^2(G,U(1))$ corresponding to different discrete torsions. Additional conditions required for a consistent gauging of a general algebra object $\mathscr{A}$ will be reviewed later.

For a CFT $\mathscr{T}$ with a $\mathbb{Z}_2$ symmetry generated by a topological line a, $H^2(\mathbb{Z}_2,U(1))$ is

trivial, and there is a unique orbifold torus partition function,
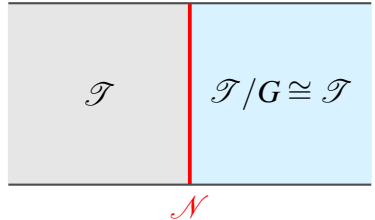
$$Z_{\mathscr{T}/\mathbb{Z}_2} = \frac{1}{2}\left(Z_{\mathscr{T}}[\mathbb{1},\mathbb{1},\mathbb{1}] + Z_{\mathscr{T}}[\mathbb{1},a,a] + Z_{\mathscr{T}}[a,\mathbb{1},a] + Z_{\mathscr{T}}[a,a,\mathbb{1}]\right). \qquad (5.20)$$

For a $\mathbb{Z}_2 \times \mathbb{Z}_2$ symmetry, generated by two topological lines a and b, $H^2(\mathbb{Z}_2 \times \mathbb{Z}_2, U(1)) = \mathbb{Z}_2$, and there are two different ways to orbifold (differing by the $\pm$ sign in the last line),

$$Z_{\mathscr{T}/\mathbb{Z}_2 \times \mathbb{Z}_2} = \frac{1}{4}(Z_{\mathscr{T}}[\mathbb{1},\mathbb{1},\mathbb{1}] + Z_{\mathscr{T}}[\mathbb{1},a,a] + Z_{\mathscr{T}}[\mathbb{1},b,b] + Z_{\mathscr{T}}[\mathbb{1},ab,ab]$$

$$+ Z_{\mathscr{T}}[a,\mathbb{1},a] + Z_{\mathscr{T}}[b,\mathbb{1},b] + Z_{\mathscr{T}}[ab,\mathbb{1},ab] + Z_{\mathscr{T}}[a,a,\mathbb{1}] + Z_{\mathscr{T}}[b,b,\mathbb{1}] + Z_{\mathscr{T}}[ab,ab,\mathbb{1}]$$

$$\pm Z_{\mathscr{T}}[a,b,ab] \pm Z_{\mathscr{T}}[a,ab,b] \pm Z_{\mathscr{T}}[b,a,ab] \pm Z_{\mathscr{T}}[b,ab,a] \pm Z_{\mathscr{T}}[ab,a,b] \pm Z_{\mathscr{T}}[ab,b,a]).$$

$$(5.21)$$

5.2.3 Half-space gauging and non-invertible symmetries

A useful way to discover a class of non-invertible, codimension-1 topological defects in general spacetime dimensions is through the "half-space gauging" (or "half-gauging" in short) [378, 88, 87]. Consider a 1+1d CFT $\mathscr{T}$ with a non-anomalous global (abelian) symmetry G. We divide the spacetime into left and right regions, and gauge the symmetry G only in the right region. At the codimension-1 interface between the left and right, we impose the topological Dirichlet boundary condition for the discrete G gauge field. If $\mathscr{T}$ is isomorphic to the gauged theory $\mathscr{T}/G$, then the interface defines a topological defect line $\mathscr{N}$ in theory $\mathscr{T}$:

$$(5.22)$$

A well-known example is the Kramers-Wannier duality in the Ising CFT, where the Ising CFT is self-dual under the $\mathbb{Z}_2$ orbifold Eq. (5.20). The half-gauging in this case produces

the Kramers-Wannier duality defect line [299, 300, 309, 137, 138, 139, 3, 2, 342]. With this additional duality line $\mathcal{N}$ as well as the $\mathbb{Z}_2$ symmetry, the symmetry of the Ising CFT is described by the Tambara-Yamagami fusion category, $\mathsf{TY}(\mathbb{Z}_2, \chi, +1)$. The notation for general Tambara-Yamagami fusion categories is explained momentarily.

More generally, if the theory is self-dual under gauging an anomaly free abelian symmetry A, then it admits a $\mathsf{TY}(A, \chi, \varepsilon)$ fusion category symmetry [374].[6] The simple objects of $\mathsf{TY}(A, \chi, \varepsilon)$ category are group-like lines g of the abelian group A, and a non-invertible line $\mathcal{N}$. These simple lines satisfy the following fusion rules,

$$g \otimes h = gh, \quad g \otimes \mathcal{N} = \mathcal{N} \otimes g = \mathcal{N}, \quad \mathcal{N} \otimes \mathcal{N} = \bigoplus_{g \in A} g. \tag{5.23}$$

The only non-trivial F-symbols are

$$[F_{\mathcal{N}}^{g\,\mathcal{N}\,h}]_{\mathcal{N},\mathcal{N}} = [F_h^{\mathcal{N}\,g\,\mathcal{N}}]_{\mathcal{N},\mathcal{N}} = \chi(g,h),$$
$$[F_{\mathcal{N}}^{\mathcal{N}\,\mathcal{N}\,\mathcal{N}}]_{g,h} = \frac{\varepsilon}{\sqrt{|A|}}\chi(g,h)^{-1}, \tag{5.24}$$

where $\varepsilon = \pm 1$ is the Frobenius-Schur indicator for $\mathcal{N}$, which is classified by $\varepsilon \in H^3(\mathbb{Z}_2, U(1)) = \mathbb{Z}_2$, and $\chi : A \times A \to U(1)$ is a non-degenerate symmetric bicharacter, which satisfies

$$\chi(g,h) = \chi(h,g), \quad \chi(gh,k) = \chi(g,k)\chi(h,k), \quad \chi(g,hk) = \chi(g,h)\chi(g,k). \tag{5.25}$$

The fusion rules Eq. (5.23) and the F-symbols Eq. (5.24) define the fusion category $\mathsf{TY}(A, \chi, \varepsilon)$ [374]. For the case of $A = \mathbb{Z}_2$, the choice of χ is unique, and there are two distinct Tambara-Yamagami fusion categories based on $\mathbb{Z}_2$ corresponding to $\varepsilon = \pm 1$. We will denote these two categories as $\mathsf{TY}(\mathbb{Z}_2)_\pm \equiv \mathsf{TY}(\mathbb{Z}_2, \chi, \pm 1)$. The $\mathsf{TY}(\mathbb{Z}_2)_+$ category is realized in the Ising CFT as mentioned above, whereas the $\mathsf{TY}(\mathbb{Z}_2)_-$ category is realized in the $SU(2)_2$ WZW model, for

---

[6]To be more precise, for there to be a $\mathsf{TY}(A, \chi, \varepsilon)$ fusion category symmetry, the theory must be self-dual under the gauging with an appropriately chosen discrete torsion such that the gauging is of order 2 [87] (see also [378]).

instance.

Similar to ordinary global symmetries, fusion category symmetries can also have an 't Hooft anomaly, which obstructs the existence of a symmetric trivially gapped phase [70, 379]. For instance, the anomaly-free condition for $\mathsf{TY}(A,\chi,\varepsilon)$ contains two parts, roughly speaking, (1) the quantum dimension of the duality line should be an integer and (2) the total Frobenius-Schur indicator should be trivial [379, 454, 373, 269, 10].

5.2.4 Group extension of a fusion category

The Tambara-Yamagami fusion category is a special example of a group extended fusion category. In general, a fusion category $\mathscr{C}$ is a G-extension of the fusion category $\mathscr{C}'$ if $\mathscr{C}$ is a G-graded fusion category whose trivial grading component $\mathscr{C}_{\mathbb{1}} = \mathscr{C}'$. Namely, $\mathscr{C}$ admits a decomposition of abelian categories

$$\mathscr{C} = \bigoplus_{g \in G} \mathscr{C}_g \tag{5.26}$$

with $\mathscr{C}_{\mathbb{1}} = \mathscr{C}'$, such that the tensor product $\otimes$ maps $\mathscr{C}_g \times \mathscr{C}_h$ to $\mathscr{C}_{gh}$ for every $g,h \in G$.

Consider the case $G = \mathbb{Z}_2 = \{\mathbb{1}, \eta\}$. In this language, the Tambara-Yamagami fusion category $\mathsf{TY}(A,\chi,\varepsilon)$ is a $\mathbb{Z}_2$-extension of the fusion category $\mathsf{Vec}_A \equiv \mathsf{TY}(A,\chi,\varepsilon)_{\mathbb{1}}$ where the non-trivial grading component $\mathsf{TY}(A,\chi,\varepsilon)_{\eta}$ contains a unique simple object $\mathscr{N}$. Note that a graded fusion category does not necessarily contain non-invertible symmetries, as one can see from the simplest G-graded fusion category Vec_G.

The trivial grading component $\mathscr{C}_{\mathbb{1}}$ is a tensor subcategory of $\mathscr{C}$, and each $\mathscr{C}_g$ is a $\mathscr{C}_{\mathbb{1}}$-bimodule category. This observation leads to the classification of G-extensions of a fusion category [125] which we briefly review now. The grading components $\mathscr{C}_g$ satisfy the G-multiplication rule under the tensor product $\boxtimes_{\mathscr{C}_{\mathbb{1}}}$ of $\mathscr{C}_{\mathbb{1}}$-bimodule categories:

$$\mathscr{C}_g \boxtimes_{\mathscr{C}_{\mathbb{1}}} \mathscr{C}_h \simeq \mathscr{C}_{gh}, \quad \forall g,h \in G. \tag{5.27}$$

In particular, this means that $\mathscr{C}_{\mathbb{1}}$ acts as an identity under $\boxtimes_{\mathscr{C}_{\mathbb{1}}}$, $\mathscr{C}_{\mathbb{1}} \boxtimes_{\mathscr{C}_{\mathbb{1}}} \mathscr{C}_g = \mathscr{C}_g \boxtimes_{\mathscr{C}_{\mathbb{1}}} \mathscr{C}_{\mathbb{1}} = \mathscr{C}_g$,

and each $\mathscr{C}_g$ admits an inverse $\mathscr{C}_{g^{-1}}$ under $\boxtimes_{\mathscr{C}_{\mathbb{1}}}$. Namely, $\mathscr{C}_g$ is an invertible $\mathscr{C}_{\mathbb{1}}$-bimodule category.

This implies that the G-extension of a fusion category $\mathscr{C}$ contains the data of a group homomorphism ρ from G to the so-called Brauer-Picard group $\mathsf{BrPic}(\mathscr{C})$ of the fusion category $\mathscr{C}$, whose elements are invertible $\mathscr{C}$-bimodule categories and the group multiplication is the tensor product $\boxtimes_{\mathscr{C}}$.

However, not every $\rho : G \to \mathsf{BrPic}(\mathscr{C})$ can be made into a G-extension of $\mathscr{C}$, and furthermore, the extension associated to a given ρ is not necessarily unique in general. The obstructions and additional data required to specify a G-extension are worked out in [125] and are interpreted physically in [25]. It starts with an important observation that $\mathsf{BrPic}(\mathscr{C})$ is isomorphic to $\mathsf{EqBr}(\mathscr{Z}(\mathscr{C}))$, the group of braided equivalences of the Drinfeld center $\mathscr{Z}(\mathscr{C})$. The latter is simply the symmetry group of the symmetry topological field theory (symTFT) of the fusion category $\mathscr{C}$ [22]. The additional data contain a choice of the symmetry fractionalization class $M \in H^2_{[\rho]}(G, A)$ where A is the group of Abelian anyons in the symTFT $\mathscr{Z}(\mathscr{C})$, and a choice of the discrete torsion $\varepsilon \in H^3(G, U(1))$. The combined data (ρ, M, ε) must satisfy the conditions that the obstruction class $O^3_{[\rho]} \in H^3_{[\rho]}(G, A)$ to the fractionalization of the symmetry $\rho : G \to \mathsf{EqBr}(\mathscr{Z}(\mathscr{C}))$ as well as the 't Hooft anomaly $O^4(\rho, M) \in H^4(G, U(1))$ of the G symmetry with the chosen fractionalization both vanish.

We introduce the following notation

$$\mathscr{E}_G^{(\rho, M, \varepsilon)}\mathscr{C} \tag{5.28}$$

to denote the G-extension of the fusion category $\mathscr{C}$ with the data (ρ, M, ε). In this work, we focus on $G = \mathbb{Z}_2 = \{\mathbb{1}, \eta\}$ and also on a special class of graded extensions in which the η-component of the extension contains a unique simple object $\mathscr{D}$, and we will denote this type of extensions

147

by adding an underline $\underline{\mathscr{E}}$. Then, the grading structure uniquely determines the fusion rules:

$$\mathscr{L} \otimes \mathscr{D} = \mathscr{D} \otimes \mathscr{L} = \langle \mathscr{L} \rangle \mathscr{D} , \quad \mathscr{D} \otimes \mathscr{D} = \bigoplus_{\text{simple} \, \mathscr{L}} \langle \mathscr{L} \rangle \mathscr{L} , \tag{5.29}$$

where $\mathscr{L}$ lines are in the trivial grading component. It immediately follows that such an extension can exist only if $\langle \mathscr{L} \rangle \in \mathbb{Z}_{>0}$ for every $\mathscr{L}$. As an example, the Tambara-Yamagami fusion category can be written as

$$\mathsf{TY}(A, \chi, \varepsilon) = \underline{\mathscr{E}}_{\mathbb{Z}_2}^{(\chi, \varepsilon)} \mathsf{Vec}_A . \tag{5.30}$$

In the case where the corresponding extension data (ρ, M, ε) are not known explicitly, we will replace the superscript by suitable labels which distinguish different extensions.

5.3 (Half-)gauging non-invertible symmetries in 1+1d

In this section, we first review how to gauge non-invertible symmetries using an algebra object [141, 39], generalizing the discussion in Section 5.2.2. We then argue that given a theory that is self-dual under gauging a non-invertible symmetry, one can obtain a new topological defect line by half-space gauging. Finally, we work out how to gauge the non-invertible $\mathrm{Rep}(H_8)$ symmetry.

5.3.1 Gauging non-invertible symmetries using algebra objects

As motivated in Section 5.2.2, to gauge a (finite) symmetry is to insert a mesh of the corresponding algebra object $\mathscr{A}$ across the spacetime manifold. To begin with, an algebra object is characterized by a triple $(\mathscr{A}, \mu, u)$. Here, $\mu \in \mathrm{Hom}_{\mathscr{C}}(\mathscr{A} \otimes \mathscr{A}, \mathscr{A})$ is a fusion junction of $\mathscr{A}$, also known as the multiplication morphism, and $u \in \mathrm{Hom}_{\mathscr{C}}(\mathbb{1}, \mathscr{A})$ is the unit morphism. They

satisfy the following consistent conditions:

$$\tag{5.31}$$

Throughout the paper, we focus on the case where $\mathscr{A}$ contains every simple object $\mathscr{L}_i$ of $\mathscr{C}$ with multiplicities given by the quantum dimensions,

$$\mathscr{A} = \bigoplus_i \langle \mathscr{L}_i \rangle \mathscr{L}_i. \tag{5.32}$$

Algebra objects $(\mathscr{A}, \mu, u)$ of this form are in 1-to-1 correspondence with fiber functors of the fusion category [303, 90]. An algebra object $\mathscr{A}$ of the form (5.32) is an example of a haploid algebra object, that is, the multiplicity of $\mathbb{1}$ in $\mathscr{A}$ is 1. This fixes the unit morphism u up to rescaling.

To insert a mesh of $\mathscr{A}$ on a Riemann surface which implements the gauging, we first choose a triangulation, and insert $\mathscr{A}$ along the edges of the dual triangulation. To do this, we need not only the fusion junction μ but also a splitting junction $\mu^\vee \in \mathrm{Hom}_{\mathscr{C}}(\mathscr{A}, \mathscr{A} \otimes \mathscr{A})$. Furthermore, in order for the gauging to be unambiguously defined, the result must be invariant under changing the triangulation of the Riemann surface. Any two triangulations of a Riemann surface can be transformed into each other via a sequence of the *fusion* and *bubble* moves [92, 143, 208],

$$\tag{5.33}$$

This leads to various additional constraints that the algebra object $\mathscr{A}$ and the junctions μ, $\mu^\vee$

must satisfy, including (5.17) and (5.18). Mathematically, these conditions are summarized by saying that $\mathscr{A}$ must be a symmetric Δ-separable Frobenius algebra object in the fusion category $\mathscr{C}$ [141, 39]. Some of them are listed below:

$$
\tag{5.34}
$$

In practice, solving the above set of conditions is enough to guarantee that one has a symmetric Δ-separable Frobenius algebra object, due to the fact that every semisimple haploid algebra object admits a unique coalgebra structure (namely $\mu^\vee$, the counit is unique up to rescaling) such that it becomes a symmetric Δ-separable Frobenius algebra [303, 141].

When we gauge a finite group symmetry, we obtain a quantum (or dual) symmetry in the gauged theory [384]. Similarly, when we gauge a general algebra object $\mathscr{A}$, we also get a quantum symmetry in the gauged theory [39, 218]. The quantum symmetry one gets after gauging $\mathscr{A}$ is described by the fusion category $_{\mathscr{A}}\mathscr{C}_{\mathscr{A}}$, that is, the category of $\mathscr{A}$-$\mathscr{A}$-bimodule objects $(\mathscr{M}, \lambda, \rho)$ in $\mathscr{C}$. Here, λ and ρ describe left/right multiplication structures of $\mathscr{A}$ on $\mathscr{M}$,

$$
\tag{5.35}
$$

satisfying

$$
\tag{5.36}
$$

150

Generally, a bimodule object can be decomposed as a direct sum of several other bimodule objects. The ones which can not be decomposed are called indecomposable bimodule objects, and they are the simple topological defect lines generating the quantum symmetry in the gauged theory. The intuition is that the conditions in (5.36) allow the line $\mathscr{M}$ to be inserted and deformed across the mesh of $\mathscr{A}$ in a consistent way.

5.3.2 Half-gauging and graded extensions

Here, we provide a description of half-gauging non-invertible symmetries, generalizing the discussion in Section 5.2.3. We begin by describing the topological interface obtained from gauging an algebra object $\mathscr{A}$ on half of the spacetime. Let us consider a CFT $\mathscr{T}$ with a fusion category symmetry $\mathscr{C}$. If $\mathscr{C}$ is anomaly-free, then we can find an algebra object $\mathscr{A}$ of the form (5.32). Gauging the algebra object $\mathscr{A}$ leads to the CFT $\mathscr{T}/\mathscr{C}$ with the quantum fusion category symmetry ${}_{\mathscr{A}}\mathscr{C}_{\mathscr{A}}$. It is then possible to consider gauging the symmetry $\mathscr{C}$ on only half of the spacetime to obtain the theory $\mathscr{T}/\mathscr{C}$ on half-space which is separated from $\mathscr{T}$ by a topological interface $\mathscr{I}$,

$$\boxed{\quad \mathscr{T} \text{ with } \mathscr{C}\text{-sym} \quad \Big| \quad \mathscr{T}/\mathscr{C} \text{ with } {}_{\mathscr{A}}\mathscr{C}_{\mathscr{A}}\text{-sym} \quad}_{\mathscr{I}} . \qquad (5.37)$$

The topological interface $\mathscr{I}$ is a simple object in the category $\mathscr{C}_{\mathscr{A}}$ of the right $\mathscr{A}$-modules in $\mathscr{C}$, given by $\mathscr{A}$ itself. Here, $\mathscr{C}_{\mathscr{A}}$ naturally carries the structure of a $\mathscr{C}$-${}_{\mathscr{A}}\mathscr{C}_{\mathscr{A}}$-bimodule category. Namely, the topological lines in $\mathscr{C}$ acts on the interface from the left, whereas the quantum topological lines in ${}_{\mathscr{A}}\mathscr{C}_{\mathscr{A}}$ acts on the interface from the right. Since we are interested in $\mathscr{A}$ of the form (5.32), $\mathscr{C}_{\mathscr{A}}$ contains a unique simple object, therefore the topological interface $\mathscr{I}$ is uniquely defined. If we have an invertible symmetry $\mathscr{C} = \mathsf{Vec}_G$, such an interface is the one coming from imposing the topological Dirichlet boundary condition for the discrete G gauge field at the interface, recovering the ordinary half-gauging construction in Section 5.2.3.

In the special case where $_{\mathscr{A}}\mathscr{C}_{\mathscr{A}} \simeq \mathscr{C}$ and $\mathscr{T} \simeq \mathscr{T}/\mathscr{C}$, the topological interface $\mathscr{I}$ can be regarded as a topological defect line $\mathscr{D}$ in the theory $\mathscr{T}$. In general, such a defect $\mathscr{D}$ is not necessarily the same as its orientation reversal $\overline{\mathscr{D}}$, but in the following we will restrict to the case where $\mathscr{D} = \overline{\mathscr{D}}$. Since the fusion category symmetry $\mathscr{C}$ (or equivalently, $_{\mathscr{A}}\mathscr{C}_{\mathscr{C}} \cong \mathscr{C}$) is gauged across the defect $\mathscr{D}$, any topological defect line $\mathscr{L} \in \mathscr{C}$ must become transparent up to its quantum dimension $\langle \mathscr{L} \rangle$ when it crosses $\mathscr{D}$. This implies the following fusion rule

$$\mathscr{L} \otimes \mathscr{D} = \mathscr{D} \otimes \mathscr{L} = \langle \mathscr{L} \rangle \mathscr{D}, \quad \forall \mathscr{L} \in \mathscr{C}. \tag{5.38}$$

Recall that $\langle \mathscr{L} \rangle \in \mathbb{Z}_{>0}$ for every $\mathscr{L}$ in an anomaly-free (unitary) fusion category, and the above fusion algebra is consistent. Since $\mathscr{D} = \overline{\mathscr{D}}$, we must also have

$$\mathscr{D} \otimes \mathscr{D} = \mathscr{D} \otimes \overline{\mathscr{D}} = \bigoplus_{\text{simple} \, \mathscr{L}} \langle \mathscr{L} \rangle \mathscr{L} = \mathscr{A}. \tag{5.39}$$

This is because the fusion $\mathscr{D} \otimes \overline{\mathscr{D}}$ corresponds to gauging $\mathscr{C}$ inside a thin slab sandwiched by the two lines $\mathscr{D}$ and $\overline{\mathscr{D}}$, and such a gauging, which is given by inserting a mesh of $\mathscr{A}$ inside the slab, reduces to a single $\mathscr{A}$ line in the limit where the thickness of the slab goes to zero, by using the consistency conditions that $\mathscr{A}$ satisfies. Comparing with (5.29), we find that the self-duality under gauging the fusion category symmetry $\mathscr{C}$ leads to a bigger fusion category symmetry described by a $\mathbb{Z}_2$-extension $\underline{\mathscr{E}}_{\mathbb{Z}_2}\mathscr{C}$ of $\mathscr{C}$, where the nontrivial grading component has the unique simple object $\mathscr{D}$. When $\mathscr{C}$ is an invertible symmetry, (5.38) and (5.39) are fusion rules for the Tambara-Yamagami fusion category.

However, as discussed in Section 5.2.4, fusion category with the fusion rules (5.38) and (5.39) is in general not unique. How does the additional data arise from the above discussion? First, when we say that the quantum symmetry $_{\mathscr{A}}\mathscr{C}_{\mathscr{A}}$ is the same as the original symmetry $\mathscr{C}$, we must explicitly specify how the topological lines and the junctions between them in $\mathscr{C}$ are

related to the ones in $_\mathscr{A}\mathscr{C}_\mathscr{A}$, and vice versa. Such a choice is not unique in general.[7] Furthermore, in general there may be more than one set of consistent local junction data we can choose for the global fusion (5.39). These choices must be made in order to unambiguously determine the larger symmetry $\underline{\mathscr{E}}_{\mathbb{Z}_2}\mathscr{C}$.

When applying this to a concrete CFT $\mathscr{T}$, the choice of the additional data mentioned above must be compatible with the other data in the $\mathscr{T}$, and we generally expect the theory $\mathscr{T}$ to realize only a subset of possible $\underline{\mathscr{E}}_{\mathbb{Z}_2}\mathscr{C}$ symmetries.

It is interesting to point out that one should not expect that $\underline{\mathscr{E}}_{\mathbb{Z}_2}\mathscr{C}$ can be uniquely fixed in a theory $\mathscr{T}$ in general. An example is the critical 3-states Potts model, see [70] for instance. There, the theory is self-dual under gauging a $\mathbb{Z}_3$ symmetry, but the theory admits two duality lines $\mathscr{N}$ and $\mathscr{N}'$ both describing this self-dual property. They realize two different $\mathbb{Z}_2$-extensions of the $\mathbb{Z}_3$ symmetry in the same theory $\mathscr{T}$.

5.3.3 Rep(H_8) **symmetry and its gauging**

Rep(H_8) is the representation category of the Hopf algebra H_8 and it is also a Tambara-Yamagami fusion category $\mathsf{TY}(\mathbb{Z}_2 \times \mathbb{Z}_2, \chi_{diag}, +1)$ describing self-duality under gauging $\mathbb{Z}_2 \times \mathbb{Z}_2$. It contains 5 simple topological defect lines–4 invertible lines $\mathbb{1}, a, b, ab$ generating the non-anomalous $\mathbb{Z}_2^a \times \mathbb{Z}_2^b$ symmetry and a non-invertible duality line $\mathscr{N}$. If we parameterize elements of $\mathbb{Z}_2^a \times \mathbb{Z}_2^b$ as $g \equiv (g_1, g_2)$ such that $a \equiv (1,0), b \equiv (0,1)$, then the bicharacter is given by $\chi_{diag}(g,h) = (-1)^{g_1 h_1 + g_2 h_2}$. For simplicity, we will drop the subscript *diag* and write χ_{diag} simply as χ for the rest of the paper. Rep(H_8) is anomaly-free and there exists a unique way of gauging it since it admits a unique fiber functor [378].

One way to obtain a theory with the Rep(H_8) symmetry is by stacking two (potentially

---

[7]In the categorical language, we need to choose a tensor equivalence between the fusion categories $\mathscr{C}$ and $_\mathscr{A}\mathscr{C}_\mathscr{A}$, and we expect it to be classified by the group $\mathrm{Aut}(\mathscr{C})$ of autoequivalences of the fusion category $\mathscr{C}$. Given a choice of tensor equivalence, we can make $\mathscr{C}_\mathscr{A}$ either to be a $\mathscr{C}$-$\mathscr{C}$-bimodule category, or to be a $_\mathscr{A}\mathscr{C}_\mathscr{A}$-$_\mathscr{A}\mathscr{C}_\mathscr{A}$-bimodule category. Both can then be used to further construct the extensions $\underline{\mathscr{E}}_{\mathbb{Z}_2}\mathscr{C}$ and $\underline{\mathscr{E}}_{\mathbb{Z}_2 \mathscr{A}}\mathscr{C}_\mathscr{A}$. Since $\mathscr{C} \simeq {}_\mathscr{A}\mathscr{C}_\mathscr{A}$, $\underline{\mathscr{E}}_{\mathbb{Z}_2}\mathscr{C}$ has the same fusion rules as $\underline{\mathscr{E}}_{\mathbb{Z}_2 \mathscr{A}}\mathscr{C}_\mathscr{A}$ but generically we do not expect them to be equivalent. Since the choice of ρ is equivalent to the choice of invertible $\mathscr{C}$-$\mathscr{C}$-bimodule categories with a unique simple object, we then expect the number of the inequivalent choices of ρ does not exceed $2|\mathrm{Aut}(\mathscr{C})|$.

different) theories with the symmetry of the Ising CFT, namely the Tambara-Yamagami fusion category $\mathsf{TY}(\mathbb{Z}_2)_+$. In this case, the $\mathbb{Z}_2^a \times \mathbb{Z}_2^b$ symmetry comes from the $\mathbb{Z}_2$ symmetries of the two theories, and the duality line $\mathcal{N}_{\mathsf{Rep}(H_8)} = \mathcal{N}_{\mathsf{Ising},1} \mathcal{N}_{\mathsf{Ising},2}$ is the diagonal duality line.

The unique algebra object of the form $\mathscr{A} = \mathbb{1} \oplus a \oplus b \oplus ab \oplus 2\mathcal{N}$ and the corresponding junctions μ, $\mu^\vee$ can be explicitly computed by solving the conditions Eq. (5.34).[8] We find that fusion junction μ and the splitting junction $\mu^\vee$ are given by

$$\tag{5.40}$$

where

$$\psi(g,h) = \frac{1}{2\sqrt{2}} \begin{pmatrix} 1 & 1 & 1 & 1 \\ 1 & 1 & 1 & 1 \\ 1 & -1 & 1 & -1 \\ 1 & -1 & 1 & -1 \end{pmatrix}, \quad L(g) = \frac{1}{2\sqrt{2}} \left(\sigma^0, -\sigma^3, -\sigma^1, -i\sigma^2 \right),$$

$$R(g) = \frac{1}{2\sqrt{2}} \left(\sigma^0, \sigma^3, \sigma^1, -i\sigma^2 \right), \quad W(g) = \frac{1}{4} \left(\sigma^3 - \sigma^1, -\sigma^0 + i\sigma^2, \sigma^0 + i\sigma^2, -\sigma^1 - \sigma^3 \right),$$

$$\tag{5.41}$$

---

[8]The $\mathsf{Rep}(H_8)$ fusion category in total contains six (Morita classes of) algebra objects that can be gauged [124, 307, 112]. They are $\mathbb{1} \oplus a \oplus b \oplus ab \oplus 2\mathcal{N}$ and $\mathbb{1} \oplus ab \oplus \mathcal{N}$, which include the non-invertible line, and the ones corresponding to gauging various invertible symmetries.

and

(5.42)

where

$$\psi^\vee(g,h) = \frac{1}{2\sqrt{2}} \begin{pmatrix} 1 & 1 & 1 & 1 \\ 1 & 1 & 1 & 1 \\ 1 & -1 & 1 & -1 \\ 1 & -1 & 1 & -1 \end{pmatrix}, \quad L^\vee(g) = \frac{1}{2\sqrt{2}} \left(\sigma^0, -\sigma^3, -\sigma^1, i\sigma^2 \right),$$

$$R^\vee(g) = \frac{1}{2\sqrt{2}} \left(\sigma^0, \sigma^3, \sigma^1, i\sigma^2 \right), \quad W^\vee(g) = \frac{1}{4} \left(\sigma^3 - \sigma^1, -\sigma^0 + i\sigma^2, \sigma^0 + i\sigma^2, -\sigma^1 - \sigma^3 \right).$$

(5.43)

More details on finding such an algebra object are given in App. E.1. The torus partition function of the gauged theory $\mathscr{T}/\mathrm{Rep}(H_8)$ is computed by expanding the following diagram in terms of simple topological defect lines:

(5.44)

155

We find

$$Z_{\mathcal{T}/\mathsf{Rep}(H_8)}(\tau) = \frac{1}{8}\Big(Z_{\mathscr{T}}[\mathbb{1},\mathbb{1},\mathbb{1}](\tau) + Z_{\mathscr{T}}[\mathbb{1},a,a](\tau) + Z_{\mathscr{T}}[a,\mathbb{1},a](\tau) + Z_{\mathscr{T}}[a,a,\mathbb{1}](\tau)$$

$$+ Z_{\mathscr{T}}[\mathbb{1},b,b](\tau) + Z_{\mathscr{T}}[b,\mathbb{1},b](\tau) + Z_{\mathscr{T}}[b,b,\mathbb{1}](\tau)$$

$$+ Z_{\mathscr{T}}[\mathbb{1},ab,ab](\tau) + Z_{\mathscr{T}}[ab,\mathbb{1},ab](\tau) + Z_{\mathscr{T}}[ab,ab,\mathbb{1}](\tau)$$

$$- Z_{\mathscr{T}}[a,b,ab](\tau) - Z_{\mathscr{T}}[b,a,ab](\tau) - Z_{\mathscr{T}}[b,ab,a](\tau)$$

$$- Z_{\mathscr{T}}[ab,a,b](\tau) - Z_{\mathscr{T}}[a,ab,b](\tau) - Z_{\mathscr{T}}[ab,b,a](\tau)$$

$$+ 2Z_{\mathscr{T}}[\mathbb{1},\mathcal{N},\mathcal{N}](\tau) + 2Z_{\mathscr{T}}[\mathcal{N},\mathbb{1},\mathcal{N}](\tau) + 2Z_{\mathscr{T}}[\mathcal{N},\mathcal{N},\mathbb{1}](\tau)$$

$$+ 2Z_{\mathscr{T}}[ab,\mathcal{N},\mathcal{N}](\tau) + 2Z_{\mathscr{T}}[\mathcal{N},ab,\mathcal{N}](\tau) + 2Z_{\mathscr{T}}[\mathcal{N},\mathcal{N},ab](\tau)\Big).$$

$$(5.45)$$

Here, the terms on the RHS that come with -1 coefficients have a sign ambiguity, due to the freedom to shift the counterterm associated to the nontrivial element of $H^2(\mathbb{Z}_2^a \times \mathbb{Z}_2^b, U(1)) \cong \mathbb{Z}_2$. On the other hand, the $\mathsf{Rep}(H_8)$ symmetry implies that the theory is invariant under gauging the $\mathbb{Z}_2^a \times \mathbb{Z}_2^b$ symmetry with an appropriate choice of such a counterterm. We fix the counterterm ambiguity by requiring the theory to be self-dual under gauging $\mathbb{Z}_2^a \times \mathbb{Z}_2^b$ with no discrete torsion. This leads to the relation

$$Z_{\mathscr{T}}[\mathbb{1},\mathbb{1},\mathbb{1}](\tau) = \frac{1}{4}\Big(Z_{\mathscr{T}}[\mathbb{1},\mathbb{1},\mathbb{1}](\tau) + Z_{\mathscr{T}}[\mathbb{1},a,a](\tau) + Z_{\mathscr{T}}[a,\mathbb{1},a](\tau) + Z_{\mathscr{T}}[a,a,\mathbb{1}](\tau)$$

$$+ Z_{\mathscr{T}}[\mathbb{1},b,b](\tau) + Z_{\mathscr{T}}[b,\mathbb{1},b](\tau) + Z_{\mathscr{T}}[b,b,\mathbb{1}](\tau)$$

$$+ Z_{\mathscr{T}}[\mathbb{1},ab,ab](\tau) + Z_{\mathscr{T}}[ab,\mathbb{1},ab](\tau) + Z_{\mathscr{T}}[ab,ab,\mathbb{1}](\tau)$$

$$+ Z_{\mathscr{T}}[a,b,ab](\tau) + Z_{\mathscr{T}}[b,a,ab](\tau) + Z_{\mathscr{T}}[b,ab,a](\tau)$$

$$+ Z_{\mathscr{T}}[ab,a,b](\tau) + Z_{\mathscr{T}}[a,ab,b](\tau) + Z_{\mathscr{T}}[ab,b,a](\tau)\Big).$$

$$(5.46)$$

Using (5.46) to simplify (5.45), we find

$$
\begin{aligned}
Z_{\mathcal{T}/\mathrm{Rep}(H_8)}(\tau) = \frac{1}{4}\Big(& -Z_{\mathcal{T}}[\mathbb{1},\mathbb{1},\mathbb{1}](\tau) + Z_{\mathcal{T}}[\mathbb{1},a,a](\tau) + Z_{\mathcal{T}}[a,\mathbb{1},a](\tau) + Z_{\mathcal{T}}[a,a,\mathbb{1}](\tau) \\
& + Z_{\mathcal{T}}[\mathbb{1},b,b](\tau) + Z_{\mathcal{T}}[b,\mathbb{1},b](\tau) + Z_{\mathcal{T}}[b,b,\mathbb{1}](\tau) \\
& + Z_{\mathcal{T}}[\mathbb{1},ab,ab](\tau) + Z_{\mathcal{T}}[ab,\mathbb{1},ab](\tau) + Z_{\mathcal{T}}[ab,ab,\mathbb{1}](\tau) \\
& + Z_{\mathcal{T}}[\mathbb{1},\mathcal{N},\mathcal{N}](\tau) + Z_{\mathcal{T}}[\mathcal{N},\mathbb{1},\mathcal{N}](\tau) + Z_{\mathcal{T}}[\mathcal{N},\mathcal{N},\mathbb{1}](\tau) \\
& + Z_{\mathcal{T}}[ab,\mathcal{N},\mathcal{N}](\tau) + Z_{\mathcal{T}}[\mathcal{N},ab,\mathcal{N}](\tau) + Z_{\mathcal{T}}[\mathcal{N},\mathcal{N},ab](\tau)\Big).
\end{aligned}
$$

$$(5.47)$$

The twisted partition functions on the RHS containing only invertible symmetries can be computed via modular transformations once their action on the Hilbert space is known. The twisted partition functions containing the duality line $\mathcal{N}$ can be computed using the following relation:

$$
Z_{\mathcal{T}}[\mathcal{N},\mathbb{1},\mathcal{N}](\tau) + Z_{\mathcal{T}}[\mathcal{N},ab,\mathcal{N}](\tau) = Z_{\mathcal{T}}[\mathcal{N},\mathbb{1},\mathcal{N}](\tau+2) + Z_{\mathcal{T}}[\mathcal{N},\mathbb{1},\mathcal{N}](\tau-2),
$$

$$(5.48)$$

where the RHS can be computed once we know the action of $\mathcal{N}$ on the Hilbert space. To see this relation, notice that

$$(5.49)$$

and use the relation $\chi(\mathbb{1},g)(1+\chi(g,g)) = 2\delta_{g_1,g_2}$. The rest of the twisted partition functions

can be obtained by performing a modular transformation to the LHS of (5.48):

$$Z_{\mathscr{T}}[\mathscr{N},\mathscr{N},\mathbb{1}](\tau)+Z_{\mathscr{T}}[\mathscr{N},\mathscr{N},ab](\tau)=Z_{\mathscr{T}}[\mathscr{N},\mathbb{1},\mathscr{N}](\tau+1)+Z_{\mathscr{T}}[\mathscr{N},ab,\mathscr{N}](\tau+1),$$

$$Z_{\mathscr{T}}[\mathbb{1},\mathscr{N},\mathscr{N}](\tau)+Z_{\mathscr{T}}[ab,\mathscr{N},\mathscr{N}](\tau)=Z_{\mathscr{T}}[\mathscr{N},\mathbb{1},\mathscr{N}]\left(-\frac{1}{\tau}\right)+Z_{\mathscr{T}}[\mathscr{N},ab,\mathscr{N}]\left(-\frac{1}{\tau}\right).$$
$$(5.50)$$

To summarize, the torus partition function of the gauged theory $\mathscr{T}/\mathrm{Rep}(H_8)$ can be computed once we know the action of $\mathrm{Rep}(H_8)$ on the (untwisted) Hilbert space of $\mathscr{T}$.

When we gauge a $\mathbb{Z}_2=\{\mathbb{1},\eta\}$ symmetry, we keep the $\mathbb{Z}_2$-invariant sector of the Hilbert space $\mathscr{H}$ as well as the $\mathbb{Z}_2$-invariant sector of the defect Hilbert space $\mathscr{H}_\eta$. It is natural to ask what is the analog in the case of gauging $\mathrm{Rep}(H_8)$. We will show that there is a similar interpretation.

Let us first study the defect Hilbert space of invertible symmetries. Different topological sectors and their charges under the $\mathrm{Rep}(H_8)$ symmetry are listed in Table 5.1. This can be obtained by solving the irreps of the algebra of lasso actions following Appendix E.3.2.

For $\mathscr{H}\equiv\mathscr{H}_{\mathbb{1}}$ and $\mathscr{H}_{ab}$, the action of the duality line $\mathscr{N}$ can be unambiguously defined, therefore we expect the gauging to keep the states where $\mathscr{N}$ acts by its quantum dimension $\langle\mathscr{N}\rangle=2$. Indeed, looking at the corresponding partition functions from (5.45),

$$Z_{\mathscr{T}/\mathrm{Rep}(H_8),\mathscr{H}}=\frac{1}{8}\left(Z_{\mathscr{T}}[\mathbb{1},\mathbb{1},\mathbb{1}]+Z_{\mathscr{T}}[\mathbb{1},a,a]+Z_{\mathscr{T}}[\mathbb{1},b,b]+Z_{\mathscr{T}}[\mathbb{1},ab,ab]+2Z_{\mathscr{T}}[\mathbb{1},\mathscr{N},\mathscr{N}]\right),$$

$$Z_{\mathscr{T}/\mathrm{Rep}(H_8),\mathscr{H}_{ab}}=$$
$$\frac{1}{8}\left(Z_{\mathscr{T}}[ab,\mathbb{1},ab]+Z_{\mathscr{T}}[ab,ab,\mathbb{1}]-Z_{\mathscr{T}}[ab,b,a]-Z_{\mathscr{T}}[ab,b,a]+2Z_{\mathscr{T}}[ab,\mathscr{N},\mathscr{N}]\right),$$
$$(5.51)$$

we see that the gauging keeps only the states with charge $(1,1,1,1,2)$ under $(\mathbb{1},a,b,ab,\mathscr{N})$ in $\mathscr{H}$ and the states with charge $(1,-1,-1,1,2)$ in $\mathscr{H}_{ab}$. In the latter case, we are keeping the states which are odd under both $\mathbb{Z}_2^a$ and $\mathbb{Z}_2^b$ because of the non-trivial discrete torsion of $\mathbb{Z}_2^a\times\mathbb{Z}_2^b$ in the algebra object.

For $\mathscr{H}_a$ and $\mathscr{H}_b$, the situation is more subtle, with no analog in the invertible symmetry

Table 5.1. Topological sectors of defect Hilbert spaces of invertible symmetries together with their charges and spins. We also use the simple anyons in the symTFT of $\mathbb{Z}_2 \times \mathbb{Z}_2$ to label the topological sectors. The duality line $\mathcal{N}$ corresponds to the $\mathbb{Z}_2^{em}$ symmetry which exchanges e_i with m_i. In the special case where the anyon is invariant under $\mathbb{Z}_2^{em}$, the corresponding topological sector will split into two where the duality line $\mathcal{N}$ acts differently.

	$\mathbb{1}$	a	b	ab	$\mathcal{N}$	$\mathcal{Z}(\mathsf{Vec}_{\mathbb{Z}_2 \times \mathbb{Z}_2})$	spin s mod 1
	1	1	1	1	2	1	0
	1	1	1	1	-2	1	0
$\mathcal{H}_{\mathbb{1}}$	1	-1	1	-1	0	e_1	0
	1	1	-1	-1	0	e_2	0
	1	-1	-1	1	0	$e_1 e_2$	0
	1	-1	1	-1	$2i$	$m_1 e_1$	$\frac{1}{2}$
	1	-1	1	-1	$-2i$	$m_1 e_1$	$\frac{1}{2}$
$\mathcal{H}_a$	1	1	1	1	0	m_1	0
	1	1	-1	-1	0	$m_1 e_2$	0
	1	-1	-1	1	0	$m_1 e_1 e_2$	$\frac{1}{2}$
	1	1	-1	-1	$2i$	$m_2 e_2$	$\frac{1}{2}$
	1	1	-1	-1	$-2i$	$m_2 e_2$	$\frac{1}{2}$
$\mathcal{H}_b$	1	1	1	1	0	m_2	0
	1	-1	1	-1	0	$m_2 e_1$	0
	1	-1	-1	1	0	$m_2 e_1 e_2$	$\frac{1}{2}$
	1	-1	-1	1	2	$m_1 m_2 e_1 e_2$	0
	1	-1	-1	1	-2	$m_1 m_2 e_1 e_2$	0
$\mathcal{H}_{ab}$	1	1	1	1	0	$m_1 m_2$	0
	1	-1	1	-1	0	$m_1 m_2 e_1$	$\frac{1}{2}$
	1	1	-1	-1	0	$m_1 m_2 e_2$	$\frac{1}{2}$

case. Here, the action of the duality $\mathcal{N}$ can not be unambiguously defined and as a result it acts as $\pm 2i$ or 0. It no longer makes sense to keep the sectors where $\mathcal{N}$ acts as $\pm 2i$, and this is confirmed by the fact that both sectors have fractional spins. From the partition functions

$$
\begin{aligned}
Z_{\mathcal{T}/\mathsf{Rep}(H_8),\mathcal{H}_a} &= \frac{1}{2} \cdot \frac{1}{4} \left(Z_{\mathcal{T}}[a,\mathbb{1},a] + Z_{\mathcal{T}}[a,a,\mathbb{1}] - Z_{\mathcal{T}}[a,ab,b] - Z_{\mathcal{T}}[a,b,ab] \right), \\
Z_{\mathcal{T}/\mathsf{Rep}(H_8),\mathcal{H}_b} &= \frac{1}{2} \cdot \frac{1}{4} \left(Z_{\mathcal{T}}[b,\mathbb{1},b] + Z_{\mathcal{T}}[b,b,\mathbb{1}] - Z_{\mathcal{T}}[b,ab,a] - Z_{\mathcal{T}}[b,a,ab] \right),
\end{aligned}
\tag{5.52}
$$

we find that we keep the states with charge $(1,1,-1,-1,0)$ in $\mathcal{H}_a$ and the states with charge $(1,-1,+1,-1,0)$ in $\mathcal{H}_b$. But in both cases, there is an extra undesired factor of $\frac{1}{2}$ in the partition function. This seems to be pathological, but notice that the two sectors are actually identical because of the self-duality under gauging $\mathbb{Z}_2^a \times \mathbb{Z}_2^b$. Therefore, we should really interpret this as keeping a single sector in $\mathcal{H}_a$ (which is identified with the corresponding sector in $\mathcal{H}_b$ in the gauged theory).

Finally, let us consider the defect Hilbert space $\mathcal{H}_{\mathcal{N}}$. In this case, the action of the duality line $\mathcal{N}$ splits into 4 operators which we denote as $\mathcal{U}_{\mathcal{N},g}$. Among these, only two of them, $\mathcal{U}_{\mathcal{N},\mathbb{1}}$ and $\mathcal{U}_{\mathcal{N},ab}$ can be unambiguously defined with charges ± 1, as shown in Table 5.2. Meanwhile, there are only two invertible lines $\mathbb{1}$ and ab acting unambiguously with charges ± 1. Therefore, it is natural to expect that the $\mathsf{Rep}(H_8)$-gauging will project $\mathcal{H}_{\mathcal{N}}$ to the states where these four operators acting trivially as $+1$. Indeed, we can confirm this from the corresponding partition function

$$
Z_{\mathcal{T}/\mathsf{Rep}(H_8),\mathcal{H}_{\mathcal{N}}} = \frac{1}{4} \left(\mathscr{Z}_{\mathcal{T}}[\mathcal{N},\mathbb{1},\mathcal{N}] + \mathscr{Z}_{\mathcal{T}}[\mathcal{N},ab,\mathcal{N}] + \mathscr{Z}_{\mathcal{T}}[\mathcal{N},\mathcal{N},\mathbb{1}] + \mathscr{Z}_{\mathcal{T}}[\mathcal{N},\mathcal{N},ab] \right).
\tag{5.53}
$$

To summarize, similar to the gauging of finite invertible symmetries, we find gauging the non-invertible $\mathsf{Rep}(H_8)$ symmetry can be understood as projecting to the invariant states (up to the quantum dimension) of the topological lines whose actions can be unambiguously defined on each defect Hilbert space.

Table 5.2. Topological sectors of $\mathcal{H}_{\mathcal{N}}$ together with their charges solved by performing similar calculations as in Appendix E.3.2. Notice that in this case, the spin s can be determined using the fact that $e^{2\pi i s}$ is the same as the $\mathcal{U}_{\mathcal{N},\mathbb{1}}$ action.

	$\mathbb{1}$	a	b	ab	$\mathcal{U}_{\mathcal{N},\mathbb{1}}$	$\mathcal{U}_{\mathcal{N},a}$	$\mathcal{U}_{\mathcal{N},b}$	$\mathcal{U}_{\mathcal{N},ab}$	spin s mod 1
	1	$-i$	$-i$	-1	$e^{\frac{3\pi i}{4}}$	$e^{-\frac{3\pi i}{4}}$	$e^{-\frac{3\pi i}{4}}$	$e^{-\frac{\pi i}{4}}$	$\frac{3}{8}$
	1	$-i$	$-i$	-1	$e^{-\frac{\pi i}{4}}$	$e^{\frac{\pi i}{4}}$	$e^{\frac{\pi i}{4}}$	$e^{\frac{3\pi i}{4}}$	$\frac{7}{8}$
	1	i	i	-1	$e^{-\frac{3\pi i}{4}}$	$e^{\frac{3\pi i}{4}}$	$e^{\frac{3\pi i}{4}}$	$e^{\frac{\pi i}{4}}$	$\frac{5}{8}$
$\mathcal{H}_{\mathcal{N}}$	1	i	i	-1	$e^{\frac{\pi i}{4}}$	$e^{-\frac{\pi i}{4}}$	$e^{-\frac{\pi i}{4}}$	$e^{-\frac{3\pi i}{4}}$	$\frac{1}{8}$
	1	i	$-i$	1	1	$-i$	i	1	0
	1	$-i$	i	1	1	i	$-i$	1	0
	1	i	$-i$	1	-1	i	$-i$	-1	$\frac{1}{2}$
	1	$-i$	i	1	-1	$-i$	i	-1	$\frac{1}{2}$

To conclude this section, we argue that the quantum symmetry after gauging is again $\mathsf{Rep}(H_8)$. As pointed out in [267], gauging any possible algebra object (not necessarily of the form (5.32)) in $\mathsf{Rep}(H_8)$ leads to either $\mathsf{Rep}(H_8)$ or $\mathsf{Vec}_{D_8}^{\omega}$ for some $[\omega] \in H^3(D_8, U(1))$. Obviously the two can be distinguished by the number of invertible lines. It is straightforward to check using (5.36) that there are only 4 indecomposable bimodule objects with quantum dimension 1. Hence, the quantum symmetry must be $\mathsf{Rep}(H_8)$.

5.4 Gauging $\mathsf{Rep}(H_8)$ at $c = 1$

The primary example with the $\mathsf{Rep}(H_8)$ symmetry that we consider will be $c = 1$ CFTs [378]. In particular, we show below that a stack of two decoupled Ising CFTs (Ising^2 in short) is invariant under gauging its $\mathsf{Rep}(H_8)$ symmetry. This in turn implies the existence of a new topological defect line in the Ising^2 CFT coming from the half-space gauging of the $\mathsf{Rep}(H_8)$ symmetry, which will be discussed in Section 5.5.

Before we begin, we briefly review the $\mathsf{Rep}(H_8)$ symmetry that is realized at $c = 1$, following [378]. First, recall that the moduli space of (known) $c = 1$ CFTs consists of two continuous branches and three isolated points [150], as shown in Figure 5.1.

One of the continuous branches, called the circle branch, corresponds to the free compact

boson CFTs parameterized by the radius R of the compact boson. The other continuous branch, also parameterized by R, arises from gauging the charge conjugation symmetry (denoted as $\mathbb{Z}_2^C$) of the free boson CFTs, and we call it the orbifold branch. The orbifold branch and circle branch meet at the Berezinskii–Kosterlitz–Thouless (BKT) transition point where the minimal winding vertex operator $V_{0,1}$ becomes relevant. In our convention, the BKT point corresponds to $R = 2$ of the circle branch and $R = 1$ of the orbifold branch, and T-duality acts as $R \leftrightarrow 1/R$.

As was discussed in [378], the $\mathrm{Rep}(H_8)$ fusion category symmetry is realized at every point along the orbifold branch. The simplest way to understand this is as follows. First, at $R = \sqrt{2}$ on the orbifold branch, the theory corresponds to the Ising^2 CFT [149], which has the $\mathrm{TY}(\mathbb{Z}_2)_+ \boxtimes \mathrm{TY}(\mathbb{Z}_2)_+$ fusion category symmetry. Denote the simple topological lines of the two $\mathrm{TY}(\mathbb{Z}_2)_+$ fusion categories as $\{1, a, \mathcal{N}_1\}$ and $\{1, b, \mathcal{N}_2\}$, respectively, where a, b are $\mathbb{Z}_2$ symmetry lines and $\mathcal{N}_1$, $\mathcal{N}_2$ are Kramers-Wannier duality lines. The $\mathrm{Rep}(H_8)$ symmetry is realized as a subcategory of the $\mathrm{TY}(\mathbb{Z}_2)_+ \boxtimes \mathrm{TY}(\mathbb{Z}_2)_+$ fusion category, consisting of the simple lines $\{1, a, b, ab, \mathcal{N}\}$ where $\mathcal{N} \equiv \mathcal{N}_1 \mathcal{N}_2$.

To arrive at other values of $R \neq \sqrt{2}$ on the orbifold branch, one can deform the Ising^2 CFT by the exactly marginal operator $\varepsilon_1 \varepsilon_2$, where ε_i's stand for the energy operators with $(h, \bar{h}) = (\frac{1}{2}, \frac{1}{2})$ from the two Ising factors. Such a deformation explicitly breaks the $\mathrm{TY}(\mathbb{Z}_2)_+ \boxtimes \mathrm{TY}(\mathbb{Z}_2)_+$ fusion category symmetry down to its $\mathrm{Rep}(H_8)$ subcategory, and this shows that the $\mathrm{Rep}(H_8)$ symmetry is preserved across the entire orbifold branch.

Throughout the paper, we consider the gauging of symmetries only at the level of torus partition functions. Generally, the torus partition function alone may not be enough to fully determine a 1+1d CFT. However, at $c = 1$, all the known CFTs have distinct torus partition functions (up to T-duality) and hence computing the torus partition function will be sufficient for identifying the theory after gauging, assuming that the classification in [150] is complete.

Finally, as a side remark, we mention that there is another $\mathbb{Z}_2 \times \mathbb{Z}_2$ Tambara-Yamagami fusion category, that is equivalent to the representation category $\mathrm{Rep}(D_8)$ of the dihedral group of order 8, which also exists as a symmetry along the orbifold branch [378]. The $\mathrm{Rep}(D_8)$

fusion category has the same fusion algebra as $\text{Rep}(H_8)$, but has different F-symbols [39, 379].

The $\text{Rep}(D_8)$ symmetry is free of an 't Hooft anomaly, and one may also consider gauging the $\text{Rep}(D_8)$ symmetry on the orbifold branch. We will leave this analysis for the future, and focus on the $\text{Rep}(H_8)$ symmetry in this work. It is worth mentioning, however, that there is one additional feature that appears when gauging the $\text{Rep}(D_8)$ symmetry which does not occur in the case of $\text{Rep}(H_8)$. Namely, there are three inequivalent ways to gauge the $\text{Rep}(D_8)$ symmetry, whereas for the $\text{Rep}(H_8)$ symmetry we do not have such multiple options. This is due to the fact that $\text{Rep}(D_8)$ admits three distinct fiber functors, whereas $\text{Rep}(H_8)$ admits a unique fiber functor [379].

5.4.1 Ising^2 is self-dual under gauging $\text{Rep}(H_8)$

Before we discuss the $c = 1$ CFTs on the orbifold branch at a generic value of R, here we first show that the Ising^2 CFT (corresponding to $R = \sqrt{2}$) is self-dual under gauging $\text{Rep}(H_8)$. The computation is simpler in this case since the $\text{Rep}(H_8)$ symmetry commutes with the fully extended chiral algebra, namely two copies of the Ising chiral algebra ($c = \frac{1}{2}$ Virasoro algebra), with respect to which the theory is rational. With respect to the extended chiral algebra, there are 9 primary operators,

$$1, \quad \sigma_1, \quad \sigma_2, \quad \varepsilon_1, \quad \varepsilon_2, \quad \sigma_1\sigma_2, \quad \sigma_1\varepsilon_2, \quad \varepsilon_1\sigma_2, \quad \varepsilon_1\varepsilon_2, \tag{5.54}$$

where σ_i and ε_i are the spin and energy operators coming from the two Ising factors, respectively. The spin operators have conformal weights $(\frac{1}{16}, \frac{1}{16})$ and the energy operators have conformal weights $(\frac{1}{2}, \frac{1}{2})$.

We now proceed to gauge the $\text{Rep}(H_8)$ symmetry of the Ising^2 CFT on a torus. From the

general analysis in Section 5.3, the torus partition function after gauging is given by

$$\begin{aligned}
Z_{\text{Ising}^2/\text{Rep}(H_8)}(\tau) = \frac{1}{4}\Big(&-Z_{\text{Ising}^2}[\mathbb{1},\mathbb{1},\mathbb{1}](\tau) \\
&+ Z_{\text{Ising}^2}[\mathbb{1},a,a](\tau) + Z_{\text{Ising}^2}[a,\mathbb{1},a](\tau) + Z_{\text{Ising}^2}[a,a,\mathbb{1}](\tau) \\
&+ Z_{\text{Ising}^2}[\mathbb{1},b,b](\tau) + Z_{\text{Ising}^2}[b,\mathbb{1},b](\tau) + Z_{\text{Ising}^2}[b,b,\mathbb{1}](\tau) \\
&+ Z_{\text{Ising}^2}[\mathbb{1},ab,ab](\tau) + Z_{\text{Ising}^2}[ab,\mathbb{1},ab](\tau) + Z_{\text{Ising}^2}[ab,ab,\mathbb{1}](\tau) \\
&+ Z_{\text{Ising}^2}[\mathbb{1},\mathcal{N},\mathcal{N}](\tau) + Z_{\text{Ising}^2}[\mathcal{N},\mathbb{1},\mathcal{N}](\tau) + Z_{\text{Ising}^2}[\mathcal{N},\mathcal{N},\mathbb{1}](\tau) \\
&+ Z_{\text{Ising}^2}[ab,\mathcal{N},\mathcal{N}](\tau) + Z_{\text{Ising}^2}[\mathcal{N},ab,\mathcal{N}](\tau) + Z_{\text{Ising}^2}[\mathcal{N},\mathcal{N},ab](\tau)\Big).
\end{aligned}$$

(5.55)

The twisted partition functions appearing on the RHS of (5.55) can be computed straightforwardly, since they are simply products of two decoupled Ising CFT partition functions twisted by various topological lines. Generally, torus partition functions of the diagonal minimal models (such as the Ising CFT) twisted by arbitrary topological lines are known [309, 70]. To begin with, we have

$$Z_{\text{Ising}^2}(\tau) \equiv Z_{\text{Ising}^2}[\mathbb{1},\mathbb{1},\mathbb{1}](\tau) = \left(|\chi_0^{\text{Ising}}(\tau)|^2 + |\chi_{\frac{1}{16}}^{\text{Ising}}(\tau)|^2 + |\chi_{\frac{1}{2}}^{\text{Ising}}(\tau)|^2\right)^2, \qquad (5.56)$$

where the Ising characters are

$$\begin{aligned}
\chi_0^{\text{Ising}} &= \frac{1}{2}\left(\sqrt{\frac{\vartheta_3}{\eta}} + \sqrt{\frac{\vartheta_4}{\eta}}\right), \\
\chi_{\frac{1}{2}}^{\text{Ising}} &= \frac{1}{2}\left(\sqrt{\frac{\vartheta_3}{\eta}} - \sqrt{\frac{\vartheta_4}{\eta}}\right), \\
\chi_{\frac{1}{16}}^{\text{Ising}} &= \frac{1}{\sqrt{2}}\sqrt{\frac{\vartheta_2}{\eta}}.
\end{aligned}$$

(5.57)

The partition functions where one of the $\mathbb{Z}_2$ symmetry lines, a, b, or ab, is inserted along

the spatial cycle can be read off from the action of the $\mathbb{Z}_2$ symmetries on the primaries (5.54):

$$
\begin{aligned}
Z_{\text{Ising}^2}[\mathbb{1},a,a](\tau) &= Z_{\text{Ising}^2}[\mathbb{1},b,b](\tau) \\
&= \left(|\chi_0^{\text{Ising}}(\tau)|^2 - |\chi_{\frac{1}{16}}^{\text{Ising}}(\tau)|^2 + |\chi_{\frac{1}{2}}^{\text{Ising}}(\tau)|^2 \right) \\
&\quad \times \left(|\chi_0^{\text{Ising}}(\tau)|^2 + |\chi_{\frac{1}{16}}^{\text{Ising}}(\tau)|^2 + |\chi_{\frac{1}{2}}^{\text{Ising}}(\tau)|^2 \right), \\
Z_{\text{Ising}^2}[\mathbb{1},ab,ab](\tau) &= \left(|\chi_0^{\text{Ising}}(\tau)|^2 - |\chi_{\frac{1}{16}}^{\text{Ising}}(\tau)|^2 + |\chi_{\frac{1}{2}}^{\text{Ising}}(\tau)|^2 \right)^2 .
\end{aligned}
\tag{5.58}
$$

Recall that the modular S and T matrices for the Ising characters (5.57) are given by

$$
S = \frac{1}{2} \begin{pmatrix} 1 & 1 & \sqrt{2} \\ 1 & 1 & -\sqrt{2} \\ \sqrt{2} & -\sqrt{2} & 0 \end{pmatrix}, \quad
T = e^{-\frac{\pi i}{24}} \begin{pmatrix} 1 & 0 & 0 \\ 0 & -1 & 0 \\ 0 & 0 & e^{\frac{\pi i}{8}} \end{pmatrix}.
\tag{5.59}
$$

Applying the S-transformation to (5.58), we obtain the twisted partition functions where the $\mathbb{Z}_2$ symmetry lines are now wrapping around the Euclidean time cycle:

$$
\begin{aligned}
Z_{\text{Ising}^2}[a,\mathbb{1},a](\tau) &= Z_{\text{Ising}^2}[b,\mathbb{1},b](\tau) \\
&= \left(\chi_0^{\text{Ising}}(\tau)\overline{\chi}_{\frac{1}{2}}^{\text{Ising}}(\tau) + \chi_{\frac{1}{2}}^{\text{Ising}}(\tau)\overline{\chi}_0^{\text{Ising}}(\tau) + |\chi_{\frac{1}{16}}^{\text{Ising}}(\tau)|^2 \right) \\
&\quad \times \left(|\chi_0^{\text{Ising}}(\tau)|^2 + |\chi_{\frac{1}{16}}^{\text{Ising}}(\tau)|^2 + |\chi_{\frac{1}{2}}^{\text{Ising}}(\tau)|^2 \right), \\
Z_{\text{Ising}^2}[ab,\mathbb{1},ab](\tau) &= \left(\chi_0^{\text{Ising}}(\tau)\overline{\chi}_{\frac{1}{2}}^{\text{Ising}}(\tau) + \chi_{\frac{1}{2}}^{\text{Ising}}(\tau)\overline{\chi}_0^{\text{Ising}}(\tau) + |\chi_{\frac{1}{16}}^{\text{Ising}}(\tau)|^2 \right)^2 .
\end{aligned}
\tag{5.60}
$$

Further performing an additional T-transformation, we get

$$
\begin{aligned}
Z_{\text{Ising}^2}[a,a,\mathbb{1}](\tau) &= Z_{\text{Ising}^2}[b,b,\mathbb{1}](\tau) \\
&= \left(-\chi_0^{\text{Ising}}(\tau)\overline{\chi}_{\frac{1}{2}}^{\text{Ising}}(\tau) - \chi_{\frac{1}{2}}^{\text{Ising}}(\tau)\overline{\chi}_0^{\text{Ising}}(\tau) + |\chi_{\frac{1}{16}}^{\text{Ising}}(\tau)|^2 \right) \\
&\quad \times \left(|\chi_0^{\text{Ising}}(\tau)|^2 + |\chi_{\frac{1}{16}}^{\text{Ising}}(\tau)|^2 + |\chi_{\frac{1}{2}}^{\text{Ising}}(\tau)|^2 \right), \\
Z_{\text{Ising}^2}[ab,ab,\mathbb{1}](\tau) &= \left(-\chi_0^{\text{Ising}}(\tau)\overline{\chi}_{\frac{1}{2}}^{\text{Ising}}(\tau) - \chi_{\frac{1}{2}}^{\text{Ising}}(\tau)\overline{\chi}_0^{\text{Ising}}(\tau) + |\chi_{\frac{1}{16}}^{\text{Ising}}(\tau)|^2 \right)^2.
\end{aligned}
\tag{5.61}
$$

Next, if we insert the $\mathcal{N} \equiv \mathcal{N}_1\mathcal{N}_2$ line along the spatial cycle, we obtain

$$
Z_{\text{Ising}^2}[\mathbb{1},\mathcal{N},\mathcal{N}](\tau) = 2\left(|\chi_0^{\text{Ising}}(\tau)|^2 - |\chi_{\frac{1}{2}}^{\text{Ising}}(\tau)|^2 \right)^2,
\tag{5.62}
$$

since the spin operators map to non-local operators and do not contribute to the torus partition function, and the energy operators flip the sign under the action of $\mathcal{N}$. The factor of 2 comes from the quantum dimension of the line, $\langle\mathcal{N}\rangle = 2$. Performing the S-transformation, we obtain

$$
Z_{\text{Ising}^2}[\mathcal{N},\mathbb{1},\mathcal{N}](\tau) = \left(\chi_0^{\text{Ising}}(\tau)\overline{\chi}_{\frac{1}{16}}(\tau) + \chi_{\frac{1}{2}}^{\text{Ising}}(\tau)\overline{\chi}_{\frac{1}{16}}(\tau) + c.c. \right)^2.
\tag{5.63}
$$

Now, we apply the identity (5.48) that was derived in Section 5.3 to obtain

$$
\begin{aligned}
&Z_{\text{Ising}^2}[\mathcal{N},\mathbb{1},\mathcal{N}](\tau) + Z_{\text{Ising}^2}[\mathcal{N},ab,\mathcal{N}](\tau) \\
&= Z_{\text{Ising}^2}[\mathcal{N},\mathbb{1},\mathcal{N}](\tau+2) + Z_{\text{Ising}^2}[\mathcal{N},\mathbb{1},\mathcal{N}](\tau-2) \\
&= \left(e^{-\frac{2\pi i}{8}}\chi_0^{\text{Ising}}(\tau)\overline{\chi}_{\frac{1}{16}}(\tau) + e^{-\frac{2\pi i}{8}}\chi_{\frac{1}{2}}^{\text{Ising}}(\tau)\overline{\chi}_{\frac{1}{16}}(\tau) + c.c. \right)^2 \\
&\quad + \left(e^{\frac{2\pi i}{8}}\chi_0^{\text{Ising}}(\tau)\overline{\chi}_{\frac{1}{16}}(\tau) + e^{\frac{2\pi i}{8}}\chi_{\frac{1}{2}}^{\text{Ising}}(\tau)\overline{\chi}_{\frac{1}{16}}(\tau) + c.c. \right)^2.
\end{aligned}
\tag{5.64}
$$

Alternatively, we can also separately obtain $Z_{\text{Ising}^2}[\mathcal{N},ab,\mathcal{N}](\tau)$ as a product of two Ising CFT partition functions, namely $Z_{\text{Ising}^2}[\mathcal{N},ab,\mathcal{N}](\tau) = Z_{\text{Ising}}[\mathcal{N}_1,a,\mathcal{N}_1](\tau) \times Z_{\text{Ising}}[\mathcal{N}_2,b,\mathcal{N}_2](\tau)$, since $\mathcal{N} = \mathcal{N}_1\mathcal{N}_2$. However, to compute the RHS of (5.55), the combination (5.64) is sufficient.

Finally, we use (5.50) to obtain

$$
\begin{aligned}
&Z_{\mathrm{Ising}^2}[\mathbb{1},\mathcal{N},\mathcal{N}](\tau)+Z_{\mathrm{Ising}^2}[ab,\mathcal{N},\mathcal{N}](\tau)= \\
&Z_{\mathrm{Ising}^2}[\mathcal{N},\mathbb{1},\mathcal{N}](-1/\tau)+Z_{\mathrm{Ising}^2}[\mathcal{N},ab,\mathcal{N}](-1/\tau), \\
&Z_{\mathrm{Ising}^2}[\mathcal{N},\mathcal{N},\mathbb{1}](\tau)+Z_{\mathrm{Ising}^2}[\mathcal{N},\mathcal{N},ab](\tau)= \\
&Z_{\mathrm{Ising}^2}[\mathcal{N},\mathbb{1},\mathcal{N}](\tau+1)+Z_{\mathrm{Ising}^2}[\mathcal{N},ab,\mathcal{N}](\tau+1).
\end{aligned}
\tag{5.65}
$$

The explicit expressions in terms of the Ising characters are easily obtained from (5.64) and the S and T matrices in (5.59).

Plugging in all the ingredients into the RHS of (5.55), we finally obtain

$$
\begin{aligned}
Z_{\mathrm{Ising}^2/\mathrm{Rep}(H_8)}(\tau) &= \left(|\chi_0^{\mathrm{Ising}}(\tau)|^2+|\chi_{\frac{1}{16}}^{\mathrm{Ising}}(\tau)|^2+|\chi_{\frac{1}{2}}^{\mathrm{Ising}}(\tau)|^2\right)^2 \\
&= Z_{\mathrm{Ising}^2}(\tau).
\end{aligned}
\tag{5.66}
$$

We conclude that the Ising^2 CFT is invariant under gauging its Rep(H_8) symmetry as claimed. To be more precise, we confirmed this fact only at the level of the torus partition function. As was mentioned earlier, this is sufficient to prove the invariance of the full theory under the gauging, under the assumption that the classification of $c=1$ CFTs given in [150] is complete.

5.4.2 $c=1$ orbifold branch: $R \leftrightarrow 2/R$

Next, we move on to gauge the Rep(H_8) symmetry at a generic point on the orbifold branch. We will find that the theory at radius R is mapped to that at radius at $2/R$ and vice versa under gauging the Rep(H_8) symmetry. The Ising^2 CFT at $R=\sqrt{2}$ is a fixed point under this gauging, consistent with the analysis in the previous subsection.

Circle branch

We begin by briefly reviewing various facts about the $c = 1$ compact boson along the circle branch to set up the conventions. The action is

$$S = \frac{R^2}{4\pi} \int d\phi \wedge \star d\phi = \frac{R^2}{2\pi} \int d^2 z \partial \phi \bar{\partial} \phi \tag{5.67}$$

where $\phi \sim \phi + 2\pi$. Our convention for the radius R is such that the T-duality acts as $R \leftrightarrow 1/R$ and the self-dual radius is at $R = 1$, where the theory is described by the $SU(2)_1$ WZW model. The model has a symmetry

$$(U(1)_m \times U(1)_w) \rtimes \mathbb{Z}_2^C. \tag{5.68}$$

The momentum symmetry $U(1)_m$ is generated by the current $J_m = \frac{-iR^2}{2\pi} \star d\phi$ and the winding symmetry $U(1)_w$ is generated by the current $J_w = \frac{1}{2\pi} d\phi$. The conservation equations are given by $dJ_m = dJ_w = 0$. The charge conjugation symmetry $\mathbb{Z}_2^C$ acts as $\phi \to -\phi$.

At every radius R, there is a $u(1) \times \overline{u(1)}$ current algebra generated by $j(z) = \partial \phi(z)$ and $\bar{j}(\bar{z}) = \bar{\partial} \phi(\bar{z})$. The current algebra primaries are the local vertex operators,

$$V_{n,w}(z,\bar{z}) = e^{in\phi(z,\bar{z}) + iw\tilde{\phi}(z,\bar{z})}, \tag{5.69}$$

where $n, w \in \mathbb{Z}$ label the charges under the $U(1)_m$ and $U(1)_w$ symmetries, respectively. Here, $\tilde{\phi}$ is the dual boson satisfying $d\tilde{\phi} = -iR^2 \star d\phi$. The conformal weights of the vertex operators are

$$h_{n,w} = \frac{1}{4} \left(\frac{n}{R} + wR \right)^2, \quad \bar{h}_{n,w} = \frac{1}{4} \left(\frac{n}{R} - wR \right)^2. \tag{5.70}$$

The torus partition function is given by

$$Z_R^{circ}(\tau) = \frac{1}{|\eta(\tau)|^2} \sum_{n,w \in \mathbb{Z}} q^{\frac{1}{4}\left(\frac{n}{R} + wR\right)^2} \bar{q}^{\frac{1}{4}\left(\frac{n}{R} - wR\right)^2}, \tag{5.71}$$

168

where $q = e^{2\pi i \tau}$ as usual. Each term of the torus partition function (5.71) is a $u(1) \times \overline{u(1)}$ current algebra character.

Alternatively, we can also consider decomposing the torus partition function (5.71) into the characters of the Virasoro algebra. This will become useful later when we consider the $\text{Rep}(H_8)$ symmetry and its gauging along the orbifold branch. At $c = 1$, the Virasoro characters are given as follows [212]. For a generic conformal weight h, we have

$$\chi_h(\tau) = \frac{q^h}{\eta(\tau)} . \tag{5.72}$$

However, when $h = \ell^2/4$ for some integer ℓ, there are null states in the Verma module and the character is instead given by

$$\chi_{\ell^2/4}(\tau) = \frac{1}{\eta(\tau)} \left(q^{\ell^2/4} - q^{(\ell+2)^2/4} \right) . \tag{5.73}$$

The precise spectrum of Virasoro primary operators on the circle branch depends on the value of the radius R. For a generic value of R (such that $R \notin \mathbb{Q}$), the torus partition function (5.71) decomposes into the Virasoro characters as follows:

$$Z_R^{circ}(\tau) =$$

$$\frac{1}{|\eta(\tau)|^2} \left(\sum_{\substack{n,w \in \mathbb{Z} \\ (n,w) \neq (0,0)}} q^{\frac{1}{4}\left(\frac{n}{R}+wR\right)^2} \bar{q}^{\frac{1}{4}\left(\frac{n}{R}-wR\right)^2} + \sum_{\ell,m \in \mathbb{Z}_{\geq 0}} \left(q^{\ell^2} - q^{(\ell+1)^2} \right) \left(\bar{q}^{m^2} - \bar{q}^{(m+1)^2} \right) \right) . \tag{5.74}$$

From this, we read off the spectrum of Virasoro primary operators at a generic value of R:

$$V_{n,w}, \quad n,w \in \mathbb{Z}, (n,w) \neq (0,0), \quad (h,\bar{h}) = \left(\frac{1}{4}\left(\frac{n}{R}+wR\right)^2, \frac{1}{4}\left(\frac{n}{R}-wR\right)^2\right),$$

$$C_{\ell,m}, \quad \ell,m \in \mathbb{Z}_{\geq 0}, \quad (h,\bar{h}) = (\ell^2, m^2) . \tag{5.75}$$

The operators $C_{\ell,m}$ are made out of the (normal-ordered) Schur polynomials of currents $j(z)$, $\bar{j}(\bar{z})$ and their derivatives [389, 114, 113]. For instance, $C_{1,1} = j(z)\bar{j}(\bar{z})$ is the exactly marginal operator (namely the kinetic term), and $C_{0,0}$ is the identity operator.

The $\mathbb{Z}_2^C$ charge conjugation symmetry acts on the Virasoro primaries as

$$\mathbb{Z}_2^C: \quad V_{n,w} \to V_{-n,-w},$$
$$C_{\ell,m} \to (-1)^{\ell+m} C_{\ell,m}. \tag{5.76}$$

Denote the topological defect line that generates the $\mathbb{Z}_2^C$ symmetry as η. From the action of the $\mathbb{Z}_2^C$ symmetry on the primary operators, we can obtain the partition function of the free boson where the η line is inserted along the spatial cycle:

$$Z_R^{circ}[\mathbb{1},\eta,\eta](\tau) = \frac{1}{|\eta(\tau)|^2} \sum_{\ell,m\in\mathbb{Z}_{\geq 0}} (-1)^{\ell+m}(q^{\ell^2} - q^{(\ell+1)^2})(\bar{q}^{m^2} - \bar{q}^{(m+1)^2})$$
$$= \frac{|\vartheta_3(\tau)\vartheta_4(\tau)|}{|\eta(\tau)|^2}. \tag{5.77}$$

By performing the *S*-transformation, we obtain the twisted partition function

$$Z_R^{circ}[\eta,\mathbb{1},\eta](\tau) = \frac{1}{|\eta(\tau)|^2} \sum_{\ell,m\in\mathbb{Z}_{\geq 0}} 2q^{\frac{1}{4}(\ell+\frac{1}{2})^2}\bar{q}^{\frac{1}{4}(m+\frac{1}{2})^2} = \frac{|\vartheta_3(\tau)\vartheta_2(\tau)|}{|\eta(\tau)|^2}. \tag{5.78}$$

From (5.78), we read off the spectrum of Virasoro primary operators in the twisted Hilbert space associated with η [113]. First of all, we see that the twisted sector operators are doubly-degenerate, which is a consequence of the fact that the $\mathbb{Z}_2^m \times \mathbb{Z}_2^w$ subgroup of the momentum and winding symmetries acts projectively on the $\mathbb{Z}_2^C$ twisted sector due to a mixed anomaly between the three symmetries [378]. We denote the Virasoro primaries in the $\mathbb{Z}_2^C$ twisted sector as

$$D_{\ell,m}^{(i)}, \quad \ell,m \in \mathbb{Z}_{\geq 0}, i = 1,2, \quad (h,\bar{h}) = (\frac{1}{4}(\ell+\frac{1}{2})^2, \frac{1}{4}(m+\frac{1}{2})^2). \tag{5.79}$$

The $\mathbb{Z}_2^C$ charge of the twisted sector operators (5.79) is given by $2(h - \bar{h}) = \frac{1}{2}(\ell - m)(\ell + m + 1)$

[70, 242]. Namely,

$$\mathbb{Z}_2^C: \quad D_{\ell,m}^{(i)} \to (-1)^{\frac{1}{2}(\ell-m)(\ell+m+1)} D_{\ell,m}^{(i)}. \tag{5.80}$$

Orbifold branch and its $\mathrm{Rep}(H_8)$ **symmetry**

By gauging the $\mathbb{Z}_2^C$ charge conjugation symmetry of the compact boson, we obtain the orbifold branch theories, which we again label by the radius R. The torus partition function is given by

$$
\begin{aligned}
Z_R^{orb}(\tau) &= \frac{1}{2} \left(Z_R^{circ}[\mathbb{1},\mathbb{1},\mathbb{1}](\tau) + Z_R^{circ}[\mathbb{1},\eta,\eta](\tau) + Z_R^{circ}[\eta,\mathbb{1},\eta](\tau) + Z_R^{circ}[\eta,\eta,\mathbb{1}](\tau) \right) \\
&= \frac{1}{2} \left(Z_R^{circ}(\tau) + \frac{|\vartheta_3(\tau)\vartheta_4(\tau)|}{|\eta(\tau)|^2} + \frac{|\vartheta_3(\tau)\vartheta_2(\tau)|}{|\eta(\tau)|^2} + \frac{|\vartheta_4(\tau)\vartheta_2(\tau)|}{|\eta(\tau)|^2} \right).
\end{aligned}
\tag{5.81}
$$

Primary operators on the orbifold branch consist of the $\mathbb{Z}_2^C$-invariant operators of the circle branch, including the twisted sector operators (5.79). At a generic radius R, they are

$$V_{n,w}^+ \equiv \frac{1}{\sqrt{2}}(V_{n,w} + V_{-n,-w}),\ n,w \in \mathbb{Z}, (n,w) \neq (0,0),\ (h,\bar{h}) = (\frac{1}{4}(\frac{n}{R}+wR)^2, \frac{1}{4}(\frac{n}{R}-wR)^2),$$

$$C_{\ell,m},\quad \ell,m \in \mathbb{Z}_{\geq 0}, \ell+m \in 2\mathbb{Z},\quad (h,\bar{h}) = (\ell^2, m^2),$$

$$D_{\ell,m}^{(i)},\ \ell,m \in \mathbb{Z}_{\geq 0}, i=1,2, \frac{1}{2}(\ell-m)(\ell+m+1) \in 2\mathbb{Z},\ (h,\bar{h}) = (\frac{1}{4}(\ell+\frac{1}{2})^2, \frac{1}{4}(m+\frac{1}{2})^2),$$

$$\tag{5.82}$$

modulo the identification $V_{n,w}^+ = V_{-n,-w}^+$. At the Ising^2 point, the exactly marginal operator $C_{1,1}$ coincides with the $\varepsilon_1\varepsilon_2$ operator.

We may decompose the torus partition function on the orbifold branch (5.81) into the

171

Virasoro characters (assuming a generic value of R),

$$Z_R^{orb}(\tau) = \frac{1}{|\eta(\tau)|^2} \left\{ \frac{1}{2} \sum_{\substack{n,w\in\mathbb{Z} \\ (n,w)\neq(0,0)}} q^{\frac{1}{4}\left(\frac{n}{R}+wR\right)^2} \bar{q}^{\frac{1}{4}\left(\frac{n}{R}-wR\right)^2} \right.$$
$$\left. + \sum_{\substack{\ell,m\in\mathbb{Z}_{\geq 0} \\ \ell+m\in 2\mathbb{Z}}} \left(q^{\ell^2} - q^{(\ell+1)^2}\right)\left(\bar{q}^{m^2} - \bar{q}^{(m+1)^2}\right) + \sum_{\substack{\ell,m\in\mathbb{Z}_{\geq 0} \\ \frac{1}{2}(\ell-m)(\ell+m+1)\in 2\mathbb{Z}}} 2q^{\frac{1}{4}(\ell+\frac{1}{2})^2}\bar{q}^{\frac{1}{4}(m+\frac{1}{2})^2} \right\}.$$

$$(5.83)$$

The factor of $1/2$ in front of the first summation is to account for the double counting coming from the identification $V_{n,w}^+ = V_{-n,-w}^+$. The first two terms in (5.83) add up to the first two terms of (5.81), and the last term of (5.83) is the same as the sum of the last two terms of (5.81).

The action of the $\mathrm{Rep}(H_8)$ symmetry on the Virasoro primary operators (5.82) along the orbifold branch is given in [378], which we quote below. First, the two $\mathbb{Z}_2$ symmetries (denoted as $\mathbb{Z}_2^a$ and $\mathbb{Z}_2^b$) act as

$$\mathbb{Z}_2^a: \quad V_{n,w}^+ \to (-1)^n V_{n,w}^+,$$
$$\left(D_{\ell,m}^{(1)}, D_{\ell,m}^{(2)}\right) \to \left(-iD_{\ell,m}^{(2)}, iD_{\ell,m}^{(1)}\right),$$
$$C_{\ell,m} \to C_{\ell,m},$$

$$(5.84)$$

and

$$\mathbb{Z}_2^b: \quad V_{n,w}^+ \to (-1)^n V_{n,w}^+,$$
$$\left(D_{\ell,m}^{(1)}, D_{\ell,m}^{(2)}\right) \to \left(iD_{\ell,m}^{(2)}, -iD_{\ell,m}^{(1)}\right),$$
$$C_{\ell,m} \to C_{\ell,m},$$

$$(5.85)$$

respectively. The operators $C_{\ell,m}$ are invariant under $\mathbb{Z}_2^a \times \mathbb{Z}_2^b$. The diagonal subgroup $\mathbb{Z}_2^{ab} \subset \mathbb{Z}_2^a \times \mathbb{Z}_2^b$ corresponds to the quantum symmetry of the charge conjugation $\mathbb{Z}_2^C$ on the circle branch, which can be seen from the fact that all the twisted sector operators $D_{\ell,m}^{(i)}$ are odd

172

under $\mathbb{Z}_2^{ab}$, whereas the other operators $V_{n,w}^+$, $C_{\ell,m}$ are even.

On the other hand, the line $\mathcal{N}$ acts as

$$\mathcal{N}: \quad V_{n,w}^+ \to 2i^n(-1)^w V_{n,w}^+ \quad \text{for } n \in 2\mathbb{Z},$$
$$C_{\ell,m} \to 2C_{\ell,m}, \tag{5.86}$$
$$\text{other operators} \to \text{non-local operators}.$$

The factors of 2 come from the quantum dimension of the $\mathcal{N}$ line. The action indicates that the operators $C_{\ell,m}$ also commute with the $\mathcal{N}$ line, and hence with the entire $\text{Rep}(H_8)$. For instance, the exactly marginal operator $C_{1,1}$ lets us move up and down on the orbifold branch, while preserving $\text{Rep}(H_8)$.

Gauging $\text{Rep}(H_8)$

We now study the $\text{Rep}(H_8)$ gauging on the orbifold branch. As discussed in Section 5.3.3, we only need to know the action of the $\text{Rep}(H_8)$ symmetry on the Hilbert space, or equivalently, on the local primary operators to compute the relevant twisted partition functions, which has been spelled out above. For simplicity, below we perform the computation at a generic irrational point. However, the conclusion remains the same for any values of R.

From (5.47), we have

$$Z_R^{orb/\text{Rep}(H_8)}(\tau) = \frac{1}{4}\Big(-Z_R^{orb}[\mathbb{1},\mathbb{1},\mathbb{1}](\tau)$$
$$+ Z_R^{orb}[\mathbb{1},a,a](\tau) + Z_R^{orb}[a,\mathbb{1},a](\tau) + Z_R^{orb}[a,a,\mathbb{1}](\tau)$$
$$+ Z_R^{orb}[\mathbb{1},b,b](\tau) + Z_R^{orb}[b,\mathbb{1},b](\tau) + Z_R^{orb}[b,b,\mathbb{1}](\tau)$$
$$+ Z_R^{orb}[\mathbb{1},ab,ab](\tau) + Z_R^{orb}[ab,\mathbb{1},ab](\tau) + Z_R^{orb}[ab,ab,\mathbb{1}](\tau)$$
$$+ Z_R^{orb}[\mathbb{1},\mathcal{N},\mathcal{N}](\tau) + Z_R^{orb}[\mathcal{N},\mathbb{1},\mathcal{N}](\tau) + Z_R^{orb}[\mathcal{N},\mathcal{N},\mathbb{1}](\tau)$$
$$+ Z_R^{orb}[ab,\mathcal{N},\mathcal{N}](\tau) + Z_R^{orb}[\mathcal{N},ab,\mathcal{N}](\tau) + Z_R^{orb}[\mathcal{N},\mathcal{N},ab](\tau)\Big).$$
$$\tag{5.87}$$

From the action of $\mathbb{Z}_2^a$, $\mathbb{Z}_2^b$ symmetries on the Virasoro primaries (5.84), (5.85), we read off

$$Z_R^{orb}[\mathbb{1},a,a](\tau) = Z_R^{orb}[\mathbb{1},b,b](\tau) = \frac{1}{2|\eta(\tau)|^2}$$

$$\sum_{\substack{n,w\in\mathbb{Z} \\ (n,w)\neq(0,0)}} (-1)^n q^{\frac{1}{4}\left(\frac{n}{R}+wR\right)^2} \bar{q}^{\frac{1}{4}\left(\frac{n}{R}-wR\right)^2} + \frac{1}{|\eta(\tau)|^2} \sum_{\substack{\ell,m\in\mathbb{Z}_{\geq 0} \\ \ell+m\in 2\bar{\mathbb{Z}}}} \left(q^{\ell^2} - q^{(\ell+1)^2}\right)\left(\bar{q}^{m^2} - \bar{q}^{(m+1)^2}\right)$$

$$= \frac{1}{2}\frac{1}{|\eta(\tau)|^2}\left(\sum_{n,w\in\mathbb{Z}} (-1)^n q^{\frac{1}{4}\left(\frac{n}{R}+wR\right)^2} \bar{q}^{\frac{1}{4}\left(\frac{n}{R}-wR\right)^2} + \sum_{\ell,m\in\mathbb{Z}} (-1)^{\ell+m} q^{\ell^2}\bar{q}^{m^2}\right)$$

$$= \frac{1}{2}\frac{1}{|\eta(\tau)|^2}\left(\sum_{n,w\in\mathbb{Z}} (-1)^n q^{\frac{1}{4}\left(\frac{n}{R}+wR\right)^2} \bar{q}^{\frac{1}{4}\left(\frac{n}{R}-wR\right)^2} + |\vartheta_3(\tau)\vartheta_4(\tau)|\right), \tag{5.88}$$

where in the second step we have used

$$\sum_{\substack{\ell,m\in\mathbb{Z}_{\geq 0} \\ \ell+m\in 2\bar{\mathbb{Z}}}} \left(q^{\ell^2} - q^{(\ell+1)^2}\right)\left(\bar{q}^{m^2} - \bar{q}^{(m+1)^2}\right) = \frac{1}{2}\sum_{\ell,m\in\mathbb{Z}} (-1)^{\ell+m} q^{\ell^2}\bar{q}^{m^2} + \frac{1}{2}, \tag{5.89}$$

and absorbed $\frac{1}{2}$ into the $(n,w)=(0,0)$ term of the first summation. In the last step, we used $\sum_n (-1)^n q^{n^2} = \vartheta_4(2\tau) = \sqrt{\vartheta_3(\tau)\vartheta_4(\tau)}$.

The modular S-transformation is computed using the Poisson resummation, and we obtain

$$Z_R^{orb}[a,\mathbb{1},a](\tau) = Z_R^{orb}[b,\mathbb{1},b](\tau)$$

$$= \frac{1}{|\eta(\tau)|^2}\left(\frac{1}{2}\sum_{n,w\in\mathbb{Z}} q^{\frac{1}{4}\left(\frac{w}{R}+(n+\frac{1}{2})R\right)^2} \bar{q}^{\frac{1}{4}\left(\frac{w}{R}-(n+\frac{1}{2})R\right)^2} + \frac{1}{4}\sum_{\ell,m\in\mathbb{Z}} q^{\frac{1}{4}(\ell+\frac{1}{2})^2}\bar{q}^{\frac{1}{4}(m+\frac{1}{2})^2}\right) \tag{5.90}$$

$$= \frac{1}{2}\frac{1}{|\eta(\tau)|^2}\left(\sum_{n,w\in\mathbb{Z}} q^{\frac{1}{4}\left(\frac{w}{R}+(n+\frac{1}{2})R\right)^2} \bar{q}^{\frac{1}{4}\left(\frac{w}{R}-(n+\frac{1}{2})R\right)^2} + |\vartheta_2(\tau)\vartheta_3(\tau)|\right).$$

We can see that the result can be combined into a non-negative integer summation over Virasoro characters if we appropriately restrict the range of the summation variables. The spin selection rule for a non-anomaous $\mathbb{Z}_2$ symmetry, $h - \bar{h} \in \mathbb{Z}/2$ is also satisfied [242]. Further performing

the T-transformation, we obtain

$$
\begin{aligned}
Z_R^{orb}[a,a,\mathbb{1}](\tau) &= Z_R^{orb}[b,b,\mathbb{1}](\tau) \\
&= \frac{1}{2|\eta(\tau)|^2} \sum_{n,w \in \mathbb{Z}} (-1)^w q^{\frac{1}{4}\left(\frac{w}{R}+(n+\frac{1}{2})R\right)^2} \bar{q}^{\frac{1}{4}\left(\frac{w}{R}-(n+\frac{1}{2})R\right)^2} \\
&+ \frac{1}{4|\eta(\tau)|^2} \sum_{\ell,m \in \mathbb{Z}} (-1)^{\frac{1}{2}(\ell-m)(\ell+m+1)} q^{\frac{1}{4}(\ell+\frac{1}{2})^2} \bar{q}^{\frac{1}{4}(m+\frac{1}{2})^2} \\
&= \frac{1}{2} \frac{1}{|\eta(\tau)|^2} \left(\sum_{n,w \in \mathbb{Z}} (-1)^w q^{\frac{1}{4}\left(\frac{w}{R}+(n+\frac{1}{2})R\right)^2} \bar{q}^{\frac{1}{4}\left(\frac{w}{R}-(n+\frac{1}{2})R\right)^2} + |\vartheta_2(\tau)\vartheta_4(\tau)| \right) .
\end{aligned}
\tag{5.91}
$$

Next, recall that the diagonal $\mathbb{Z}_2^{ab} \subset \mathbb{Z}_2^a \times \mathbb{Z}_2^b$ symmetry generated by the line ab is the quantum symmetry of the $\mathbb{Z}_2^C$ charge conjugation symmetry on the circle branch [378]. Therefore, gauging $\mathbb{Z}_2^{ab}$ brings us back to the circle branch,

$$
Z_R^{circ}(\tau) = \frac{1}{2} \left(Z_R^{orb}[\mathbb{1},\mathbb{1},\mathbb{1}](\tau) + Z_R^{orb}[\mathbb{1},ab,ab](\tau) + Z_R^{orb}[ab,\mathbb{1},ab](\tau) + Z_R^{orb}[ab,ab,\mathbb{1}](\tau) \right) .
\tag{5.92}
$$

From this, we obtain

$$
\begin{aligned}
& Z_R^{orb}[\mathbb{1},ab,ab](\tau) + Z_R^{orb}[ab,\mathbb{1},ab](\tau) + Z_R^{orb}[ab,ab,\mathbb{1}](\tau) \\
&= 2Z_R^{circ}(\tau) - Z_R^{orb}[\mathbb{1},\mathbb{1},\mathbb{1}](\tau) \\
&= \frac{3}{2} \frac{1}{|\eta(\tau)|^2} \sum_{n,w \in \mathbb{Z}} q^{\frac{1}{4}\left(\frac{n}{R}+wR\right)^2} \bar{q}^{\frac{1}{4}\left(\frac{n}{R}-wR\right)^2} \\
&\quad - \frac{1}{2|\eta(\tau)|^2} \left(|\vartheta_3(\tau)\vartheta_4(\tau)| + |\vartheta_2(\tau)\vartheta_3(\tau)| + |\vartheta_2(\tau)\vartheta_4(\tau)| \right) .
\end{aligned}
\tag{5.93}
$$

Finally, we have [378]

$$
\begin{aligned}
& Z_R^{orb}[\mathcal{N},\mathbb{1},\mathcal{N}](\tau) \\
&= \frac{1}{2|\eta(\tau)|^2} \left(\sum_{m,n \in \mathbb{Z}} q^{\frac{1}{4}\left(\frac{n+1/2}{R}+\frac{(m+1/2)R}{2}\right)^2} \bar{q}^{\frac{1}{4}\left(\frac{n+1/2}{R}-\frac{(m+1/2)R}{2}\right)^2} + \sum_{m,n \in \mathbb{Z}} q^{\frac{1}{4}(m+1/2)^2} \bar{q}^{\frac{1}{4}(n+1/2)^2} \right) .
\end{aligned}
\tag{5.94}
$$

By applying the identity (5.48), we obtain

$$
Z_R^{orb}[\mathcal{N},\mathbb{1},\mathcal{N}](\tau) + Z_R^{orb}[\mathcal{N},ab,\mathcal{N}](\tau) = \frac{1}{|\eta(\tau)|^2} \sum_{m,n\in\mathbb{Z}} q^{\frac{1}{4}(m+1/2)^2}\bar{q}^{\frac{1}{4}(n+1/2)^2}
$$
$$
= \frac{2}{|\eta(\tau)|^2}|\vartheta_2(\tau)\vartheta_3(\tau)|\,.
$$
(5.95)

We then use the identities (5.50) to obtain

$$
Z_R^{orb}[\mathbb{1},\mathcal{N},\mathcal{N}](\tau) + Z_R^{orb}[ab,\mathcal{N},\mathcal{N}](\tau) = \frac{2}{|\eta(\tau)|^2}|\vartheta_3(\tau)\vartheta_4(\tau)|\,,
$$
$$
Z_R^{orb}[\mathcal{N},\mathcal{N},\mathbb{1}](\tau) + Z_R^{orb}[\mathcal{N},\mathcal{N},ab](\tau) = \frac{2}{|\eta(\tau)|^2}|\vartheta_2(\tau)\vartheta_4(\tau)|\,.
$$
(5.96)

By plugging all the twisted partition functions into the RHS of (5.87), we find

$$
Z_R^{orb/\mathsf{Rep}(H_8)}(\tau) = Z_{2/R}^{orb}(\tau)\,.
$$
(5.97)

That is, the orbifold theories at radii R and $2/R$ are mapped into each other under gauging the $\mathsf{Rep}(H_8)$ symmetry as claimed. In particular, at the Ising^2 point $R = \sqrt{2}$, we confirm again that the theory is self-dual under gauging the $\mathsf{Rep}(H_8)$ symmetry.

5.5   A new topological defect line in the Ising^2 CFT

The fact that the Ising^2 CFT is invariant under gauging the $\mathsf{Rep}(H_8)$ symmetry implies the existence of a new topological defect line $\mathscr{D}$ coming from the half-space gauging of the $\mathsf{Rep}(H_8)$ symmetry, according to the general considerations in Section 5.3. In this section, we (partially) bootstrap the action of the topological line $\mathscr{D}$ on the $c = 1$ Virasoro primary operators. Upon the modular S-transformation, we then also obtain the spectrum of operators in the twisted Hilbert space associated with $\mathscr{D}$.

The topological line $\mathscr{D}$ does not commute with the fully extended chiral algebra, but preserves the $c = 1$ Virasoro algebra. Moreover, there does not exist any relevant or marginal

operator which is invariant under the action of $\mathscr{D}$. The exactly marginal operator $\varepsilon_1 \varepsilon_2 = C_{1,1}$ anticommutes with $\mathscr{D}$. The latter property is reminiscent of the fact that the energy operator in the Ising CFT anticommutes with the Kramers-Wannier duality line. See [379, 378] for many other known topological defect lines in the Ising^2 CFT.

5.5.1 Virasoro primaries

The fact that the new topological line $\mathscr{D}$ does not commute with the fully extended chiral algebra of the Ising^2 CFT, namely two copies of the Ising chiral algebra, is easy to check, since the Ising^2 CFT is a diagonal rational CFT for that extended chiral algebra. In any diagonal rational CFT, the full spectrum of topological line operators which commute with the extended chiral algebra is known, where they are referred to as Verlinde lines [386, 309]. The Verlinde lines in the Ising^2 CFT form the fusion category $\mathsf{TY}(\mathbb{Z}_2)_+ \boxtimes \mathsf{TY}(\mathbb{Z}_2)_+$, and by inspecting the fusion algebra, it is straightforward to confirm that $\mathscr{D}$ is not one of the Verlinde lines.

Being topological, $\mathscr{D}$ commutes with the $c = 1$ Virasoro algebra, and we will attempt to find the action of $\mathscr{D}$ on the $c = 1$ Virasoro primaries. The spectrum of Virasoro primaries at a generic point on the orbifold branch was reviewed in Section 5.4 (see (5.82)). However, at $R = \sqrt{2}$ corresponding to the Ising^2 CFT, there are additional null states that do not appear at generic values of R, and the full spectrum of Virasoro primaries is more involved. Below we list all the $c = 1$ Virasoro primaries of the Ising^2 CFT and their conformal weights:

$$
\begin{aligned}
&V_{n,w}^+, &&n, w \in \mathbb{Z}, n \neq \pm 2w, &&(h, \bar{h}) = \left(\tfrac{1}{8}(n+2w)^2, \tfrac{1}{8}(n-2w)^2\right), \\
&A_{w,m}^+, &&w \in \mathbb{Z}_{>0}, m \in \mathbb{Z}_{\geq 0}, &&(h, \bar{h}) = \left(2w^2, m^2\right), \\
&B_{w,\ell}^+, &&w \in \mathbb{Z}_{>0}, \ell \in \mathbb{Z}_{\geq 0}, &&(h, \bar{h}) = \left(\ell^2, 2w^2\right), \\
&C_{\ell,m}, &&\ell, m \in \mathbb{Z}_{\geq 0}, \ell + m \in 2\mathbb{Z}, &&(h, \bar{h}) = \left(\ell^2, m^2\right), \\
&D_{\ell,m}^{(i)}, &&\ell, m \in \mathbb{Z}_{\geq 0}, i = 1, 2, \tfrac{1}{2}(\ell - m)(\ell + m + 1) \in 2\mathbb{Z}, &&(h, \bar{h}) = \left(\tfrac{1}{4}(\ell + \tfrac{1}{2})^2, \tfrac{1}{4}(m + \tfrac{1}{2})^2\right).
\end{aligned}
$$

$$\tag{5.98}$$

177

We review (5.98) in more detail in Appendix E.2. The operators $V_{n,w}^+$, $C_{\ell,m}$ and $D_{\ell,m}^{(i)}$ are identical to those in (5.82) at generic R, whereas the operators $A_{w,m}^+$ and $B_{w,\ell}^+$ are new primary operators appearing at $R = \sqrt{2}$ due to some of the generic modules at generic R splitting into infinitely-many degenerate modules at $R = \sqrt{2}$. There is an identification $V_{n,w}^+ = V_{-n,-w}^+$, and to avoid double-counting, we may restrict to $n \geq 1, w \in \mathbb{Z}$ or $n = 0, w \geq 1$.

The torus partition function of the Ising^2 CFT decomposes into a sum over the $c = 1$ Virasoro characters given in (5.72) and (5.73) as follows:

$$
\begin{aligned}
Z_{\text{Ising}^2}(\tau) = \frac{1}{|\eta(\tau)|^2} \Bigg\{ & \sum_{\substack{n \in \mathbb{Z}_{\geq 1}, w \in \mathbb{Z} \\ n \neq \pm 2w}} q^{\frac{1}{8}(n+2w)^2} \bar{q}^{\frac{1}{8}(n-2w)^2} + \sum_{w \in \mathbb{Z}_{\geq 1}} q^{\frac{1}{2}w^2} \bar{q}^{\frac{1}{2}w^2} \\
& + \sum_{w \in \mathbb{Z}_{\geq 1}, m \in \mathbb{Z}_{\geq 0}} q^{2w^2} \left(\bar{q}^{m^2} - \bar{q}^{(m+1)^2} \right) + \sum_{w \in \mathbb{Z}_{\geq 1}, \ell \in \mathbb{Z}_{\geq 0}} \left(q^{\ell^2} - q^{(\ell+1)^2} \right) \bar{q}^{2w^2} \\
& + \sum_{\substack{\ell, m \in \mathbb{Z}_{\geq 0} \\ \ell + m \in 2\mathbb{Z}}} \left(q^{\ell^2} - q^{(\ell+1)^2} \right) \left(\bar{q}^{m^2} - \bar{q}^{(m+1)^2} \right) + \sum_{\substack{\ell, m \in \mathbb{Z}_{\geq 0} \\ \frac{1}{2}(\ell-m)(\ell+m+1) \in 2\mathbb{Z}}} 2 q^{\frac{1}{4}(\ell+\frac{1}{2})^2} \bar{q}^{\frac{1}{4}(m+\frac{1}{2})^2} \Bigg\}.
\end{aligned}
\tag{5.99}
$$

Individual terms appearing in the torus partition function can be recognized as the contributions coming from the $c = 1$ Virasoro families corresponding to (5.98).

5.5.2 Bootstrapping the action of $\mathscr{D}$

Here, we will partially determine the action of $\mathscr{D}$ on the Virasoro primary operators (5.98) by demanding the following set of conditions:

- Consistency with the fusion algebra (5.39)

- Well-defined defect Hilbert space of $\mathscr{D}$

- Spin selection rule (5.137)

Let us elaborate on the conditions in more detail. First, recall that (from (5.39))

$$
\mathscr{D} \otimes \mathscr{D} = 1 \oplus a \oplus b \oplus ab \oplus 2\mathcal{N}.
\tag{5.100}
$$

This fusion algebra implies that $\mathscr{D}$ acts non-invertibly on local operators which are not invariant under the Rep(H_8) symmetry. That is, such operators are annihilated when surrounded by a closed loop of $\mathscr{D}$, or equivalently, they are mapped to non-local operators when $\mathscr{D}$ sweeps past them. Moreover, on the local operators which are Rep(H_8)-invariant, the action of $\mathscr{D}$ is order 2, up to the quantum dimension $\langle \mathscr{D} \rangle = \sqrt{8}$. Specifically, we have

$$\mathscr{D} \cdot (\mathscr{D} \cdot \mathscr{O}) = 8\mathscr{O} \quad \text{if } \mathscr{O} \text{ is Rep}(H_8)\text{-invariant}\,,$$
$$\mathscr{D} \cdot \mathscr{O} = 0 \quad \text{if } \mathscr{O} \text{ is not Rep}(H_8)\text{-invariant}\,,$$

(5.101)

where the notation $\mathscr{D} \cdot \mathscr{O}$ means the action of $\mathscr{D}$ on a local operator $\mathscr{O}$ by surrounding $\mathscr{O}$ with a closed loop of $\mathscr{D}$ (see Figure 5.2). By the state-operator map, such an action is related to the action of $\mathscr{D}$ as an operator on the state $|\mathscr{O}\rangle$.

Second, we require the twisted Hilbert space associated with $\mathscr{D}$ to decompose properly into a direct sum of $c = 1$ Virasoro representations [309]. Namely, we require the twisted torus partition function to decompose into $c = 1$ Virasoro characters with non-negative integer coefficients,

$$Z_{\text{Ising}^2}[\mathscr{D}, \mathbb{1}, \mathscr{D}](\tau) \overset{!}{=} \sum_{h,\bar{h}} n_{h,\bar{h}} \chi_h(\tau) \overline{\chi}_{\bar{h}}(\tau)\,, \quad n_{h,\bar{h}} \in \mathbb{Z}_{\geq 0}\,. \tag{5.102}$$

Such a condition is also known as a modular bootstrap condition. Since the twisted partition function (5.102) is related by the S-transformation to the partition function where $\mathscr{D}$ is inserted along the spatial cycle, $Z_{\text{Ising}^2}[\mathscr{D}, \mathbb{1}, \mathscr{D}](\tau) = Z_{\text{Ising}^2}[\mathbb{1}, \mathscr{D}, \mathscr{D}](-1/\tau)$, the condition that $n_{h,\bar{h}} \in \mathbb{Z}_{\geq 0}$ significantly constrains the action of $\mathscr{D}$ on the primaries.

Finally, the spin $s = h - \bar{h}$ of the operators in the twisted Hilbert space of $\mathscr{D}$ is constrained to take only a particular set of values, shown in (5.137). Such conditions on the spin of twisted sector operators are commonly referred to as spin selection rules [70]. The spin selection rule depends on the structure of the full fusion category formed by $\mathscr{D}$ and the topological lines of Rep(H_8), namely it is determined by the fusion algebra as well as the F-symbols. In Section 5.7, by solving the pentagon equations, we show that there are 8 fusion categories with the fusion

algebra (5.4). All of the 8 fusion categories are distinguished from each other by different spin selection rules. Here, we will use the spin selection rule (5.137) but postpone its derivation until Section 5.7. The spin selection rule not only imposes a consistency condition on the action of $\mathscr{D}$, but it also lets us to determine which of the 8 fusion categories are actually realized in the Ising^2 CFT once the action of $\mathscr{D}$ is obtained.

We now proceed to find the action of $\mathscr{D}$ on the primaries which solves the consistency conditions listed above. In particular, we focus on the action of $\mathscr{D}$ on the Rep(H_8)-invariant operators. The $\mathbb{Z}_2^a$ and $\mathbb{Z}_2^b$ symmetries act on $V_{n,w}^+$ as $V_{n,w}^+ \to (-1)^n V_{n,w}^+$, and leaves $A_{w,m}^+$, $B_{w,\ell}^+$, $C_{\ell,m}$ invariant. They also act nontrivially on $D_{\ell,m}^{(i)}$ operators for all values of ℓ and m. The line $\mathscr{N}$ acts on the Virasoro primaries as [378]

$$\mathscr{N}: \quad V_{2k,w}^+ \to 2(-1)^{k+w} V_{2k,w}^+,$$
$$A_{w,m}^+, B_{w,\ell}^+, C_{\ell,m} \text{ are left invariant up to quantum dimension}, \quad (5.103)$$
$$\text{other operators} \to \text{non-local operators}.$$

We see that $V_{2k,w}^+$ with $k + w \in 2\mathbb{Z}$ as well as $A_{w,m}^+$, $B_{w,\ell}^+$, $C_{\ell,m}$ operators are invariant under the Rep(H_8)-symmetry. Taking into account the fact that $\mathscr{O}$ and $\mathscr{D} \cdot \mathscr{O}$ should have the same conformal dimensions $(h, \bar{h})$, the general ansatz for the action of $\mathscr{D}$ we can consider is

$$\mathscr{D}: \quad \begin{pmatrix} V_{2k,w}^+ \\ V_{2w,k}^+ \end{pmatrix} \to \sqrt{8} X_{k,w} \begin{pmatrix} V_{2k,w}^+ \\ V_{2w,k}^+ \end{pmatrix},$$
$$A_{w,m}^+ \to \sqrt{8}(-1)^{f(w,m)} A_{w,m}^+,$$
$$B_{w,\ell}^+ \to \sqrt{8}(-1)^{g(w,\ell)} B_{w,\ell}^+, \quad (5.104)$$
$$C_{\ell,m} \to \sqrt{8}(-1)^{h(\ell,m)} C_{\ell,m},$$
$$\text{other operators} \to \text{non-local operators}.$$

Here, $X_{k,w}$ are 2×2 matrices satisfying $X_{k,w}^2 = 1$, and f, g, h are $\mathbb{Z}_2$-valued functions. Note that

$V_{2k,w}^+$ and $V_{2w,k}^+$ have the same conformal dimensions, and they can mix with each other under the action of $\mathscr{D}$ (also recall that $k \neq w$ from (5.98)). The general ansatz (5.104) solves the first consistency condition (5.101).

It turns out that the set of consistency conditions we impose is not sufficient to fully determine the form of the matrices $X_{k,w}$. However, we propose that

$$\operatorname{Tr} X_{k,w} = 0 \quad \text{for all } k \text{ and } w. \tag{5.105}$$

Under this assumption, we can write down the torus partition function with the $\mathscr{D}$ line wrapping around the spatial cycle as

$$Z_{\text{Ising}^2}[\mathbb{1}, \mathscr{D}, \mathscr{D}](\tau) = \frac{\sqrt{8}}{|\eta(\tau)|^2} \left\{ \sum_{w \in \mathbb{Z}_{\geq 1}, m \in \mathbb{Z}_{\geq 0}} (-1)^{f(w,m)} q^{2w^2} \left(\bar{q}^{m^2} - \bar{q}^{(m+1)^2} \right) \right.$$
$$+ \sum_{w \in \mathbb{Z}_{\geq 1}, \ell \in \mathbb{Z}_{\geq 0}} (-1)^{g(w,\ell)} \left(q^{\ell^2} - q^{(\ell+1)^2} \right) \bar{q}^{2w^2} \tag{5.106}$$
$$\left. + \sum_{\substack{\ell,m \in \mathbb{Z}_{\geq 0} \\ \ell+m \in 2\mathbb{Z}}} (-1)^{h(\ell,m)} \left(q^{\ell^2} - q^{(\ell+1)^2} \right) \left(\bar{q}^{m^2} - \bar{q}^{(m+1)^2} \right) \right\}.$$

The $A_{w,m}^+$, $B_{w,\ell}^+$, $C_{\ell,m}$ operators contribute to the above partition function.

Next, we proceed to constrain the $\mathbb{Z}_2$-valued functions f, g, h by imposing the condition (5.102). We find that the following solves (5.102):

$$f(w,m) = m + \alpha w,$$
$$g(w,\ell) = \ell + \beta w, \tag{5.107}$$
$$h(\ell,m) = \ell.$$

Here, $\alpha, \beta = 0, 1$, whose values will be further constrained below by imposing the spin selection

181

rule. More specifically, (5.107) leads to

$$Z_{\text{Ising}^2}[\mathscr{D}, \mathbb{1}, \mathscr{D}](\tau) = \frac{1}{|\eta(\tau)|^2} \left\{ \sum_{w \in \mathbb{Z}, m \in \mathbb{Z}_{\geq 0}} q^{\frac{1}{8}(w + \frac{\alpha}{2})^2} \bar{q}^{\frac{1}{4}(m + \frac{1}{2})^2} + \sum_{w \in \mathbb{Z}, \ell \in \mathbb{Z}_{\geq 0}} q^{\frac{1}{4}(\ell + \frac{1}{2})^2} \bar{q}^{\frac{1}{8}(w + \frac{\beta}{2})^2} \right\},$$

(5.108)

and we explicitly see that the condition (5.102) is satisfied.

The twisted torus partition function (5.108) provides us with the information about the spectrum of operators in the twisted Hilbert space of $\mathscr{D}$. In particular, we see the primary operators of conformal dimensions $(\frac{1}{8}(w + \frac{\alpha}{2})^2, \frac{1}{4}(m + \frac{1}{2})^2)$ for all $w \in \mathbb{Z}$, $m \in \mathbb{Z}_{\geq 0}$, as well as those with dimensions $(\frac{1}{4}(\ell + \frac{1}{2})^2, \frac{1}{8}(w + \frac{\beta}{2})^2)$ for all $\ell \in \mathbb{Z}_{\geq 0}$, $w \in \mathbb{Z}$. To further constrain the values of α and β, we now impose the spin selection rule (5.137). Namely, as explained in more detail in Section 5.7, the spin $s = h - \bar{h}$ mod $\frac{1}{2}$ of every operator in the twisted sector of $\mathscr{D}$ must take one of the 4 allowed values appearing in one of the 8 rows in (5.137). A priori, we do not know which of the 8 fusion categories, corresponding to the 8 rows in (5.137), is realized by $\mathscr{D}$. We find that

$$(\alpha, \beta) = (0, 1) \quad \text{is consistent with } \underline{\mathscr{E}}_{\mathbb{Z}_2}^{(-,+,+)} \text{Rep}(H_8) \text{ in Tab. 5.4},$$
$$(\alpha, \beta) = (1, 0) \quad \text{is consistent with } \underline{\mathscr{E}}_{\mathbb{Z}_2}^{(+,+,+)} \text{Rep}(H_8) \text{ in Tab. 5.3},$$

(5.109)

whereas $(\alpha, \beta) = (0, 0)$ and $(\alpha, \beta) = (1, 1)$ do not satisfy any of the 8 spin selection rules in (5.137).

Therefore, we have so far two possible candidate actions of $\mathscr{D}$ corresponding to the choice of $(\alpha, \beta) = (0, 1)$ or $(\alpha, \beta) = (1, 0)$. In fact, these two choices are related by another $\mathbb{Z}_2$-symmetry that is present in the Ising^2 CFT, namely the $\mathbb{Z}_2$ symmetry which swaps the two Ising factors. We denote this symmetry as $\mathbb{Z}_2^{\text{swap}}$, and the corresponding topological line as r. It combines with $\mathbb{Z}_2^a \times \mathbb{Z}_2^b$ to form a dihedral group of order 8. By tracking the decomposition of the Ising^2 characters into the $c = 1$ Virasoro characters, one can show that $\mathbb{Z}_2^{\text{swap}}$ acts on $A_{w,m}^+$ and $B_{w,\ell}^+$ as $(-1)^w$, and composing $\mathscr{D}$ with the $\mathbb{Z}_2^{\text{swap}}$ line has the effect of shifting both α and β

by 1 mod 2, see (5.104) and (5.107).

Without loss of generality, we may let $\mathscr{D}$ to be the topological line corresponding to the solution $(\alpha, \beta) = (0, 1)$. Then, another topological line $\mathscr{D}' \equiv \mathscr{D}r$ obtained by composing $\mathscr{D}$ with the $\mathbb{Z}_2^{\text{swap}}$-symmetry line r also satisfy the same fusion algebra (5.4), but it has different F-symbols and correspond to the other solution $(\alpha, \beta) = (1, 0)$. To conclude, we find that two of the 8 possible fusion categories, that are found in Section 5.7, are realized in the Ising^2 CFT. Namely, the two $\mathbb{Z}_2$-extensions of $\text{Rep}(H_8)$, denoted as $\underline{\mathscr{E}}_{\mathbb{Z}_2}^{(-,+,+)}\text{Rep}(H_8)$ and $\underline{\mathscr{E}}_{\mathbb{Z}_2}^{(+,+,+)}\text{Rep}(H_8)$, are realized respectively by $\mathscr{D}$ and $\mathscr{D}'$. The notation is explained in more detail in Section 5.7. The Fronbenius-Schur indicator for the $\mathscr{D}$ line is $\varepsilon_{\mathscr{D}} = +1$, and similarly for $\mathscr{D}'$.

As claimed earlier, we see that there are no relevant operators preserving $\mathscr{D}$, simply due to the fact there are no relevant operators preserving $\text{Rep}(H_8)$ and (5.101). Furthermore, the only marginal operator $C_{1,1}$, which is $\text{Rep}(H_8)$-invariant, anticommutes with $\mathscr{D}$, namely $\mathscr{D} \cdot C_{1,1} = -\sqrt{8}C_{1,1}$ where the factor of $\sqrt{8}$ comes from the quantum dimension of $\mathscr{D}$. The fact that $C_{1,1}$ should anticommute with $\mathscr{D}$ is intuitively clear. Starting from the Ising^2 point on the orbifold branch, one may deform the theory by $C_{1,1}$ either with a positive coefficient or with a negative coefficient. Since $C_{1,1}$ anticommutes with $\mathscr{D}$, $\mathscr{D}$ now becomes a topological interface between the two deformed theories. This is nothing but the topological interface between the theories at R and $2/R$ (in the vicinity of $R = \sqrt{2}$) coming from the half-space gauging of $\text{Rep}(H_8)$.

5.6 Stacking two theories with $\mathsf{TY}(\mathbb{Z}_2)_+$ symmetries

In this section, we study gauging the $\text{Rep}(H_8)$ symmetry of the theories obtained by stacking two (potentially different) theories with $\mathsf{TY}(\mathbb{Z}_2)_+$ symmetries. Motivated by the previous example, i.e. Ising^2, of self-duality under gauging $\text{Rep}(H_8)$, we want to see if it is true that every theory obtained in such a way is self-dual under gauging $\text{Rep}(H_8)$. We will start with a generic analysis and show that this is not the case in general. We will provide some additional special examples which are self-dual under gauging, and then provide some examples which are

not.

5.6.1 General analysis

Here, we consider taking two generic CFTs, both with $\mathsf{TY}(\mathbb{Z}_2)_+$ fusion category symmetry, and gauge the $\mathsf{Rep}(H_8)$ subcategory. We will find that, in general, the theory is not self-dual under gauging $\mathsf{Rep}(H_8)$, and we will also see from the general result why the known example is self-dual under $\mathsf{Rep}(H_8)$ gauging–essentially it requires some factorization property of topological sectors. Below, the nontrivial simple lines of the $\mathsf{TY}(\mathbb{Z}_2)_+$ categories of the two CFTs are denoted as $\{\eta_1, \mathscr{N}_1\}$ and $\{\eta_2, \mathscr{N}_2\}$, respectively.

First, note that the topological sectors and their modular properties of a 1+1d CFT with a $\mathsf{TY}(\mathbb{Z}_2)_+$ symmetry can be characterized by the anyons in the symTFT $\mathscr{Z}(\mathsf{TY}(\mathbb{Z}_2)_+) = \mathsf{Ising} \boxtimes \overline{\mathsf{Ising}}$. Since $\mathsf{TY}(\mathbb{Z}_2)_+$ fusion category itself can be equipped with a braiding structure to become a modular tensor category (MTC) Ising, the bulk symTFT is simply the Ising MTC together with its orientation reversal $\overline{\mathsf{Ising}}$. For more details on this theory, see [22].

We denote the simple anyons in the 3d Ising TFT as $(\mathbb{1}, \psi, \sigma)$, and the simple anyons in its orientation reversal $\overline{\mathsf{Ising}}$ as $(\overline{\mathbb{1}}, \overline{\psi}, \overline{\sigma})$. Let us order the 9 anyons in $\mathsf{Ising} \times \overline{\mathsf{Ising}}$ as

$$(1, \overline{1}), (1, \overline{\psi}), (1, \overline{\sigma}), (\psi, \overline{1}), (\psi, \overline{\psi}), (\psi, \overline{\sigma}), (\sigma, \overline{1}), (\sigma, \overline{\psi}), (\sigma, \overline{\sigma}). \qquad (5.110)$$

In this basis, the S and T matrices are given by

$$S = \begin{pmatrix}
\frac{1}{4} & \frac{1}{4} & \frac{1}{2\sqrt{2}} & \frac{1}{4} & \frac{1}{4} & \frac{1}{2\sqrt{2}} & \frac{1}{2\sqrt{2}} & \frac{1}{2\sqrt{2}} & \frac{1}{2} \\[6pt]
\frac{1}{4} & \frac{1}{4} & -\frac{1}{2\sqrt{2}} & \frac{1}{4} & \frac{1}{4} & -\frac{1}{2\sqrt{2}} & \frac{1}{2\sqrt{2}} & \frac{1}{2\sqrt{2}} & -\frac{1}{2} \\[6pt]
\frac{1}{2\sqrt{2}} & -\frac{1}{2\sqrt{2}} & 0 & \frac{1}{2\sqrt{2}} & -\frac{1}{2\sqrt{2}} & 0 & \frac{1}{2} & -\frac{1}{2} & 0 \\[6pt]
\frac{1}{4} & \frac{1}{4} & \frac{1}{2\sqrt{2}} & \frac{1}{4} & \frac{1}{4} & \frac{1}{2\sqrt{2}} & -\frac{1}{2\sqrt{2}} & -\frac{1}{2\sqrt{2}} & -\frac{1}{2} \\[6pt]
\frac{1}{4} & \frac{1}{4} & -\frac{1}{2\sqrt{2}} & \frac{1}{4} & \frac{1}{4} & -\frac{1}{2\sqrt{2}} & -\frac{1}{2\sqrt{2}} & -\frac{1}{2\sqrt{2}} & \frac{1}{2} \\[6pt]
\frac{1}{2\sqrt{2}} & -\frac{1}{2\sqrt{2}} & 0 & \frac{1}{2\sqrt{2}} & -\frac{1}{2\sqrt{2}} & 0 & -\frac{1}{2} & \frac{1}{2} & 0 \\[6pt]
\frac{1}{2\sqrt{2}} & \frac{1}{2\sqrt{2}} & \frac{1}{2} & -\frac{1}{2\sqrt{2}} & -\frac{1}{2\sqrt{2}} & -\frac{1}{2} & 0 & 0 & 0 \\[6pt]
\frac{1}{2\sqrt{2}} & \frac{1}{2\sqrt{2}} & -\frac{1}{2} & -\frac{1}{2\sqrt{2}} & -\frac{1}{2\sqrt{2}} & \frac{1}{2} & 0 & 0 & 0 \\[6pt]
\frac{1}{2} & -\frac{1}{2} & 0 & -\frac{1}{2} & \frac{1}{2} & 0 & 0 & 0 & 0
\end{pmatrix}, \qquad (5.111)$$

$$T = \begin{pmatrix}
1 & 0 & 0 & 0 & 0 & 0 & 0 & 0 & 0 \\[4pt]
0 & -1 & 0 & 0 & 0 & 0 & 0 & 0 & 0 \\[4pt]
0 & 0 & e^{-\frac{i\pi}{8}} & 0 & 0 & 0 & 0 & 0 & 0 \\[4pt]
0 & 0 & 0 & -1 & 0 & 0 & 0 & 0 & 0 \\[4pt]
0 & 0 & 0 & 0 & 1 & 0 & 0 & 0 & 0 \\[4pt]
0 & 0 & 0 & 0 & 0 & -e^{-\frac{i\pi}{8}} & 0 & 0 & 0 \\[4pt]
0 & 0 & 0 & 0 & 0 & 0 & e^{\frac{i\pi}{8}} & 0 & 0 \\[4pt]
0 & 0 & 0 & 0 & 0 & 0 & 0 & -e^{\frac{i\pi}{8}} & 0 \\[4pt]
0 & 0 & 0 & 0 & 0 & 0 & 0 & 0 & 1
\end{pmatrix}. \qquad (5.112)$$

Let us denote the torus partition function of the topological sector corresponding to an anyon $\mathbf{a}$ as $Z_{i,\mathbf{a}}(\tau)$ where $i = 1, 2$ labels the two stacked CFTs. Then, we can express the following

twisted partition functions as

$$Z_i[\mathbb{1},\mathbb{1},\mathbb{1}](\tau) = Z_{i,(\mathbb{1},\overline{\mathbb{1}})}(\tau) + Z_{i,(\psi,\overline{\psi})}(\tau) + Z_{i,(\sigma,\overline{\sigma})}(\tau),$$

$$Z_i[\eta_i,\mathbb{1},\eta_i](\tau) = Z_{i,(\mathbb{1},\overline{\psi})}(\tau) + Z_{i,(\psi,\overline{\mathbb{1}})}(\tau) + Z_{i,(\sigma,\overline{\sigma})}(\tau), \tag{5.113}$$

$$Z_i[\mathcal{N}_i,\mathbb{1},\mathcal{N}_i](\tau) = Z_{i,(\mathbb{1},\overline{\sigma})}(\tau) + Z_{i,(\sigma,\overline{\mathbb{1}})}(\tau) + Z_{i,(\sigma,\overline{\psi})}(\tau) + Z_{i,(\psi,\overline{\sigma})}(\tau).$$

The twisted partition functions of the stacked theory $\mathscr{T}_1 \times \mathscr{T}_2$ can be computed from the twisted partition functions Z_i. For instance,

$$Z_{\mathscr{T}_1 \times \mathscr{T}_2}[\mathbb{1},\mathbb{1},\mathbb{1}] = Z_1[\mathbb{1},\mathbb{1},\mathbb{1}]Z_2[\mathbb{1},\mathbb{1},\mathbb{1}], \quad Z_{\mathscr{T}_1 \times \mathscr{T}_2}[a,\mathbb{1},a] = Z_1[\eta_1,\mathbb{1},\eta_1]Z_2[\mathbb{1},\mathbb{1},\mathbb{1}],$$

$$Z_{\mathscr{T}_1 \times \mathscr{T}_2}[b,\mathbb{1},b] = Z_1[\mathbb{1},\mathbb{1},\mathbb{1}]Z_2[\eta_2,\mathbb{1},\eta_2], \quad Z_{\mathscr{T}_1 \times \mathscr{T}_2}[ab,\mathbb{1},ab] = Z_1[\eta_1,\mathbb{1},\eta_1]Z_2[\eta_2,\mathbb{1},\eta_2],$$

$$Z_{\mathscr{T}_1 \times \mathscr{T}_2}[\mathcal{N},\mathbb{1},\mathcal{N}] = Z_1[\mathcal{N}_1,\mathbb{1},\mathcal{N}_1]Z_2[\mathcal{N}_2,\mathbb{1},\mathcal{N}_2].$$

$$\tag{5.114}$$

Using modular transformations (5.111) and the general formula in Section 5.3.3, we find

$$Z_{\mathscr{T}_1 \times \mathscr{T}_2 / \mathsf{Rep}(H_8)}(\tau) = Z_{1,(1,\overline{1})}(\tau)Z_{2,(1,\overline{1})}(\tau) + Z_{1,(\psi,\overline{1})}(\tau)Z_{2,(1,\overline{\psi})}(\tau) + Z_{1,(1,\overline{\psi})}(\tau)Z_{2,(\psi,\overline{1})}(\tau)$$

$$+ Z_{1,(\psi,\overline{\psi})}(\tau)Z_{2,(\psi,\overline{\psi})}(\tau) + Z_{1,(\psi,\overline{\sigma})}(\tau)Z_{2,(\sigma,\overline{\psi})}(\tau) + Z_{1,(\sigma,\overline{\psi})}(\tau)Z_{2,(\psi,\overline{\sigma})}(\tau)$$

$$+ Z_{1,(\sigma,\overline{\sigma})}(\tau)Z_{2,(\sigma,\overline{\sigma})}(\tau) + Z_{1,(1,\overline{\sigma})}(\tau)Z_{2,(\sigma,\overline{1})}(\tau) + Z_{1,(\sigma,\overline{1})}(\tau)Z_{2,(1,\overline{\sigma})}(\tau), \tag{5.115}$$

while

$$Z_{\mathscr{T}_1 \times \mathscr{T}_2}(\tau) = \left(Z_{1,(1,\overline{1})}(\tau) + Z_{1,(\psi,\overline{\psi})}(\tau) + Z_{1,(\sigma,\overline{\sigma})}(\tau) \right)$$

$$\left(Z_{2,(1,\overline{1})}(\tau) + Z_{2,(\psi,\overline{\psi})}(\tau) + Z_{2,(\sigma,\overline{\sigma})}(\tau) \right). \tag{5.116}$$

Thus we have shown that stacking two theories with $\mathsf{TY}(\mathbb{Z}_2)_+$ symmetries does not necessarily lead to self-duality under gauging $\mathsf{Rep}(H_8)$.

5.6.2 Additional examples

Here, we provide a sufficient condition for self-duality under gauging $\mathsf{Rep}(H_8)$, which allows us to find additional examples which are self-dual.

Comparing two partition functions (5.115) and (5.116), we notice that a sufficient condition for the theory $\mathcal{T}_1 \times \mathcal{T}_2$ to be self-dual under gauging $\text{Rep}(H_8)$ is

$$Z_{i,(a,\bar{b})}(\tau) = Z_{i,a}(\tau) Z_{i,\bar{b}}(\tau), \quad \forall a, b, \tag{5.117}$$

as well as

$$Z_{1,a}(\tau) = Z_{2,a}(\tau) \quad \text{or} \quad Z_{1,\bar{a}}(\tau) = Z_{2,\bar{a}}(\tau). \tag{5.118}$$

Then,

$$
\begin{aligned}
Z_{\mathcal{T}_1 \times \mathcal{T}_2/\text{Rep}(H_8)}(\tau) &= \left(Z_{1,1}(\tau) Z_{2,\bar{1}}(\tau) + Z_{1,\psi}(\tau) Z_{2,\bar{\psi}}(\tau) + Z_{1,\sigma}(\tau) Z_{2,\bar{\sigma}}(\tau) \right) \\
&\quad \times \left(Z_{2,1}(\tau) Z_{1,\bar{1}}(\tau) + Z_{2,\psi}(\tau) Z_{1,\bar{\psi}}(\tau) + Z_{2,\sigma}(\tau) Z_{1,\bar{\sigma}}(\tau) \right) \\
&= \left(Z_{1,1}(\tau) Z_{1,\bar{1}}(\tau) + Z_{1,\psi}(\tau) Z_{1,\bar{\psi}}(\tau) + Z_{1,\sigma}(\tau) Z_{1,\bar{\sigma}}(\tau) \right) \\
&\quad \times \left(Z_{2,1}(\tau) Z_{2,\bar{1}}(\tau) + Z_{2,\psi}(\tau) Z_{2,\bar{\psi}}(\tau) + Z_{2,\sigma}(\tau) Z_{2,\bar{\sigma}}(\tau) \right) = Z_{\mathcal{T}_1 \times \mathcal{T}_2}(\tau), \\
\end{aligned}
\tag{5.119}
$$

where in the first equal sign we used (5.117) and the in the second equal sign we used (5.118).

Indeed, in the case of the Ising^2 CFT, the partition function for the Ising CFT does factorize as (5.117) with

$$
\begin{aligned}
\left(Z_{\text{Ising},1}(\tau), Z_{\text{Ising},\psi}(\tau), Z_{\text{Ising},\sigma}(\tau) \right) &= \left(\chi_0^{\text{Ising}}(\tau), \chi_{\frac{1}{2}}^{\text{Ising}}(\tau), \chi_{\frac{1}{16}}^{\text{Ising}}(\tau) \right), \\
\left(Z_{\text{Ising},\bar{1}}(\tau), Z_{\text{Ising},\bar{\psi}}(\tau), Z_{\text{Ising},\bar{\sigma}}(\tau) \right) &= \left(\overline{\chi_0^{\text{Ising}}(\tau)}, \overline{\chi_{\frac{1}{2}}^{\text{Ising}}(\tau)}, \overline{\chi_{\frac{1}{16}}^{\text{Ising}}(\tau)} \right).
\end{aligned}
\tag{5.120}
$$

To search for additional examples, we notice that the partition function of the Monster CFT also has the property (5.117). The Monster CFT is a holomorphic CFT with central charge $c_L = c = 24$ [136, 135], and it enjoys a $\text{TY}(\mathbb{Z}_2)_+$ symmetry [241]. Its twisted partition functions can be expressed in terms of the Ising characters ($c = 1/2$) and the Baby Monster ($c = 47/2$)

characters in a factorized way as (5.117), where

$$\left(Z_{\text{Monster},\mathbb{1}}(\tau), Z_{\text{Monster},\psi}(\tau), Z_{\text{Monster},\sigma}(\tau)\right) = \left(\chi_0^{\text{Ising}}(\tau), \chi_{\frac{1}{2}}^{\text{Ising}}(\tau), \chi_{\frac{1}{16}}^{\text{Ising}}(\tau)\right),$$

$$\left(Z_{\text{Monster},\overline{\mathbb{1}}}(\tau), Z_{\text{Monster},\overline{\psi}}(\tau), Z_{\text{Monster},\overline{\sigma}}(\tau)\right) = \left(\chi_0^{\text{Baby}}(\tau), \chi_{\frac{3}{2}}^{\text{Baby}}(\tau), \chi_{\frac{31}{16}}^{\text{Baby}}(\tau)\right). \tag{5.121}$$

Then, by (5.117), (5.118), (5.119), we conclude that both Monster^2 CFT and the Ising $\times$ Monster CFT are self-dual under gauging $\text{Rep}(H_8)$ (at the level of the torus partition functions), and therefore it is natural to suspect that the new topological defect line $\mathscr{D}$ exists in these theories as well. The self-duality under gauging $\text{Rep}(H_8)$ can alternatively be checked by directly calculating the twisted partition functions of the Monster CFT following [241]. More detailed analysis on these new topological lines is left for the future.

5.6.3 Non-examples

In this subsection, we provide two examples which are not self-dual under gauging the $\text{Rep}(H_8)$ symmetry. One of them is a nontrivial CFT and the other is a TQFT.

Two copies of $U(1)_4$

Here, we consider a stack of 2 copies of $c = 1$ compact boson theories at radius $R = \sqrt{2}$. The compact boson at radius $R = \sqrt{2}$ has $\text{TY}(\mathbb{Z}_2)_+$ symmetry [378]. It also enjoys the $U(1)_4$ extended chiral algebra under which the theory is rational. We have the following twisted partition functions [378]:

$$Z_{U(1)_4}[\mathbb{1}, \mathbb{1}, \mathbb{1}] = \sum_{m=-1}^{2} |K_m^2(\tau)|^2,$$

$$Z_{U(1)_4}[\mathbb{1}, \eta, \eta] = \sum_{m=-1}^{2} (-1)^m |K_m^2(\tau)|^2, \tag{5.122}$$

$$Z_{U(1)_4}[\mathbb{1}, \mathcal{N}, \mathcal{N}] = \sqrt{2} K_0^2(\tau) \left(\sum_{m \in \mathbb{Z}_{\geq 0}} (-1)^m \chi_{m^2}(\overline{\tau})\right).$$

Here, $\chi_{m^2}(\tau)$ are the Virasoro characters with scaling dimension m^2 (see (5.73)), and K_m^2 are characters of the $U(1)_4$ chiral algebra and given by

$$K_m^2(\tau) = \frac{1}{\eta(\tau)} \sum_{r \in \mathbb{Z}} q^{2\left(r + \frac{m}{4}\right)^2}, \quad m = -1, 0, 1, 2. \tag{5.123}$$

$K_m^2(\tau)$'s have the modular properties

$$K_n^2\left(-\frac{1}{\tau}\right) = \frac{1}{2} \sum_{m=-1}^{2} e^{-\frac{\pi i m n}{2}} K_m^2(\tau), \quad K_n^2(\tau+1) = e^{\frac{\pi i n^2}{4} - \frac{\pi i}{12}} K_n^2(\tau). \tag{5.124}$$

It is then straightforward to use modular transformations together with (5.114) to compute the partition function of $(U(1)_4 \times U(1)_4)/\mathrm{Rep}(H_8)$ following the general analysis in Section 5.3.3. We find

$$Z_{(U(1)_4 \times U(1)_4)/\mathrm{Rep}(H_8)}(\tau) = \frac{1}{2} K_0^2(\tau)^2 \left(\overline{K_0^2(\tau)}^2 + A^2 \right) + 4 K_0^2(\tau) K_1^2(\tau)(B^2 + C^2)$$

$$+ 4 K_1^2(\tau)^2 \overline{K_1^2(\tau)}^2 + 8 K_2^1(\tau) K_2^2(\tau) BC + 3 K_0^2(\tau) \overline{K_0^2(\tau)} K_2^2(\tau) \overline{K_2^2(\tau)} + \frac{1}{2} K_2^2(\tau)^2 \overline{K_2^2(\tau)}^2 \tag{5.125}$$

$$= q^{\frac{1}{12}} \overline{q}^{\frac{1}{12}} + 4 q^{\frac{5}{24}} \overline{q}^{\frac{5}{24}} + 4 q^{\frac{1}{3}} \overline{q}^{\frac{1}{3}} + 12 q^{\frac{7}{12}} \overline{q}^{\frac{7}{12}} + \cdots,$$

where

$$A = \sum_{m \in \mathbb{Z}_{\geq 0}} (-1)^m \chi_{m^2}(\overline{\tau}), \; B = \sum_{\substack{m \in \mathbb{Z}_{\geq 0}, \\ m = 0,3 \mod 4}} \chi_{\frac{(m+1/2)^2}{4}}(\overline{\tau}), \; C = \sum_{\substack{m \in \mathbb{Z}_{\geq 0}, \\ m = 1,2 \mod 4}} \chi_{\frac{(m+1/2)^2}{4}}(\overline{\tau}). \tag{5.126}$$

On the other hand,

$$Z_{U(1)_4 \times U(1)_4}(\tau) = \left(\sum_{m=-1}^{2} |K_m^2(\tau)|^2 \right)^2 = q^{\frac{1}{12}} \overline{q}^{\frac{1}{12}} + 4 q^{\frac{5}{24}} \overline{q}^{\frac{5}{24}} + 4 q^{\frac{1}{3}} \overline{q}^{\frac{1}{3}} + 8 q^{\frac{7}{12}} \overline{q}^{\frac{7}{12}} + \cdots. \tag{5.127}$$

Hence, we conclude that $U(1)_4 \times U(1)_4$ is not self-dual under gauging $\mathrm{Rep}(H_8)$.

Regular Ising^2 TQFT

Given a fusion category $\mathscr{C}$, 1+1d $\mathscr{C}$-symmetric TQFTs are classified by the module categories over $\mathscr{C}$ [181]. Here we consider a 1+1d TQFT which has the $\mathscr{C} = \mathsf{TY}(\mathbb{Z}_2)_+ \boxtimes \mathsf{TY}(\mathbb{Z}_2)_+$ symmetry. The nontrivial simple objects in the first $\mathsf{TY}(\mathbb{Z}_2)_+$ factor are denoted as η_1, $\mathscr{N}_1$, and those in the second factor as η_2, $\mathscr{N}_2$. We will consider the TQFT which corresponds to the regular module category of $\mathscr{C}$, that is, $\mathscr{C}$ viewed as a module category over itself. The untwisted (closed) Hilbert space $\mathscr{H}$ is spanned by the states labeled by the simple objects in $\mathscr{C}$,

$$\mathscr{H} = \mathrm{span}\left\{|\mathbb{1}\rangle, |\eta_1\rangle, |\eta_2\rangle, |\eta_1\eta_2\rangle, |\mathscr{N}_1\rangle, |\mathscr{N}_2\rangle, |\eta_2\mathscr{N}_1\rangle, |\eta_1\mathscr{N}_2\rangle, |\mathscr{N}\rangle\right\}, \qquad (5.128)$$

where $\mathscr{N} \equiv \mathscr{N}_1\mathscr{N}_2$. In particular, the theory has 9 degenerate states, and it represents a phase where the $\mathscr{C}$-symmetry is spontaneously broken completely. More generally, the twisted Hilbert space of a simple topological line $\mathscr{L}_i$ is given by

$$\mathscr{H}_{\mathscr{L}_i} \cong \bigoplus_j \mathrm{Hom}(\mathscr{L}_j, \mathscr{L}_i \otimes \mathscr{L}_j). \qquad (5.129)$$

We now consider gauging the $\mathrm{Rep}(H_8)$ subcategory of $\mathscr{C} = \mathsf{TY}(\mathbb{Z}_2)_+ \boxtimes \mathsf{TY}(\mathbb{Z}_2)_+$. The action of $\mathscr{C}$ on $\mathscr{H}$ is determined by the fusion coefficients. Namely, when a simple topological line $\mathscr{L}_i$ in $\mathscr{C}$ acts on a basis state $|\mathscr{L}_j\rangle$, we have $\mathscr{L}_i|\mathscr{L}_j\rangle = \sum_k N_{ij}^k |\mathscr{L}_k\rangle$, and then the action is linearly extended to arbitrary states in $\mathscr{H}$. The action on the twisted sectors are determined from the lasso actions. We can obtain the following twisted torus partition functions which are needed

for the Rep(H_8) gauging:

$$Z_{TQFT}[\mathbb{1},\mathbb{1},\mathbb{1}] = 9\,,$$

$$Z_{TQFT}[\mathbb{1},\eta_1,\eta_1] = Z_{TQFT}[\eta_1,\mathbb{1},\eta_1] = Z_{TQFT}[\eta_1,\eta_1,\mathbb{1}] = 3\,,$$

$$Z_{TQFT}[\mathbb{1},\eta_2,\eta_2] = Z_{TQFT}[\eta_2,\mathbb{1},\eta_2] = Z_{TQFT}[\eta_2,\eta_2,\mathbb{1}] = 3\,,$$

$$Z_{TQFT}[\mathbb{1},\eta_1\eta_2,\eta_1\eta_2] = Z_{TQFT}[\eta_1\eta_2,\mathbb{1},\eta_1\eta_2] = Z_{TQFT}[\eta_1\eta_2,\eta_1\eta_2,\mathbb{1}] = 1\,, \qquad (5.130)$$

$$Z_{TQFT}[\eta_1,\eta_2,\eta_1\eta_2] = Z_{TQFT}[\eta_2,\eta_1,\eta_1\eta_2] = Z_{TQFT}[\eta_2,\eta_1\eta_2,\eta_1] = 1\,,$$

$$Z_{TQFT}[\eta_1\eta_2,\eta_1,\eta_2] = Z_{TQFT}[\eta_1,\eta_1\eta_2,\eta_2] = Z_{TQFT}[\eta_1\eta_2,\eta_2,\eta_1] = 1\,,$$

$$Z_{TQFT}[\mathbb{1},\mathcal{N},\mathcal{N}] = Z_{TQFT}[\mathcal{N},\mathbb{1},\mathcal{N}] = Z_{TQFT}[\mathcal{N},\mathcal{N},\mathbb{1}] = 0\,.$$

The torus partition function after gauging Rep(H_8) is then given by

$$Z_{TQFT/\text{Rep}(H_8)} = 3 \qquad (5.131)$$

which differs from the original torus partition function $Z_{TQFT} = 9$.[9] Therefore, this TQFT serves as another non-example, which has the Ising^2 fusion category symmetry and yet is not invariant under gauging the Rep(H_8) subcategory.

5.7 Fusion categories including the new topological line: $\underline{\mathscr{E}}_{\mathbb{Z}_2}^{(i,\kappa_{\mathscr{D}},\varepsilon_{\mathscr{D}})}\text{Rep}(H_8)$

The fusion rules involving the new topological defect line $\mathscr{D}$ are given by (5.4). The fusion rules and F-symbols only involving $1, a, b, ab, \mathcal{N}$ are inherited from Rep(H_8). In this section, we solve the pentagon equations with the additional $\mathscr{D}$ line, and calculate the spin selection rules using the lasso action of topological defect lines on defect operators. There are 8 gauge-inequivalent solutions to the pentagon equations, which differ by three $\mathbb{Z}_2$-valued phases. The spin selection rules can unambiguously distinguish all 8 fusion categories. In particular, the

---

[9]The resulting theory after gauging Rep(H_8) would correspond to a module category of $\mathscr{C}$ with 3 simple objects.

Ising^2 CFT realizes 2 of the 8 solutions in Tab. 5.3 and Tab. 5.4. More details on calculations are presented in App. E.3.

5.7.1 F-symbols

Recall that non-trivial F-symbols of $\mathrm{Rep}(H_8)$ are

$$
\begin{aligned}
[F^{g\,\mathcal{N}\,h}_{\mathcal{N}}]_{(\mathcal{N},1,1),(\mathcal{N},1,1)} &= \chi(g,h), \quad [F^{\mathcal{N}\,g\,\mathcal{N}}_{h}]_{(\mathcal{N},1,1),(\mathcal{N},1,1)} = \chi(g,h), \\
[F^{\mathcal{N}\,\mathcal{N}\,\mathcal{N}}_{\mathcal{N}}]_{(g,1,1),(h,1,1)} &= \frac{1}{2}\chi^{-1}(g,h).
\end{aligned}
\tag{5.132}
$$

All other F-symbols of $\mathrm{Rep}(H_8)$ are trivial. With the additional $\mathscr{D}$ line, we explicitly solve the pentagon equations. The 8 inequivalent solutions for the F-symbols are listed in Tab. 5.3 and Tab. 5.4. We denote these 8 fusion categories as $\underline{\mathscr{E}}^{(i,\kappa_{\mathscr{D}},\varepsilon_{\mathscr{D}})}_{\mathbb{Z}_2}\mathrm{Rep}(H_8)$ with $i=\pm, \kappa_{\mathscr{D}}=\pm, \varepsilon_{\mathscr{D}}=\pm$.

Table 5.3. First 4 sets of F-symbols for $\underline{\mathscr{C}}^{(+,\kappa_\mathscr{D},\varepsilon_\mathscr{D})}_{\mathbb{Z}_2}\,\mathrm{Rep}(H_8)$ involving the $\mathscr{D}$ line, specified by $\kappa_\mathscr{D} = \pm 1,\ \varepsilon_\mathscr{D} = \pm 1$. $g,h = (1,a,b,ab)$, Greek letters $= 1,2$ due to the multiplicity $N^{\mathscr{N}\mathscr{N}}_{\mathscr{D}\mathscr{D}} = N^{\mathscr{D}}_{\mathscr{D}\mathscr{D}} = N^{\mathscr{D}}_{\mathscr{N}\mathscr{D}} = N^{\mathscr{D}}_{\mathscr{N}\mathscr{D}} = 2$.

Label	Value
$[F^{gh\mathscr{D}}_{\mathscr{D}}]_{(gh,1,1),(\mathscr{D},1,1)}$ $[F^{\mathscr{D}gh}_{\mathscr{D}}]_{(\mathscr{D},1,1),(gh,1,1)}$	$\begin{pmatrix}1&1&1&1\\1&1&-1&-1\\1&-1&-1&1\\1&-1&1&-1\end{pmatrix}$
$[F^{g\mathscr{N}\mathscr{D}}_{\mathscr{D}}]_{(\mathscr{N},1,\mu),(\mathscr{D},\nu,1)}$ $[F^{\mathscr{D}\mathscr{N}g}_{\mathscr{D}}]_{(\mathscr{D},\mu,1),(\mathscr{N},1,\nu)}$	$(\sigma^0,\ \sigma^1,\ \sigma^3,\ -i\sigma^2)$
$[F^{\mathscr{N}g\mathscr{D}}_{\mathscr{D}}]_{(\mathscr{N},1,\mu),(\mathscr{D},1,\nu)}$ $[F^{\mathscr{D}g\mathscr{N}}_{\mathscr{D}}]_{(\mathscr{D},1,\mu),(\mathscr{N},1,\nu)}$	$(\sigma^0,\ -\sigma^3,\ -\sigma^1,\ -i\sigma^2)$
$[F^{\mathscr{N}\mathscr{D}\mathscr{N}}_{\mathscr{D}}]_{(g,1,1),(\mathscr{D},\mu,\nu)}$ $[F^{\mathscr{D}g\mathscr{N}\mathscr{N}}_{\mathscr{D}}]_{(\mathscr{D},\mu,\nu),(g,1,1)}$	$\left(\dfrac{\sigma^1-\sigma^3}{2},\ \dfrac{\sigma^0-i\sigma^2}{2},\ -\dfrac{\sigma^0+i\sigma^2}{2},\ \mp\dfrac{\sigma^1+\sigma^3}{2}\right)$
$[F^{\mathscr{D}\mathscr{D}g}_{h}]_{(gh,1,1),(\mathscr{D},1,1)}$	$\begin{pmatrix}1&1&1&1\\1&1&-1&-1\\1&-1&-1&1\\1&-1&1&-1\end{pmatrix}$
$[F^{\mathscr{D}\mathscr{D}g}_{\mathscr{N}}]_{(\mathscr{N},\mu,1),(\mathscr{D},1,\nu)}$	$(\sigma^0,\ \sigma^1,\ \sigma^3,\ -i\sigma^2)$
$[F^{\mathscr{D}\mathscr{D}\mathscr{N}}_{g}]_{(\mathscr{N},\mu,1),(\mathscr{D},\nu,1)}$	$\left(-\dfrac{\sigma^1+\sigma^3}{\sqrt2},\ -\dfrac{\sigma^0+i\sigma^2}{\sqrt2},\ \dfrac{\sigma^0+i\sigma^2}{\sqrt2},\ \dfrac{\sigma^1+\sigma^3}{\sqrt2}\right)$
$[F^{\mathscr{D}\mathscr{D}\mathscr{N}}_{\mathscr{N}}]_{(g,1,1),(\mathscr{D},\mu,\nu)}$	$\left(-\dfrac{\sigma^0}{\sqrt2},\ \dfrac{\sigma^3}{\sqrt2},\ \dfrac{\sigma^1}{\sqrt2},\ -\dfrac{i\sigma^2}{\sqrt2}\right)$
$[F^{g\mathscr{D}\mathscr{D}}_{h}]_{(\mathscr{D},1,1),(gh,1,1)}$	$\begin{pmatrix}1&1&1&1\\1&1&-1&-1\\1&-1&-1&1\\1&-1&1&-1\end{pmatrix}$
$[F^{g\mathscr{D}\mathscr{D}}_{\mathscr{N}}]_{(\mathscr{D},1,\mu),(\mathscr{N},\nu,1)}$	$(\sigma^0,\ -\sigma^3,\ -\sigma^1,\ i\sigma^2)$
$[F^{\mathscr{N}\mathscr{D}\mathscr{D}}_{g}]_{(\mathscr{D},\mu,1),(\mathscr{N},\nu,1)}$	$(\sigma^0,\ \sigma^1,\ \sigma^3,\ i\sigma^2)$
$[F^{\mathscr{N}\mathscr{D}\mathscr{D}}_{\mathscr{N}}]_{(\mathscr{D},\mu,\nu),(g,1,1)}$	$\left(\dfrac{\sigma^1-\sigma^3}{2},\ \dfrac{\sigma^0-i\sigma^2}{2},\ -\dfrac{\sigma^0+i\sigma^2}{2},\ -\dfrac{\sigma^1+\sigma^3}{2}\right)$
$[F^{gh\mathscr{D}}_{\mathscr{D}}]_{(\mathscr{D},1,1),(\mathscr{D},1,1)}$	$\begin{pmatrix}1&1&1&1\\1&1&-1&-1\\1&-1&1&-1\\1&-1&-1&1\end{pmatrix}$
$[F^{\mathscr{N}\mathscr{D}g}_{\mathscr{D}}]_{(\mathscr{D},\mu,1),(\mathscr{D},1,\nu)}$	$(\sigma^0,\ \sigma^2,\ -\sigma^2,\ -\sigma^0)$
$[F^{g\mathscr{D}\mathscr{N}}_{\mathscr{D}}]_{(\mathscr{D},1,\mu),(\mathscr{D},\nu,1)}$	$(\sigma^0,\ -\sigma^2,\ \sigma^2,\ -\sigma^0)$
$[F^{\mathscr{N}\mathscr{D}\mathscr{N}}_{\mathscr{D}}]_{(\mathscr{D},\mu,\nu),(\mathscr{D},\rho,\sigma)}$	$\dfrac{\kappa_\mathscr{D}}{2\sqrt2}\begin{pmatrix}1+i&-1+i&-1+i&1+i\\-1+i&-1-i&1+i&1-i\\-1+i&1+i&-1-i&1-i\\1+i&1-i&1-i&-1-i\end{pmatrix}$
$[F^{\mathscr{D}\mathscr{D}g}_{h}]_{(\mathscr{D},1,1),(\mathscr{D},1,1)}$	$\begin{pmatrix}1&1&1&1\\1&1&-1&-1\\1&-1&1&-1\\1&-1&-1&1\end{pmatrix}$
$[F^{\mathscr{D}\mathscr{D}g}_{\mathscr{N}}]_{(\mathscr{D},1,\mu),(\mathscr{D},1,\nu)}$	$(\sigma^0,\ \sigma^2,\ -\sigma^2,\ -\sigma^0)$
$[F^{\mathscr{D}\mathscr{D}\mathscr{N}}_{g}]_{(\mathscr{D},\mu,1),(\mathscr{D},\nu,1)}$	$\left(-\dfrac{\sigma^1+\sigma^3}{\sqrt2},\ -i\dfrac{\sigma^1+\sigma^3}{\sqrt2},\ i\dfrac{\sigma^1+\sigma^3}{\sqrt2},\ \dfrac{\sigma^1-\sigma^3}{\sqrt2}\right)$
$[F^{\mathscr{D}\mathscr{N}\mathscr{D}}_{\mathscr{N}}]_{(\mathscr{D},\mu,\nu),(\mathscr{D},\rho,\sigma)}$	$\kappa_\mathscr{D}\begin{pmatrix}-\tfrac12&-\tfrac12&-\tfrac12&-\tfrac12\\-\tfrac12&\tfrac12&-\tfrac12&\tfrac12\\-\tfrac12&-\tfrac12&\tfrac12&\tfrac12\\-\tfrac12&\tfrac12&\tfrac12&-\tfrac12\end{pmatrix}$
$[F^{\mathscr{D}\mathscr{D}\mathscr{D}}_{\mathscr{D}}]_{(g,1,1),(h,1,1)}$	$\dfrac{\varepsilon_\mathscr{D}}{2\sqrt2}\begin{pmatrix}1&1&1&1\\1&-1&-1&1\\1&-1&1&-1\\1&1&-1&-1\end{pmatrix}$
$[F^{\mathscr{D}\mathscr{D}\mathscr{D}}_{\mathscr{D}}]_{(g,1,1),(\mathscr{N},\mu,\nu)}$	$\varepsilon_\mathscr{D}\left(-\dfrac{\sigma^0}{2},\ \dfrac{\sigma^2}{2},\ -\dfrac{\sigma^2}{2},\ -\dfrac{\sigma^0}{2}\right)$
$[F^{\mathscr{D}\mathscr{D}\mathscr{D}}_{\mathscr{D}}]_{(\mathscr{N},\mu,\nu),(g,1,1)}$	$\varepsilon_\mathscr{D}\left(\dfrac{\sigma^1-\sigma^3}{2\sqrt2},\ \dfrac{-i(\sigma^1+\sigma^3)}{2\sqrt2},\ \dfrac{i(\sigma^1+\sigma^3)}{2\sqrt2},\ \dfrac{\sigma^1-\sigma^3}{2\sqrt2}\right)$
$[F^{\mathscr{D}\mathscr{D}\mathscr{D}}_{\mathscr{D}}]_{(\mathscr{N},\mu,\nu),(\mathscr{N},\rho,\sigma)}$	$\dfrac{\varepsilon_\mathscr{D}\kappa_\mathscr{D}}{2\sqrt2}\begin{pmatrix}1&-1&-1&1\\-1&-1&1&1\\-1&1&-1&1\\i&-i&i&-1\end{pmatrix}$

Table 5.4. The other 4 sets of F-symbols for $\mathscr{E}_{\mathbb{Z}_2}^{(-,\kappa_\mathscr{D},\varepsilon_\mathscr{D})}\mathrm{Rep}(H_8)$ involving the $\mathscr{D}$ line, specified by $\kappa_\mathscr{D} = \pm 1, \varepsilon_\mathscr{D} = \pm 1$. Omitted F-symbols (left part in Tab. 5.3) are the same as Tab. 5.3. The two sets of F-symbols cannot be nicely grouped together because the difference is not an overall phase.

$[F_\mathscr{D}^{g\mathscr{D}h}]_{(\mathscr{D},1,1),(\mathscr{D},1,1)}$	$\begin{pmatrix} 1 & 1 & 1 & 1 \\ 1 & -1 & -1 & 1 \\ 1 & -1 & -1 & 1 \\ 1 & 1 & 1 & 1 \end{pmatrix}$
$[F_\mathscr{D}^{\mathscr{N}\mathscr{D}g}]_{(\mathscr{D},\mu,1),(\mathscr{D},1,\nu)}$	$(\sigma^0, -\sigma^2, \sigma^2, -\sigma^0)$
$[F_\mathscr{D}^{g\mathscr{D}\mathscr{N}}]_{(\mathscr{D},1,\mu),(\mathscr{D},\nu,1)}$	$(\sigma^0, \sigma^2, -\sigma^2, -\sigma^0)$
$[F_\mathscr{D}^{\mathscr{N}\mathscr{D}\mathscr{N}}]_{(\mathscr{D},\mu,\nu),(\mathscr{D},\rho,\sigma)}$	$\frac{\kappa_\mathscr{D}}{2\sqrt{2}} \begin{pmatrix} \begin{pmatrix} 1-i & -1-i \\ -1-i & 1-i \end{pmatrix} & \begin{pmatrix} -1-i & 1-i \\ -1+i & 1+i \end{pmatrix} \\ \begin{pmatrix} -1-i & -1+i \\ 1-i & 1+i \end{pmatrix} & \begin{pmatrix} 1-i & 1+i \\ 1+i & 1-i \end{pmatrix} \end{pmatrix}$
$[F_h^{\mathscr{D}g\mathscr{D}}]_{(\mathscr{D},1,1),(\mathscr{D},1,1)}$	$\begin{pmatrix} 1 & 1 & 1 & 1 \\ 1 & -1 & -1 & 1 \\ 1 & -1 & -1 & 1 \\ 1 & 1 & 1 & 1 \end{pmatrix}$
$[F_\mathscr{N}^{\mathscr{D}g\mathscr{D}}]_{(\mathscr{D},1,\mu),(\mathscr{D},1,\nu)}$	$(\sigma^0, -\sigma^2, \sigma^2, -\sigma^0)$
$[F_g^{\mathscr{D}\mathscr{N}\mathscr{D}}]_{(\mathscr{D},\mu,1),(\mathscr{D},\nu,1)}$	$(\frac{-\sigma^1+\sigma^3}{\sqrt{2}}, i\frac{\sigma^1+\sigma^3}{\sqrt{2}}, -i\frac{\sigma^1+\sigma^3}{\sqrt{2}}, \frac{\sigma^1-\sigma^3}{\sqrt{2}})$
$[F_\mathscr{N}^{\mathscr{D}\mathscr{N}\mathscr{D}}]_{(\mathscr{D},\mu,\nu),(\mathscr{D},\rho,\sigma)}$	$\kappa_\mathscr{D} \begin{pmatrix} \begin{pmatrix} \frac{1}{2} & -\frac{1}{2} \\ -\frac{i}{2} & -\frac{i}{2} \end{pmatrix} & \begin{pmatrix} -\frac{1}{2} & -\frac{1}{2} \\ -\frac{i}{2} & \frac{i}{2} \end{pmatrix} \\ \begin{pmatrix} \frac{i}{2} & \frac{i}{2} \\ \frac{1}{2} & -\frac{1}{2} \end{pmatrix} & \begin{pmatrix} \frac{i}{2} & -\frac{i}{2} \\ -\frac{1}{2} & -\frac{1}{2} \end{pmatrix} \end{pmatrix}$
$[F_\mathscr{D}^{\mathscr{D}\mathscr{D}\mathscr{D}}]_{(g,1,1),(h,1,1)}$	$\frac{\varepsilon_\mathscr{D}}{2\sqrt{2}} \begin{pmatrix} 1 & 1 & 1 & -1 \\ 1 & -1 & -1 & -1 \\ 1 & -1 & -1 & -1 \\ -1 & -1 & -1 & 1 \end{pmatrix}$
$[F_\mathscr{D}^{\mathscr{D}\mathscr{D}\mathscr{D}}]_{(g,1,1),(\mathscr{N},\mu,\nu)}$	$\varepsilon_\mathscr{D}(\frac{-\sigma^0}{2}, \frac{-\sigma^2}{2}, \frac{\sigma^2}{2}, \frac{-\sigma^0}{2})$
$[F_\mathscr{D}^{\mathscr{D}\mathscr{D}\mathscr{D}}]_{(\mathscr{N},\mu,\nu),(g,1,1)}$	$\varepsilon_\mathscr{D}(\frac{\sigma^1-\sigma^3}{2\sqrt{2}}, \frac{i(\sigma^1+\sigma^3)}{2\sqrt{2}}, -\frac{i(\sigma^1+\sigma^3)}{2\sqrt{2}}, \frac{\sigma^1-\sigma^3}{2\sqrt{2}})$
$[F_\mathscr{D}^{\mathscr{D}\mathscr{D}\mathscr{D}}]_{(\mathscr{N},\mu,\nu),(\mathscr{N},\rho,\sigma)}$	$\frac{\varepsilon_\mathscr{D}\kappa_\mathscr{D}}{2\sqrt{2}} \begin{pmatrix} \begin{pmatrix} 1 & -1 \\ -1 & -1 \end{pmatrix} & \begin{pmatrix} i & i \\ i & -i \end{pmatrix} \\ \begin{pmatrix} -i & -i \\ -i & i \end{pmatrix} & \begin{pmatrix} 1 & -1 \\ -1 & -1 \end{pmatrix} \end{pmatrix}$

The 8 solutions differ by the three $\mathbb{Z}_2$-valued phases $i = \pm, \kappa_\mathscr{D} = \pm, \varepsilon_\mathscr{D} = \pm$ appearing in $F_\mathscr{D}^{L\mathscr{D}R}, F_R^{\mathscr{D}L\mathscr{D}}, [F_\mathscr{D}^{\mathscr{D}\mathscr{D}\mathscr{D}}]_{L,R}$, where $L, R \in \{1, a, b, ab, \mathscr{N}\}$. In particular, $\varepsilon_\mathscr{D} \in H^3(\mathbb{Z}_2, U(1))$ is the Frobenius-Schur indicator for the new topological line $\mathscr{D}$.

We briefly discuss how to interpret the above 8 solutions in terms of the classification data (ρ, M, ε). First, specifying $\rho : \mathbb{Z}_2 \to \mathrm{BrPic}(\mathrm{Rep}(H_8))$ is equivalent to specifying a bimodule category $\mathscr{C}_\eta$ with a unique simple object $\mathscr{D}$ and the corresponding F-symbols are $F_\mathscr{D}^{r_1 r_2 \mathscr{D}}, F_\mathscr{D}^{r_1 \mathscr{D} r_2}, F_\mathscr{D}^{\mathscr{D} r_1 r_2}$'s. Next, we need to verify that indeed $\mathscr{C}_\eta$ is an *invertible* $\mathrm{Rep}(H_8)$-bimodule category, and if so, we make a choice of the $\mathrm{Rep}(H_8)$-bimodule equivalence functor

between $\mathscr{C}_\eta \boxtimes_{\mathsf{Rep}(H_8)} \mathscr{C}_\eta$ and $\mathsf{Rep}(H_8)$. This data is equivalent to the choice of the symmetry fractionalization class $M \in H^2_{[\rho]}(\mathbb{Z}_2, A)$ in the symTFT point of view and the corresponding F-symbols are $F_{r_2}^{\mathscr{D}\mathscr{D}r_1}, F_{r_2}^{\mathscr{D}r_1\mathscr{D}}, F_{r_2}^{r_1\mathscr{D}\mathscr{D}}$. Finally, the choice of the Frobenius-Schur indicator $\varepsilon_\mathscr{D}$ is the choice of the discrete torsion of $\mathbb{Z}_2$ in the symTFT picture, and the corresponding F-symbol data is the $\pm$ sign in $\left[F_\mathscr{D}^{\mathscr{D}\mathscr{D}\mathscr{D}}\right]_{\mathbb{1}\mathbb{1}}$. We summarize the above discussion in Table 5.5.

Table 5.5. The correspondence between the abstract structure appearing in the classification analysis and the concrete F-symbols, where $r_i \in \mathsf{Rep}(H_8)$. We drop the labels for the internal channel of the F-symbol for simplicity.

Abstract structure	F-symbols	Classification data
Left $\mathsf{Rep}(H_8)$-module category structure	$F_\mathscr{D}^{r_1 r_2 \mathscr{D}}$	$\rho : \mathbb{Z}_2 \to \mathsf{BrPic}(\mathsf{Rep}(H_8))$
Right $\mathsf{Rep}(H_8)$-module category structure	$F_\mathscr{D}^{\mathscr{D}r_1 r_2}$	
Bimodule structure that glues the left/right module structure together	$F_\mathscr{D}^{r_1 \mathscr{D}r_2}$	
A choice of the equivalence functor $\mathscr{C}_\eta \boxtimes_{\mathsf{Rep}(H_8)} \mathscr{C}_\eta \simeq \mathsf{Rep}(H_8)$	$F_{r_2}^{\mathscr{D}\mathscr{D}r_1}, F_{r_2}^{\mathscr{D}r_1\mathscr{D}}, F_{r_2}^{r_1\mathscr{D}\mathscr{D}}$	$M \in H^2_{[\rho]}(\mathbb{Z}_2, A)$
A choice of the FS indicator	the $\pm$ sign in $\left[F_\mathscr{D}^{\mathscr{D}\mathscr{D}\mathscr{D}}\right]_{\mathbb{1}\mathbb{1}}$	$\varepsilon_\mathscr{D} \in H^3(\mathbb{Z}_2, U(1))$

As one can see in Tables 5.3 and 5.4, there are 4 distinct sets of $(F_\mathscr{D}^{r_1 r_2 \mathscr{D}}, F_\mathscr{D}^{r_1 \mathscr{D}r_2}, F_\mathscr{D}^{\mathscr{D}r_1 r_2})$'s. This implies there are 4 distinct choices of ρ. For each given ρ, there is a unique choice of M, and two choices for the Frobenius-Schur indicator.[10]

5.7.2 Lasso actions and spin selection rules

Here, we derive the spin selection rules for the defect Hilbert space $\mathscr{H}_\mathscr{D}$ following [249, 70]. By using the lasso actions of the topological defect lines on the defect Hilbert space $\mathscr{H}_\mathscr{D}$, the allowed values of the spin s of operators in $\mathscr{H}_\mathscr{D}$ are constrained.

The lasso actions of topological defect lines $\{\mathbb{1}, a, b, ab, \mathscr{N}\}$ define maps acting on the defect Hilbert space of $\mathscr{D}$. The corresponding defect line configurations are shown both on the

---

[10]On the other hand, $\mathsf{Aut}(\mathsf{TY}(A, \chi, \varepsilon))$ is given by $\mathsf{Aut}(A, \chi)$ which is the group of automorphisms of A preserving χ, see [146, Section 4.2]. We can then compute $\mathsf{Aut}(\mathsf{Rep}(H_8)) = \mathbb{Z}_2$, and the discussion in Footnote 7 suggests there should be no more than 4 distinct choices of ρ, which is consistent with the above analysis.

cylinder (left) and on the plane (right) below:

$$\text{(5.133)}$$

Both $\mathcal{U}_g, \mathcal{U}_{\mathcal{N},\mu\nu}$ maps $\mathcal{H}_{\mathcal{D}} \to \mathcal{H}_{\mathcal{D}}$. The compositions of the lasso actions in Eq. (5.133) satisfy

$$\mathcal{U}_g \cdot \mathcal{U}_h = [F_{\mathcal{D}}^{h\mathcal{D}g}]_{(\mathcal{D},1,1),(\mathcal{D},1,1)}[F_{\mathcal{D}}^{\mathcal{D}hg}]_{(\mathcal{D},1,1),(hg,1,1)}[F_{\mathcal{D}}^{gh\mathcal{D}}]^{-1}_{(\mathcal{D},1,1),(gh,1,1)}\mathcal{U}_{gh},$$

$$\mathcal{U}_g \cdot \mathcal{U}_{\mathcal{N},\mu\nu} = [F_{\mathcal{D}}^{\mathcal{N}\mathcal{D}g}]_{(\mathcal{D},\mu,1),(\mathcal{D},1,\rho)}[F_{\mathcal{D}}^{g\mathcal{N}\mathcal{D}}]^{-1}_{(\mathcal{D},\rho,1),(\mathcal{N},1,\sigma)}[F_{\mathcal{D}}^{\mathcal{D}\mathcal{N}g}]_{(\mathcal{D},\nu,1),(\mathcal{N},1,\lambda)}\mathcal{U}_{\mathcal{N},\sigma\lambda},$$

$$\mathcal{U}_{\mathcal{N},\mu\nu} \cdot \mathcal{U}_g = [F_{\mathcal{D}}^{g\mathcal{D}\mathcal{N}}]_{(\mathcal{D},1,\nu),(\mathcal{D},\rho,1)}[F_{\mathcal{D}}^{\mathcal{N}g\mathcal{D}}]^{-1}_{(\mathcal{D},1,\mu),(\mathcal{N},1,\sigma)}[F_{\mathcal{D}}^{\mathcal{D}g\mathcal{N}}]_{(\mathcal{D},1,\rho),(\mathcal{N},1,\lambda)}\mathcal{U}_{\mathcal{N},\sigma\lambda},$$

$$\mathcal{U}_{\mathcal{N},\mu\nu} \cdot \mathcal{U}_{\mathcal{N},\rho\sigma} = 2[F_{\mathcal{N}}^{\mathcal{D}\mathcal{N}\mathcal{D}}]_{(\mathcal{D},\rho,\nu),(\mathcal{D},\rho',\nu')}$$

$$\sum_g [F_{\mathcal{D}}^{\mathcal{N}\mathcal{N}\mathcal{D}}]^{-1}_{(\mathcal{D},\nu',\mu),(g,1,1)}[F_{\mathcal{D}}^{\mathcal{D}\mathcal{N}\mathcal{N}}]_{(\mathcal{D},\sigma,\rho'),(g,1,1)}\mathcal{U}_g.$$

$$\text{(5.134)}$$

The composition of more general lasso actions are listed in App. E.3.2. There are 8 1-dimensional representations for this algebra of $\mathcal{U}_g, \mathcal{U}_{\mathcal{N},\mu\nu}$, for each set of F-symbols. The spin mod $\frac{1}{2}$ of the operators in the defect Hilbert space is obtained by

$$e^{4\pi i s} = \sum_g F_{\mathcal{D},(1,1,1),(g,1,1)}^{\mathcal{D}\mathcal{D}\mathcal{D}}\mathcal{U}_g + \sum_{\mu\nu} F_{\mathcal{D},(1,1,1),(\mathcal{N},\mu,\nu)}^{\mathcal{D}\mathcal{D}\mathcal{D}}\mathcal{U}_{\mathcal{N},\mu\nu}, \qquad (5.135)$$

which is derived using the following diagram,

$$
\mathscr{D} = \sum_g F^{\mathscr{DDD}}_{\mathscr{D},(1,1,1),(g,1,1)}\,\mathscr{D}^g + \sum_{\mu\nu} F^{\mathscr{DDD}}_{\mathscr{D},(1,1,1),(\mathscr{N},\mu,\nu)}\,\mathscr{N}^{\mu\,\nu}_{\mathscr{D}}
$$
$$
= \sum_g F^{\mathscr{DDD}}_{\mathscr{D},(1,1,1),(g,1,1)}\,\mathscr{D}_g + \sum_{\mu\nu} F^{\mathscr{DDD}}_{\mathscr{D},(1,1,1),(\mathscr{N},\mu,\nu)}\,\mathscr{D}^{v\ \mu}_{\mathscr{N}}\,.
$$
(5.136)

The spin selection rules $s \bmod \frac{1}{2}$ for the 8 different solutions of F-symbols in Tab. 5.3 and Tab. 5.4 are given by

$$
\begin{array}{l|cccc}
\underline{\mathscr{E}}^{(+,+,+)}_{\mathbb{Z}_2}\mathsf{Rep}(H_8);\mathrm{Tab.}\,5.3,\kappa_{\mathscr{D}}=+,\varepsilon_{\mathscr{D}}=+ & \frac{1}{16} & \frac{7}{32} & \frac{7}{16} & \frac{15}{32} \\[4pt]
\underline{\mathscr{E}}^{(+,+,-)}_{\mathbb{Z}_2}\mathsf{Rep}(H_8);\mathrm{Tab.}\,5.3,\kappa_{\mathscr{D}}=+,\varepsilon_{\mathscr{D}}=- & \frac{3}{16} & \frac{7}{32} & \frac{5}{16} & \frac{15}{32} \\[4pt]
\underline{\mathscr{E}}^{(+,-,+)}_{\mathbb{Z}_2}\mathsf{Rep}(H_8);\mathrm{Tab.}\,5.3,\kappa_{\mathscr{D}}=-,\varepsilon_{\mathscr{D}}=+ & \frac{1}{16} & \frac{3}{32} & \frac{11}{32} & \frac{7}{16} \\[4pt]
\underline{\mathscr{E}}^{(+,-,-)}_{\mathbb{Z}_2}\mathsf{Rep}(H_8);\mathrm{Tab.}\,5.3,\kappa_{\mathscr{D}}=-,\varepsilon_{\mathscr{D}}=- & \frac{3}{32} & \frac{3}{16} & \frac{5}{16} & \frac{11}{32} \\[4pt]
\underline{\mathscr{E}}^{(-,+,+)}_{\mathbb{Z}_2}\mathsf{Rep}(H_8);\mathrm{Tab.}\,5.4,\kappa_{\mathscr{D}}=+,\varepsilon_{\mathscr{D}}=+ & \frac{1}{32} & \frac{1}{16} & \frac{9}{32} & \frac{7}{16} \\[4pt]
\underline{\mathscr{E}}^{(-,+,-)}_{\mathbb{Z}_2}\mathsf{Rep}(H_8);\mathrm{Tab.}\,5.4,\kappa_{\mathscr{D}}=+,\varepsilon_{\mathscr{D}}=- & \frac{1}{32} & \frac{3}{16} & \frac{9}{32} & \frac{5}{16} \\[4pt]
\underline{\mathscr{E}}^{(-,-,+)}_{\mathbb{Z}_2}\mathsf{Rep}(H_8);\mathrm{Tab.}\,5.4,\kappa_{\mathscr{D}}=-,\varepsilon_{\mathscr{D}}=+ & \frac{1}{16} & \frac{5}{32} & \frac{13}{32} & \frac{7}{16} \\[4pt]
\underline{\mathscr{E}}^{(-,-,-)}_{\mathbb{Z}_2}\mathsf{Rep}(H_8);\mathrm{Tab.}\,5.4,\kappa_{\mathscr{D}}=-,\varepsilon_{\mathscr{D}}=- & \frac{5}{32} & \frac{3}{16} & \frac{5}{16} & \frac{13}{32} \\
\end{array}
$$
(5.137)

The spin selection rules for $\underline{\mathscr{E}}^{(+,\kappa_{\mathscr{D}},\varepsilon_{\mathscr{D}})}_{\mathbb{Z}_2}\mathsf{Rep}(H_8)$ and $\underline{\mathscr{E}}^{(-,\kappa_{\mathscr{D}},\varepsilon_{\mathscr{D}})}_{\mathbb{Z}_2}\mathsf{Rep}(H_8)$ are related by $s \leftrightarrow -s$.

Chapter. 5, in full, is a reprint of the material as it appears in Yichul Choi, Da-Chuan Lu, and Zhengdi Sun. Self-duality under gauging a non-invertible symmetry. *Journal of High Energy Physics*, 2024(1):142, January 2024. The dissertation author was one of the primary investigator and author of this paper.

Appendix A

Appendix to Chapter. 1

A.1 Large-N renormalization group

The theory considered in the main text is the QED_3 with level-k Chern-Simons term and Yukawa coupling between the fermion bilinear terms and the scalar fields,

$$
\begin{aligned}
\mathscr{L} &= \bar{\psi}(\mathbb{1}_{N_f} \otimes \gamma^\mu)(\partial_\mu - i a_\mu)\psi + \phi_a \bar{\psi}(M^a \otimes \mathbb{1}_2)\psi \\
&+ \frac{1}{2g^2}\phi_a(r_a - \partial^2)\phi_a + \frac{\lambda}{4}(\phi_a\phi_a)^2 \\
&+ \frac{ik}{4\pi}\varepsilon^{\mu\nu\lambda}a_\mu\partial_\nu a_\lambda + \frac{1}{4e^2}f_{\mu\nu}f^{\mu\nu}
\end{aligned}
\tag{A.1}
$$

where $\psi, \bar{\psi}$ represents N_f flavors of 2-component Dirac fermion fields, $\mathbb{1}_N, M^a$ act on the N_f-dimensional flavor space while $\mathbb{1}_2, \gamma^\mu, \Gamma^{(m),I}$ act on the 2-dimensional spinor space. $\Gamma^{(m),\mu_1,...,\mu_m}$ is defined as $\gamma^{[\mu_1}...\gamma^{\mu_m]}$ (antisymmetrize the indices) and any product of γ matrices can be reduced to this form. Since the spacetime dimension is 3, $\Gamma^{(i)}$ and $\Gamma^{(3-i)}$ are related by the Levi-Civita tensor. ϕ_a with $a = 1,...,N_b$ represent the scalar fields which are coupled to the fermion bilinears via a Yukawa type interaction. The last term in the Lagrangian is the Chern-Simons term with level k.

The bare propagators and vertices can be read off from the Lagrangian Eq. (A.1),

$$
\longrightarrow \; = -i\frac{p_\mu(\mathbb{1}_{N_f}\otimes\gamma^\mu)}{p^2}, \quad a \;\text{-----}\; b = D^{(0)}_{ab}(q) = \frac{g^2}{q^2}\delta_{a,b}
$$

$$
\mu \;\sim\!\!\sim\!\!\sim\; \nu = \Pi^{(0)}_{\mu\nu}(q) = \frac{e^2}{q^2}\left(\frac{q^2\delta_{\mu\nu}-q_\mu q_\nu + \frac{k}{2\pi}e^2\varepsilon_{\mu\nu\rho}q^\rho}{q^2+(\frac{k}{2\pi})^2 e^4}+\xi\frac{q_\mu q_\nu}{q^2}\right)
$$

(A.2)

where ξ is the gauge parameter. The vertices are,

$$
\mu \;\sim\!\!\sim\!\!\prec\; = i\mathbb{1}_{N_f}\otimes\gamma^\mu, \quad a \;\text{----}\prec\; = M^a\otimes\mathbb{1}_2
$$

(A.3)

The bare gauge and critical boson propagator will receive corrections, in the large-N limit, the corrections are dominated by fermion loops, for the gauge propagator,

$$
\begin{aligned}
\mu \;\sim\!\!\bigcirc\!\!\sim\; \nu &= (-1)[i\mathbb{1}_{N_f}\otimes\gamma^\mu][-i\frac{k_\rho(\mathbb{1}_{N_f}\otimes\gamma^\rho)}{k^2}][i\mathbb{1}_{N_f}\otimes\gamma^\nu][-i\frac{(k+q)_\sigma(\mathbb{1}_{N_f}\otimes\gamma^\sigma)}{(k+q)^2}] \\
&= (-1)\,\mathrm{tr}\big[\mathbb{1}_{N_f}\otimes\gamma^\mu\gamma^\rho\gamma^\nu\gamma^\sigma\big]\int\frac{d^3k}{(2\pi)^3}\frac{k_\rho(k+q)_\sigma}{k^2(k+q)^2} \\
&= -\frac{N_f|q|}{16}(\delta_{\mu\nu}-\frac{q_\mu q_\nu}{q^2})
\end{aligned}
$$

(A.4)
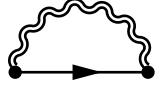
where N_f comes from trace over the identity matrix $\mathbb{1}_{N_f}$. Similar for the critical boson propagator,

$$
\begin{aligned}
a \;\text{--}\bigcirc\text{--}\; b &= (-1)[M^a\otimes\mathbb{1}_2][-i\frac{k_\rho(\mathbb{1}_{N_f}\otimes\gamma^\rho)}{k^2}][M^b\otimes\mathbb{1}_2][-i\frac{(k+q)_\sigma(\mathbb{1}_{N_f}\otimes\gamma^\sigma)}{(k+q)^2}] \\
&= \mathrm{tr}\big[M^aM^b\otimes\gamma^\rho\gamma^\sigma\big]\int\frac{d^3k}{(2\pi)^3}\frac{k_\rho(k+q)_\sigma}{k^2(k+q)^2} \\
&= -\mathrm{tr}\big[M^aM^b\big]\frac{|q|}{8}\equiv -\mathbb{M}\frac{|q|}{8}\delta_{ab}
\end{aligned}
$$

(A.5)
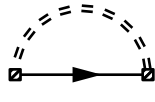
where in the last step we define $\mathrm{tr}\big[M^aM^b\big]=\mathbb{M}\delta_{ab}$, this is true when M^a is irreducible

representation. The corrected propagator can be found by using Dyson's equation,

$$\Pi(q) = \{[\Pi^{(0)}(q)]^{-1} - \Sigma^{(0)}(q)\}^{-1}$$

Note that in the large-N limit, this model flows to an interacting conformal field theory in the infrared limit, where the momentum scale q is much smaller than the coupling constants e, g, therefore the leading order of the dressed gauge and critical boson propagators are,

$$\mu \, \text{\textasciitilde\textasciitilde} \, \nu = \mu \, \text{\textasciitilde\textasciitilde} \, \nu + \mu \, \text{\textasciitilde}\bigcirc\text{\textasciitilde} \, \nu + \mu \, \text{\textasciitilde}\bigcirc\!\bigcirc\text{\textasciitilde} \, \nu$$

$$\Pi_{\mu\nu}(q) \simeq \frac{\mathbb{A}}{N_f |q|} \left(\delta_{\mu\nu} - \xi \frac{q_\mu q_\nu}{q^2} \right) + \frac{\mathbb{B}}{N_f} \frac{\varepsilon^{\mu\nu\rho} q_\rho}{q^2} + \mathcal{O}(|q|/e^2)$$

(A.6)

$$a \, \text{=====} \, b = a \, \text{------} \, b + a \, \text{--}\bigcirc\text{--} \, b + a \, \text{--}\bigcirc\!\bigcirc\text{--} \, b$$

$$D_{ab}(q) \simeq \frac{8}{\mathbb{M} |q|} \delta_{ab} + \mathcal{O}(|q|/g^2) \equiv D(q)\delta_{ab}$$

(A.7)

where $\mathbb{A} = \left(16^{-1} + 16\kappa^2\right)^{-1}, \mathbb{B} = \left((256\kappa)^{-1} + \kappa\right)^{-1}$, and $\kappa = k/(2\pi N_f)$, a simple check is when $k = 0$, $\mathbb{A} = 16, \mathbb{B} = 0$ match the coefficients in the large-N analysis of QED$_3$ theory. Note that κ is not inverse proportional to the 't Hooft coupling and can be any real number, the large-N limit is to take N_f, k to ∞ while keeping κ fixed. We also keep the gauge parameter ξ in the calculation and check that the final result does not depend on ξ.

A.1.1 Basic diagrams for $1/N$ corrections: self-energy

We extract the logarithmic divergences from the diagrams and using k, Λ to denote the external momentum and UV cutoff respectively, the self-energy corrections are,

$$= \int \frac{d^3q}{(2\pi)^3} [\Pi_{\mu\nu}(q)][i\mathbb{1}_{N_f} \otimes \gamma^\mu][-i\frac{(k+q)_\sigma(\mathbb{1}_{N_f} \otimes \gamma^\sigma)}{(k+q)^2}][i\mathbb{1}_{N_f} \otimes \gamma^\nu]$$

$$= (i\mathbb{1}_{N_f} \otimes \gamma^\mu)k_\mu \frac{\mathbb{A}(1-3\xi)}{6\pi^2 N_f}\ln(k/\Lambda) + reg. \tag{A.8}$$

$$= \int \frac{d^3q}{(2\pi)^3} [D(q)\delta_{ab}][M^a \otimes \mathbb{1}_2][-i\frac{(k+q)_\sigma(\mathbb{1}_{N_f} \otimes \gamma^\sigma)}{(k+q)^2}][M^b \otimes \mathbb{1}_2]$$

$$= (i\mathbb{1}_{N_f} \otimes \gamma^\mu)k_\mu \frac{8C_M}{6\pi^2 \mathbb{M}}\ln(k/\Lambda) + reg. \tag{A.9}$$

where we define $M^a M^a = C_M \mathbb{1}_{N_f}$ in analogy of the Casimir.

A.1.2 Basic diagrams for $1/N$ corrections: vertex corrections

The four-fermion interactions in general can be added to the Lagrangian perturbatively, and assuming the small four-fermion perturbations won't drive the system to other fixed points. The general form for such interactions is,

$$K_{(\alpha,(m_1),I),(\beta,(m_2),J)}\bar{\psi}(V^\alpha \otimes \Gamma^{(m_1),I})\psi\bar{\psi}(V^\beta \otimes \Gamma^{(m_2),J})\psi$$

For simplicity and physical relevance, we will consider a subset of the four-fermion interactions with the form,

$$\mathscr{L} \supset \mathscr{L}_{\text{int}} = u_{\alpha,(m),I}(\bar{\psi}(V^\alpha \otimes \Gamma^{(m),I})\psi)^2 \tag{A.10}$$

We introduce the diagrams for the interaction vertices as,

$$= u_{\alpha,(m),I}(V^\alpha \otimes \Gamma^{(m),I}), \qquad = K_{(\alpha,(m_1),I),(\beta,(m_2),J)}\begin{bmatrix} (V^\alpha \otimes \Gamma^{(m_1),I}) \\ \otimes \\ (V^\beta \otimes \Gamma^{(m_2),J}) \end{bmatrix}$$

$$(A.11)$$

The vertex corrections are

$$= u_{\alpha,(m),I}(V^\alpha \otimes \Gamma^{(m),I})\frac{\mathbb{A}(-3 - 2C_{\gamma,(m),I} + 3\xi)}{6\pi^2 N_f}\ln(k/\Lambda) + reg. \qquad (A.12)$$

$$= u_{\alpha,(m),I}(V^\alpha \otimes \Gamma^{(m),I})\frac{8C_{\gamma,(m),I}C_{M,\alpha}}{6\pi^2 \mathbb{M}}\ln(k/\Lambda) + reg. \qquad (A.13)$$

where we define $C_{M,\alpha}, C_{\gamma,(m),I}$ as $M^a V^\alpha M^a \equiv C_{M,\alpha} V^\alpha$ and $\gamma^\mu \Gamma^{(m),I}\gamma^\mu \equiv C_{\gamma,(m),I}\Gamma^{(m),I}$, repeated indices a, μ mean summation.

Note that there are also two-loop diagrams for the $1/N$ corrections, we begin with the calculation of the mass bubbles,

$$\Pi_{L,R}^{\text{Anticlockwise}} = -iu_{\alpha,(m),I}\,\text{tr}\left[(V_L)(\mathbb{1}_{N_f} \otimes \gamma^a)(V_R)(V^\alpha \otimes (\gamma^b \Gamma^{(m),I}\gamma^c))\right]$$
$$\frac{1}{128q^3}(q_a q_b q_c - q^2 q_c \delta_{a,b} - q^2 q_b \delta_{a,c} + q^2 q_a \delta_{b,c}),$$

$$(A.14)$$

$$\Pi_{L,R}^{\text{Clockwise}} = iu_{\alpha,(m),I}\,\text{tr}\left[(V_L)(V^\alpha \otimes (\gamma^b \Gamma^{(m),I}\gamma^c))(V_R)(\mathbb{1}_{N_f} \otimes \gamma^a))\right]$$
$$\frac{1}{128q^3}(q_a q_b q_c - q^2 q_c \delta_{a,b} - q^2 q_b \delta_{a,c} + q^2 q_a \delta_{b,c}),$$

$$(A.15)$$

where V_L, V_R stands for the vertex insertion, they could be gauge-gauge, boson-boson or gauge-boson. The formula is complicated in general. For the 3-dimensional theory, the γ-matrices are simply the Pauli matrices and m in $\Gamma^{(m),I}$ is up to 3. Besides, $\Gamma^{(3),\{i_1,i_2,i_3\}} = i\varepsilon^{i_1,i_2,i_3}\Gamma^{(0)}$,

$$\Gamma^{(2),\{i_1,i_2\}} = i\varepsilon^{i_1,i_2}{}_l \Gamma^{(1),l}.$$

The gauge-gauge insertion:

Only $\Gamma^{(0)}, \Gamma^{(3)}$ will have non-zero contribution, as their relation is discussed previously, we can calculate $\Gamma^{(0)}$ and derive the result for $\Gamma^{(3)}$. The mass bubble result for $\Gamma^{(0)}$ is,

$$\text{(diagram)} = u_{\alpha,(0)} \, \text{tr}(V) \frac{q_l \varepsilon^{lij}}{4q} \tag{A.16}$$

The two-loop diagrams give similar results for $\Gamma^{(0)}, \Gamma^{(3)}$,

$$\text{(diagram)} = \begin{cases} u_{\alpha,(0)} (\mathbb{1}_{N_f} \otimes \Gamma^{(0)}) \dfrac{\text{tr}(V)}{N_f} \dfrac{(\mathbb{A}^2 - \mathbb{B}^2)}{4\pi^2 N_f} \ln(k/\Lambda) + reg. & \text{for } m = 0 \\[2ex] u_{\alpha,(3),\{i_1,i_2,i_3\}} (\mathbb{1}_{N_f} \otimes \Gamma^{(3),\{i_1,i_2,i_3\}}) \dfrac{\text{tr}(V)}{N_f} \dfrac{(\mathbb{A}^2 - \mathbb{B}^2)}{4\pi^2 N_f} \ln(k/\Lambda) + reg. & \text{for } m = 3 \end{cases} \tag{A.17}$$

The boson-boson insertion:

The non-zero contributions will occur only if $\text{tr}(M^i M^j V^\alpha) = -\text{tr}(M^i V^\alpha M^j)$, this requires non-trivial choices of the M^a, V^α. If so, the two-loop contributions are,

for $\text{tr}(M^i M^j V^\alpha) = -\text{tr}(M^i V^\alpha M^j)$

$$\text{(diagram)} = \begin{cases} -iu_{\alpha,(1),i_1} \, \text{tr}(M^i V^\alpha M^j) \dfrac{q_{i_1}}{4q} & \text{for } m = 1 \\[2ex] -iu_{\alpha,(2),\{i_1,i_2\}} \, \text{tr}(M^i V^\alpha M^j) \dfrac{iq_l \varepsilon^{l,i_1,i_2}}{2q} & \text{for } m = 2 \end{cases} \tag{A.18}$$

$$
\begin{aligned}
&\text{(diagram)} = \begin{cases}
u_{\alpha,(1),i_1}(M^i M^j \otimes \Gamma^{(1),i_1}) \dfrac{-8\,\mathrm{tr}(M^i V^\alpha M^j)}{3\pi^2 \mathbb{M}^2}\ln(k/\Lambda) + reg. & \text{for } m=1 \\[3mm]
u_{\alpha,(2),\{i_1,i_2\}}(M^i M^j \otimes \Gamma^{(2),\{i_1,i_2\}}) \dfrac{-8\,\mathrm{tr}(M^i V^\alpha M^j)}{3\pi^2 \mathbb{M}^2}\ln(k/\Lambda) + reg. & \text{for } m=2
\end{cases}
\end{aligned}
\tag{A.19}
$$

For example, the boson 2-loop will contribute when $M^a = \{\mathbb{1}_2, \sigma^1, \sigma^2\}$ and $V^\alpha = \{\mathbb{1}_2, \sigma^1, \sigma^2, \sigma^3\}$ and it will only contribute to the current-current interaction.

Mixed gauge-boson insertion

The mixed gauge-boson insertion will vanish for all the choices of V^α and $\Gamma^{(m),I}$, part of the reason is because $\mathrm{tr}(M^i V^\alpha) = \mathrm{tr}(V^\alpha M^i)$ and it will never have a minus sign.

A.1.3 Basic diagrams for $1/N$ corrections: ladder corrections

The four-fermion interaction vertices as depicted in Eq. (A.11) will receive $\mathscr{O}(1/N)$ correction from gauge and boson propagators as well,

$$
\text{(diagrams)}
$$

$$
= K_{(\alpha,(m_1),I),(\beta,(m_2),J)} \begin{bmatrix} V^\alpha \\ \otimes \\ V^\beta \end{bmatrix} \otimes \left(\begin{bmatrix} \Gamma^{(m_1),I}\gamma^\mu \\ \otimes \\ \Gamma^{(m_2),J}\gamma^\mu \end{bmatrix} + \begin{bmatrix} \Gamma^{(m_1),I}\gamma^\mu \\ \otimes \\ \gamma^\mu \Gamma^{(m_2),J} \end{bmatrix} \right) \frac{-2\mathbb{A}}{6\pi^2 N_f}\ln(k/\Lambda) + reg.
\tag{A.20}
$$

$$
\Rightarrow u_{(\alpha,(m),I)} \begin{bmatrix} V^\alpha \\ \otimes \\ V^\alpha \end{bmatrix} \otimes \left(\begin{bmatrix} \Gamma^{(m),I}\gamma^\mu \\ \otimes \\ \Gamma^{(m),I}\gamma^\mu \end{bmatrix} + \begin{bmatrix} \Gamma^{(m),I}\gamma^\mu \\ \otimes \\ \gamma^\mu \Gamma^{(m),I} \end{bmatrix} \right) \frac{-2\mathbb{A}}{6\pi^2 N_f}\ln(k/\Lambda) + reg.
\tag{A.21}
$$

where the last equation is the correction for the simplified four-fermion interaction as in Eq. A.10.

Table A.1. The definition for the coefficients that are universal for chosen fermion-boson vertex and interaction matrix.

Notation	Definition
κ	$k/(2\pi N_f)$
$\mathbb{A}$	$\mathbb{A} = \left(16^{-1} + 16\kappa^2\right)^{-1}$
$\mathbb{B}$	$\mathbb{B} = \left((256\kappa)^{-1} + \kappa\right)^{-1}$
$\mathbb{M}$	$\text{tr}\left[M^a M^b\right] = \mathbb{M}\delta_{ab}$
C_M	$M^a M^a = C_M \mathbb{1}_{N_f}$
$C_{M,\alpha}$	$M^a V^\alpha M^a \equiv C_{M,\alpha} V^\alpha$
$C_{\gamma,(m),I}$	$\gamma^\mu \Gamma^{(m),I}\gamma^\mu \equiv C_{\gamma,(m),I}\Gamma^{(m),I}$ $C_{\gamma,(0),} = 3, C_{\gamma,(1),\mu} = -1$
f_c^{ab}	$\sigma^a\sigma^b = f_c^{ab}\sigma^c,\ \frac{1}{2}\text{tr}\left(\sigma^a\sigma^b\sigma^c\right)$
$\mathbf{F}_\beta^\alpha(\{M^a\}), \tilde{\mathbf{F}}_\beta^\alpha(\{M^a\})$	$\mathbf{F}_\beta^\alpha(\{M^a\}) = \sum_{a\in\{M^a\}} f_\beta^{\alpha a} f_\beta^{\alpha a},$ $\tilde{\mathbf{F}}_\beta^\alpha(\{M^a\}) = \sum_{a\in\{M^a\}} f_\beta^{\alpha a} f_\beta^{a\alpha},\ \alpha,\beta \in \{V^\alpha\}$

$$= K_{(\alpha,(m_1),I),(\beta,(m_2),J)}\left(\begin{bmatrix} V^\alpha M^a \\ \otimes \\ V^\beta M^a \end{bmatrix} \otimes \begin{bmatrix} \Gamma^{(m_1),I}\gamma^\mu \\ \otimes \\ \Gamma^{(m_2),J}\gamma^\mu \end{bmatrix} - \begin{bmatrix} V^\alpha M^a \\ \otimes \\ M^a V^\beta \end{bmatrix} \otimes \begin{bmatrix} \Gamma^{(m_1),I}\gamma^\mu \\ \otimes \\ \gamma^\mu\Gamma^{(m_2),J} \end{bmatrix}\right)$$

$$\frac{-8}{6\pi^2\mathbb{M}}\ln(k/\Lambda) + reg. \tag{A.22}$$

$$= u_{(\alpha,(m),I)}\left(\begin{bmatrix} V^\alpha M^a \\ \otimes \\ V^\alpha M^a \end{bmatrix} \otimes \begin{bmatrix} \Gamma^{(m),I}\gamma^\mu \\ \otimes \\ \Gamma^{(m),I}\gamma^\mu \end{bmatrix} - \begin{bmatrix} V^\alpha M^a \\ \otimes \\ M^a V^\alpha \end{bmatrix} \otimes \begin{bmatrix} \Gamma^{(m),I}\gamma^\mu \\ \otimes \\ \gamma^\mu\Gamma^{(m),I} \end{bmatrix}\right)\frac{-8}{6\pi^2\mathbb{M}}\ln(k/\Lambda) + reg.$$

$$\tag{A.23}$$

the repeated indices μ, a should be summed over.

A.1.4 Examples

Above general calculations will be concrete with certain assumptions,

1. Since $\Gamma^{(i)}$ and $\Gamma^{(3-i)}$ are related by Levi-Civita symbol in 3 dimension, we only need to consider $\Gamma^{(0)} = \mathbb{1}_2$ and $\Gamma^{(1),\mu} = \gamma^\mu$.

2. For the physical relevance, we consider the four-fermion interactions in the form of $u_{\alpha,m}(\bar{\psi}(V^\alpha \otimes \mathbb{1}_2)\psi)^2$ and $u_{\alpha,\mu}(\bar{\psi}(V^\alpha \otimes \gamma^\mu)\psi)^2$ with $\mu = 0,1,2$.

3. We further assume V^α, M^a are represented by Pauli matrices. This kind of interaction vertices arise when doing fermionic parton construction of the spin models, i.e. the spin operators correspond to the fermion bilinears with Pauli matrices inserted in the middle.

4. We also view V^αs as the basis of certain vector space and form a set $\{V^\alpha\}$ as well as M^as form a set $\{M^a\}$, such that $V^\alpha M^a \in \{V^\alpha\}$. For example, for $\{M^a\} = \{\mathbb{1}_2\}$ or $\{M^a\} = \{\mathbb{1}_2, \sigma^3\}$, $\{V^\alpha\}$ can be $\{V^\alpha\} = \{\mathbb{1}_2, \sigma^3\}$ or $\{V^\alpha\} = \{\mathbb{1}_2, \sigma^1, \sigma^2, \sigma^3\}$

Since V^α, M^a can be represented by Pauli matrices as assumed, we can exploit the underlying algebraic structure of Pauli matrices. We further define the structure constants when multiplying the V^α, M^a as

$$V^\alpha M^b = \sum_\beta f_\beta^{\alpha b} V^\beta, \quad M^b V^\alpha = \sum_\beta f_\beta^{b\alpha} V^\beta \tag{A.24}$$

where $f_\beta^{\alpha b}, f_\beta^{b\alpha}$ can be viewed as $\sigma^a \sigma^b = \sum_c f_c^{ab} \sigma^c$ with a,b,c being restricted. The f_c^{ab} for Pauli matrices are,

$$f_c^{ab} = i\varepsilon_c^{ab}, \text{with } a,b,c = 1,2,3, \quad f_b^{0a} = \delta_b^a, \; f_b^{a0} = \delta_b^a, \; f_0^{ab} = \delta^{ab}, \text{with } a,b = 0,1,2,3. \tag{A.25}$$

The structure constants are also calculated by,

$$f_c^{ab} = \frac{1}{2}\text{tr}\left(\sigma^a \sigma^b \sigma^c\right) \tag{A.26}$$

The γ, Γ matrices are also represented by Pauli matrices and therefore have this structure as well,

$$\Gamma^i \gamma^\mu = \sum_j f_j^{i\mu} \Gamma^j, \quad \gamma^\mu \Gamma^i = \sum_j f_j^{\mu i} \Gamma^j. \tag{A.27}$$

We arrange the coupling constants in a vector as $u_{\alpha,i} = (u_{\alpha,m}, u_{\alpha,0}, u_{\alpha,1}, u_{\alpha,2})$, where the first term is the mass-mass interaction and the last 3 terms are the current-current interactions in τ, x, y directions. The corresponding γ-matrices are $\Gamma^i = \{\mathbb{1}_2, \gamma^0, \gamma^1, \gamma^2\} = \{\mathbb{1}_2, \sigma^3, \sigma^1, \sigma^2\}$.

With the structure constants, the ladder corrections Eq. A.20 can be simplified as,

$$u_{(\alpha,(m),I)} \begin{bmatrix} V^\alpha \\ \otimes \\ V^\alpha \end{bmatrix} \otimes \left(\begin{bmatrix} \Gamma^{(m),I} \gamma^\mu \\ \otimes \\ \Gamma^{(m),I} \gamma^\mu \end{bmatrix} + \begin{bmatrix} \Gamma^{(m),I} \gamma^\mu \\ \otimes \\ \gamma^\mu \Gamma^{(m),I} \end{bmatrix} \right) \frac{-2\mathbb{A}}{6\pi^2 N_f} \ln(k/\Lambda) + reg. \tag{A.28}$$

$$= u_{(\alpha,i)} \begin{bmatrix} V^\alpha \\ \otimes \\ V^\alpha \end{bmatrix} \otimes \begin{bmatrix} \Gamma^j \\ \otimes \\ \Gamma^j \end{bmatrix} \sum_\mu \left(f_j^{i\mu} f_j^{i\mu} + f_j^{i\mu} f_j^{\mu i} \right) \frac{-2\mathbb{A}}{6\pi^2 N_f} \ln(k/\Lambda) + reg. \tag{A.29}$$

$$= u_{(\alpha,i)} \begin{bmatrix} V^\alpha \\ \otimes \\ V^\alpha \end{bmatrix} \otimes \begin{bmatrix} \Gamma^j \\ \otimes \\ \Gamma^j \end{bmatrix} \left(\mathbb{1}_{\dim\{V^\alpha\}} \otimes \left(\mathbf{F}_j^i + \tilde{\mathbf{F}}_j^i \right) \right) \frac{-2\mathbb{A}}{6\pi^2 N_f} \ln(k/\Lambda) + reg. \tag{A.30}$$

where $\mathbf{F}_j^i \equiv \sum_{\mu=\{3,1,2\}} f_j^{i\mu} f_j^{i\mu}$, $\tilde{\mathbf{F}}_j^i \equiv \sum_{\mu=\{3,1,2\}} f_j^{i\mu} f_j^{\mu i}$, $i,j = 0,3,1,2$ and Eq. A.22 can be

simplified as,

$$u_{(\alpha,(m),I)} \left(\begin{bmatrix} V^\alpha M^a \\ \otimes \\ V^\alpha M^a \end{bmatrix} \otimes \begin{bmatrix} \Gamma^{(m),I}\gamma^\mu \\ \otimes \\ \Gamma^{(m),I}\gamma^\mu \end{bmatrix} - \begin{bmatrix} V^\alpha M^a \\ \otimes \\ M^a V^\alpha \end{bmatrix} \otimes \begin{bmatrix} \Gamma^{(m),I}\gamma^\mu \\ \otimes \\ \gamma^\mu \Gamma^{(m),I} \end{bmatrix} \right) \frac{-8}{6\pi^2 \mathbb{M}} \ln(k/\Lambda) + reg.$$

(A.31)

$$= u_{(\alpha,i)} \begin{bmatrix} V^\beta \\ \otimes \\ V^\beta \end{bmatrix} \otimes \begin{bmatrix} \Gamma^j \\ \otimes \\ \Gamma^j \end{bmatrix} \left(\left(\sum_a f_\beta^{\alpha a} f_\beta^{\alpha a} \right) \left(\sum_\mu f_j^{i\mu} f_j^{i\mu} \right) - \left(\sum_a f_\beta^{\alpha a} f_\beta^{a\alpha} \right) \left(\sum_\mu f_j^{i\mu} f_j^{\mu i} \right) \right)$$

$$\frac{-8}{6\pi^2 \mathbb{M}} \ln(k/\Lambda) + reg.$$

(A.32)

$$= u_{(\alpha,i)} \begin{bmatrix} V^\beta \\ \otimes \\ V^\beta \end{bmatrix} \otimes \begin{bmatrix} \Gamma^j \\ \otimes \\ \Gamma^j \end{bmatrix} \left(\mathbf{F}_\beta^\alpha(\{M^a\}) \otimes \mathbf{F}_j^i - \tilde{\mathbf{F}}_\beta^\alpha(\{M^a\}) \otimes \tilde{\mathbf{F}}_j^i \right) \frac{-8}{6\pi^2 \mathbb{M}} \ln(k/\Lambda) + reg. \quad \text{(A.33)}$$

Both of the ladder contributions will depend on the structure constants with specific forms, and we define $\mathbf{F}_\beta^\alpha(\{M^a\}) \equiv \sum_{a \in \{M^a\}} f_\beta^{\alpha a} f_\beta^{\alpha a}$, $\tilde{\mathbf{F}}_\beta^\alpha(\{M^a\}) \equiv \sum_{a \in \{M^a\}} f_\beta^{\alpha a} f_\beta^{a\alpha}$, $\alpha, \beta \in \{V^\alpha\}$ similar to the above definition for the Γ-matrices.

The self-energy corrections and the vertex corrections will be diagonal matrices acting on the vector $u_{\alpha,i}$. The self-energy corrections are the same for every $u_{\alpha,i}$, while the vertex corrections depend on the α, i. As listed in the Table. A.1, the coefficient $C_{\gamma,(0),} = 3, C_{\gamma,(1),\mu} = -1$ are distinct for mass-mass and current-current. The structure constants in Eq. A.25 also have these distinctions, this suggests the RG equations are in block forms.

A.1.5 Renormalization group equation for four-fermion interactions

The $1/N$ corrections for the four-fermion interaction vertices are,

$$(A.34)$$

As discussed previously, for generic boson-fermion vertices, the ladder correction diagram of one interaction vertex will contribute to another interaction vertex, therefore, one need to include all the possible interaction vertices as the basis. For example, if $\{M^a\} = \{\mathbb{1}_2, \sigma^3\}$ and $\{V^\alpha\} = \{\mathbb{1}_2, \sigma^1\}$, then σ^2, σ^3 also need to be included in $\{V^\alpha\}$.

We will analyze the example in the main text Section. 1.3.2 in detail. Due to the reason provided in the previous paragraph, we choose the interaction vertex to be $\{V^\alpha\} = \{\mathbb{1}_2, \sigma^1, \sigma^2, \sigma^3\} \otimes \mathbb{1}_N$ and $\{M^a\} = \{\}, \{\mathbb{1}_2\} \otimes \mathbb{1}_N, \{\sigma^3\} \otimes \mathbb{1}_N, \{\mathbb{1}_2, \sigma^3\} \otimes \mathbb{1}_N$. Combining with the Γ-matrices, the basis of the interaction vertices $u_{\alpha,i} = (u_{\alpha,m}, u_{\alpha,0}, u_{\alpha,1}, u_{\alpha,2})$ is $4 \times 4 = 16$ dimensional. The RG equation is organized as,

$$\frac{du_{\alpha,i}}{d\ell} = \left(-\mathbb{1} + \frac{64}{3\pi^2(2N)} \mathbf{M}_{(\alpha,i),(\beta,j)} \right) u_{\beta,j} \qquad (A.35)$$

where α, β are the indices of the flavors, and i, j are the indices of the Γ-matrices, $i = 0, 1, 2, 3$ corresponds to $\{\mathbb{1}_2, \gamma^0, \gamma^1, \gamma^2\} = \{\mathbb{1}_2, \sigma^3, \sigma^1, \sigma^2\}$ in 3d.

The matrix $\mathbf{M}_{(\alpha,i),(\beta,j)}$ contains several parts,

$$\mathbf{M}_{(\alpha,i),(\beta,j)} = \mathbf{M}^{sv}_{(\alpha,i),(\beta,j)} + \mathbf{M}^{gL}_{(\alpha,i),(\beta,j)} + \mathbf{M}^{bL}_{(\alpha,i),(\beta,j)} \qquad (A.36)$$

The self-energy and vertex corrections are in the diagonal,

$$\mathbf{M}^{sv}_{(\alpha,0),(\beta,0)} = \left(\frac{16\mathbb{A}}{6\pi^2 N_f} + \frac{-2\,\mathrm{tr}(V^\alpha)}{N_f} \frac{(\mathbb{A}^2 - \mathbb{B}^2)}{4\pi^2 N_f} + \frac{-16(C_M + 3C_{M,\alpha})}{6\pi^2 \mathbb{M}} \right) \mathbb{1}_{\alpha,\beta} \tag{A.37}$$

$$\mathbf{M}^{sv}_{(\alpha,i),(\beta,i)} = \left(0 + \frac{-16(C_M - C_{M,\alpha})}{6\pi^2 \mathbb{M}} \right) \mathbb{1}_{\alpha,\beta}, \quad \text{with } i = 1,2,3 \tag{A.38}$$

The ladder correction from the gauge vertex contributes the off-diagonal part,

$$\mathbf{M}^{gL}_{(\alpha,0),(\beta,i)} = \mathbf{M}^{gL}_{(\alpha,i),(\beta,0)} = \frac{8\mathbb{A}}{6\pi^2 N_f} \mathbb{1}_{\alpha,\beta}, \quad \text{with } i = 1,2,3. \tag{A.39}$$

The ladder corrections from the boson vertex are complicated, in the (i,j) space, there are two parts,

$$\mathbf{M}^{bL}_{(\alpha,0),(\beta,i)} = \mathbf{M}^{bL}_{(\alpha,i),(\beta,0)} = \frac{16}{6\pi^2 \mathbb{M}} (\mathbf{F}^\alpha_\beta(\{M^a\}) - \tilde{\mathbf{F}}^\alpha_\beta(\{M^a\})), \quad \text{with } i = 1,2,3 \tag{A.40}$$

$$\mathbf{M}^{bL}_{(\alpha,i),(\beta,j)} = \frac{16}{6\pi^2 \mathbb{M}} (-\mathbf{F}^\alpha_\beta(\{M^a\}) - \tilde{\mathbf{F}}^\alpha_\beta(\{M^a\})), \quad \text{with } i,j = 1,2,3, i \neq j \tag{A.41}$$

where $\mathbf{F}^\alpha_\beta(\{M^a\}) = \sum_{a \in \{M^a\}} f^{\alpha a}_\beta f^{\alpha a}_\beta, \tilde{\mathbf{F}}^\alpha_\beta(\{M^a\}) = \sum_{a \in \{M^a\}} f^{\alpha a}_\beta f^{a\alpha}_\beta, \; \alpha, \beta \in \{V^\alpha\}$ is defined previously. This can be simplified if we take subset of $\{V^\alpha\}$ with proper $\{M^a\}$, and restrict the indices α, β in the subset.

The first quadrant, continuous $\mathrm{O}(4)$ **DQCP:** There is no critical boson in the system, $\{M^a\} = \{\}$. There is no mixture in the flavor space of the eigen-channel. For $V^a = \mathbb{1}_{2N}$,

$$\frac{du_{0,i}}{d\ell} = \left(-1 + \frac{64}{3\pi^2(2N)} \mathbf{M}_{(0,i),(0,j)} \right) u_{0,j}, \quad \mathbf{M} = \frac{1}{256\kappa^2 + 1} \begin{pmatrix} \frac{4(512\kappa^2 - 1)}{256\kappa^2 + 1} & 1 & 1 & 1 \\ 1 & 0 & 0 & 0 \\ 1 & 0 & 0 & 0 \\ 1 & 0 & 0 & 0 \end{pmatrix} \tag{A.42}$$

In our case, $2N = 2, \kappa = 0$, the RG equation becomes,

$$\frac{du_{0,i}}{d\ell} = \begin{pmatrix} -1 - \frac{128}{3\pi^2} & \frac{32}{3\pi^2} & \frac{32}{3\pi^2} & \frac{32}{3\pi^2} \\ \frac{32}{3\pi^2} & -1 & 0 & 0 \\ \frac{32}{3\pi^2} & 0 & -1 & 0 \\ \frac{32}{3\pi^2} & 0 & 0 & -1 \end{pmatrix} u_{0,j} \tag{A.43}$$

And the eigenvalues of this matrix are all negative, meaning the perturbation is irrelevant among all the channels.

For $V^\alpha = \sigma^\alpha \otimes \mathbb{1}_N, \alpha = 1, 2, 3$, the RG equations are the same for different αs,

$$\frac{du_{\alpha,i}}{d\ell} = \left(-1 + \frac{64}{3\pi^2(2N)} \mathbf{M}_{(\alpha,i),(\alpha,j)} \right) u_{\alpha,j}, \quad \mathbf{M} = \frac{1}{256\kappa^2 + 1} \begin{pmatrix} 2 & 1 & 1 & 1 \\ 1 & 0 & 0 & 0 \\ 1 & 0 & 0 & 0 \\ 1 & 0 & 0 & 0 \end{pmatrix} \tag{A.44}$$

In our case, there is one relevant channel, and plug that into the Eq. A.44, we get,

$$u_{\alpha,i} = g_\alpha (3, 1, 1, 1)^T, \quad \frac{dg_\alpha}{d\ell} = 2.24 g_\alpha. \tag{A.45}$$

Follow the same procedure, we will present the RG equations and the relevant channel results for other cases.

The r_2 axis, continuous $\mathsf{SO}(5)$ **DQCP**: The boson corresponding to the singlet mass is critical,

$\{M^a\} = \{\mathbb{1}_{2N}\}$. There is also no mixture in the flavor space. For $V^\alpha = \mathbb{1}_{2N}$,

$$\frac{du_{0,i}}{d\ell} = \left(-1 + \frac{64}{3\pi^2(2N)}\mathbf{M}_{(0,i),(0,j)}\right) u_{0,j}, \tag{A.46}$$

$$\mathbf{M} = \begin{pmatrix} \frac{4(512\kappa^2-1)}{(256\kappa^2+1)^2} - \frac{1}{2} & \frac{1}{256\kappa^2+1} & \frac{1}{256\kappa^2+1} & \frac{1}{256\kappa^2+1} \\ \frac{1}{256\kappa^2+1} & 0 & -\frac{1}{4} & -\frac{1}{4} \\ \frac{1}{256\kappa^2+1} & -\frac{1}{4} & 0 & -\frac{1}{4} \\ \frac{1}{256\kappa^2+1} & -\frac{1}{4} & -\frac{1}{4} & 0 \end{pmatrix}. \tag{A.47}$$

There is no relevant channel in this case.

Again, for $V^\alpha = \sigma^\alpha \otimes \mathbb{1}_N, \alpha = 1,2,3$, the RG equations are the same for different αs,

$$\frac{du_{\alpha,i}}{d\ell} = \left(-1 + \frac{64}{3\pi^2(2N)}\mathbf{M}_{(\alpha,i),(\alpha,j)}\right) u_{\alpha,j}, \tag{A.48}$$

$$\mathbf{M} = \begin{pmatrix} \frac{2}{256\kappa^2+1} - \frac{1}{2} & \frac{1}{256\kappa^2+1} & \frac{1}{256\kappa^2+1} & \frac{1}{256\kappa^2+1} \\ \frac{1}{256\kappa^2+1} & 0 & -\frac{1}{4} & -\frac{1}{4} \\ \frac{1}{256\kappa^2+1} & -\frac{1}{4} & 0 & -\frac{1}{4} \\ \frac{1}{256\kappa^2+1} & -\frac{1}{4} & -\frac{1}{4} & 0 \end{pmatrix} \tag{A.49}$$

And the relevant channel is the same as the case of the first quadrant, but with a smaller eigenvalue,

$$u_{\alpha,i} = g_\alpha(3,1,1,1)^T, \quad \frac{dg_\alpha}{d\ell} = 1.70g_\alpha. \tag{A.50}$$

The r_1 axis, transition between the $O(4)$ DQCP and first-order transition: The boson corresponding to the triplet mass is critical, $\{M^a\} = \{\sigma^3 \otimes \mathbb{1}_N\}$. There are mixture between V^0, V^3 and also between V^1, V^2, we will present the RG equation for V^0, V^3 and V^1, V^2 separately.

For $\{V^0, V^3\}$,

$$\frac{du_{\alpha,i}}{d\ell} = \left(-1 + \frac{64}{3\pi^2(2N)} \mathbf{M}_{(\alpha,i),(\beta,j)}\right) u_{\beta,j}, \tag{A.51}$$

$$\mathbb{M} = \begin{pmatrix} \mathsf{P} & (256\kappa^2+1)^{-1}\mathbb{1}_2 & (256\kappa^2+1)^{-1}\mathbb{1}_2 & (256\kappa^2+1)^{-1}\mathbb{1}_2 \\ (256\kappa^2+1)^{-1}\mathbb{1}_2 & 0_2 & -\frac{1}{4}\sigma^1 & -\frac{1}{4}\sigma^1 \\ (256\kappa^2+1)^{-1}\mathbb{1}_2 & -\frac{1}{4}\sigma^1 & 0_2 & -\frac{1}{4}\sigma^1 \\ (256\kappa^2+1)^{-1}\mathbb{1}_2 & -\frac{1}{4}\sigma^1 & -\frac{1}{4}\sigma^1 & 0_2 \end{pmatrix} \tag{A.52}$$

where $\mathsf{P} = \begin{pmatrix} \frac{4(512\kappa^2-1)}{(256\kappa^2+1)^2} - \frac{1}{2} & 0 \\ 0 & \frac{2}{256\kappa^2+1} - \frac{1}{2} \end{pmatrix}$. And the 2×2 matrices act on the $\{V^0, V^3\}$ space, 0_2 is 2×2 matrix with all entries being 0. The only relevant channel is,

$$u_{\alpha,i} = g_{(0,3)}((-0.03, 0.82), (-0.071, 0.32), (-0.071, 0.32), (-0.071, 0.32))^T, \tag{A.53}$$

$$\frac{dg_{(0,3)}}{d\ell} = 1.89 g_{(0,3)}. \tag{A.54}$$

For $\{V^1, V^2\}$,

$$\frac{du_{\alpha,i}}{d\ell} = \left(-1 + \frac{64}{3\pi^2(2N)} \mathbf{M}_{(\alpha,i),(\beta,j)}\right) u_{\beta,j}, \tag{A.55}$$

$$\mathbb{M} = \begin{pmatrix} \left(\frac{2}{256\kappa^2+1} + \frac{1}{4}\right)\mathbb{1}_2 & \mathsf{S} & \mathsf{S} & \mathsf{S} \\ \mathsf{S} & -\frac{1}{4}\mathbb{1}_2 & 0_2 & 0_2 \\ \mathsf{S} & 0_2 & -\frac{1}{4}\mathbb{1}_2 & 0_2 \\ \mathsf{S} & 0_2 & 0_2 & -\frac{1}{4}\mathbb{1}_2 \end{pmatrix}. \tag{A.56}$$

where $S = (256\kappa^2 + 1)^{-1}\mathbb{1}_2 - \frac{1}{4}\sigma^1$. There are two relevant channels,

$$u_{\alpha,i} = g^{(1)}_{(1,2)}((-3,3),(-1,1),(-1,1),(-1,1))^T, \quad \frac{dg^{(1)}_{(1,2)}}{d\ell} = 2.78g^{(1)}_{(1,2)}, \tag{A.57}$$

$$u_{\alpha,i} = g^{(2)}_{(1,2)}((4.1,4.1),(1,1),(1,1),(1,1))^T, \quad \frac{dg^{(2)}_{(1,2)}}{d\ell} = 2.02g^{(2)}_{(1,2)}. \tag{A.58}$$

The first channel is antisymmetric combination of V^1, V^2 and the second is symmetric combination.

The origin, multi-critical point: Both bosons are critical, the boson-fermion vertices are $\{M^a\} = \{\mathbb{1}_{2N}, \sigma^3 \otimes \mathbb{1}_N\}$. Again, there will be mixture between V^0, V^3 and also between V^1, V^2. For $\{V^0, V^3\}$,

$$\frac{du_{\alpha,i}}{d\ell} = \left(-1 + \frac{64}{3\pi^2(2N)}\mathbf{M}_{(\alpha,i),(\beta,j)}\right)u_{\beta,j}, \tag{A.59}$$

$$\mathbb{M} = \begin{pmatrix} \mathsf{K} & \mathsf{R} & \mathsf{R} & \mathsf{R} \\ \mathsf{R} & 0_2 & -\frac{1}{4}(\mathbb{1}_2 + \sigma^1) & -\frac{1}{4}(\mathbb{1}_2 + \sigma^1) \\ \mathsf{R} & -\frac{1}{4}(\mathbb{1}_2 + \sigma^1) & 0_2 & -\frac{1}{4}(\mathbb{1}_2 + \sigma^1) \\ \mathsf{R} & -\frac{1}{4}(\mathbb{1}_2 + \sigma^1) & -\frac{1}{4}(\mathbb{1}_2 + \sigma^1) & 0_2 \end{pmatrix}. \tag{A.60}$$

where $\mathsf{K} = \begin{pmatrix} \frac{4(512\kappa^2 - 1)}{(256\kappa^2 + 1)^2} - 1 & 0 \\ 0 & \frac{2}{256\kappa^2 + 1} - 1 \end{pmatrix}$ and $\mathsf{R} = (256\kappa^2 + 1)^{-1}\mathbb{1}_2$. And the relevant channel is the same as previous case with a smaller eigenvalue,

$$u_{\alpha,i} = g_{(0,3)}((-0.03, 0.82), (-0.071, 0.32), (-0.071, 0.32), (-0.071, 0.32))^T, \tag{A.61}$$

$$\frac{dg_{(0,3)}}{d\ell} = 1.35g_{(0,3)}. \tag{A.62}$$

For $\{V^1, V^2\}$,

$$\frac{du_{\alpha,i}}{d\ell} = \left(-1 + \frac{64}{3\pi^2(2N)} \mathbf{M}_{(\alpha,i),(\beta,j)}\right) u_{\beta,j}, \tag{A.63}$$

$$\mathbb{M} = \begin{pmatrix} \mathsf{Q} & \mathsf{S} & \mathsf{S} & \mathsf{S} \\ \mathsf{S} & -\frac{1}{4}\mathbb{1}_2 & -\frac{1}{4}\mathbb{1}_2 & -\frac{1}{4}\mathbb{1}_2 \\ \mathsf{S} & -\frac{1}{4}\mathbb{1}_2 & -\frac{1}{4}\mathbb{1}_2 & -\frac{1}{4}\mathbb{1}_2 \\ \mathsf{S} & -\frac{1}{4}\mathbb{1}_2 & -\frac{1}{4}\mathbb{1}_2 & -\frac{1}{4}\mathbb{1}_2 \end{pmatrix}. \tag{A.64}$$

where $\mathsf{Q} = \left(\frac{2}{256\kappa^2+1} - \frac{1}{4}\right)\mathbb{1}_2$, $\mathsf{S} = (256\kappa^2 + 1)^{-1}\mathbb{1}_2 - \frac{1}{4}\sigma^1$. There are two relevant channels,

$$u_{\alpha,i} = g_{(1,2)}^{(1)}((-3,3),(-1,1),(-1,1),(-1,1))^T, \quad \frac{dg_{(1,2)}^{(1)}}{d\ell} = 2.24 g_{(1,2)}^{(1)}, \tag{A.65}$$

$$u_{\alpha,i} = g_{(1,2)}^{(2)}((4.1,4.1),(1,1),(1,1),(1,1))^T, \quad \frac{dg_{(1,2)}^{(2)}}{d\ell} = 1.49 g_{(1,2)}^{(2)}. \tag{A.66}$$

The first relevant channel is the antisymmetric combination of V^1, V^2, it is interesting that this relevant channel has the same scaling dimension as the relevant channel V^3 with $(3,1,1,1)^T$ in the O(4) DQCP (Eq. A.45).

A.1.6   Mass scaling

Combining the diagrams in previous sections allows us to calculate the scaling dimension for the fermion mass term, which corresponds to the vertex $\bar{\psi}V^\alpha \otimes \Gamma^{(0)}\psi \equiv \bar{\psi}V^\alpha \otimes \mathbb{1}_2\psi$. As discussed in the main text, we use the $N_f = 2$ QED$_3$ description of DQCP, and consider its large-N generalization. The vertex of singlet mass is thus $V^\alpha = \mathbb{1}_{2N}$ and for the triplet mass is

$V^{\alpha} = \sigma^3 \otimes \mathbb{1}_N$. The diagram equation for the corrections of the mass scaling dimension is,

$$\text{(A.67)}$$

For M^a being full rank, $\mathbb{M} = 2N$, C_M equals to the number of critical boson N_b. For singlet mass term, $C_{M,\alpha} = N_b$, but for the triplet mass, $C_{M,\alpha}$ depends on the choices of M^a, the coefficient is calculated explicitly by $C_{M,\alpha} = \text{tr}[(\sum_a M^a V^{\alpha} M^a) V^{\alpha}] / \text{tr}[V^{\alpha} V^{\alpha}]$. For boson associated to singlet mass, the result is simple, $M^a = \mathbb{1}$, with $a = 1, ..., N_b$, $C_{M,\alpha} = N_b$.

For the mass scaling, $m = 0$, $C_{\gamma,(0),\{\}} = 3$, and there is no two-loop correction by critical boson. Collecting the logarithmic divergent part, we get,

$$\Delta_{\bar{\psi} \mathbb{1}_{2N} \psi} = 2 - \frac{128(512\kappa^2 - 1)}{3\pi^2(2N)(1 + 256\kappa^2)^2} + \frac{16 N_b}{3\pi^2(2N)} \tag{A.68}$$

$$\Delta_{\bar{\psi}(\sigma^3 \otimes \mathbb{1}_N)\psi} = 2 - \frac{64}{3\pi^2(2N)(1 + 256\kappa^2)} + \frac{4(3 C_{M,\alpha} + N_b)}{3\pi^2(2N)} \tag{A.69}$$

where the last term in each equation comes from the critical boson contribution. This general result agrees with previous work with certain parameters.

A.1.7 Boson mass scaling

We can also calculate the scaling dimension of the boson operator ϕ_a^2. Following Ref. [47], we define the scalar two-point function as $G_{ab}^{\phi} \equiv \langle \phi_a(p) \phi_b(-p) \rangle$, and its $\mathscr{O}(1/N)$ 1PI scalar self-energy contribution is represented by $\Sigma_{ab}^{\phi(1)}(p)$. From the Dyson's equation, the two-point function to $\mathscr{O}(1/N)$ is,

$$G_{ab}^{\phi} = D_{ab}(p) + D_{ac}(p) \Sigma_{cd}^{\phi(1)}(p) G_{db}^{\phi}(p) \simeq D_{ab}(p) + D_{ac}(p) \Sigma_{cd}^{\phi(1)}(p) D_{db}(p) \tag{A.70}$$

where the self-energy is obtained by summing over the basic diagrams for fermion mass scaling but with nontrivial choices of M^as. Because of the coupling $\phi_a \bar{\psi} M^a \psi$, the self-energy corrections depend on M^as and can therefore change the scaling dimensions of the corresponding bosons. The self-energy has the following generic form,

$$\Sigma_{ab}^{\phi(1)}(p) = \delta_{ab} \frac{c_a |p|}{\pi^2 N} \ln\left(\frac{\Lambda^2}{p^2}\right) \tag{A.71}$$

For example, for $M^a = \mathbb{1}$, $c = \frac{2}{3} - \frac{16(512\kappa^2 - 1)}{3(256\kappa^2 + 1)^2} \stackrel{\kappa \to 0}{=} 6$, and for M^a is traceless, $c = \frac{2}{3} - \frac{8}{3(256\kappa^2 + 1)} \stackrel{\kappa \to 0}{=} -2$. The self-energy will contribute to the scaling dimension of the ϕ^2 in the following diagram,

$$\tag{A.72}$$

where the shaded bubble is the self-energy correction $\Sigma_{ab}^{\phi(1)}(p)$. There is one more diagram at $\mathcal{O}(1/N)$ will contribute to the scaling of ϕ^2, as following,

$$\tag{A.73}$$

the fermion "box" is the summation of fermions running clockwise and anti-clockwise. The scaling dimension of ϕ^2 is combining Eq. A.72 and Eq. A.73, this gives,

$$\Delta_{\phi_a^2} = 2 - \frac{16 c_a}{\pi^2 N} + \frac{8}{\pi^2 N}. \tag{A.74}$$

Note that the hourglass diagram (the first diagram in Eq. A.75) won't contribute to the anomalous dimension, a simple argument is that similar diagram with one internal boson line appears in the self-energy correction (second and third diagram in Eq. A.75) and it contributes to the anomalous dimension, while the hourglass diagram has two internal boson line, the power in the

Table A.2. The scaling dimensions of ϕ_a^2 with several choices of the boson-fermion vertices, these choices correspond to the axis and origin of the phase diagram Fig. 1.3 in the main text.

$\{M^a\}$	$\Delta_{\phi_a^2}$
$\{\mathbb{1}_2\}$	$2 - \frac{8}{3\pi^2 N} + \frac{256(512\kappa^2 - 1)}{3\pi^2(256\kappa^2 + 1)^2 N} \overset{\kappa \to 0}{=} 2 - \frac{88}{\pi^2 N}$
$\{\sigma^3\}$	$2 - \frac{8}{3\pi^2 N} + \frac{128}{3\pi^2(256\kappa^2 + 1)N} \overset{\kappa \to 0}{=} 2 + \frac{40}{\pi^2 N}$
$\{\mathbb{1}_2, \sigma^3\}$	$\{2 - \frac{40}{3\pi^2 N} + \frac{256(512\kappa^2 - 1)}{3\pi^2(256\kappa^2 + 1)^2 N}, 2 - \frac{40}{3\pi^2 N} + \frac{128}{3\pi^2(256\kappa^2 + 1)N}\} \overset{\kappa \to 0}{=} \{2 - \frac{296}{3\pi^2 N}, 2 + \frac{88}{3\pi^2 N}\}$

denominator is larger by 1, hence, it won't contribute to the anomalous dimension.

$$= = \left\langle \!\!\!\begin{array}{c} \end{array}\!\!\! \right\rangle = =, \quad = = = \left\langle \!\!\!\begin{array}{c} \end{array}\!\!\! \right\rangle = = = \subset = = = \bigcirc = = \tag{A.75}$$

With $\mathcal{O}(1/N)$ correction, the scaling dimension of the boson operator ϕ_a^2 are listed in the Tabel. A.2. These scaling dimensions are not trustworthy for small fermion flavors N, but they show a trend for the scaling dimensions when having different boson-fermion vertices in large N.

A.2   Details of $N_f = 2$ QED$_3$ and self-duality

The single flavor fermion coupled to the $\mathsf{U}(1)$ gauge field is dual to free fermion theory and this is dubbed as fermion/fermion duality[177, 340],

$$i\bar{\Psi}\slashed{D}_{A_1}\Psi \Longleftrightarrow i\bar{\chi}\slashed{D}_{a_1}\chi - \frac{2}{4\pi}b_1 db_1 + \frac{1}{2\pi}a_1 db_1 + \frac{1}{2\pi}A_1 db_1 - \frac{1}{4\pi}A_1 dA_1 - 2CS_g, \tag{A.76}$$

$$i\bar{\Psi}\slashed{D}_{A_2}\Psi \Longleftrightarrow i\bar{\chi}\slashed{D}_{a_2}\chi + \frac{1}{4\pi}a_2 da_2 + \frac{2}{4\pi}b_2 db_2 - \frac{1}{2\pi}a_2 db_2 - \frac{1}{2\pi}A_2 db_2 + 2CS_g, \tag{A.77}$$

where CS_g denotes the gravitational Chern-Simons term which will vanish in the flat spacetimes. The second line is the orientation reversed (time-reversal) version of the first one. We can then product them together on each side with the substitution $A_1 \to A, A_2 \to A - 2X$. Next, adding the counterterms $\frac{1}{2\pi}Ad(Y - X) + \frac{1}{4\pi}(XdX - YdY) + \frac{1}{4\pi}AdA + 2CS_g$ to both sides and gauging

A, after integrating out most of the gauge fields, we get,

$$i\bar{\Psi}_1 \not{D}_a \Psi_1 + i\bar{\Psi}_2 \not{D}_{a-2X} \Psi_2 + \frac{1}{4\pi}ada + \frac{1}{2\pi}ad(Y-X) + \frac{1}{4\pi}(XdX - YdY) + 2CS_g \Longleftrightarrow \quad (A.78)$$

$$i\bar{\chi}_1 \not{D}_{\tilde{a}-2Y} \chi_1 + i\bar{\chi}_2 \not{D}_{\tilde{a}} \chi_2 + \frac{1}{4\pi}\tilde{a}d\tilde{a} + \frac{1}{2\pi}\tilde{a}d(X-Y) + \frac{1}{4\pi}(YdY - XdX) + 2CS_g, \quad (A.79)$$

the self-duality exchanges $X \leftrightarrow Y$ and $\chi_i \leftrightarrow \Psi_{\bar{i}}$. After relabeling the dynamical gauge fields $a, \tilde{a}$, it gives back Eq. (1.1) and Eq. (1.2).

The self-duality exchanges the monopole symmetry and the Cartan subgroup of the flavor symmetry. It is also the duality between strong and weak couplings, this can be seen from the duality transformations amongst the derivation and their corresponding transformations in the 3+1d bulk. Considering the 2+1d $U(1)$ gauge matter theories live at the boundary of 3+1d $U(1)$ gauge theory with the coupling constant τ,

$$I(A) = \frac{1}{8\pi}\int_X d^4x\sqrt{g}\left(\frac{2\pi}{e^2}F_{mn}F^{mn} + \frac{i\theta}{4\pi}\varepsilon_{mnpq}F^{mn}F^{pq}\right) \quad (A.80)$$

$$= \frac{i}{8\pi}\int_X d^4x\sqrt{g}(\bar{\tau}F_{mn}^+F^{+mn} - \tau F_{mn}^-F^{-mn}), \quad \tau = \frac{\theta}{2\pi} + \frac{2\pi i}{e^2} \quad (A.81)$$

where g is the metric for the spacetime, the theory and the transformation properties are well-defined also in the curved spacetime. $F = dA$ and F is decomposed into self-dual and anti-self-dual pieces, $F_{mn}^{\pm} = \frac{1}{2}(F_{mn} \pm (\star F)_{mn})$ with $(\star F)_{mn} = \frac{1}{2}\varepsilon_{mnpq}F^{pq}$, also $(\star F)_{mn}(\star F)^{mn} = F_{mn}F^{mn}$. The S transformation and T transformation act as,

$$S: \quad \tau \to \tau' = -\frac{1}{\tau}, \quad \begin{pmatrix} 0 & -1 \\ 1 & 0 \end{pmatrix}, \quad \int_{\partial X} J \cdot A \to \int_{\partial X} J \cdot a - \frac{1}{2\pi}adA' \quad (A.82)$$

$$-S: \quad \tau \to \tau' = -\frac{1}{\tau}, \quad \begin{pmatrix} 0 & -1 \\ 1 & 0 \end{pmatrix}, \quad \int_{\partial X} J \cdot A \to \int_{\partial X} J \cdot a + \frac{1}{2\pi}adA' \quad (A.83)$$

$$T[k]: \quad \tau \to \tau' = \tau + k, \quad \begin{pmatrix} 1 & k \\ 0 & 1 \end{pmatrix}, \quad \int_{\partial X} J \cdot A \to \int_{\partial X} J \cdot A - \frac{k}{4\pi} A dA \tag{A.84}$$

The $SL(2,\mathbb{Z})$ matrix acts on the coupling constant τ as,

$$\tau \to \tau' = \frac{a\tau + b}{c\tau + d}, \quad \begin{pmatrix} a & b \\ c & d \end{pmatrix} \in SL(2,\mathbb{Z}) \tag{A.85}$$

The fermion/fermion duality in the derivation of the $N_f = 2$ QED$_3$ self-duality is essential in connecting the left-hand-side and the right-hand-side (the other procedures, adding the counterterms and gauging the background gauge fields are the same for both hand sides). Using the above notation, the fermion/fermion duality and its orientation reversed version is,

$$T[1] \circ (-S) \circ T[2] \circ (-S), \; \tau \to \frac{1}{2} - \frac{1}{2(2\tau - 1)} \tag{A.86}$$

$$S \circ T[-2] \circ S \circ T[-1], \; \tau \to \frac{1}{2} - \frac{1}{2(2\tau - 1)}. \tag{A.87}$$

Take the coupling of the bulk theory $\tau = \frac{1}{2} + \frac{2\pi i}{e^2}$, under the duality $\tau \to \frac{1}{2} - \frac{1}{2(2\tau-1)} = \frac{1}{2} + \frac{e^2 i}{8\pi}$. If $e \to 0$, which is the weak coupling limit, the dual theory has the strong coupling with $\tau \to \frac{1}{2} + 0i$. This suggests the fermion/fermion duality is a strong-weak duality, and similar calculation can be done for the $N_f = 2$ QED$_3$, which involves the U(1) × U(1) gauge theory in the bulk.

A.3 Connection to the gapless $\mathbb{Z}_2$ spin liquid in Ref. [352]

A.3.1 Matrix form of fermion operators

The 2 flavor Nambu spinor can be written in matrix form,

$$\mathscr{X}_i = \begin{pmatrix} f_{i\uparrow} & -f_{i\downarrow}^\dagger \\ f_{i\downarrow} & f_{i\uparrow}^\dagger \end{pmatrix} \tag{A.88}$$

220

The $\mathsf{SU}(2)$ gauge symmetry and physical spin symmetry act as,

$$\mathsf{SU}(2)_g : \mathscr{X}_i \to \mathscr{X}_i U^\dagger_{g,i} \tag{A.89}$$

$$\mathsf{SU}(2)_s : \mathscr{X}_i \to U_{s,i}\mathscr{X}_i. \tag{A.90}$$

In majorana basis, one has,

$$\mathscr{X}_i = \frac{1}{\sqrt{2}}(\chi_0 + i\chi_a\sigma^a). \tag{A.91}$$

Note that there is a discrepancy in the conventional notation and this, but it is merely relabeling,

$$
\begin{pmatrix} f_\uparrow \\ f_\uparrow^\dagger \\ f_\downarrow \\ f_\downarrow^\dagger \end{pmatrix} =
\begin{pmatrix} 1 & i & 0 & 0 \\ 1 & -i & 0 & 0 \\ 0 & 0 & 1 & i \\ 0 & 0 & 1 & -i \end{pmatrix}
\begin{pmatrix} \chi_{1,1} \\ \chi_{1,2} \\ \chi_{2,1} \\ \chi_{2,2} \end{pmatrix} =
\begin{pmatrix} 1 & 0 & 0 & i \\ 1 & 0 & 0 & -i \\ 0 & i & -1 & 0 \\ 0 & -i & -1 & 0 \end{pmatrix}
\begin{pmatrix} \chi_0 \\ \chi_1 \\ \chi_2 \\ \chi_3 \end{pmatrix}
\tag{A.92}
$$

the relabeling is,

$$
\begin{pmatrix} \chi_0 \\ \chi_1 \\ \chi_2 \\ \chi_3 \end{pmatrix} =
\begin{pmatrix} 1 & 0 & 0 & 0 \\ 0 & 0 & 0 & 1 \\ 0 & 0 & 1 & 0 \\ 0 & 1 & 0 & 0 \end{pmatrix}
\begin{pmatrix} \chi_{1,1} \\ \chi_{1,2} \\ \chi_{2,1} \\ \chi_{2,2} \end{pmatrix}.
\tag{A.93}
$$

$\chi_a \to \chi_{a_1,a_2}$.

A.3.2   Hamiltonian and Higgs fields

Define the 4×2 matrix operator,

$$X_{\alpha,v;\beta} = \frac{1}{\sqrt{2}}(\chi_{0,v}\mathbb{1}_{\alpha\beta} + i\chi_{a,v}\sigma^a_{\alpha\beta}) \tag{A.94}$$

$$X_v = \frac{1}{\sqrt{2}}(\chi_{0,v}\sigma^0 + i\chi_{a,v}\sigma^a) \tag{A.95}$$

with $\chi_{a,v}, a = 0 \sim 3, v = 1, 2$. The γ-matrices act on the spinor index m in $\chi_{m,a,v}$, and it is left implicit. The mean-field Lagrangian is,

$$
\begin{aligned}
\mathscr{L} &= \mathrm{i}\,\mathrm{Tr}\{\bar{X}\gamma^\mu \partial_\mu X\} \\
&= \mathrm{i}\,\mathrm{Tr}\Big\{(\chi_{0,v}^T \gamma^0 \sigma^0 - \mathrm{i}\chi_{a,v}^T \gamma^0 \sigma^a)\gamma^\mu \partial_\mu (\chi_{0,v}\sigma^0 + \mathrm{i}\chi_{b,v}\sigma^b)\Big\} \\
&= \sum_{a,v} \mathrm{i}\chi_{a,v}^T \gamma^0 \gamma^\mu \partial_\mu \chi_{a,v}
\end{aligned}
$$

where $\gamma^\mu = \{\sigma^2, \sigma^3, \sigma^1\}$ and $\bar{X} = X^\dagger \gamma^0$.

Let's now proceed to translate the Lagrangian for the Higgs fields in Ref. [352], the matrix μ^i acts on the v indices, one of the $\mathbb{Z}_2$ Higgs field is,

$$
\begin{aligned}
&\Phi_1^a \mathrm{Tr}\{\sigma^a \bar{X}\mu^z \gamma^x X\} \\
={}&\Phi_1^c \mathrm{Tr}\Big\{\sigma^c(\chi_{0,v}^T \gamma^0 \sigma^0 - \mathrm{i}\chi_{a,v}^T \gamma^0 \sigma^a)\mu_{v,w}^z \gamma^x(\chi_{0,w}\sigma^0 + \mathrm{i}\chi_{b,w}\sigma^b)\Big\} \\
={}&\Phi_1^c \mathrm{i}(\chi_{0,v}^T \gamma^0 \gamma^x \mu_{v,w}^z \chi_{c,w} - \chi_{c,v}^T \gamma^0 \gamma^x \mu_{v,w}^z \chi_{0,w})
\end{aligned}
\tag{A.96}
$$

one can also get the matrices that act on the index a,

$$
c = 1, \delta_{i,0}\delta_{j,1} - \delta_{i,1}\delta_{j,0} = -\mathrm{i}(\sigma^{02} + \sigma^{32})
\tag{A.97}
$$

$$
c = 2, \delta_{i,0}\delta_{j,1} - \delta_{i,1}\delta_{j,0} = -\mathrm{i}(\sigma^{20} + \sigma^{23})
\tag{A.98}
$$

$$
c = 3, \delta_{i,0}\delta_{j,1} - \delta_{i,1}\delta_{j,0} = -\mathrm{i}(\sigma^{12} + \sigma^{21})
\tag{A.99}
$$

To compare with our model, we need to change the basis following Eq. A.93,

$$
c = 1, -\mathrm{i}M^1 = -\mathrm{i}(\sigma^{12} + \sigma^{21})
\tag{A.100}
$$

$$
c = 2, -\mathrm{i}M^2 = -\mathrm{i}(\sigma^{20} + \sigma^{23})
\tag{A.101}
$$

$$
c = 3, -\mathrm{i}M^3 = -\mathrm{i}(\sigma^{02} + \sigma^{32})
\tag{A.102}
$$

and using the basis χ_{m,v,a_1,a_2}, therefore, the Higgs field becomes,

$$\Phi_1^c \chi^T [(\gamma^0 \gamma^x) \otimes \mu^z \otimes M^c] \chi \tag{A.103}$$

the other $\mathbb{Z}_2$ Higgs field is,

$$\Phi_2^c \chi^T [(\gamma^0 \gamma^y) \otimes \mu^x \otimes M^c] \chi \tag{A.104}$$

and the $\mathsf{U}(1)$ Higgs field is,

$$\Phi_3^c \chi^T [\gamma^0 (\gamma^y k_x + \gamma^x k_y) \otimes \mu^y \otimes M^c] \chi \tag{A.105}$$

A.3.3 The Higgs configuration

Ref. [352] proposes the staggered flux state is obtained when $\langle \Phi_3 \rangle \propto (0,0,\delta\phi)$ and the Z2Azz13 state follows from $\langle \Phi_1 \rangle \propto (\gamma_1 - \gamma_2, \gamma_1 + \gamma_2, 0)$ and $\langle \Phi_2 \rangle \propto (-\gamma_1 - \gamma_2, \gamma_1 - \gamma_2, 0)$. Recall that, $\gamma^\mu = \{\sigma^2, \sigma^3, \sigma^1\}$ and

$$c = 1, -\mathrm{i}M^1 = -\mathrm{i}(\sigma^{12} + \sigma^{21}) \tag{A.106}$$

$$c = 2, -\mathrm{i}M^2 = -\mathrm{i}(\sigma^{20} + \sigma^{23}) \tag{A.107}$$

$$c = 3, -\mathrm{i}M^3 = -\mathrm{i}(\sigma^{02} + \sigma^{32}). \tag{A.108}$$

When condensing the Higgs fields, it corresponds to generate the mass for the combination of the fermion bilinears,

$$\Phi_1^{1,2} : \sigma^{1312} + \sigma^{1321}, \sigma^{1320} + \sigma^{1323} \tag{A.109}$$

$$\Phi_2^{1,2} : \sigma^{3112} + \sigma^{3121}, \sigma^{3120} + \sigma^{3123} \tag{A.110}$$

$$\Phi_3^3 : \sigma^{1202} k_y + \sigma^{1232} k_y, \sigma^{3202} k_x + \sigma^{3232} k_x \tag{A.111}$$

and the kinetic terms are,

$$\sigma^{1000}k_x, \sigma^{3000}k_y. \tag{A.112}$$

The only Pauli matrix commutes with the above matrices is σ^{0230}, which is also the symmetry generator.

Our model

In our model, the kinetic terms are,

$$\sigma^{100}k_x, \sigma^{300}k_y \tag{A.113}$$

and the pairing terms are

$$\sigma^{323}, \sigma^{321}, \sigma^{123}, \sigma^{121} \tag{A.114}$$

and the Pauli matrices that commute with the above are,

$$\sigma^{012}, \sigma^{020}, \sigma^{032} \tag{A.115}$$

A.3.4 Basis rotation

We can match both theories by examining their symmetry generators. The only matrix σ^{0230} that commutes with other matrices in Ref. [352] can be rotated to,

$$\sigma^{0012}, \text{ by } e^{i\frac{\pi}{4}\sigma^{0222}} \tag{A.116}$$

$$\sigma^{0020}, \text{ by } e^{i\frac{\pi}{4}\sigma^{0210}} \tag{A.117}$$

$$\sigma^{0332}, \text{ by } e^{i\frac{\pi}{4}\sigma^{0102}} \tag{A.118}$$

where the rotation is generated by $\sigma^I \rightarrow e^{-i\frac{\pi}{4}\sigma^J}\sigma^I e^{i\frac{\pi}{4}\sigma^J}$. The $\mathbb{Z}_2$ Higgs fields in Eq. (A.109) will be rotated to,

$$
\begin{aligned}
&\Phi_1^{1,2} : \sigma^{1312} + \sigma^{1321}, \sigma^{1102} + \sigma^{1323} \\
&\Phi_2^{1,2} : \sigma^{3112} + \sigma^{3121}, -\sigma^{3302} + \sigma^{3123} \text{ by } e^{i\frac{\pi}{4}\sigma^{0222}}
\end{aligned} \tag{A.119}
$$

$$
\begin{aligned}
&\Phi_1^{1,2} : \sigma^{1102} + \sigma^{1321}, \sigma^{1320} + \sigma^{1323} \\
&\Phi_2^{1,2} : -\sigma^{3302} + \sigma^{3121}, \sigma^{3120} + \sigma^{3123} \text{ by } e^{i\frac{\pi}{4}\sigma^{0210}}
\end{aligned} \tag{A.120}
$$

$$
\begin{aligned}
&\Phi_1^{1,2} : -\sigma^{1210} + \sigma^{1321}, -\sigma^{1222} + \sigma^{1323} \\
&\Phi_2^{1,2} : \sigma^{3112} - \sigma^{3023}, \sigma^{3120} + \sigma^{3021} \text{ by } e^{i\frac{\pi}{4}\sigma^{0102}}
\end{aligned} \tag{A.121}
$$

If one takes the second index as labeling the original theory and the dual theory in our model, some terms of the $\mathbb{Z}_2$ Higgs fields in Ref. [352] correspond to the pairing in the form of $\sigma^{121}, \sigma^{123}, \sigma^{321}, \sigma^{323}$ that appear in both the original theory and the dual theory according to the Eq. (A.121). For example,

$$
... + \chi^T \sigma^{1321} \chi = ... + \chi_1^T \sigma^{121} \chi_1 - \chi_2^T \sigma^{121} \chi_2 \sim ... + \psi^\intercal \sigma^2 \gamma^0 \gamma^x \psi - \tilde{\psi}^\intercal \sigma^2 \gamma^0 \gamma^x \tilde{\psi} \tag{A.122}
$$
$$
... + \chi^T \sigma^{3021} \chi = ... + \chi_1^T \sigma^{321} \chi_1 + \chi_2^T \sigma^{321} \chi_2 \sim ... + \psi^\intercal \sigma^2 \gamma^0 \gamma^y \psi + \tilde{\psi}^\intercal \sigma^2 \gamma^0 \gamma^y \tilde{\psi} \tag{A.123}
$$

where ψ is the original fermion and $\tilde{\psi}$ is the dual fermion, they are corresponding to the pairing fermion bilinears that appear in the $\mathbb{Z}_2$ Higgs fields Eq. (A.121). However, the dual fermion pairings are not explicit in the self-dual $N_f = 2$ QED$_3$ theory and the linear combinations with another fermion bilinears are crucial to obtain the $\mathbb{Z}_2$ Higgs fields in Ref. [352], for example, $\Phi_1^1 \chi^T(-\sigma^{1210} + \sigma^{1321})\chi$ in the first line of Eq. (A.121).

Appendix B

Appendix to Chapter. 2

B.1   de Rham cohomology of Lie groups and homogeneous spaces

B.1.1   de Rham complex

Let e_i denote the basis for the Lie algebra $\mathfrak{g}$ and θ^i for the 1-forms for $\mathfrak{g}^*$, which is the dual space of $\mathfrak{g}$. The p-forms on $\mathfrak{g}$ are the alternating multi-linear maps $\omega : \mathfrak{g} \times ... \times \mathfrak{g} \to \mathbb{R}$. For x_a being the basis for space V, the V-valued p-form on $\mathfrak{g}$, $\omega \in \Lambda^p(\mathfrak{g}^*, V)$ can be written as,

$$\omega = A^{\alpha}_{i_1,...,i_p} x_{\alpha} \theta^{i_1} \wedge ... \wedge \theta^{i_p}. \tag{B.1}$$

For example, the Maurer-Cartan 1-forms are Lie algebra valued 1-forms,

$$\theta = \theta^A T^A \in \Lambda^1(\mathfrak{g}^*, \mathfrak{g}). \tag{B.2}$$

The exterior derivative sends the p-forms to $p+1$-forms $d : \Lambda^p(\mathfrak{g}^*, V) \to \Lambda^{p+1}(\mathfrak{g}^*, V)$ and follows the rule,

$$d\theta^i = -\frac{1}{2} f^i_{jk} \theta^j \wedge \theta^k, \quad dx_{\alpha} = B^{\beta}_{\alpha i} x_{\beta} \theta^i, \tag{B.3}$$

where f^i_{jk} is the structure factor for the Lie algebra and $B^{\beta}_{\alpha i}$ is a certain linear map for the V-space.

For $\mathfrak{h} \subset \mathfrak{g}$ being a subalgebra of $\mathfrak{g}$, the relative cochain is given by,

$$\Lambda^p(\mathfrak{g}^*, \mathfrak{h}, V) = \{\omega \in \Lambda^p(\mathfrak{g}^*, V) | i_y(\omega) = 0 \text{ and } i_y(d\omega) = 0, \forall y \in \mathfrak{h}\}. \tag{B.4}$$

where i_y is the interior product, in other words, the forms ωs as well as $d\omega$s do not contain θ^is from the subalgebra $\mathfrak{h}$ parts, and the forms are invariant under adjoint action of H. In the following, we will mainly consider $\Lambda^p(\mathfrak{g}^*, \mathbb{R})$ and $\Lambda^p(\mathfrak{g}^*, \mathfrak{h}, \mathbb{R})$ which is relevant to the Wess-Zumino-Witten term for $G, G/H$ and other topological terms in the physical actions, thus, no x_α dependence.

The condition to construct relative cochain implies

$$\mathcal{L}_y \omega = (d i_y + i_y d) \omega = 0 \tag{B.5}$$

where $\mathcal{L}_y$ is the Lie derivative with respect to y, the relative cochain is then given by,

$$\Lambda^p(\mathfrak{g}^*, \mathfrak{h}, \mathbb{R}) = \{\omega \in \overset{p}{\bigwedge}(\mathfrak{g}/\mathfrak{h})^* | \mathcal{L}_y \omega = 0, \forall y \in \mathfrak{h}\}. \tag{B.6}$$

the Lie derivative action is explicitly expressed in terms of the components of the Maurer-Cartan 1-form,

$$\mathcal{L}_y \omega^{(n)} = -\sum_{i=1}^n \frac{1}{n!} \omega_{a_1,\dots,a_n} f^{b_j, y, a_j} \theta^{a_1} \wedge \dots \wedge \theta^{b_j} \wedge \dots \wedge \theta^{a_n} = 0. \tag{B.7}$$

The relative cochain can be constructed by first finding the space spanned by $\bigwedge^p(\mathfrak{g}/\mathfrak{h})^*$ and then using $\mathcal{L}_y, y \in H$ iteratively to eliminate non-invariant bases.

B.1.2 Cohomology

A p-form $\omega \in \Lambda^p(\mathfrak{g}^*, \mathfrak{h}, \mathbb{R})$ is **closed**, if $d\omega = 0$; and **exact** if it can be expressed by a $(p-1)$-form η by $\omega = d\eta$. Since $d^2 = 0$ for any differential forms ω, the exact forms are necessarily closed but the closed forms can be non-exact.

The cohomology $H^*(G, \mathbb{R})$ and $H^*(G/H, \mathbb{R})$ measures the closed forms not being exact. Consequently, the p-forms cannot be expressed locally in $p-1$ dimension by Stokes theorem.

We explicitly calculate the cohomology group using the basis of the general p-form generated by the exterior product of the 1-form components θ^is. For example, the basis for the 2-forms in $\Lambda^2(\mathfrak{g}^*, \mathbb{R})$ are,

$$\{\theta^1 \wedge \theta^2, \theta^1 \wedge \theta^3, ..., \theta^{\dim(G)-1} \wedge \theta^{\dim(G)}\}. \tag{B.8}$$

The exterior derivative can therefore be expressed as a matrix $\tilde{d}_{ab}$,

$$\mathrm{d}\{(\theta^i)^{\wedge p}\}_a = \tilde{d}^p_{ab}\{(\theta^i)^{\wedge(p+1)}\}_b \tag{B.9}$$

The matrix $\tilde{d}^p_{ab}$ is a $\binom{\dim(G)}{p} \times \binom{\dim(G)}{p+1}$ matrix. The subspace of the closed p-forms C^p is the null-space or the kernel of the matrix $(\tilde{d}^p_{ab})^T$,

$$\text{subspace of the closed } p\text{-forms: } C^p = \ker(\tilde{d}^p_{ab})^\mathsf{T} \tag{B.10}$$

The subspace of the exact p-forms Z^p is the the orthogonal complement of the kernel of $(\tilde{d}^{p-1}_{ab})$,

$$\text{subspace of the exact } p\text{-forms: } Z^p = (\ker \tilde{d}^{p-1}_{ab})^\perp \tag{B.11}$$

This can be obtained by Gaussian elimination of the matrix $\tilde{d}^{p-1}_{ab}$. Therefore, the cohomology is the quotient,

$$H^p = \frac{\ker(\tilde{d}^p_{ab})^\mathsf{T}}{(\ker \tilde{d}^{p-1}_{ab})^\perp} \tag{B.12}$$

Algorithmically, we denoted the space of closed p-form as C^p and exact p-form as Z^p, they are both matrices, and the cohomology is,

$$[\ker C^p \cdot (Z^p)^\mathsf{T} \cdot Z^p \cdot (C^p)^\mathsf{T}] \cdot C^p \tag{B.13}$$

228

For the relative cochain, one needs to further impose the constraint in Eq. (B.6). This constraint corresponds to dropping the basis which contains indices corresponding to that in $\mathfrak{h}$ and invariant under the adjoint transformation of H. One can start with the basis constructed by wedge product of θ^as, where $a \in \mathfrak{g}/\mathfrak{h}$, and then use the Lie derivative for each $h \in H$ to eliminate non-zero bases.

B.1.3 Examples

Using the de Rham cohomology, we are able to calculate the following examples. And we compare our results with the general results which are cited from [274] if not citing others.

SU(4): Our calculation gives,

$$H^3(\mathsf{SU}(4), \mathbb{R}) = \mathbb{R}, \quad H^5(\mathsf{SU}(4), \mathbb{R}) = \mathbb{R}. \tag{B.14}$$

In general, $H^*(\mathsf{SU}(n)) = \Lambda(e_3, e_5, ..., e_{2n-1})$, where $e_i \in H^i(\mathsf{SU}(n), \mathbb{R})$, the cohomology ring is generated by wedge product.

SO(6)/(SO(4)$\times$ SO(2)), dim $= 15 - 7 = 8$ even dimensional: Our calculation gives,

$$H^2\left(\frac{\mathsf{SO}(6)}{\mathsf{SO}(4) \times \mathsf{SO}(2)}, \mathbb{R}\right) = \mathbb{R}, \quad H^4\left(\frac{\mathsf{SO}(6)}{\mathsf{SO}(4) \times \mathsf{SO}(2)}, \mathbb{R}\right) = \mathbb{R} \oplus \mathbb{R}. \tag{B.15}$$

In general,

$$H^*(\mathsf{SO}(2n+2)/(\mathsf{SO}(2n) \times \mathsf{SO}(2))) = (1 + t^{2n})(1 + t^2 + t^4 + ... + t^{2n}) \tag{B.16}$$

For $n = 2, H^*(\mathsf{SO}(6)/(\mathsf{SO}(4) \times \mathsf{SO}(2))) = 1 + t^2 + 2t^4 + t^6 + t^8$, where t^n corresponds to the degree n generator, $2t^4$ means 2 independent degree 4 generators. In general, the Poincare

polynomial for $H^*(\frac{\mathsf{SO}(2n)}{\mathsf{SO}(2k)\times\mathsf{SO}(2n-2k)})$ is in [167],

$$\frac{H^*(\frac{\mathsf{SO}(8)}{\mathsf{SO}(4)\times\mathsf{SO}(4)})\ \Big|\ 1+3t^4+4t^8+...}{H^*(\frac{\mathsf{SO}(10)}{\mathsf{SO}(4)\times\mathsf{SO}(6)})\ \Big|\ 1+2t^4+t^6+3t^8...} \tag{B.17}$$

also,

$$\frac{H^*(\frac{\mathsf{SO}(8)}{\mathsf{SO}(2)^4})\ \Big|\ 1+4t^2+9t^4+...}{H^*(\frac{\mathsf{SO}(10)}{\mathsf{SO}(2)^5})\ \Big|\ 1+5t^2+14t^4...} \tag{B.18}$$

Our explicit calculation of cohomology up to 4 degree agrees with the general results.

SO(6)/U(3): Our calculation gives,

$$H^2\left(\frac{\mathsf{SO}(6)}{\mathsf{U}(3)},\mathbb{R}\right)=\mathbb{R},\quad H^4\left(\frac{\mathsf{SO}(6)}{\mathsf{U}(3)},\mathbb{R}\right)=\mathbb{R}. \tag{B.19}$$

In general, $H^*(\mathsf{SO}(2n)/\mathsf{U}(n))=\Delta(e_2,e_4,...,e_{2n-2})$.

Our calculation of other cohomology of cosets with $G=\mathsf{SO}$,

$$
\begin{array}{c|c|c|c|c}
 & \frac{\mathsf{SO}(8)}{\mathsf{SO}(4)\times\mathsf{SO}(4)} & \mathsf{SO}(8)/\mathsf{U}(4) & \frac{\mathsf{SO}(10)}{\mathsf{SO}(4)\times\mathsf{SO}(6)} & \mathsf{SO}(10)/\mathsf{U}(5) \\
\hline
H^2(G/H,\mathbb{R}) & \varnothing(\mathbb{Z}_2) & \mathbb{R} & \varnothing(\mathbb{Z}_2) & \mathbb{R}
\end{array}
\tag{B.20}
$$

The torsion $\mathbb{Z}_2$ of $H^2(\frac{\mathsf{SO}(8)}{\mathsf{SO}(4)\times\mathsf{SO}(4)})$ cannot be detected by de Rham cohomology.

Cohomology of G/K

The cohomology of G/K is relevant to the symmetry defects in spontaneously symmetry-breaking phases. The Lie group K is generated by the Lie algebra $\mathfrak{k}=\mathfrak{h}_1\cap\mathfrak{h}_2$, and our cohomology calculation gives,

$$
\begin{array}{c|c|c|c}
 & \frac{\mathsf{SO}(6)}{\mathsf{SO}\mathsf{SO}\cap\mathsf{U}} & \frac{\mathsf{SO}(8)}{\mathsf{SO}\mathsf{SO}\cap\mathsf{U}} & \frac{\mathsf{SO}(10)}{\mathsf{SO}\mathsf{SO}\cap\mathsf{U}} \\
\hline
H^2(G/H,\mathbb{R}) & \mathbb{R}\oplus\mathbb{R} & \mathbb{R}\oplus\mathbb{R} & \mathbb{R}\oplus\mathbb{R}
\end{array}
\tag{B.21}
$$

where $\mathbb{R} \oplus \mathbb{R}$ in $H^2(\mathsf{SO}(6)/(\mathsf{SOSO} \cap \mathsf{U}))$ are the same generators of $H^2(G/H_1), H^2(G/H_2)$. For $\mathsf{SO}(8), \mathsf{SO}(10)$, one is the same generator of SO/U, another is the new from both SO/U and SO/SO parts.

Other cosets

SU(4)/SO(4): Our calculation shows,

$$H^4\left(\frac{SU(4)}{SO(4)}, \mathbb{R}\right) = \mathbb{R}, \quad H^5\left(\frac{SU(4)}{SO(4)}, \mathbb{R}\right) = \mathbb{R} \tag{B.22}$$

In general,

$$H^*\left(\frac{SU(n)}{SO(n)}, \mathbb{R}\right) = \begin{cases} \Lambda(e_5, ..., e_{4m+1}) & n = 2m+1 \\ \\ \Lambda(e_5, ..., e_{4m-2}) \otimes \Delta(e_{2m}) & n = 2m \end{cases} \tag{B.23}$$

SO(6)/(SO(3)× SO(3)), $\dim = 15 - 6 = 9$ odd dimensional: Our calculation shows,

$$H^4\left(\frac{SO(6)}{SO(3) \times SO(3)}, \mathbb{R}\right) = \mathbb{R}, \quad H^5\left(\frac{SO(6)}{SO(3) \times SO(3)}, \mathbb{R}\right) = \mathbb{R} \tag{B.24}$$

B.2   Cartan homotopy formula

B.2.1   Review of Cartan homotopy method

If two connections are of the same bundle, one can consider the interpolation [286],

$$\mathscr{A}_t = \mathscr{A}_0 + t(\mathscr{A}_1 - \mathscr{A}_0), \quad \mathscr{F}_t \equiv d\mathscr{A}_t + \mathscr{A}_t^2 \tag{B.25}$$

Another useful formula,

$$\mathscr{D}_{\mathscr{A}}\eta = d\eta + [\mathscr{A}, \eta], \tag{B.26}$$

$$[\eta^{(p)}, \omega^{(q)}] = \eta^{(p)} \wedge \omega^{(q)} - (-1)^{pq} \omega^{(q)} \wedge \eta^{(p)} \tag{B.27}$$

Define the anti-deriviative operator ℓ_t,

$$\ell_t \mathscr{A}_t = 0, \quad \ell_t \mathscr{F}_t = \delta t (\mathscr{A}_1 - \mathscr{A}_0), \tag{B.28}$$

$$\ell_t(\eta^{(p)}\omega^{(q)}) = (\ell_t\eta^{(p)})\omega^{(q)} + (-1)^p \eta^{(p)}(\ell_t\omega^{(q)}) \tag{B.29}$$

we have,

$$(d\ell_t + \ell_t d)\mathscr{A}_t = \delta t \frac{\partial \mathscr{A}_t}{\partial t} \tag{B.30}$$

$$(d\ell_t + \ell_t d)\mathscr{F}_t = \delta t \frac{\partial \mathscr{F}_t}{\partial t} \tag{B.31}$$

This shows that for any polynomial $S(\mathscr{A}, \mathscr{F})$, we have

$$(d\ell_t + \ell_t d)S(\mathscr{A}_t, \mathscr{F}_t) = \delta t \frac{\partial}{\partial t} S(\mathscr{A}_t, \mathscr{F}_t) \tag{B.32}$$

this yields,

$$S(\mathscr{A}_1, \mathscr{F}_1) - S(\mathscr{A}_0, \mathscr{F}_0) = (dk_{01} + k_{01}d)S(\mathscr{A}_t, \mathscr{F}_t) \tag{B.33}$$

where

$$k_{01}S(\mathscr{A}_t, \mathscr{F}_t) \equiv \int_0^1 \delta t \ell_t S(\mathscr{A}_t, \mathscr{F}_t) \tag{B.34}$$

B.2.2 Details of gauged WZW term

We would like to use the Carton homotopy method to derive the additional exact form in the gauged WZW term. As discussed around Eq. (2.33), the general gauged WZW for symmetry breaking of $G \to H$ has the form,

$$\underline{\Gamma}^{(d+1)}(U, A, A_{\mathfrak{h}}) \equiv \mathsf{CS}(A^U, A_{\mathfrak{h}}^U) - \mathsf{CS}(A, A_{\mathfrak{h}}) = \Gamma^{(d+1)}(U) + d\alpha^{(d)}(U, A, A_{\mathfrak{h}}). \tag{B.35}$$

For $\mathfrak{h} = \varnothing$, the gauged WZW term is given by the Chern-Simons form,

$$\underline{\Gamma}^{(d+1)}(U,A) \equiv \mathsf{CS}(A^U) - \mathsf{CS}(A) = \Gamma^{(d+1)}(U) + d\alpha^{(d)}(U,A). \tag{B.36}$$

For presentation simplicity, we focus on $d = 2$ and first calculate the case when $\mathfrak{h} = \varnothing$, then $\mathfrak{h} \neq \varnothing$.

The case when $\mathfrak{h} = \varnothing$

Consider the path of interpolation, $A_t = tU^{-1}AU + U^{-1}dU = tU^{-1}AU + \theta$, such that $A_1 = A^U, A_0 = \theta$. The difference between Chern-Simons forms is then,

$$\mathsf{CS}^{(3)}(A^U) - \mathsf{CS}^{(3)}(\theta) = d\int_t \ell_t \mathsf{CS}^{(3)}(A_t) + \int_t \ell_t d\mathsf{CS}^{(3)}(A_t). \tag{B.37}$$

The last term on the right-hand side (RHS) gives $\mathsf{CS}^{(3)}(A)$, while the first term in the RHS gives,

$$d\int_t \ell_t (A_t F_t - \frac{1}{3}A_t^3) = -d\int_t (A_t A) = d(-dUU^{-1}A), \tag{B.38}$$

since $\ell_t F_t = U^{-1}AU$, $\ell_t A_t = 0$. Therefore, $\alpha^{(2)} = -dUU^{-1}A$. In short,

$$\mathsf{CS}^{(3)}(A^U) - \mathsf{CS}^{(3)}(\theta) = \mathsf{CS}^{(3)}(A) - d(dUU^{-1}A). \tag{B.39}$$

Hence, the gauged WZW term in $d = 2$ is,

$$\underline{\Gamma}^{(3)}(U,A) = \Gamma_G^{(3)}(U) + d(dUU^{-1}A), \tag{B.40}$$

where $\Gamma_G^{(3)}(U)$ is given in Eq. (2.49). This indeed shows that the gauge field only supports on d-dimensional manifold.

The case when $\mathfrak{h} \neq \varnothing$

Consider the path of interpolation, $A_t = tU^{-1}AU + \theta, A_{\mathfrak{h},t} = tU^{-1}A_{\mathfrak{h}}U + V$, the difference of the relative Chern-Simons form is,

$$\mathsf{CS}^{(3)}(A^U, A_{\mathfrak{h}}^U) - \mathsf{CS}^{(3)}(\theta, V) = d \int_t \ell_t \mathsf{CS}^{(3)}(A_t, A_{\mathfrak{h},t}) + \int_t \ell_t d\mathsf{CS}^{(3)}(A_t, A_{\mathfrak{h},t}). \tag{B.41}$$

Similarly, the last term in the RHS gives $\mathsf{CS}^{(3)}(A, A_{\mathfrak{h}})$, the first term in RHS is,

$$d \int_t \ell_t \operatorname{tr}\left((A_t - A_{\mathfrak{h},t})F_t + (A_t - A_{\mathfrak{h},t})F_{\mathfrak{h},t} + \ldots \right) \tag{B.42}$$

$$= d \int_t \operatorname{tr}(tU^{-1}A_{\mathfrak{f}}U + \phi)U^{-1}(A + A_{\mathfrak{h}})U \tag{B.43}$$

$$= d \operatorname{tr}(U\phi U^{-1}(A + A_{\mathfrak{h}})) \tag{B.44}$$

where $\ell_t F_{t,i} = A_i$, $\ell_t A_i = 0$, and $\ldots$ is the polynomial $A_t^2 - A_t A_{\mathfrak{h},t}^2 - \frac{1}{3}(A_t^3 - A_{\mathfrak{h},t}^3)$ which vanishes under ℓ_t. Then the gauged WZW term is given by,

$$\underline{\Gamma}^{(3)}(U, A, A_{\mathfrak{h}}) = \mathsf{CS}(A^U, A_{\mathfrak{h}}^U) - \mathsf{CS}(A, A_{\mathfrak{h}}) = \Gamma^{(3)}(U) + d\operatorname{tr}(U\phi U^{-1}(A + A_{\mathfrak{h}})) \tag{B.45}$$

where $\Gamma^{(3)}(U)$ is given in Eq. (2.47).

Appendix C

Appendix to Chapter. 3

C.1 Emergent $\mathsf{U}(1)$ Symmetries in the (1+1)D Two-Band Model

Start from the definition of charge $\mathsf{U}(1)$ (parameterized by a periodic angle $\phi \in [0, 2\pi)$) and lattice translation $\mathbb{Z}$ (parameterized by an integer $n \in \mathbb{Z}$) symmetries as defined in Eq. (3.7)

$$
\begin{aligned}
\mathsf{U}(1) : c_{iA} &\to e^{iq_A\phi} c_{iA}, \quad c_{iB} \to e^{iq_B\phi} c_{iB}; \\
\mathbb{Z} : c_{iA} &\to c_{(i+n)A}, \quad c_{iB} \to c_{(i+n)B}.
\end{aligned}
\tag{C.1}
$$

Follow the definition Eq. (3.9) of the fermion operators in the momentum space

$$
c_{kA} = \sum_i c_{iA} e^{-iki}, \quad c_{kB} = \sum_i c_{iB} e^{-iki},
\tag{C.2}
$$

where the wave number $k \in [-\pi, \pi)$ is a dimensionless periodic variable defined in the first Brillouin zone. (Note: the *dimensionful* momentum p should be related to the *dimensionless* wave number k by $p = \hbar k / a$ with a being the lattice constant and the site coordinate $x \in \mathbb{R}$ is related to the site index $i \in \mathbb{Z}$ by $x = ai$, such that the Fourier factor $e^{-ipx/\hbar} = e^{-iki}$ is consistent with the quantum mechanics convention.) It is straightforward to show that the $\mathsf{U}(1) \times \mathbb{Z}$ symmetry acts

in the momentum space as

$$\mathsf{U}(1): c_{kA} \to e^{iq_A\phi}c_{kA}, c_{kB} \to e^{iq_B\phi}c_{kB};$$

$$\mathbb{Z}: c_{kA} \to e^{ikn}c_{kA}, c_{kB} \to e^{ikn}c_{kB}. \tag{C.3}$$

Apply these transformations to the low-energy fermion near the four Fermi points. According to Eq. (3.12)

$$
\begin{aligned}
c_{AR} &= c_{(3k_F)A}, \\
c_{BR} &= c_{(-k_F)B}, \\
c_{BL} &= c_{(k_F)B}, \\
c_{AL} &= c_{(-3k_F)A},
\end{aligned}
\tag{C.4}
$$

Eq. (C.3) becomes

$$
\mathsf{U}(1): \begin{cases}
c_{AR} & \to \quad e^{iq_A\phi}c_{AR}, \\
c_{BR} & \to \quad e^{iq_B\phi}c_{BR}, \\
c_{BL} & \to \quad e^{iq_B\phi}c_{BL}, \\
c_{AL} & \to \quad e^{iq_A\phi}c_{AL};
\end{cases}
$$

$$
\mathbb{Z}: \begin{cases}
c_{AR} & \to \quad e^{3ik_Fn}c_{AR}, \\
c_{BR} & \to \quad e^{-ik_Fn}c_{BR}, \\
c_{BL} & \to \quad e^{ik_Fn}c_{BL}, \\
c_{AL} & \to \quad e^{-3ik_Fn}c_{AL}.
\end{cases}
\tag{C.5}
$$

Because $k_F = |v_B|\pi$ is *almost always* (i.e., with probability 1) a irrational multiple of π (because $|v_B|$ is almost always an irrational number without fine tuning), $k_Fn \mod 2\pi$ can approach any angle in $[0, 2\pi)$ (with 2π periodicity) as close as we want (given $n \in \mathbb{Z}$). This allows us to define

two angular variables ϕ_V and ϕ_A, both are periodic in $[0, 2\pi)$,

$$\phi_V = \phi, \quad \phi_A = k_F n \mod 2\pi, \tag{C.6}$$

then Eq. (C.5) can be compactly written as

$$\text{UV symmetry} \Rightarrow \text{IR symmetry}$$

$$U(1) \Rightarrow U(1)_V : c_a \rightarrow e^{iq_a^V \phi_V} c_a, \tag{C.7}$$

$$\mathbb{Z} \Rightarrow U(1)_A : c_a \rightarrow e^{iq_a^A \phi_A} c_a,$$

for $a = AR, BR, BL, AL$ enumerating over the four Fermi point labels, together with the charge vectors (given that $q_A = 1$ and $q_B = 3$):

$$\boldsymbol{q}^V = \begin{bmatrix} q_A \\ q_B \\ q_B \\ q_A \end{bmatrix} = \begin{bmatrix} 1 \\ 3 \\ 3 \\ 1 \end{bmatrix}, \quad \boldsymbol{q}^A = \begin{bmatrix} 3 \\ -1 \\ 1 \\ -3 \end{bmatrix}. \tag{C.8}$$

Therefore, the global charge $U(1)$ symmetry is simply reinterpreted as the $U(1)_V$ vector symmetry, and the translation symmetry (described by a non-compact $\mathbb{Z}$ group) in the UV becomes an emergent $U(1)_A$ axial symmetry (described by a compact $U(1)$ group) in the IR. The symmetry transformation in Eq. (C.7) precisely matches Eq. (3.14) in the main text with the correct charge assignment as listed in Tab. 3.1.

Recombining the charge vectors of $U(1)_V$ and $U(1)_A$, we can define two alternative emergent $U(1)$ symmetries, denoted as $U(1)_{\frac{3V \pm A}{2}}$ with the charge vectors

$$\boldsymbol{q}^{\frac{3V \pm A}{2}} = \frac{1}{2}(3\boldsymbol{q}^V \pm \boldsymbol{q}^A), \tag{C.9}$$

as their names implied. More explicitly, the charge vectors match the chiral charge assignements

237

for the 3-4-5-0 fermions:

$$
\boldsymbol{q}^{\frac{3V+A}{2}} = \begin{bmatrix} 3 \\ 4 \\ 5 \\ 0 \end{bmatrix}, \quad \boldsymbol{q}^{\frac{3V-A}{2}} = \begin{bmatrix} 0 \\ 5 \\ 4 \\ 3 \end{bmatrix}. \tag{C.10}
$$

The fermions are expected to transform under $\mathsf{U}(1)_{\frac{3V\pm A}{2}}$ as (parameterized by the periodic angles $\phi_\pm \in [0, 2\pi)$)

$$
\mathsf{U}(1)_{\frac{3V\pm A}{2}} : c_a \to e^{i\frac{1}{2}(3q_a^V \pm q_a^A)\phi_\pm} c_a. \tag{C.11}
$$

This can be viewed as the combined transformation of $\mathsf{U}(1)_V$ and $\mathsf{U}(1)_A$ with the vector rotation angle ϕ_V and the axial rotation angle ϕ_A given by

$$
\phi_V = \frac{3}{2}\phi_\pm, \quad \phi_A = \pm\frac{1}{2}\phi_\pm, \tag{C.12}
$$

as can be verified by comparing Eq. (C.11) with Eq. (C.7). Now we can connect these rotation angle back to the original $\mathsf{U}(1) \times \mathbb{Z}$ symmetry of the lattice fermions using the relation Eq. (C.6),

$$
\phi = \frac{3}{2}\phi_\pm, \quad \pm\frac{1}{2}\phi_\pm = k_F n \quad \mathrm{mod}\ 2\pi. \tag{C.13}
$$

Eliminate $\phi_\pm$ from the equations, we obtain the relation

$$
\phi = \pm 3k_F n \quad \mathrm{mod}\ 2\pi, \tag{C.14}
$$

for the $\mathsf{U}(1)_{\frac{3V\pm A}{2}}$ symmetries. Therefore, in order to reproduce the IR emergent $\mathsf{U}(1)_{\frac{3V\pm A}{2}}$ symmetries, the corresponding UV symmetries (at the lattice level) must be such implemented that every n-step translation should be followed by a charge $\mathsf{U}(1)$ rotation with the rotation angle

$\phi = \pm 3k_F n$. So we establish the following correspondence between the IR and UV symmetries

IR symmetry $\Rightarrow$ UV symmetry

$$\mathsf{U}(1)_{\frac{3V\pm A}{2}} \Rightarrow \mathbb{Z}(\tfrac{3V\pm A}{2}) : \begin{cases} c_{iA} \to \mathrm{e}^{\pm 3iq_A k_F n} c_{(i+n)A}, \\[2mm] c_{iB} \to \mathrm{e}^{\pm 3iq_B k_F n} c_{(i+n)B}. \end{cases} \qquad (C.15)$$

Here the compact $\mathsf{U}(1)$ symmetries in the IR get mapped to the non-compact symmetries $\mathbb{Z}$ in the UV, because the UV symmetries are parameterized by the integer variable $n \in \mathbb{Z}$. Given that $q_A = 1$ and $q_B = 3$, Eq. (C.15) becomes Eq. (3.15), as claimed in the main text. Therefore the 3-4-5-0 chiral fermion model is indeed realized in by the (1+1)D two-band lattice model at low energy.

C.2 Wang-Wen Interaction

In the bonsonization language, the Wang-Wen interaction is described by

$$\mathscr{L}_{\mathrm{int}} = \sum_{\alpha=1,2} g_\alpha \cos\left(l_\alpha^\mathsf{T} \varphi\right) \qquad (C.16)$$

with $\varphi = (\varphi_{AR}, \varphi_{BR}, \varphi_{BL}, \varphi_{AL})^\mathsf{T}$ and the interaction vectors given by

$$l_1 = \begin{bmatrix} 1 \\ -2 \\ 1 \\ 2 \end{bmatrix}, \quad l_2 = \begin{bmatrix} 2 \\ 1 \\ -2 \\ 1 \end{bmatrix}. \qquad (C.17)$$

Mapping back to the chiral fermions by the correspondence $c_a \sim :\mathrm{e}^{\mathrm{i}\varphi_a}:$, the interaction reads

$$\begin{aligned} H_{\mathrm{int}} &= \frac{g_1}{2}(c_{AR}c_{BL})(c_{BR}^\dagger c_{AL})^2 + \mathrm{h.c.} \\ &+ \frac{g_2}{2}(c_{BR}c_{AL})(c_{AR}c_{BL}^\dagger)^2 + \mathrm{h.c..} \end{aligned} \qquad (C.18)$$

According to Eq. (3.12) and use the inverse Fourier transformation,

$$c_{AR} = c_{(3k_F)A} = \sum_i c_{iA} e^{3ik_F i},$$

$$c_{BR} = c_{(-k_F)B} = \sum_i c_{iB} e^{-ik_F i},$$

$$c_{BL} = c_{(k_F)B} = \sum_i c_{iB} e^{ik_F i}, \tag{C.19}$$

$$c_{AL} = c_{(-3k_F)A} = \sum_i c_{iA} e^{-3ik_F i}.$$

Plugging Eq. (C.19) into Eq. (C.18), the interaction becomes

$$H_{\text{int}} = \sum_{i_1,\cdots,i_6} g_{i_1\cdots i_6} (c^\dagger_{i_1 B} c_{i_2 A})(c_{i_3 B} c_{i_4 A})(c^\dagger_{i_5 B} c_{i_6 A}) + \text{h.c.}, \tag{C.20}$$

with

$$g_{i_1\cdots i_6} = \frac{g_1}{2} e^{ik_F(i_1 - 3i_2 + i_3 + 3i_4 + i_5 - 3i_6)}$$
$$+ \frac{g_2}{2} e^{ik_F(-i_1 + 3i_2 - i_3 - 3i_4 - i_5 + 3i_6)}. \tag{C.21}$$

Notice that under lattice reflection symmetry $\mathbb{Z}_2 : c_{iA} \to c_{(-i)A}, c_{iB} \to c_{(-i)B}$, g_1 and g_2 maps to each other. To simplify, we can impose the reflection symmetry and requires $g_1 = g_2 = g$, then the coupling coefficient is

$$g_{i_1\cdots i_6} = g\cos\left(k_F(i_1 - 3i_2 + i_3 + 3i_4 + i_5 - 3i_6)\right). \tag{C.22}$$

The dominant s-wave interaction is given by

$$i_1 - 3i_2 + i_3 + 3i_4 + i_5 - 3i_6 = 0, \tag{C.23}$$

such that $g_{i_1 \cdots i_6} = g$ is uniform. We seek a local interaction that has minimal span on the lattice. The optimal solution of Eq. (C.23) is given by

$$i_1 = i_2 = i - 1, i_3 = i_4 = i, i_5 = i_6 = i + 1, \tag{C.24}$$

for any choice of i. With this solution Eq. (C.24), Eq. (C.20) reduces to

$$H_{\text{int}} = g \sum_i c^\dagger_{(i-1)B} c_{(i-1)A} c_{iB} c_{iA} c^\dagger_{(i+1)B} c_{(i+1)A} + \text{h.c..} \tag{C.25}$$

which is the SMG interaction Eq. (3.16) proposed in the main text.

C.3 Full Renormalization Group Equations

We start with the interaction $H_{\text{int, CF}}$

$$H_{\text{int, CF}} = g_{rs} \sum_\alpha \varepsilon^{ijk} c^\dagger_{B\alpha} c_{A_i\alpha} c_{A_j\alpha} c_{A_k\alpha}$$

$$+ g_{rt} \sum_{\alpha \neq \beta} \varepsilon^{ijk} c^\dagger_{B\alpha} c_{A_i\alpha} c_{A_j\beta} c_{A_k\beta} + \text{h.c.} \tag{C.26}$$

Under RG, the following density-density and exchange interactions will be generated

$$H_{\text{int, AA}} = g_{as} \sum_{\alpha,st} n_{A_s\alpha} n_{A_t\alpha} + g_{at} \sum_{\alpha \neq \beta,st} n_{A_s\alpha} n_{A_t\beta}$$

$$+ g_{ae} \sum_{\alpha \neq \beta,st} c^\dagger_{A_s\alpha} c_{A_s\beta} c^\dagger_{A_t\beta} c_{A_t\alpha} + (A_s \leftrightarrow A_t) + \text{h.c.} \tag{C.27}$$

and

$$H_{\text{int, AB}} = g_{bs} \sum_{\alpha,s} n_{B\alpha} n_{A_s\alpha} + g_{bt} \sum_{\alpha \neq \beta,s} n_{B\alpha} n_{A_s\beta}$$

$$+ g_{be} \sum_{\alpha \neq \beta,s} c^\dagger_{B\alpha} c_{B\beta} c^\dagger_{A_s\beta} c_{A_s\alpha} + (A_s \leftrightarrow B) + \text{h.c.} \tag{C.28}$$

There is an additional density-density interaction that will correct $H_{\text{int, AA}}, H_{\text{int, AB}}$,

$$H_{\text{int, BB}} = g_{\text{bb}} \sum_{\alpha\beta} n_{B\alpha} n_{B\beta} - c_{B\alpha}^{\dagger} c_{B\beta} c_{B\beta}^{\dagger} c_{B\alpha}. \tag{C.29}$$

Putting all interactions together, the complete RG equations are

$$\frac{dg_{\text{bb}}}{d\ell} = 4d_0 d_{\text{BB}} g_{\text{bb}}^2 + 3d_0 g_{\text{be}}^2$$

$$\frac{dg_{\text{bs}}}{d\ell} = -2d_{\text{AB}} g_{\text{bs}}^2 + \frac{9g_{\text{rs}}^2}{2} + g_{\text{rt}}^2$$

$$\frac{dg_{\text{bt}}}{d\ell} = 2d_0 d_{\text{AB}} g_{\text{bt}}^2$$

$$\frac{dg_{\text{be}}}{d\ell} = -6d_0 g_{\text{ae}} g_{\text{be}} + 2d_0 g_{\text{at}} g_{\text{be}} + 4d_0 d_{\text{BB}} g_{\text{bb}} g_{\text{be}} + 3g_{\text{rs}} g_{\text{rt}} + \frac{g_{\text{rt}}^2}{2}$$

$$\frac{dg_{\text{as}}}{d\ell} = -2g_{\text{as}}^2$$

$$\frac{dg_{\text{at}}}{d\ell} = 2d_0 g_{\text{at}}^2 - d_0 d_{\text{AB}} g_{\text{rt}}^2$$

$$\frac{dg_{\text{ae}}}{d\ell} = -d_0 d_{\text{AB}} g_{\text{rt}}^2 + 4d_0 g_{\text{ae}} g_{\text{at}} - 6d_0 g_{\text{ae}}^2 - 2d_0 d_{\text{BB}} g_{\text{be}}^2$$

$$\frac{dg_{\text{rs}}}{d\ell} = -6g_{\text{as}} g_{\text{rs}}$$

$$\frac{dg_{\text{rt}}}{d\ell} = 4d_0 d_{\text{AB}} g_{\text{bt}} g_{\text{rt}} - 2g_{\text{as}} g_{\text{rt}}$$

where $d_{\text{AB}} = d\chi_{pp,\text{AB}}(\mathbf{0})/d\ell, d_{\text{BB}} = d\chi_{pp,\text{BB}}(\mathbf{0})/d\ell$. These ratios depend on the energies of A and B-type fermions near the VHSs. The two types of fermions have similar band structures, which can be approximated as $E_{\mathbf{k}}^{A,B} = \varepsilon^{A,B} f(\mathbf{k})$. The ratios are then given by $d_{\text{AB}} = \frac{2|\varepsilon^A|}{|\varepsilon^A|+|\varepsilon^B|}$ and $d_{\text{BB}} = \frac{|\varepsilon^A|}{|\varepsilon^B|}$. If A and B-type fermions have the same band structure, then $d_{\text{AB}} = d_{\text{BB}} = 1$.

Appendix D

Appendix to Chapter. 4

D.1   Cluster Perturbation Theory

Here we review the details of cluster perturbation theory (CPT) originally developed in [345]. Denote the superlattice lattice points by $\boldsymbol{R}$, then the position of any original lattice point would be given by $\boldsymbol{R} + \boldsymbol{r}$, where $\boldsymbol{r}$ is the relative position of the lattice point to the location $\boldsymbol{R}$ of the cluster containing that particular lattice point. For clusters of size L, the generic Green's function in real space can be denoted by $G_{i,j}^{\boldsymbol{R},\boldsymbol{R}'}$, with $i, j = 1,...,L$, where the time-dependence is implicitly assumed and same goes for the frequency-dependence in Fourier space. Due to the translation invariance of the clusters on the *superlattice*, the real space Green's function can be firstly partially Fourier-transformed to give,

$$G_{i,j}^{\boldsymbol{R},\boldsymbol{R}'} = \frac{1}{N}\sum_{\boldsymbol{q}} G(\boldsymbol{q})_{ij} e^{i\boldsymbol{q}\cdot(\boldsymbol{R}-\boldsymbol{R}')}, \tag{D.1}$$

where the $\boldsymbol{q}$-summation is over the Brillouin zone (BZ) of the superlattice and N is the number of clusters on the superlattice, which goes to infinity in the thermodynamic limit. In contrast to the translation invariance of the $(\boldsymbol{R},\boldsymbol{R}')$-part of $G_{i,j}^{\boldsymbol{R},\boldsymbol{R}'}$, or equivalently it only depends on the difference $\boldsymbol{R} - \boldsymbol{R}'$ as can be seen in Eq. (D.1), the (i,j)-part of the Green's function loses translation invariance due to the introduction of clusters. This is so because correlation between two points within the same cluster is not manifestly the same with the correlation between

another pair of equally separated points *across* clusters. Therefore, it takes two lattice momenta to fully characterize $G_{i,j}^{R,R'}$ in Fourier space. More precisely, we have,

$$G(\boldsymbol{k},\boldsymbol{k'}) = \frac{1}{NL} \sum_{\boldsymbol{R},\boldsymbol{R'}} \sum_{i,j} G_{i,j}^{\boldsymbol{R},\boldsymbol{R'}} e^{i\boldsymbol{k}\cdot(\boldsymbol{R}+\boldsymbol{r}_i)-i\boldsymbol{k'}\cdot(\boldsymbol{R'}+\boldsymbol{r}_j)}. \tag{D.2}$$

Then we can plug Eq. (D.1) into Eq. (D.2) and integrate out the superlattice lattice vectors $\boldsymbol{R},\boldsymbol{R'}$ to obtain the following,

$$G(\boldsymbol{k},\boldsymbol{k'}) = \frac{1}{L} \sum_{i,j} \sum_{\boldsymbol{q}} G(\boldsymbol{q})_{ij} \tilde{\delta}_{\boldsymbol{k},\boldsymbol{q}} \tilde{\delta}_{\boldsymbol{k'},\boldsymbol{q}} e^{i(\boldsymbol{k}\cdot\boldsymbol{r}_i-\boldsymbol{k'}\cdot\boldsymbol{r}_j)}, \tag{D.3}$$

where the $\tilde{\delta}$-function denotes the fact that the two wavevectors are equivalent only up to a superlattice reciprocal lattice vector $\boldsymbol{Q}$ because $\boldsymbol{Q}\cdot\boldsymbol{R} = 2\pi\mathbb{Z}$ in the phase factor. More precisely, we have

$$\tilde{\delta}_{\boldsymbol{k},\boldsymbol{q}} = \sum_{s=1}^{L} \delta_{\boldsymbol{k},\boldsymbol{q}+\boldsymbol{Q}_s}, \tag{D.4}$$

where $\boldsymbol{Q}_s$ with $s = 1,...,L$ are the L inequivalent wave vectors in the reciprocal lattice of the original lattice (see the 1d case shown in Fig. D.1). Then we can perform the $\boldsymbol{q}$-summation in Eq. (D.3) to have,

$$\begin{aligned} G(\boldsymbol{k},\boldsymbol{k'}) &= \frac{1}{L} \sum_{i,j} \sum_{s,s'} G(\boldsymbol{k}-\boldsymbol{Q}_s)_{ij} \delta_{\boldsymbol{k'}-\boldsymbol{k},\boldsymbol{Q}_s-\boldsymbol{Q}_{s'}} e^{i(\boldsymbol{k}\cdot\boldsymbol{r}_i-\boldsymbol{k'}\cdot\boldsymbol{r}_j)} \\ &= \sum_{i,j} \sum_{\Delta\boldsymbol{Q}} G(\boldsymbol{k})_{ij} \delta_{\boldsymbol{k'}-\boldsymbol{k},\Delta\boldsymbol{Q}} e^{i(\boldsymbol{k}\cdot\boldsymbol{r}_i-\boldsymbol{k'}\cdot\boldsymbol{r}_j)}, \end{aligned} \tag{D.5}$$

where we have used the fact that $G(\boldsymbol{q})_{ij}$ is invariant under the shift by a superlattice reciprocal lattice vector $\boldsymbol{Q}_s$.

The translation invariant approximation for the Green's function on the original lattice is

- Original reciprocal space
- Superlattice reciprocal space

Figure D.1. Reciprocal lattice in 1d for a 4-site cluster. K labels the reciprocal lattice vector for the original lattice and Q labels the reciprocal lattice vector for the superlattice. More precisely, $K_s = \frac{2\pi}{a}s$ and $Q_s = \frac{2\pi}{La}s$, where a is the lattice constant of the original lattice, $L = 4$ here and $s \in \mathbb{Z}$.

obtained when $\Delta \boldsymbol{Q} = 0$, i.e. $\boldsymbol{k} = \boldsymbol{k}'$. Therefore, the Green's function becomes,

$$G(\boldsymbol{k}) = \sum_{i,j} G(\boldsymbol{k})_{ij} e^{i\boldsymbol{k}\cdot(\boldsymbol{r}_i - \boldsymbol{r}_j)}. \tag{D.6}$$

Now we just need to calculate $G_{i,j}(\boldsymbol{k})$ using cluster perturbation. The idea is to treat hopping between clusters as perturbation when consider strong on-site interactions. In particular,

$$\hat{H} = \hat{H}_0 + \hat{V}, \tag{D.7}$$

where $\hat{H}_0$ contains intra-cluster terms and $\hat{V}$ contains inter-cluster hopping. Considering nearest-neighbor hopping between the square clusters used in the main text. The cluster construction is reproduced in Fig. D.2 with the 4 sites in each cluster labeled by $1, 2, 3, 4$. The hopping matrix is given by (setting lattice constant $a = 1$)

$$
\begin{aligned}
V_{i,j}^{\boldsymbol{R},\boldsymbol{R}'} = & -t\delta_{\boldsymbol{R},\boldsymbol{R}'-2\hat{x}}(\delta_{i,2}\delta_{j,1} + \delta_{i,3}\delta_{j,4}) \\
& -t\delta_{\boldsymbol{R},\boldsymbol{R}'+2\hat{x}}(\delta_{i,1}\delta_{j,2} + \delta_{i,4}\delta_{j,3}) \\
& -t\delta_{\boldsymbol{R},\boldsymbol{R}'-2\hat{y}}(\delta_{i,1}\delta_{j,4} + \delta_{i,2}\delta_{j,3}) \\
& -t\delta_{\boldsymbol{R},\boldsymbol{R}'+2\hat{y}}(\delta_{i,3}\delta_{j,2} + \delta_{i,4}\delta_{j,1})
\end{aligned}
\tag{D.8}
$$
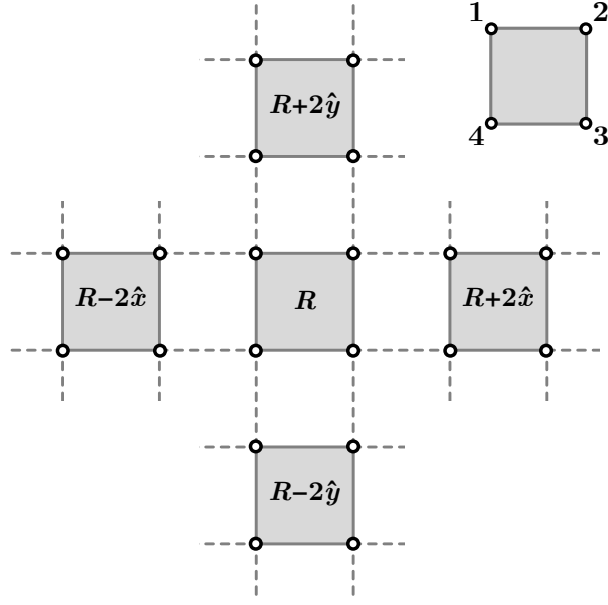
Figure D.2. Cluster diagram showing the hopping between neighboring clusters (dashed line). The four sites inside each cluster are numbered as shown.

Fourier transforming $V_{i,j}^{R,R'}$ into the superlattice reciprocal space, we have

$$
\begin{aligned}
V_{i,j}(\boldsymbol{q}) &= -t e^{i2q_x}(\delta_{i,2}\delta_{j,1} + \delta_{i,3}\delta_{j,4}) \\
&\quad - t e^{-i2q_x}(\delta_{i,1}\delta_{j,2} + \delta_{i,4}\delta_{j,3}) \\
&\quad - t e^{i2q_y}(\delta_{i,1}\delta_{j,4} + \delta_{i,2}\delta_{j,3}) \\
&\quad - t e^{-i2q_y}(\delta_{i,3}\delta_{j,2} + \delta_{i,4}\delta_{j,1}) \\
&= -t \begin{pmatrix} 0 & e^{-i2\boldsymbol{q}_x} & 0 & e^{i2\boldsymbol{q}_y} \\ e^{i2\boldsymbol{q}_x} & 0 & e^{i2\boldsymbol{q}_y} & 0 \\ 0 & e^{-i2\boldsymbol{q}_y} & 0 & e^{i2\boldsymbol{q}_x} \\ e^{-i2\boldsymbol{q}_y} & 0 & e^{-i2\boldsymbol{q}_x} & 0 \end{pmatrix}_{i,j},
\end{aligned}
\tag{D.9}
$$

which is the form presented in Eq. (4.17) in the main text. Then the interacting Green's function

is given by

$$
\begin{aligned}
\hat{G}(\boldsymbol{q}) &= \frac{1}{\omega - \hat{H}} = \frac{1}{\omega - \hat{H}_0 - \hat{V}(\boldsymbol{q})} \\
&= \frac{\hat{G}_0}{1 - \hat{V}(\boldsymbol{q})\hat{G}_0},
\end{aligned}
\tag{D.10}
$$

where $\hat{G}_0 \equiv (\omega - \hat{H}_0)^{-1}$ is the intra-cluster Green's function that can be easily obtained by exact diagonalization as long as the cluster size is not too big. The obtained $G(\boldsymbol{q})_{ij}$ can now be plugged into Eq. (D.6) to calculate the CPT Green's function for the interacting system.

Appendix E

Appendix to Chapter. 5

E.1 Details on solving the algebra object in $\mathrm{Rep}(H_8)$

The fusion and splitting junctions satisfy the conditions in Eq. (5.34). The first two conditions can fix the form of the junctions and the last one fixes the normalization. From the first condition in Eq. (5.34), we have

$$\psi(g,h)\psi(gh,k) = \psi(g,hk)\psi(h,k), \tag{E.1}$$

$$L(h)L(g) = \psi(g,h)L(gh), \quad R(g)R(h) = \psi(g,h)R(gh), \tag{E.2}$$

$$L(g)R(h) = \chi(g,h)R(h)L(g), \tag{E.3}$$

$$W(gh)R(h)^{\mathsf{T}} = \psi(g,h)W(g), \quad L(g)W(gh) = \psi(g,h)W(h), \tag{E.4}$$

$$R(g)W(h) = \chi(g,h)W(h)L(g)^{\mathsf{T}}, \tag{E.5}$$

$$[W(g)]_{ab}[L(g)]_{cd} = \sum_h \frac{1}{2}\chi(g,h)^{-1}[W(h)]_{bc}[R(h)]_{ad}, \tag{E.6}$$

where $L(g), R(g), W(g)$ are 2×2 matrices and their multiplication is matrix multiplication. χ is the bicharacter in $\mathrm{Rep}(H_8)$. Eq. (E.1) states that $\psi(g,h)$ is a 2-cocycle of $\mathbb{Z}_2 \times \mathbb{Z}_2$, and is classified by $H^2(\mathbb{Z}_2 \times \mathbb{Z}_2, U(1)) = \mathbb{Z}_2$. Only the non-trivial one will solve the following equations. Eq. (E.2) states $L(g), R(g)$ furnish the projective representation of $\mathbb{Z}_2 \times \mathbb{Z}_2$, and $W(g)$ can be solved accordingly. The splitting junctions can be solved similarly. The junctions are normalized such that the last condition in Eq. (5.34) is satisfied.

E.2 More on Virasoro primaries of Ising^2

Here we work out the spectrum of $c = 1$ Virasoro primary operators at the Ising^2 point. To do so, we begin from the $R = \sqrt{2}$ point on the circle branch. The conformal weights of the vertex operators $V_{n,w}$ are

$$h_{n,w} = \frac{1}{4}\left(\frac{n}{\sqrt{2}} + w\sqrt{2}\right)^2 = \frac{1}{8}(n+2w)^2 \,,$$
$$\bar{h}_{n,w} = \frac{1}{4}\left(\frac{n}{\sqrt{2}} - w\sqrt{2}\right)^2 = \frac{1}{8}(n-2w)^2 \,. \tag{E.7}$$

When $n = 2w \neq 0$, there are null states since $\bar{h}_{2w,w} = 0$, and the Verma module corresponding to the vertex operator $V_{2w,w}$ breaks into infinitely many irreducible $c = 1$ Virasoro modules. We denote the corresponding $c = 1$ Virasoro primaries as $A_{w,m}$, where $w \in \mathbb{Z} \setminus \{0\}$ and $m \in \mathbb{Z}_{\geq 0}$. The conformal weights of $A_{w,m}$ are $(h, \bar{h}) = (2w^2, m^2)$. Similarly, when $n = -2w \neq 0$, we have null states since $h_{-2w,w} = 0$, and the Verma module decomposes into infinitely many irreducible $c = 1$ Virasoro modules. The corresponding Virasoro primaries are denoted as $B_{w,\ell}$ with $w \in \mathbb{Z} \setminus \{0\}$ and $\ell \in \mathbb{Z}_{\geq 0}$, whose conformal weights are $(h, \bar{h}) = (\ell^2, 2w^2)$. Finally, the $(n, w) = (0,0)$ module decomposes into the irreducible $c = 1$ Virasoro modules with the primary operators denoted as $C_{\ell,m}$ with $\ell, m \in \mathbb{Z}_{\geq 0}$, whose conformal weights are $(h, \bar{h}) = (\ell^2, m^2)$.

To summarize, the $c = 1$ Virasoro primaries at $R = \sqrt{2}$ on the circle branch are

$$\begin{aligned}
V_{n,w}\,, &\quad n, w \in \mathbb{Z}\,, n \neq \pm 2w\,, &\quad (h,\bar{h}) = \left(\tfrac{1}{8}(n+2w)^2, \tfrac{1}{8}(n-2w)^2\right), \\
A_{w,m}\,, &\quad w \in \mathbb{Z} \setminus \{0\}\,, m \in \mathbb{Z}_{\geq 0}\,, &\quad (h,\bar{h}) = (2w^2, m^2), \\
B_{w,\ell}\,, &\quad w \in \mathbb{Z} \setminus \{0\}\,, \ell \in \mathbb{Z}_{\geq 0}\,, &\quad (h,\bar{h}) = (\ell^2, 2w^2), \\
C_{\ell,m}\,, &\quad \ell, m \in \mathbb{Z}_{\geq 0}\,, &\quad (h,\bar{h}) = (\ell^2, m^2).
\end{aligned} \tag{E.8}$$

Correspondingly, the torus partition function can be decomposed into the $c = 1$ Virasoro

characters:

$$
\begin{aligned}
Z^{circ}_{R=\sqrt{2}}(\tau) &= \frac{1}{|\eta(\tau)|^2} \sum_{n,w\in\mathbb{Z}} q^{\frac{1}{8}(n+2w)^2} \bar{q}^{\frac{1}{8}(n-2w)^2} \\
&= \frac{1}{|\eta(\tau)|^2} \sum_{\substack{n,w\in\mathbb{Z} \\ n\neq\pm 2w}} q^{\frac{1}{8}(n+2w)^2} \bar{q}^{\frac{1}{8}(n-2w)^2} + \frac{1}{|\eta(\tau)|^2} \sum_{\substack{w\in\mathbb{Z}\setminus\{0\} \\ m\in\mathbb{Z}_{\geq 0}}} q^{2w^2}\left(\bar{q}^{m^2} - \bar{q}^{(m+1)^2}\right) \\
&\quad + \frac{1}{|\eta(\tau)|^2} \sum_{\substack{w\in\mathbb{Z}\setminus\{0\} \\ \ell\in\mathbb{Z}_{\geq 0}}} \left(q^{\ell^2} - q^{(\ell+1)^2}\right) \bar{q}^{2w^2} \\
&\quad + \frac{1}{|\eta(\tau)|^2} \sum_{\ell,m\in\mathbb{Z}_{\geq 0}} \left(q^{\ell^2} - q^{(\ell+1)^2}\right)\left(\bar{q}^{m^2} - \bar{q}^{(m+1)^2}\right).
\end{aligned}
\tag{E.9}
$$

The $\mathbb{Z}_2^C$ charge conjugation symmetry acts on the Virasoro primaries (E.8) as

$$
\begin{aligned}
\mathbb{Z}_2^C: \quad V_{n,w} &\to V_{-n,-w}, \\
A_{w,m} &\to (-1)^m A_{-w,m}, \\
B_{w,\ell} &\to (-1)^\ell B_{-w,\ell}, \\
C_{\ell,m} &\to (-1)^{\ell+m} C_{\ell,m}.
\end{aligned}
\tag{E.10}
$$

The $\mathbb{Z}_2^C$ twisted sector spectrum can be read off from the twisted partition function (which actually does not depend on the value of R)

$$
Z^{circ}_{R=\sqrt{2}}[\eta,\mathbb{1},\eta](\tau) = \frac{1}{|\eta(\tau)|^2} \sum_{\ell,m\in\mathbb{Z}_{\geq 0}} 2q^{\frac{1}{4}(\ell+\frac{1}{2})^2} \bar{q}^{\frac{1}{4}(m+\frac{1}{2})^2}.
\tag{E.11}
$$

We see that the twisted sector operators are doubly-degenerate, which is a consequence of the fact that the $\mathbb{Z}_2^m \times \mathbb{Z}_2^w$ subgroup of the momentum and winding symmetries acts projectively on the $\mathbb{Z}_2^C$ twisted sector due to a mixed anomaly between the three symmetries. We denote the Virasoro primaries in the $\mathbb{Z}_2^C$ twisted sector as

$$
D^{(i)}_{\ell,m}, \quad \ell,m \in \mathbb{Z}_{\geq 0}, i = 1,2, \quad (h,\bar{h}) = (\frac{1}{4}(\ell+\frac{1}{2})^2, \frac{1}{4}(m+\frac{1}{2})^2).
\tag{E.12}
$$

The $\mathbb{Z}_2^C$ charge of a twisted sector operator is given by $2(h - \bar{h}) = \frac{1}{2}(\ell - m)(\ell + m + 1)$. Namely,

$$\mathbb{Z}_2^C: \quad D_{\ell,m}^{(i)} \to (-1)^{\frac{1}{2}(\ell-m)(\ell+m+1)} D_{\ell,m}^{(i)}. \tag{E.13}$$

We are ready to write down all the $c = 1$ Virasoro primaries at the Ising^2 point, namely at $R = \sqrt{2}$ on the orbifold branch. These are the operators on the circle branch which are $\mathbb{Z}_2^C$ invariant:

$$V_{n,w}^+ \equiv \frac{1}{\sqrt{2}}(V_{n,w} + V_{-n,-w}), \quad n, w \in \mathbb{Z}, n \neq \pm 2w, \quad (h, \bar{h}) = (\frac{1}{8}(n + 2w)^2, \frac{1}{8}(n - 2w)^2),$$

$$A_{w,m}^+ \equiv \frac{1}{\sqrt{2}}(A_{w,m} + (-1)^m A_{-w,m}), \quad w \in \mathbb{Z}_{>0}, m \in \mathbb{Z}_{\geq 0}, \quad (h, \bar{h}) = (2w^2, m^2),$$

$$B_{w,\ell}^+ \equiv \frac{1}{\sqrt{2}}(B_{w,\ell} + (-1)^\ell B_{-w,\ell}), \quad w \in \mathbb{Z}_{>0}, \ell \in \mathbb{Z}_{\geq 0}, \quad (h, \bar{h}) = (\ell^2, 2w^2),$$

$$C_{\ell,m}, \quad \ell, m \in \mathbb{Z}_{\geq 0}, \ell + m \in 2\mathbb{Z}, \quad (h, \bar{h}) = (\ell^2, m^2),$$

$$D_{\ell,m}^{(i)}, \quad \ell, m \in \mathbb{Z}_{\geq 0}, i = 1, 2, \frac{1}{2}(\ell - m)(\ell + m + 1) \in 2\mathbb{Z}, \quad (h, \bar{h}) = (\frac{1}{4}(\ell + \frac{1}{2})^2, \frac{1}{4}(m + \frac{1}{2})^2),$$

$$\tag{E.14}$$

modulo the identification $V_{n,w}^+ = V_{-n,-w}^+$.

E.3 Calculation details for $\underline{\mathscr{E}}_{\mathbb{Z}_2}^{(i,\kappa_{\mathscr{D}},\varepsilon_{\mathscr{D}})}\mathsf{Rep}(H_8)$

We provide some details on the pentagon equations for $\underline{\mathscr{E}}_{\mathbb{Z}_2}^{(i,\kappa_{\mathscr{D}},\varepsilon_{\mathscr{D}})}\mathsf{Rep}(H_8)$ and lasso actions in the defect Hilbert space of $\mathscr{D}$.

E.3.1 Gauge fixing

The fusion vertices generally can be transformed by unitary matrices, and the F-symbols related by these transformations lead to equivalent fusion categories. For the purpose of classifying inequivalent fusion categories, this introduces tremendous redundancies when solving the pentagon equations. We will follow the physics convention to refer these redundancies as gauge redundancies in this context.

The finite number of inequivalent solutions can be obtained by gauge fixing. To solve the pentagon equations for $\underline{\mathscr{E}}_{\mathbb{Z}_2}^{(i,\kappa_{\mathscr{D}},\varepsilon_{\mathscr{D}})}\mathsf{Rep}(H_8)$, the fusion vertices involving the new defect $\mathscr{D}$ need to be gauge fixed. In particular, we set F-symbols with at least one of $a,b,c = \mathbb{1}$ to be 1, and also fix the expressions for

$$[F_{\mathscr{D}}^{ab\mathscr{D}}]_{(ab,1,1),(\mathscr{D},1,1)}, \quad [F_{\mathscr{D}}^{a\mathscr{N}\mathscr{D}}]_{(\mathscr{N},1,\mu),(\mathscr{D},\nu,1)}, \quad [F_{\mathscr{D}}^{\mathscr{D}ab}]_{(\mathscr{D},1,1),(ab,1,1)}, \quad [F_{\mathscr{D}}^{\mathscr{D}\mathscr{N}a}]_{(\mathscr{D},\mu,1),(\mathscr{N},1,\nu)},$$

$$[F_b^{\mathscr{D}\mathscr{D}a}]_{(ba^{-1},1,1),(\mathscr{D},1,1)}, \quad [F_{\mathscr{N}}^{\mathscr{D}\mathscr{D}a}]_{(\mathscr{N},\mu,1),(\mathscr{D},1,\nu)}.$$

$$(E.15)$$

There will be residual gauge transformations which will further eliminate gauge-equivalent solutions. The explicit expressions for the choices and gauge-inequivalent solutions are listed in Tab. 5.3 and Tab. 5.4.

E.3.2 General lasso actions in the defect Hilbert space of $\mathscr{D}$

In this section, we derive the composition of general lasso actions in the defect Hilbert space of $\mathscr{D}$. We define the notation,

$$\equiv \mathscr{U}[a,b][\mu,\nu] \equiv \qquad , \qquad (E.16)$$

where $a, b \in \mathscr{E}_{\mathbb{Z}_2}^{\circ(i,\kappa_{\mathscr{D}},\varepsilon_{\mathscr{D}})}\mathsf{Rep}(H_8)$. We only keep the start and end points of the a line for simplicity. The multiplication is given by,

$$= \sum_{f',\sigma',\mu'} F^{cda}_{b,(\mathscr{D},\sigma,\mu)(f',\sigma',\mu')}$$

$$= \sum_{\substack{f',\mu',\nu' \\ f'',\mu'',\nu'' \\ e,\alpha,\beta}} F^{cda}_{b,(\mathscr{D},\sigma,\mu)(f',\sigma',\mu')} F^{\mathscr{D}ca}_{f',(d,\rho,\mu'),(f'',\mu'',\nu'')} (F^{acf'}_{\mathscr{D}})^{-1}_{(b,\nu',\nu)(e,\alpha,\beta)}$$

$$\qquad\qquad\qquad\qquad\qquad\qquad\qquad\qquad\qquad\qquad\qquad\qquad\qquad\qquad (E.17)$$

$$= \sum_{\substack{f',\mu',\nu',\nu'' \\ e,\alpha,\beta}} \sqrt{\frac{d_a d_c}{d_e}} F^{cda}_{b,(\mathscr{D},\sigma,\mu)(f',\sigma',\mu')} F^{\mathscr{D}ca}_{f',(d,\rho,\mu'),(e,\alpha,\nu'')} (F^{acf'}_{\mathscr{D}})^{-1}_{(b,\nu',\nu)(e,\alpha,\beta)} \ $$

$$\cdot$$

Bibliography

[1] David Aasen, Parsa Bonderson, and Christina Knapp. Characterization and Classification of Fermionic Symmetry Enriched Topological Phases. *arXiv e-prints*, page arXiv:2109.10911, September 2021.

[2] David Aasen, Paul Fendley, and Roger S. K. Mong. Topological Defects on the Lattice: Dualities and Degeneracies. 8 2020.

[3] David Aasen, Roger S. K. Mong, and Paul Fendley. Topological defects on the lattice: I. The Ising model. *Journal of Physics A Mathematical General*, 49(35):354001, September 2016.

[4] AG Abanov and Paul B Wiegmann. Theta-terms in nonlinear sigma-models. *Nuclear Physics B*, 570(3):685–698, 2000.

[5] Stephen L. Adler. Axial-vector vertex in spinor electrodynamics. *Phys. Rev.*, 177:2426–2438, Jan 1969.

[6] Tommi Alanne and Simone Blasi. Abelian gauge-yukawa β-functions at large N_f. *Phys. Rev. D*, 98:116004, Dec 2018.

[7] B. L. Altshuler, A. V. Chubukov, A. Dashevskii, A. M. Finkel'stein, and D. K. Morr. Luttinger theorem for a spin-density-wave state. *EPL (Europhysics Letters)*, 41(4):401–406, February 1998.

[8] P. W. Anderson. Plasmons, Gauge Invariance, and Mass. *Physical Review*, 130(1):439–442, April 1963.

[9] Philip W Anderson. More is different: Broken symmetry and the nature of the hierarchical structure of science. *Science*, 177(4047):393–396, 1972.

[10] Andrea Antinucci, Francesco Benini, Christian Copetti, Giovanni Galati, and Giovanni Rizi. Anomalies of non-invertible self-duality symmetries: fractionalization and gauging. *arXiv e-prints*, page arXiv:2308.11707, August 2023.

[11] Julius Ashkin and Edward Teller. Statistics of two-dimensional lattices with four components. *Physical Review*, 64(5-6):178, 1943.

[12] V. Ayyar. Search for a continuum limit of the PMS phase. *ArXiv e-prints*, November 2016.

[13] V. Ayyar and S. Chandrasekharan. Fermion masses through four-fermion condensates. *Journal of High Energy Physics*, 10:58, October 2016.

[14] V. Ayyar and S. Chandrasekharan. Origin of fermion masses without spontaneous symmetry breaking. *Phys. Rev. D*, 93(8):081701, April 2016.

[15] Venkitesh Ayyar and Shailesh Chandrasekharan. Massive fermions without fermion bilinear condensates. *Phys. Rev. D*, 91(6):065035, March 2015.

[16] Venkitesh Ayyar and Shailesh Chandrasekharan. Generating a nonperturbative mass gap using Feynman diagrams in an asymptotically free theory. *Phys. Rev. D*, 96(11):114506, December 2017.

[17] C. Bachas and I. Brunner. Fusion of conformal interfaces. *JHEP*, 02:085, 2008.

[18] Matthias Bal, Dominic J. Williamson, Robijn Vanhove, Nick Bultinck, Jutho Haegeman, and Frank Verstraete. Mapping topological to conformal field theories through strange correlators. *arXiv e-prints*, page arXiv:1801.05959, January 2018.

[19] T. Banks and A. Dabholkar. Decoupling a fermion whose mass comes from a Yukawa coupling: Nonperturbative considerations. *Phys. Rev. D*, 46(9):4016–4028, November 1992.

[20] Tom Banks and Nathan Seiberg. Symmetries and strings in field theory and gravity. *Physical Review D*, 83(8):084019, 2011.

[21] M. Barkeshli, N. Y. Yao, and C. R. Laumann. Continuous preparation of a fractional chern insulator. *Phys. Rev. Lett.*, 115(2):026802, 2015.

[22] Maissam Barkeshli, Parsa Bonderson, Meng Cheng, and Zhenghan Wang. Symmetry Fractionalization, Defects, and Gauging of Topological Phases. *Phys. Rev. B*, 100(11):115147, 2019.

[23] Maissam Barkeshli, Yu-An Chen, Po-Shen Hsin, and Naren Manjunath. Classification of (2 +1)D invertible fermionic topological phases with symmetry. *Physical Review B*, 105(23):235143, June 2022.

[24] Maissam Barkeshli and John McGreevy. Continuous transition between fractional

quantum hall and superfluid states. *Phys. Rev. B*, 89(23):235116, 2014.

[25] Alexander Barvels, Simon Lentner, and Christoph Schweigert. Partially dualized Hopf algebras have equivalent Yetter-Drinfel'd modules. *arXiv e-prints*, page arXiv:1402.2214, February 2014.

[26] Vladimir Bashmakov, Michele Del Zotto, and Azeem Hasan. Four-manifolds and Symmetry Categories of 2d CFTs. 5 2023.

[27] Melanie Becker, Yaniel Cabrera, and Daniel Robbins. Conformal interfaces between free boson orbifold theories. *JHEP*, 09:148, 2017.

[28] J. S. Bell and R. Jackiw. A PCAC puzzle: $\pi^0 \to \gamma\gamma$ in the σ-model. *Il Nuovo Cimento A (1965-1970)*, 60(1):47–61, 1969.

[29] Francesco Benini, Po-Shen Hsin, and Nathan Seiberg. Comments on global symmetries, anomalies, and duality in (2+ 1) d. *Journal of High Energy Physics*, 2017(4):135, 2017.

[30] Y. BenTov. Fermion masses without symmetry breaking in two spacetime dimensions. *Journal of High Energy Physics*, 7:34, July 2015.

[31] Y. BenTov and A. Zee. Origin of families and SO(18) grand unification. *Phys. Rev. D*, 93(6):065036, March 2016.

[32] V. L. Berezinskiĭ. Destruction of Long-range Order in One-dimensional and Two-dimensional Systems having a Continuous Symmetry Group I. Classical Systems. *Soviet Journal of Experimental and Theoretical Physics*, 32:493, January 1971.

[33] V. L. Berezinskiĭ. Destruction of Long-range Order in One-dimensional and Two-dimensional Systems Possessing a Continuous Symmetry Group. II. Quantum Systems. *Soviet Journal of Experimental and Theoretical Physics*, 34:610, January 1972.

[34] E. Berg, E. Fradkin, and S. A. Kivelson. Charge-4e superconductivity from pair-density-wave order in certain high-temperature superconductors. *Nature Physics*, 5:830–833, November 2009.

[35] E. Berg, E. Fradkin, and S. A. Kivelson. Theory of the striped superconductor. *Physical Review B*, 79(6):064515, February 2009.

[36] Lakshya Bhardwaj, Lea E. Bottini, Ludovic Fraser-Taliente, Liam Gladden, Dewi S. W. Gould, Arthur Platschorre, and Hannah Tillim. Lectures on Generalized Symmetries. 7 2023.

[37] Lakshya Bhardwaj, Lea E. Bottini, Daniel Pajer, and Sakura Schafer-Nameki. Categorical

Landau Paradigm for Gapped Phases. 10 2023.

[38] Lakshya Bhardwaj, Lea E. Bottini, Daniel Pajer, and Sakura Schafer-Nameki. Gapped Phases with Non-Invertible Symmetries: (1+1)d. 10 2023.

[39] Lakshya Bhardwaj and Yuji Tachikawa. On finite symmetries and their gauging in two dimensions. *JHEP*, 03:189, 2018.

[40] Tanmoy Bhattacharya, Matthew R. Martin, and Erich Poppitz. Chiral lattice gauge theories from warped domain walls and Ginsparg-Wilson fermions. *Phys. Rev. D*, 74(8):085028, October 2006.

[41] Zhen Bi, Alex Rasmussen, Kevin Slagle, and Cenke Xu. Classification and description of bosonic symmetry protected topological phases with semiclassical nonlinear sigma models. *Physical Review B*, 91(13):134404, 2015.

[42] Zhen Bi and T. Senthil. Adventure in Topological Phase Transitions in 3+1 -D: Non-Abelian Deconfined Quantum Criticalities and a Possible Duality. *Phys. Rev. X*, 9(2):021034, 2019.

[43] Zhen Bi, Kevin Slagle, and Cenke Xu. Self-dual quantum electrodynamics on the boundary of 4d bosonic symmetry protected topological states. *arXiv preprint arXiv:1504.04373*, 2015.

[44] R. Blankenbecler, D. J. Scalapino, and R. L. Sugar. Monte carlo calculations of coupled boson-fermion systems. i. *Phys. Rev. D*, 24:2278–2286, Oct 1981.

[45] M. Blume, V. J. Emery, and Robert B. Griffiths. Ising model for the λ transition and phase separation in he^3-he^4 mixtures. *Phys. Rev. A*, 4:1071–1077, Sep 1971.

[46] Luis J Boya, ECG Sudarshan, and Todd Tilma. Volumes of compact manifolds. *Reports on Mathematical Physics*, 52(3):401–422, 2003.

[47] Rufus Boyack, Ahmed Rayyan, and Joseph Maciejko. Deconfined criticality in the qed 3 gross-neveu-yukawa model: The 1/n expansion revisited. *Phys. Rev. B*, 99(19):195135, 2019.

[48] Tomáš Brauner and Helena Kolešová. Gauged wess-zumino terms for a general coset space. *Nuclear Physics B*, 945:114676, 2019.

[49] T. Daniel Brennan and Sungwoo Hong. Introduction to Generalized Global Symmetries in QFT and Particle Physics. 6 2023.

[50] Ilka Brunner, Nils Carqueville, and Daniel Plencner. Discrete torsion defects. *Commun.*

Math. Phys., 337(1):429–453, 2015.

[51] Matthew Buican and Andrey Gromov. Anyonic Chains, Topological Defects, and Conformal Field Theory. *Communications in Mathematical Physics*, 356(3):1017–1056, December 2017.

[52] Daniel Bulmash, Pavan Hosur, Shou-Cheng Zhang, and Xiao-Liang Qi. Unified Topological Response Theory For Gapped and Gapless Free Fermions. *Physical Review X*, 5(2):021018, April 2015.

[53] Nick Bultinck and Meng Cheng. Filling constraints on fermionic topological order in zero magnetic field. *Physical Review B*, 98(16):161119, October 2018.

[54] Ivan M. Burbano, Justin Kulp, and Jonas Neuser. Duality defects in E_8. *JHEP*, 10:186, 2022.

[55] N. Butt and S. Catterall. Four fermion condensates in SU(2) Yang-Mills-Higgs theory on a lattice. In *The 36th Annual International Symposium on Lattice Field Theory. 22-28 July*, page 294, July 2018.

[56] Nouman Butt, Simon Catterall, Arnab Pradhan, and Goksu Can Toga. Anomalies and symmetric mass generation for Kähler-Dirac fermions. *Phys. Rev. D*, 104(9):094504, November 2021.

[57] Nouman Butt, Simon Catterall, and David Schaich. SO(4) invariant Higgs-Yukawa model with reduced staggered fermions. *Phys. Rev. D*, 98(11):114514, December 2018.

[58] Nouman Butt, Simon Catterall, and Goksu Can Toga. Symmetric Mass Generation in Lattice Gauge Theory. *arXiv e-prints*, page arXiv:2111.01001, November 2021.

[59] Curtis G Callan Jr, Sidney Coleman, Julius Wess, and Bruno Zumino. Structure of phenomenological lagrangians. ii. *Physical Review*, 177(5):2247, 1969.

[60] Nils Carqueville and Ingo Runkel. Orbifold completion of defect bicategories. *Quantum Topol.*, 7:203, 2016.

[61] S. Catterall. Fermion mass without symmetry breaking. *Journal of High Energy Physics*, 1:121, January 2016.

[62] S. Catterall and D. Schaich. Novel phases in strongly coupled four-fermion theories. *ArXiv e-prints*, September 2016.

[63] Simon Catterall. Chiral lattice fermions from staggered fields. *Phys. Rev. D*, 104(1):014503, July 2021.

[64] Simon Catterall. 't Hooft anomalies for staggered fermions. *Phys. Rev. D*, 107(1):014501, January 2023.

[65] Simon Catterall and Nouman Butt. Topology and strong four fermion interactions in four dimensions. *Phys. Rev. D*, 97(9):094502, May 2018.

[66] Simon Catterall, Nouman Butt, and David Schaich. Exotic Phases of a Higgs-Yukawa Model with Reduced Staggered Fermions. *arXiv e-prints*, page arXiv:2002.00034, January 2020.

[67] Simon Catterall and Arnab Pradhan. Induced topological gravity and anomaly inflow from Kähler-Dirac fermions in odd dimensions. *Phys. Rev. D*, 106(1):014509, July 2022.

[68] Chi-Ming Chang, Jin Chen, and Fengjun Xu. Topological Defect Lines in Two Dimensional Fermionic CFTs. 8 2022.

[69] Chi-Ming Chang and Ying-Hsuan Lin. Lorentzian dynamics and factorization beyond rationality. *JHEP*, 10:125, 2021.

[70] Chi-Ming Chang, Ying-Hsuan Lin, Shu-Heng Shao, Yifan Wang, and Xi Yin. Topological defect lines and renormalization group flows in two dimensions. *Journal of High Energy Physics*, 2019(1):26, January 2019.

[71] K. A. Chao, J. Spałek, and A. M. Oleś. Canonical perturbation expansion of the hubbard model. *Phys. Rev. B*, 18:3453–3464, Oct 1978.

[72] Arkya Chatterjee and Xiao-Gang Wen. Holographic theory for the emergence and the symmetry protection of gaplessness and for continuous phase transitions. *arXiv preprint arXiv:2205.06244*, 2022.

[73] Chen Chen, Joel Giedt, and Erich Poppitz. On the decoupling of mirror fermions. *Journal of High Energy Physics*, 2013:131, April 2013.

[74] Chuang Chen, Xiao Yan Xu, Yang Qi, and Zi Yang Meng. Metal to Orthogonal Metal Transition. *Chinese Physics Letters*, 37(4):047103, April 2020.

[75] Jin Chen, Babak Haghighat, and Qing-Rui Wang. Para-fusion Category and Topological Defect Lines in $\mathbb{Z}_N$-parafermionic CFTs. 9 2023.

[76] Wei-Qiang Chen, Chao-Ming Jian, Liang Kong, Yi-Zhuang You, and Hao Zheng. Topological phase transition on the edge of two-dimensional Z_2 topological order. *Physical Review B*, 102(4):045139, July 2020.

[77] Xie Chen, Arpit Dua, Po-Shen Hsin, Chao-Ming Jian, Wilbur Shirley, and Cenke Xu.

Loops in 4+ 1d topological phases. *arXiv preprint arXiv:2112.02137*, 2021.

[78] Yu-An Chen and Po-Shen Hsin. Exactly solvable lattice hamiltonians and gravitational anomalies. *arXiv preprint arXiv:2110.14644*, 2021.

[79] Meng Cheng, Zhen Bi, Yi-Zhuang You, and Zheng-Cheng Gu. Classification of Symmetry-Protected Phases for Interacting Fermions in Two Dimensions. *arXiv e-prints*, page arXiv:1501.01313, January 2015.

[80] Meng Cheng and Nathan Seiberg. Lieb-Schultz-Mattis, Luttinger, and 't Hooft - anomaly matching in lattice systems. *SciPost Physics*, 15(2):051, August 2023.

[81] Meng Cheng and Cenke Xu. Series of (2+1)-dimensional stable self-dual interacting conformal field theories. *Physical Review B*, 94(21):214415, December 2016.

[82] Meng Cheng, Michael Zaletel, Maissam Barkeshli, Ashvin Vishwanath, and Parsa Bonderson. Translational Symmetry and Microscopic Constraints on Symmetry-Enriched Topological Phases: A View from the Surface. *Physical Review X*, 6(4):041068, December 2016.

[83] Shai M. Chester and Ning Su. Bootstrapping Deconfined Quantum Tricriticality. *Phys. Rev. Lett.*, 132(11):111601, March 2024.

[84] Gennady Y. Chitov and David Sénéchal. Renormalization-group study of interacting electrons. *Physical Review B*, 52(18):13487–13496, November 1995.

[85] Gennady Y. Chitov and David Sénéchal. Fermi liquid as a renormalization-group fixed point: The role of interference in the Landau channel. *Physical Review B*, 57(3):1444–1456, January 1998.

[86] Gil Young Cho, Chang-Tse Hsieh, and Shinsei Ryu. Anomaly manifestation of Lieb-Schultz-Mattis theorem and topological phases. *Physical Review B*, 96(19):195105, November 2017.

[87] Yichul Choi, Clay Cordova, Po-Shen Hsin, Ho Tat Lam, and Shu-Heng Shao. Non-invertible Condensation, Duality, and Triality Defects in 3+1 Dimensions. 4 2022.

[88] Yichul Choi, Clay Córdova, Po-Shen Hsin, Ho Tat Lam, and Shu-Heng Shao. Noninvertible duality defects in 3 +1 dimensions. *Phys. Rev. D*, 105(12):125016, June 2022.

[89] Yichul Choi, Da-Chuan Lu, and Zhengdi Sun. Self-duality under gauging a non-invertible symmetry. *Journal of High Energy Physics*, 2024(1):142, January 2024.

[90] Yichul Choi, Brandon C. Rayhaun, Yaman Sanghavi, and Shu-Heng Shao. Comments on Boundaries, Anomalies, and Non-Invertible Symmetries. 5 2023.

[91] Chong-Sun Chu, Pei-Ming Ho, and Bruno Zumino. Non-abelian anomalies and effective actions for a homogeneous space g/h. *Nuclear Physics B*, 475(1-2):484–504, 1996.

[92] Stephen-wei Chung, Masafumi Fukuma, and Alfred Shapere. Structure of topological lattice field theories in three dimensions. *International Journal of Modern Physics A*, 9(08):1305–1360, 1994.

[93] TE Clark and ST Love. The chiral anomaly and goldstone-wilczek current in even dimensions. *Physics Letters B*, 158(3):234–238, 1985.

[94] Sidney Coleman. *Aspects of symmetry: selected Erice lectures*. Cambridge University Press, 1988.

[95] Sidney Coleman, Julius Wess, and Bruno Zumino. Structure of phenomenological lagrangians. i. *Physical Review*, 177(5):2239, 1969.

[96] Clay Cordova, Thomas T. Dumitrescu, Kenneth Intriligator, and Shu-Heng Shao. Snowmass White Paper: Generalized Symmetries in Quantum Field Theory and Beyond. In *2022 Snowmass Summer Study*, 5 2022.

[97] Clay Córdova, Daniel S. Freed, Ho Tat Lam, and Nathan Seiberg. Anomalies in the Space of Coupling Constants and Their Dynamical Applications I. *SciPost Phys.*, 8(1):001, 2020.

[98] Clay Córdova, Kantaro Ohmori, Shu-Heng Shao, and Fei Yan. Decorated $\mathbb{Z}_2$ symmetry defects and their time-reversal anomalies. *Phys. Rev. D*, 102(4):045019, 2020.

[99] Philippe Curty and Hans Beck. Thermodynamics and Phase Diagram of High Temperature Superconductors. *Phys. Rev. Lett.*, 91(25):257002, December 2003.

[100] Predrag Cvitanović. *Group theory: birdtracks, Lie's, and exceptional groups*. Princeton University Press, 2008.

[101] C. Dasgupta and B. I. Halperin. *Phys. Rev. Lett.*, 47(21):1556, 1981.

[102] Joe Davighi and Ben Gripaios. Homological classification of topological terms in sigma models on homogeneous spaces. *Journal of High Energy Physics*, 2018(9):1–41, 2018.

[103] Joe Davighi and Nakarin Lohitsiri. Anomaly interplay in U(2) gauge theories. *Journal of High Energy Physics*, 2020(5):98, May 2020.

[104] Joe Davighi and Nakarin Lohitsiri. The algebra of anomaly interplay. *SciPost Physics*, 10(3):074, March 2021.

[105] Luca Delacrétaz, Diego Hofman, and Grégoire Mathys. Superfluids as higher-form anomalies. *SciPost Physics*, 8(3):047, 2020.

[106] Luca V Delacretaz, Yi-Hsien Du, Umang Mehta, and Dam Thanh Son. Nonlinear bosonization of fermi surfaces: The method of coadjoint orbits. *arXiv preprint arXiv:2203.05004*, 2022.

[107] Michael DeMarco and Xiao-Gang Wen. A Novel Non-Perturbative Lattice Regularization of an Anomaly-Free $1 + 1d$ Chiral $SU(2)$ Gauge Theory. *arXiv e-prints*, page arXiv:1706.04648, June 2017.

[108] Nisheeta Desai and Ribhu K. Kaul. First-order phase transitions in the square-lattice easy-plane J-Q model. *Physical Review B*, 102(19):195135, November 2020.

[109] Dennis DeTurck and Herman Gluck. Linking integrals in the n-sphere. *arXiv preprint arXiv:0802.0320*, 2008.

[110] Eric D'Hoker. Invariant effective actions, cohomology of homogeneous spaces and anomalies. *Nuclear Physics B*, 451(3):725–748, 1995.

[111] Lorenzo Di Pietro, Davide Gaiotto, Edoardo Lauria, and Jingxiang Wu. 3d abelian gauge theories at the boundary. *Journal of High Energy Physics*, 2019(5):1–60, 2019.

[112] Oleksandr Diatlyk, Conghuan Luo, Yifan Wang, and Quinten Weller. Gauging Non-Invertible Symmetries: Topological Interfaces and Generalized Orbifold Groupoid in 2d QFT. 11 2023.

[113] Robbert Dijkgraaf, Cumrun Vafa, Erik P. Verlinde, and Herman L. Verlinde. The Operator Algebra of Orbifold Models. *Commun. Math. Phys.*, 123:485, 1989.

[114] Robbert Dijkgraaf, Erik P. Verlinde, and Herman L. Verlinde. C = 1 Conformal Field Theories on Riemann Surfaces. *Commun. Math. Phys.*, 115:649–690, 1988.

[115] Zhihao Duan, Qiang Jia, and Sungjay Lee. $\mathbb{Z}_N$ Duality and Parafermions Revisited. 9 2023.

[116] N. Dupuis, L. Canet, A. Eichhorn, W. Metzner, J. M. Pawlowski, M. Tissier, and N. Wschebor. The nonperturbative functional renormalization group and its applications. *Physics Reports*, 910:1–114, May 2021.

[117] N. Dupuis and G. Y. Chitov. Renormalization-group approach to Fermi-liquid theory.

Physical Review B, 54(5):3040–3043, August 1996.

[118] Igor Dzyaloshinskii. Some consequences of the Luttinger theorem: The Luttinger surfaces in non-Fermi liquids and Mott insulators. *Physical Review B*, 68(8):085113, August 2003.

[119] Estia Eichten and John Preskill. Chiral Gauge Theories on the Lattice. *Nucl. Phys. B*, 268:179–208, 1986.

[120] S. Elitzur and V. P. Nair. Non perturbative anomalies in higher dimensions. *Nuclear Physics B*, 243(2):205–211, September 1984.

[121] Dominic V. Else and T. Senthil. Strange Metals as Ersatz Fermi Liquids. *Phys. Rev. Lett.*, 127(8):086601, August 2021.

[122] Dominic V. Else, Ryan Thorngren, and T. Senthil. Non-Fermi Liquids as Ersatz Fermi Liquids: General Constraints on Compressible Metals. *Physical Review X*, 11(2):021005, April 2021.

[123] F. Englert and R. Brout. Broken Symmetry and the Mass of Gauge Vector Mesons. *Phys. Rev. Lett.*, 13(9):321–323, August 1964.

[124] Pavel Etingof, Ryan Kinser, and Chelsea Walton. Tensor algebras in finite tensor categories. *International Mathematics Research Notices*, 2021(24):18529–18572, 2021.

[125] Pavel Etingof, Dmitri Nikshych, Victor Ostrik, and with an appendix by Ehud Meir. Fusion categories and homotopy theory. *arXiv e-prints*, page arXiv:0909.3140, September 2009.

[126] Lukasz Fidkowski, Jeongwan Haah, and Matthew B Hastings. Gravitational anomaly of 3+ 1 dimensional z_2 toric code with fermionic charges and fermionic loop self-statistics. *arXiv preprint arXiv:2110.14654*, 2021.

[127] Lukasz Fidkowski and Alexei Kitaev. Effects of interactions on the topological classification of free fermion systems. *Phys. Rev. B*, 81(13):134509, April 2010.

[128] Lukasz Fidkowski and Alexei Kitaev. Topological phases of fermions in one dimension. *Physical Review B*, 83(7):075103, February 2011.

[129] Jose M Figueroa-O'Farrill and Sonia Stanciu. Equivariant cohomology and gauged bosonic sigma-models. *arXiv preprint hep-th/9407149*, 1994.

[130] Matthew P. A. Fisher and Leonid I. Glazman. Transport in a one-dimensional Luttinger liquid. *arXiv e-prints*, pages cond–mat/9610037, October 1996.

[131] M. Franz and A. J. Millis. Phase fluctuations and spectral properties of underdoped cuprates. *Physical Review B*, 58(21):14572–14580, December 1998.

[132] M. Franz and Z. Tešanović. Algebraic Fermi Liquid from Phase Fluctuations: "Topological" Fermions, Vortex "Berryons," and QED$_3$ Theory of Cuprate Superconductors. *Phys. Rev. Lett.*, 87(25):257003, December 2001.

[133] Daniel S Freed. Pions and generalized cohomology. *Journal of Differential Geometry*, 80(1):45–77, 2008.

[134] Daniel S Freed, Zohar Komargodski, and Nathan Seiberg. The sum over topological sectors and θ in the 2+ 1-dimensional $\mathbb{CP}^1\sigma$-model. *Communications in Mathematical Physics*, 362(1):167–183, 2018.

[135] Igor Frenkel, James Lepowsky, and Arne Meurman. *Vertex operator algebras and the Monster*. Academic press, 1989.

[136] Igor B Frenkel, James Lepowsky, and Arne Meurman. A natural representation of the fischer-griess monster with the modular function j as character. *Proceedings of the National Academy of Sciences*, 81(10):3256–3260, 1984.

[137] Jurg Frohlich, Jurgen Fuchs, Ingo Runkel, and Christoph Schweigert. Kramers-Wannier duality from conformal defects. *Phys. Rev. Lett.*, 93:070601, 2004.

[138] Jurg Frohlich, Jurgen Fuchs, Ingo Runkel, and Christoph Schweigert. Duality and defects in rational conformal field theory. *Nucl. Phys.*, B763:354–430, 2007.

[139] Jurg Frohlich, Jurgen Fuchs, Ingo Runkel, and Christoph Schweigert. Defect lines, dualities, and generalised orbifolds. In *Proceedings, 16th International Congress on Mathematical Physics (ICMP09): Prague, Czech Republic, August 3-8, 2009*, 2009.

[140] Jurgen Fuchs, Matthias R. Gaberdiel, Ingo Runkel, and Christoph Schweigert. Topological defects for the free boson CFT. *J. Phys. A*, 40:11403, 2007.

[141] Jurgen Fuchs, Ingo Runkel, and Christoph Schweigert. TFT construction of RCFT correlators 1. Partition functions. *Nucl. Phys. B*, 646:353–497, 2002.

[142] F. Fucito, E. Marinari, G. Parisi, and C. Rebbi. A proposal for monte carlo simulations of fermionic systems. *Nuclear Physics B*, 180(3):369–377, 1981.

[143] Masafumi Fukuma, Shinobu Hosono, and Hikaru Kawai. Lattice topological field theory in two dimensions. *Communications in mathematical physics*, 161:157–175, 1994.

[144] Nobuo Furukawa, T. M. Rice, and Manfred Salmhofer. Truncation of a Two-Dimensional

Fermi Surface due to Quasiparticle Gap Formation at the Saddle Points. *Phys. Rev. Lett.*, 81(15):3195–3198, October 1998.

[145] Davide Gaiotto, Anton Kapustin, Nathan Seiberg, and Brian Willett. Generalized Global Symmetries. *JHEP*, 02:172, 2015.

[146] César Galindo. Trivializing group actions on braided crossed tensor categories and graded braided tensor categories. *arXiv e-prints*, page arXiv:2010.00847, October 2020.

[147] Snir Gazit, Fakher F. Assaad, and Subir Sachdev. Fermi Surface Reconstruction without Symmetry Breaking. *Physical Review X*, 10(4):041057, October 2020.

[148] Joel Giedt and Erich Poppitz. Chiral lattice gauge theories and the strong coupling dynamics of a Yukawa-Higgs model with Ginsparg-Wilson fermions. *Journal of High Energy Physics*, 2007(10):076, October 2007.

[149] Paul H. Ginsparg. APPLIED CONFORMAL FIELD THEORY. In *Les Houches Summer School in Theoretical Physics: Fields, Strings, Critical Phenomena*, 9 1988.

[150] Paul H. Ginsparg. Curiosities at c = 1. *Nucl. Phys. B*, 295:153–170, 1988.

[151] Nico Gneist, Dominik Kiese, Ravn Henkel, Ronny Thomale, Laura Classen, and Michael M. Scherer. Functional renormalization of spinless triangular-lattice fermions: N-patch vs. truncated-unity scheme. *European Physical Journal B*, 95(9):157, September 2022.

[152] Nikolay V. Gnezdilov and Yuxuan Wang. Solvable model for a charge-4 e superconductor. *Physical Review B*, 106(9):094508, September 2022.

[153] Jeffrey Goldstone, Abdus Salam, and Steven Weinberg. Broken Symmetries. *Physical Review*, 127(3):965–970, August 1962.

[154] Jeffrey Goldstone and Frank Wilczek. Fractional quantum numbers on solitons. *Physical Review Letters*, 47(14):986, 1981.

[155] Pedro R. S. Gomes. An introduction to higher-form symmetries. *SciPost Phys. Lect. Notes*, 74:1, 2023.

[156] J A Gracey. Critical point analysis of various fermionic field theories in the large n expansion. *Journal of Physics A: Mathematical and General*, 25(3):L109–L113, feb 1992.

[157] Tarun Grover and T Senthil. Topological spin hall states, charged skyrmions, and superconductivity in two dimensions. *Physical review letters*, 100(15):156804, 2008.

[158] Y. Gu and X.-L. Qi. Axion field theory approach and the classification of interacting topological superconductors. *ArXiv e-prints*, December 2015.

[159] Z.-C. Gu and M. Levin. Effect of interactions on two-dimensional fermionic symmetry-protected topological phases with Z_2 symmetry. *Physical Review B*, 89(20):201113, May 2014.

[160] Meng Guo, Kantaro Ohmori, Pavel Putrov, Zheyan Wan, and Juven Wang. Fermionic Finite-Group Gauge Theories and Interacting Symmetric/Crystalline Orders via Cobordisms. *Communications in Mathematical Physics*, 376(2):1073–1154, January 2020.

[161] Yuxuan Guo and Yi-Zhuang You. Symmetric Mass Generation of Kähler-Dirac Fermions from the Perspective of Symmetry-Protected Topological Phases. *arXiv e-prints*, page arXiv:2306.17420, June 2023.

[162] V. Gurarie. Single-particle Green's functions and interacting topological insulators. *Physical Review B*, 83(8):085426, February 2011.

[163] Martin C. Gutzwiller. Effect of correlation on the ferromagnetism of transition metals. *Phys. Rev.*, 134:A923–A941, May 1964.

[164] Babak Haghighat and Youran Sun. Topological Defect Lines in bosonized Parafermionic CFTs. 6 2023.

[165] F. D. M. Haldane. Luttinger's Theorem and Bosonization of the Fermi Surface. *arXiv e-prints*, pages cond–mat/0505529, May 2005.

[166] M. B. Hastings. Sufficient conditions for topological order in insulators. *EPL (Europhysics Letters)*, 70(6):824–830, June 2005.

[167] Chen He. Equivariant cohomology rings of the real flag manifolds. *arXiv preprint arXiv:1610.07968*, 2016.

[168] Egil V. Herland, Egor Babaev, and Asle Sudbo. Phase transitions in a three dimensional $U(1) \times U(1)$ lattice London superconductor. *arXiv e-prints*, page arXiv:1006.3311, June 2010.

[169] A. C. Hewson. Renormalization group and Fermi liquid theory. *Advances in Physics*, 43(4):543–575, July 1994.

[170] Peter W. Higgs. Broken Symmetries and the Masses of Gauge Bosons. *Phys. Rev. Lett.*, 13(16):508–509, October 1964.

[171] J. E. Hirsch. Two-dimensional hubbard model: Numerical simulation study. *Phys. Rev. B*, 31:4403–4419, Apr 1985.

[172] J. E. Hirsch, D. J. Scalapino, R. L. Sugar, and R. Blankenbecler. Efficient monte carlo procedure for systems with fermions. *Phys. Rev. Lett.*, 47:1628–1631, Nov 1981.

[173] Martin Hohenadler and Fakher F. Assaad. Fractionalized Metal in a Falicov-Kimball Model. *Phys. Rev. Lett.*, 121(8):086601, August 2018.

[174] Gary T Horowitz and Mark Srednicki. A quantum field theoretic description of linking numbers and their generalization. *Communications in Mathematical Physics*, 130(1):83–94, 1990.

[175] J. Hou, P. T. Yang, Z. Y. Liu, J. Y. Li, P. F. Shan, L. Ma, G. Wang, N. N. Wang, H. Z. Guo, J. P. Sun, Y. Uwatoko, M. Wang, G. M. Zhang, B. S. Wang, and J. G. Cheng. Emergence of high-temperature superconducting phase in the pressurized La3Ni2O7 crystals. *arXiv e-prints*, page arXiv:2307.09865, July 2023.

[176] Wanda Hou and Yi-Zhuang You. Variational Monte Carlo Study of Symmetric Mass Generation in a Bilayer Honeycomb Lattice Model. *arXiv e-prints*, page arXiv:2212.13364, December 2022.

[177] Po-Shen Hsin and Nathan Seiberg. Level/rank duality and chern-simons-matter theories. *Journal of High Energy Physics*, 2016(9):95, 2016.

[178] Rui-Zhen Huang, Da-Chuan Lu, Yi-Zhuang You, Zi Yang Meng, and Tao Xiang. Emergent symmetry and conserved current at a one-dimensional incarnation of deconfined quantum critical point. *Physical Review B*, 100(12):125137, September 2019.

[179] Rui-Zhen Huang, Da-Chuan Lu, Yi-Zhuang You, Zi Yang Meng, and Tao Xiang. Emergent Symmetry and Conserved Current at a One Dimensional Incarnation of Deconfined Quantum Critical Point. *Phys. Rev. B*, 100(12):125137, 2019.

[180] Sheng-Jie Huang and Meng Cheng. Topological holography, quantum criticality, and boundary states. 10 2023.

[181] Tzu-Chen Huang, Ying-Hsuan Lin, and Sahand Seifnashri. Construction of two-dimensional topological field theories with non-invertible symmetries. *JHEP*, 12:028, 2021.

[182] Yen-Ta Huang and Dung-Hai Lee. Non-abelian bosonization in two and three spatial dimensions and applications. *Nuclear Physics B*, 972:115565, 2021.

[183] Yen-Ta Huang and Dung-Hai Lee. The electromagnetic duality and the 3+ 1d o

(6) non-linear sigma model with a level-1 wess-zumino-witten term. *arXiv preprint arXiv:2206.09392*, 2022.

[184] CM Hull and B Spence. The gauged nonlinear sigma model with wess-zumino term. *Physics Letters B*, 232(2):204–210, 1989.

[185] CM Hull and B Spence. The geometry of the gauged sigma-model with wess-zumino term. *Nuclear Physics B*, 353(2):379–426, 1991.

[186] Hiroki Isobe, Noah F. Q. Yuan, and Liang Fu. Unconventional Superconductivity and Density Waves in Twisted Bilayer Graphene. *Physical Review X*, 8(4):041041, October 2018.

[187] Lukas Janssen and Yin-Chen He. Critical behavior of the qed 3-gross-neveu model: Duality and deconfined criticality. *Physical Review B*, 96(20):205113, 2017.

[188] Wenjie Ji, Shu-Heng Shao, and Xiao-Gang Wen. Topological Transition on the Conformal Manifold. *Phys. Rev. Res.*, 2(3):033317, 2020.

[189] Wenjie Ji and Xiao-Gang Wen. Noninvertible anomalies and mapping-class-group transformation of anomalous partition functions. *Phys. Rev. Research*, 1(3):033054, October 2019.

[190] Wenjie Ji and Xiao-Gang Wen. Categorical symmetry and noninvertible anomaly in symmetry-breaking and topological phase transitions. *Phys. Rev. Res.*, 2(3):033417, 2020.

[191] Chao-Ming Jian, Zhen Bi, and Cenke Xu. Lieb-Schultz-Mattis theorem and its generalizations from the perspective of the symmetry-protected topological phase. *Physical Review B*, 97(5):054412, February 2018.

[192] Chao-Ming Jian, Alex Rasmussen, Yi-Zhuang You, and Cenke Xu. Emergent Symmetry and Tricritical Points near the deconfined Quantum Critical Point. *arXiv e-prints*, page arXiv:1708.03050, August 2017.

[193] Shenghan Jiang, Meng Cheng, Yang Qi, and Yuan-Ming Lu. Generalized lieb-schultz-mattis theorem on bosonic symmetry protected topological phases. *SciPost Physics*, 11(2):024, 2021.

[194] Shenghan Jiang and Olexei I. Motrunich. Ising ferromagnet to valence bond solid transition in a one-dimensional spin chain: Analogies to deconfined quantum critical points. *Phys. Rev. B*, 99(7):075103, 2019.

[195] Y.-F. Jiang, Z.-X. Li, S. A. Kivelson, and H. Yao. Charge-4e superconductors: a Majorana quantum Monte Carlo study. *ArXiv e-prints*, July 2016.

[196] Jorge V. José, Leo P. Kadanoff, Scott Kirkpatrick, and David R. Nelson. Renormalization, vortices, and symmetry-breaking perturbations in the two-dimensional planar model. *Phys. Rev. B*, 16:1217–1241, Aug 1977.

[197] Justin Kaidi, Emily Nardoni, Gabi Zafrir, and Yunqin Zheng. Symmetry TFTs and anomalies of non-invertible symmetries. *JHEP*, 10:053, 2023.

[198] Justin Kaidi, Kantaro Ohmori, and Yunqin Zheng. Kramers-Wannier-like Duality Defects in (3+1)D Gauge Theories. *Phys. Rev. Lett.*, 128(11):111601, 2022.

[199] Justin Kaidi, Kantaro Ohmori, and Yunqin Zheng. Symmetry TFTs for Non-Invertible Defects. 9 2022.

[200] Hidekazu Kamei and Kazumasa Miyake. On Quartet Superfluidity of Fermionic Atomic Gas. *Journal of the Physical Society of Japan*, 74(7):1911–1913, July 2005.

[201] David B. Kaplan. A method for simulating chiral fermions on the lattice. *Physics Letters B*, 288(3):342–347, 1992.

[202] Anton Kapustin. Bosonic Topological Insulators and Paramagnets: a view from cobordisms. 4 2014.

[203] Anton Kapustin. Symmetry Protected Topological Phases, Anomalies, and Cobordisms: Beyond Group Cohomology. 3 2014.

[204] Anton Kapustin and Ryan Thorngren. Anomalies of discrete symmetries in various dimensions and group cohomology. *arXiv e-prints*, page arXiv:1404.3230, April 2014.

[205] Anton Kapustin and Ryan Thorngren. Fermionic SPT phases in higher dimensions and bosonization. *Journal of High Energy Physics*, 2017(10):80, October 2017.

[206] Anton Kapustin, Ryan Thorngren, Alex Turzillo, and Zitao Wang. Fermionic symmetry protected topological phases and cobordisms. *Journal of High Energy Physics*, 2015:52, December 2015.

[207] Andreas Karch and David Tong. Particle-vortex duality from 3d bosonization. *Phys. Rev. X*, 6(3):031043, 2016.

[208] Vahid Karimipour and Ali Mostafazadeh. Lattice topological field theory on nonorientable surfaces. *Journal of Mathematical Physics*, 38(1):49–66, 1997.

[209] B. Keimer, S. A. Kivelson, M. R. Norman, S. Uchida, and J. Zaanen. From quantum matter to high-temperature superconductivity in copper oxides. *Nature*, 518(7538):179, February 2015.

[210] Y. Kikukawa. Why is the mission impossible? Decoupling the mirror Ginsparg-Wilson fermions in the lattice models for two-dimensional Abelian chiral gauge theories. *Progress of Theoretical and Experimental Physics*, 2019(7):073B02, July 2019.

[211] Yoshio Kikukawa. On the gauge invariant path-integral measure for the overlap Weyl fermions in $\underline{16}$ of SO(10). *PTEP*, 2019(11):113B03, 2019.

[212] Elias B. Kiritsis. Proof of the Completeness of the Classification of Rational Conformal Theories With $c = 1$. *Phys. Lett. B*, 217:427–430, 1989.

[213] S. A. Kivelson, V. J. Emery, and H. Q. Lin. Doped antiferromagnets in the weak-hopping limit. *Physical Review B*, 42:6523–6530, October 1990.

[214] Ryohei Kobayashi, Yasunori Lee, Ken Shiozaki, and Yuya Tanizaki. Topological terms of (2+ 1) d flag-manifold sigma models. *Journal of High Energy Physics*, 2021(8):1–28, 2021.

[215] Ryohei Kobayashi, Kantaro Ohmori, and Yuji Tachikawa. On gapped boundaries for SPT phases beyond group cohomology. *Journal of High Energy Physics*, 2019(11):131, November 2019.

[216] Mahito Kohmoto, Marcel den Nijs, and Leo P Kadanoff. Hamiltonian studies of the d= 2 ashkin-teller model. *Physical Review B*, 24(9):5229, 1981.

[217] Masataka Koide, Yuta Nagoya, and Satoshi Yamaguchi. Non-invertible topological defects in 4-dimensional $\mathbb{Z}_2$ pure lattice gauge theory. *PTEP*, 2022(1):013B03, 2022.

[218] Zohar Komargodski, Kantaro Ohmori, Konstantinos Roumpedakis, and Sahand Seifnashri. Symmetries and strings of adjoint QCD$_2$. *JHEP*, 03:103, 2021.

[219] Zohar Komargodski, Adar Sharon, Ryan Thorngren, and Xinan Zhou. Comments on abelian higgs models and persistent order. *SciPost Physics*, 6(1):003, 2019.

[220] Liang Kong and Hao Zheng. A mathematical theory of gapless edges of 2d topological orders. Part I. *Journal of High Energy Physics*, 2020(2):150, February 2020.

[221] J M Kosterlitz. The critical properties of the two-dimensional xy model. *Journal of Physics C: Solid State Physics*, 7(6):1046, 1974.

[222] John Michael Kosterlitz and David James Thouless. Ordering, metastability and phase transitions in two-dimensional systems. *Journal of Physics C: Solid State Physics*, 6(7):1181, 1973.

[223] H. A. Kramers and G. H. Wannier. Statistics of the two-dimensional ferromagnet. part i.

Phys. Rev., 60:252–262, Aug 1941.

[224] Shauna Kravec, John McGreevy, and Brian Swingle. All-fermion electrodynamics and fermion number anomaly inflow. *Physical Review D*, 92(8):085024, 2015.

[225] Hyok-Jon Kwon and Alan T. Dorsey. Effect of phase fluctuations on the single-particle properties of underdoped cuprates. *Physical Review B*, 59(9):6438–6448, March 1999.

[226] Hyok-Jon Kwon, Alan T. Dorsey, and P. J. Hirschfeld. Observability of Quantum Phase Fluctuations in Cuprate Superconductors. *Phys. Rev. Lett.*, 86(17):3875–3878, April 2001.

[227] Ethan Lake. Higher-form symmetries and spontaneous symmetry breaking. *arXiv preprint arXiv:1802.07747*, 2018.

[228] L.D. Landau and E.M. Lifshitz. *Statistical Physics: Volume 5*. Number v. 5. Elsevier Science, 2013.

[229] Jong Yeon Lee, Chao-Ming Jian, and Cenke Xu. Quantum criticality under decoherence or weak measurement. *arXiv e-prints*, page arXiv:2301.05238, January 2023.

[230] Patrick A. Lee, Naoto Nagaosa, and Xiao-Gang Wen. Doping a Mott Insulator: Physics of High Temperature Superconductivity. *Rev. Mod. Phys.*, 78(1):17–85, January 2006.

[231] Yasunori Lee, Kantaro Ohmori, and Yuji Tachikawa. Revisiting Wess-Zumino-Witten terms. *SciPost Physics*, 10(3):061, March 2021.

[232] Michael Levin and T. Senthil. Deconfined quantum criticality and Néel order via dimer disorder. *Physical Review B*, 70(22):220403(R), December 2004.

[233] Tao Li and Da-Wei Yao. Pairing origin of the pseudogap as observed in ARPES measurement in the underdoped cuprates. *arXiv e-prints*, page arXiv:1805.05530, May 2018.

[234] Tao Li and Da-Wei Yao. Why is the antinodal quasiparticle in the electron-doped cuprate $Pr_{1.3-x}La_{0.7}Ce_xCuO_4$ immune to the antiferromagnetic band-folding effect? *EPL (Europhysics Letters)*, 124(4):47001, November 2018.

[235] Zi-Xiang Li, Shao-Kai Jian, and Hong Yao. Deconfined quantum criticality and emergent so (5) symmetry in fermionic systems. *arXiv preprint arXiv:1904.10975*, 2019.

[236] Biao Lian. A Quantum Breakdown Model: from Many-body Localization to Chaos with Scars. *arXiv e-prints*, page arXiv:2208.10509, August 2022.

[237] Tsuf Lichtman, Ryan Thorngren, Netanel H. Lindner, Ady Stern, and Erez Berg. Bulk

Anyons as Edge Symmetries: Boundary Phase Diagrams of Topologically Ordered States. *arXiv e-prints*, page arXiv:2003.04328, March 2020.

[238] Elliott Lieb, Theodore Schultz, and Daniel Mattis. Two soluble models of an antiferromagnetic chain. *Annals of Physics*, 16(3):407–466, 1961.

[239] Evgenii Mikhailovich Lifshitz and Lev Petrovich Pitaevskii. *Statistical physics: theory of the condensed state*, volume 9. Elsevier, 2013.

[240] Ying-Hsuan Lin, Masaki Okada, Sahand Seifnashri, and Yuji Tachikawa. Asymptotic density of states in 2d CFTs with non-invertible symmetries. 8 2022.

[241] Ying-Hsuan Lin and Shu-Heng Shao. Duality Defect of the Monster CFT. *J. Phys. A*, 54(6):065201, 2021.

[242] Ying-Hsuan Lin and Shu-Heng Shao. $\mathbb{Z}_N$ symmetries, anomalies, and the modular bootstrap. *Phys. Rev. D*, 103(12):125001, 2021.

[243] Ying-Hsuan Lin and Shu-Heng Shao. Bootstrapping Non-invertible Symmetries. 2 2023.

[244] Yu-Ping Lin and Rahul M. Nandkishore. Chiral twist on the high-T_c phase diagram in moiré heterostructures. *Physical Review B*, 100(8):085136, August 2019.

[245] Yu-Ping Lin and Rahul M. Nandkishore. Parquet renormalization group analysis of weak-coupling instabilities with multiple high-order Van Hove points inside the Brillouin zone. *Physical Review B*, 102(24):245122, December 2020.

[246] Wen-Yuan Liu, Juraj Hasik, Shou-Shu Gong, Didier Poilblanc, Wei-Qiang Chen, and Zheng-Cheng Gu. Emergence of Gapless Quantum Spin Liquid from Deconfined Quantum Critical Point. *Physical Review X*, 12(3):031039, July 2022.

[247] Da-Chuan Lu. Nonlinear sigma model description of deconfined quantum criticality in arbitrary dimensions. *SciPost Physics Core*, 6(3):047, July 2023.

[248] Da-Chuan Lu, Miao Li, Zhao-Yi Zeng, Wanda Hou, Juven Wang, Fan Yang, and Yi-Zhuang You. Superconductivity from Doping Symmetric Mass Generation Insulators: Application to $La_3Ni_2O_7$ under Pressure. August 2023.

[249] Da-Chuan Lu and Zhengdi Sun. On triality defects in 2d CFT. *Journal of High Energy Physics*, 2023(2):173, March 2023.

[250] Da-Chuan Lu, Juven Wang, and Yi-Zhuang You. Definition and classification of Fermi surface anomalies. *Physical Review B*, 109(4):045123, January 2024.

[251] Da-Chuan Lu, Taige Wang, Shubhayu Chatterjee, and Yi-Zhuang You. Correlated metals and unconventional superconductivity in rhombohedral trilayer graphene: A renormalization group analysis. *Physical Review B*, 106(15):155115, October 2022.

[252] Da-Chuan Lu, Cenke Xu, and Yi-Zhuang You. Self-duality protected multicriticality in deconfined quantum phase transitions. *Physical Review B*, 104(20):205142, November 2021.

[253] Da-Chuan Lu, Cenke Xu, and Yi-Zhuang You. Self-duality protected multicriticality in deconfined quantum phase transitions. *Physical Review B*, 104(20):205142, 2021.

[254] Da-Chuan Lu, Meng Zeng, Juven Wang, and Yi-Zhuang You. Fermi Surface Symmetric Mass Generation. *arXiv e-prints*, page arXiv:2210.16304, October 2022.

[255] Da-Chuan Lu, Meng Zeng, Juven Wang, and Yi-Zhuang You. Fermi surface symmetric mass generation. *Physical Review B*, 107(19):195133, May 2023.

[256] Da-Chuan Lu, Meng Zeng, and Yi-Zhuang You. Green's function zeros in Fermi surface symmetric mass generation. *Physical Review B*, 108(20):205117, November 2023.

[257] Yuan-Ming Lu, Ying Ran, and Masaki Oshikawa. Filling-enforced constraint on the quantized Hall conductivity on a periodic lattice. *arXiv e-prints*, page arXiv:1705.09298, May 2017.

[258] Ran Luo, Qing-Rui Wang, and Yi-Nan Wang. Lecture Notes on Generalized Symmetries and Applications. 7 2023.

[259] J. M. Luttinger. Fermi surface and some simple equilibrium properties of a system of interacting fermions. *Phys. Rev.*, 119:1153–1163, Aug 1960.

[260] J. M. Luttinger and J. C. Ward. Ground-state energy of a many-fermion system. ii. *Phys. Rev.*, 118:1417–1427, Jun 1960.

[261] JM Luttinger. An exactly soluble model of a many-fermion system. *Journal of mathematical physics*, 4(9):1154–1162, 1963.

[262] Nvsen Ma, Guang-Yu Sun, Yi-Zhuang You, Cenke Xu, Ashvin Vishwanath, Anders W. Sandvik, and Zi Yang Meng. Dynamical signature of fractionalization at a deconfined quantum critical point. *Physical Review B*, 98(17):174421, November 2018.

[263] Ruochen Ma and Chong Wang. Theory of deconfined pseudocriticality. *Physical Review B*, 102(2):020407, July 2020.

[264] Ruochen Ma and Chong Wang. Average Symmetry-Protected Topological Phases. *arXiv*

e-prints, page arXiv:2209.02723, September 2022.

[265] JL Manes. Differential geometric construction of the gauged wess-zumino action. *Nuclear Physics B*, 250(1-4):369–384, 1985.

[266] Juan Manes, Raymond Stora, and Bruno Zumino. Algebraic study of chiral anomalies. *Communications in Mathematical Physics*, 102(1):157–174, 1985.

[267] Ian Marshall and Dmitri Nikshych. On the Brauer-Picard groups of fusion categories. *arXiv e-prints*, page arXiv:1603.04318, March 2016.

[268] John McGreevy. Generalized Symmetries in Condensed Matter. *Annual Review of Condensed Matter Physics*, 14:57–82, March 2023.

[269] Ehud Meir and Evgeny Musicantov. Module categories over graded fusion categories. *arXiv e-prints*, page arXiv:1010.4333, October 2010.

[270] N David Mermin. The topological theory of defects in ordered media. *Reviews of Modern Physics*, 51(3):591, 1979.

[271] Max A. Metlitski, Lukasz Fidkowski, Xie Chen, and Ashvin Vishwanath. Interaction effects on 3D topological superconductors: surface topological order from vortex condensation, the 16 fold way and fermionic Kramers doublets. *arXiv e-prints*, page arXiv:1406.3032, June 2014.

[272] Max A. Metlitski and Ryan Thorngren. Intrinsic and emergent anomalies at deconfined critical points. *Physical Review B*, 98(8):085140, August 2018.

[273] Max A Metlitski and Ashvin Vishwanath. Particle-vortex duality of two-dimensional dirac fermion from electric-magnetic duality of three-dimensional topological insulators. *Phys. Rev. B*, 93(24):245151, 2016.

[274] Mamoru Mimura and Hiroshi Toda. *Topology of Lie groups, I and II*, volume 91. American Mathematical Soc., 1991.

[275] G. Misguich, C. Lhuillier, M. Mambrini, and P. Sindzingre. Degeneracy of the ground-state of antiferromagnetic spin-1/2 Hamiltonians. *European Physical Journal B*, 26(2):167–183, March 2002.

[276] I. Montvay. Mirror fermions in chiral gauge theories. *Nuclear Physics B Proceedings Supplements*, 29(2):159–170, December 1992.

[277] E.-G. Moon. Skyrmions with quadratic band touching fermions: A way to achieve charge 4e superconductivity. *Physical Review B*, 85(24):245123, June 2012.

[278] Eun-Gook Moon and Andrey Chubukov. Quantum-critical Pairing with Varying Exponents. *Journal of Low Temperature Physics*, 161(1-2):263–281, October 2010.

[279] Gregory W Moore. Introduction to chern-simons theories. *Available on the internet*, 2019.

[280] Gregory W. Moore and Nathan Seiberg. Classical and Quantum Conformal Field Theory. *Commun. Math. Phys.*, 123:177, 1989.

[281] Christopher Mudry, Akira Furusaki, Takahiro Morimoto, and Toshiya Hikihara. Quantum phase transitions beyond landau-ginzburg theory in one-dimensional space revisited. *Physical Review B*, 99(20):205153, 2019.

[282] Yuta Nagoya and Soichiro Shimamori. Non-invertible duality defect and non-commutative fusion algebra. 9 2023.

[283] Adam Nahum. Note on wess-zumino-witten models and quasiuniversality in 2+ 1 dimensions. *arXiv preprint arXiv:1912.13468*, 2019.

[284] Adam Nahum, JT Chalker, P Serna, M Ortuño, and AM Somoza. Deconfined quantum criticality, scaling violations, and classical loop models. *Phys. Rev. X*, 5(4):041048, 2015.

[285] Adam Nahum, P Serna, JT Chalker, M Ortuño, and AM Somoza. Emergent so (5) symmetry at the néel to valence-bond-solid transition. *Physical review letters*, 115(26):267203, 2015.

[286] Mikio Nakahara. *Geometry, topology and physics*. CRC press, 2018.

[287] Y. Nambu and G. Jona-Lasinio. Dynamical Model of Elementary Particles Based on an Analogy with Superconductivity. I. *Physical Review*, 122(1):345–358, April 1961.

[288] Yoichiro Nambu. Quasi-Particles and Gauge Invariance in the Theory of Superconductivity. *Physical Review*, 117(3):648–663, February 1960.

[289] Rahul Nandkishore, L. S. Levitov, and A. V. Chubukov. Chiral superconductivity from repulsive interactions in doped graphene. *Nature Physics*, 8(2):158–163, February 2012.

[290] Rahul Nandkishore, Max A. Metlitski, and T. Senthil. Orthogonal metals: The simplest non-Fermi liquids. *Physical Review B*, 86(4):045128, July 2012.

[291] H. B. Nielsen and M. Ninomiya. A no-go theorem for regularizing chiral fermions. *Physics Letters B*, 105:219–223, October 1981.

[292] H. B. Nielsen and M. Ninomiya. Absence of neutrinos on a lattice (I). Proof by homotopy theory. *Nuclear Physics B*, 185:20–40, July 1981.

[293] H. B. Nielsen and M. Ninomiya. Absence of neutrinos on a lattice: (ii). intuitive topological proof. *Nuclear Physics B*, 193(1):173–194, 1981.

[294] B. Nienhuis, A. N. Berker, Eberhard K. Riedel, and M. Schick. First- and second-order phase transitions in potts models: Renormalization-group solution. *Phys. Rev. Lett.*, 43:737–740, Sep 1979.

[295] Alexander Nikolaenko, Maria Tikhanovskaya, Subir Sachdev, and Ya-Hui Zhang. Small to large Fermi surface transition in a single-band model using randomly coupled ancillas. *Physical Review B*, 103(23):235138, June 2021.

[296] Edward O'Brien and Paul Fendley. Lattice Supersymmetry and Order-Disorder Coexistence in the Tricritical Ising Model. *Phys. Rev. Lett.*, 120(20):206403, May 2018.

[297] Masaki Oshikawa. Commensurability, Excitation Gap, and Topology in Quantum Many-Particle Systems on a Periodic Lattice. *Phys. Rev. Lett.*, 84(7):1535–1538, February 2000.

[298] Masaki Oshikawa. Topological Approach to Luttinger's Theorem and the Fermi Surface of a Kondo Lattice. *Phys. Rev. Lett.*, 84(15):3370–3373, April 2000.

[299] Masaki Oshikawa and Ian Affleck. Defect lines in the Ising model and boundary states on orbifolds. *Phys. Rev. Lett.*, 77:2604–2607, 1996.

[300] Masaki Oshikawa and Ian Affleck. Boundary conformal field theory approach to the critical two-dimensional Ising model with a defect line. *Nucl. Phys. B*, 495:533–582, 1997.

[301] Masaki Oshikawa and T. Senthil. Fractionalization, Topological Order, and Quasiparticle Statistics. *Phys. Rev. Lett.*, 96(6):060601, February 2006.

[302] Masaki Oshikawa, Masanori Yamanaka, and Ian Affleck. Magnetization Plateaus in Spin Chains: "Haldane Gap" for Half-Integer Spins. *Phys. Rev. Lett.*, 78(10):1984–1987, March 1997.

[303] Victor Ostrik. Module categories, weak hopf algebras and modular invariants. *Transformation groups*, 8:177–206, 2003.

[304] Sridip Pal and Zhengdi Sun. High Energy Modular Bootstrap, Global Symmetries and Defects. *JHEP*, 08:064, 2020.

[305] Arun Paramekanti and Ashvin Vishwanath. Extending Luttinger's theorem to $\mathbb{Z}_2$ fractionalized phases of matter. *Physical Review B*, 70(24):245118, December 2004.

[306] Takamori Park, Mengxing Ye, and Leon Balents. Electronic instabilities of kagome metals: Saddle points and Landau theory. *Physical Review B*, 104(3):035142, July 2021.

[307] A. Perez-Lona, D. Robbins, E. Sharpe, T. Vandermeulen, and X. Yu. Notes on gauging noninvertible symmetries, part 1: Multiplicity-free cases. 11 2023.

[308] Michael E Peskin. Mandelstam-'t hooft duality in abelian lattice models. *Annals of Physics*, 113(1):122 – 152, 1978.

[309] V. B. Petkova and J. B. Zuber. Generalized twisted partition functions. *Phys. Lett. B*, 504:157–164, 2001.

[310] Erich Poppitz and Yanwen Shang. Chiral Lattice Gauge Theories via Mirror-Fermion Decoupling:. a Mission (im)possible? *International Journal of Modern Physics A*, 25(14):2761–2813, January 2010.

[311] Abhishodh Prakash, Michele Fava, and S. A. Parameswaran. Multiversality and Unnecessary Criticality in One Dimension. *Phys. Rev. Lett.*, 130(25):256401, 2023.

[312] Abhishodh Prakash and Juven Wang. Unwinding Fermionic SPT Phases: Supersymmetry Extension. *Phys. Rev. B*, 103(8):085130, 2021.

[313] Abhishodh Prakash, Juven Wang, and Tzu-Chieh Wei. Unwinding Short-Range Entanglement. *Phys. Rev.*, B98(12):125108, 2018.

[314] X.-L. Qi. A new class of (2 + 1)-dimensional topological superconductors with $\mathbb{Z}_8$ topological classification. *New Journal of Physics*, 15(6):065002, June 2013.

[315] Yan Qi Qin, Yuan-Yao He, Yi-Zhuang You, Zhong-Yi Lu, Arnab Sen, Anders W. Sandvik, Cenke Xu, and Zi Yang Meng. Duality between the Deconfined Quantum-Critical Point and the Bosonic Topological Transition. *Phys. Rev. X*, 7(3):031052, July 2017.

[316] R. Queiroz, E. Khalaf, and A. Stern. Dimensional Hierarchy of Fermionic Interacting Topological Phases. *Physical Review Letters*, 117(20):206405, November 2016.

[317] Louk Rademaker and Miguel Ortuño. Explicit Local Integrals of Motion for the Many-Body Localized State. *Phys. Rev. Lett.*, 116(1):010404, January 2016.

[318] L. Radzihovsky and A. Vishwanath. Quantum Liquid Crystals in an Imbalanced Fermi Gas: Fluctuations and Fractional Vortices in Larkin-Ovchinnikov States. *Physical Review Letters*, 103(1):010404, July 2009.

[319] S. Raghu and S. A. Kivelson. Superconductivity from repulsive interactions in the two-dimensional electron gas. *Physical Review B*, 83(9):094518, March 2011.

[320] Brandon C. Rayhaun. Bosonic Rational Conformal Field Theories in Small Genera, Chiral Fermionization, and Symmetry/Subalgebra Duality. 3 2023.

[321] Shlomo S. Razamat and David Tong. Gapped Chiral Fermions. *Physical Review X*, 11(1):011063, January 2021.

[322] Jun-Won Rhim and Bohm-Jung Yang. Classification of flat bands according to the band-crossing singularity of Bloch wave functions. *Physical Review B*, 99(4):045107, January 2019.

[323] Brenden Roberts, Shenghan Jiang, and Olexei I Motrunich. Deconfined quantum critical point in one dimension. *Physical Review B*, 99(16):165143, 2019.

[324] Dale Rolfsen. *Knots and links*, volume 346. American Mathematical Soc., 2003.

[325] Robert Rüger, Luca F. Tocchio, Roser Valentí, and Claudius Gros. The phase diagram of the square lattice bilayer Hubbard model: a variational Monte Carlo study. *New Journal of Physics*, 16(3):033010, March 2014.

[326] S. Ryu and S.-C. Zhang. Interacting topological phases and modular invariance. *Physical Review B*, 85(24):245132, June 2012.

[327] Shinsei Ryu, Joel E. Moore, and Andreas W. W. Ludwig. Electromagnetic and gravitational responses and anomalies in topological insulators and superconductors. *Physical Review B*, 85(4):045104, January 2012.

[328] Shinsei Ryu, Christopher Mudry, Chang-Yu Hou, and Claudio Chamon. Masses in graphenelike two-dimensional electronic systems: Topological defects in order parameters and their fractional exchange statistics. *Physical Review B*, 80(20):205319, 2009.

[329] Subir Sachdev. Topological order, emergent gauge fields, and Fermi surface reconstruction. *Reports on Progress in Physics*, 82(1):014001, January 2019.

[330] H Saleur. Partition functions of the two-dimensional ashkin-teller model on the critical line. *Journal of Physics A: Mathematical and General*, 20(16):L1127, 1987.

[331] M. Salmhofer and C. Honerkamp. Fermionic Renormalization Group Flows —Technique and Theory—. *Progress of Theoretical Physics*, 105(1):1–35, January 2001.

[332] Anders W Sandvik. Evidence for deconfined quantum criticality in a two-dimensional heisenberg model with four-spin interactions. *Physical review letters*, 98(22):227202, 2007.

[333] Thomas Scaffidi, Daniel E. Parker, and Romain Vasseur. Gapless Symmetry Protected

Topological Order. *Phys. Rev. X*, 7(4):041048, 2017.

[334] D. J. Scalapino and R. L. Sugar. Method for performing monte carlo calculations for systems with fermions. *Phys. Rev. Lett.*, 46:519–521, Feb 1981.

[335] Sakura Schafer-Nameki. ICTP Lectures on (Non-)Invertible Generalized Symmetries. 5 2023.

[336] David Schaich and Simon Catterall. Phases of a strongly coupled four-fermion theory. In *European Physical Journal Web of Conferences*, volume 175 of *European Physical Journal Web of Conferences*, page 03004, March 2018.

[337] Mathias S. Scheurer, Shubhayu Chatterjee, Wei Wu, Michel Ferrero, Antoine Georges, and Subir Sachdev. Topological order in the pseudogap metal. *Proceedings of the National Academy of Science*, 115(16):E3665–E3672, April 2018.

[338] U. Schollwöck. The density-matrix renormalization group. *Reviews of Modern Physics*, 77(1):259–315, January 2005.

[339] Nathan Seiberg, Sahand Seifnashri, and Shu-Heng Shao. Non-invertible symmetries and LSM-type constraints on a tensor product Hilbert space. *arXiv e-prints*, page arXiv:2401.12281, January 2024.

[340] Nathan Seiberg, T. Senthil, Chong Wang, and Edward Witten. A duality web in 2 + 1 dimensions and condensed matter physics. *Annals of Physics*, 374:395–433, November 2016.

[341] Nathan Seiberg, T Senthil, Chong Wang, and Edward Witten. A duality web in 2+ 1 dimensions and condensed matter physics. *Annals of Physics*, 374:395–433, 2016.

[342] Nathan Seiberg and Shu-Heng Shao. Majorana chain and Ising model – (non-invertible) translations, anomalies, and emanant symmetries. 7 2023.

[343] Nathan Seiberg and Edward Witten. Gapped boundary phases of topological insulators via weak coupling. *Progress of Theoretical and Experimental Physics*, 2016(12), 2016.

[344] Sahand Seifnashri and Shu-Heng Shao. Cluster state as a non-invertible symmetry protected topological phase. *arXiv e-prints*, page arXiv:2404.01369, April 2024.

[345] D. Sénéchal, D. Perez, and M. Pioro-Ladrière. Spectral Weight of the Hubbard Model through Cluster Perturbation Theory. *Phys. Rev. Lett.*, 84(3):522–525, January 2000.

[346] David Sénéchal, Danny Perez, and Dany Plouffe. Cluster perturbation theory for Hubbard models. *Physical Review B*, 66(7):075129, August 2002.

[347] T. Senthil. Symmetry Protected Topological phases of Quantum Matter. *Ann. Rev. Condensed Matter Phys.*, 6:299, 2015.

[348] T. Senthil, Leon Balents, Subir Sachdev, Ashvin Vishwanath, and Matthew P. A. Fisher. Quantum criticality beyond the Landau-Ginzburg-Wilson paradigm. *Physical Review B*, 70(14):144407, October 2004.

[349] T. Senthil, Subir Sachdev, and Matthias Vojta. Fractionalized Fermi Liquids. *Phys. Rev. Lett.*, 90(21):216403, May 2003.

[350] T. Senthil, Ashvin Vishwanath, Leon Balents, Subir Sachdev, and Matthew P. A. Fisher. Deconfined Quantum Critical Points. *Science*, 303(5663):1490–1494, March 2004.

[351] T. Senthil, Matthias Vojta, and Subir Sachdev. Weak magnetism and non-Fermi liquids near heavy-fermion critical points. *Physical Review B*, 69(3):035111, January 2004.

[352] Henry Shackleton, Alex Thomson, and Subir Sachdev. Deconfined criticality and a gapless $\mathbb{Z}_2$ spin liquid in the square-lattice antiferromagnet. *Phys. Rev. B*, 104:045110, Jul 2021.

[353] R. Shankar. Renormalization group for interacting fermions in $d > 1$. *Physica A Statistical Mechanics and its Applications*, 177(1):530–536, September 1991.

[354] R. Shankar. Renormalization-group approach to interacting fermions. *Reviews of Modern Physics*, 66(1):129–192, January 1994.

[355] Shu-Heng Shao. What's Done Cannot Be Undone: TASI Lectures on Non-Invertible Symmetry. 8 2023.

[356] Zhengyan Shi, Hart Goldman, Dominic Else, and Todadri Senthil. Gifts from anomalies: Exact results for Landau phase transitions in metals. *SciPost Physics*, 13(5):102, November 2022.

[357] Madhav Sinha, Fei Yan, Linnea Grans-Samuelsson, Ananda Roy, and Hubert Saleur. Lattice Realizations of Topological Defects in the critical (1+1)-d Three-State Potts Model. 10 2023.

[358] Jan Skolimowski and Michele Fabrizio. Luttinger's theorem in the presence of Luttinger surfaces. *Physical Review B*, 106(4):045109, July 2022.

[359] K. Slagle, Y.-Z. You, and C. Xu. Exotic quantum phase transitions of strongly interacting topological insulators. *Physical Review B*, 91(11):115121, March 2015.

[360] J. Smit. Fermions on a Lattice. *Acta Phys. Polon. B*, 17:531, 1986.

[361] Andrés M. Somoza, Pablo Serna, and Adam Nahum. Self-Dual Criticality in Three-Dimensional Z2 Gauge Theory with Matter. *Phys. Rev. X*, 11(4):041008, 2021.

[362] D. T. Son. Superconductivity by long-range color magnetic interaction in high-density quark matter. *Phys. Rev. D*, 59(9):094019, May 1999.

[363] Dam Thanh Son. Is the composite fermion a dirac particle? *Phys. Rev. X*, 5(3):031027, 2015.

[364] X.-Y. Song and A. P. Schnyder. Interaction effects on the classification of crystalline topological insulators and superconductors. *ArXiv e-prints*, September 2016.

[365] Xue-Yang Song, Yin-Chen He, Ashvin Vishwanath, and Chong Wang. Electric polarization as a nonquantized topological response and boundary Luttinger theorem. *arXiv e-prints*, page arXiv:1909.08637, September 2019.

[366] Xue-Yang Song and Ya-Hui Zhang. Deconfined criticalities and dualities between chiral spin liquid, topological superconductor and charge density wave chern insulator. *arXiv preprint arXiv:2206.08939*, 2022.

[367] Tudor D. Stanescu, Philip Phillips, and Ting-Pong Choy. Theory of the Luttinger surface in doped Mott insulators. *Physical Review B*, 75(10):104503, March 2007.

[368] Hualei Sun, Mengwu Huo, Xunwu Hu, Jingyuan Li, Zengjia Liu, Yifeng Han, Lingyun Tang, Zhongquan Mao, Pengtao Yang, Bosen Wang, Jinguang Cheng, Dao-Xin Yao, Guang-Ming Zhang, and Meng Wang. Signatures of superconductivity near 80 k in a nickelate under high pressure. *Nature*, 2023.

[369] P.V.D. Swift. The electroweak theory on the lattice. *Physics Letters B*, 145(3):256–260, 1984.

[370] Gerard 't Hooft. Naturalness, chiral symmetry, and spontaneous chiral symmetry breaking. *NATO Sci. Ser. B*, 59:135–157, 1980.

[371] Yuji Tachikawa. On gauging finite subgroups. *SciPost Phys.*, 8(1):015, 2020.

[372] Yuji Tachikawa and Kazuya Yonekura. Gauge interactions and topological phases of matter. *Progress of Theoretical and Experimental Physics*, 2016(9):093B07, 2016.

[373] Daisuke Tambara. Representations of tensor categories with fusion rules of self-duality for abelian groups. *Israel Journal of Mathematics*, 118:29–60, 2000.

[374] Daisuke Tambara and Shigeru Yamagami. Tensor categories with fusion rules of self-duality for finite abelian groups. *Journal of Algebra*, 209(2):692–707, 1998.

[375] Akihiro Tanaka and Xiao Hu. Many-body spin berry phases emerging from the π-flux state: Competition between antiferromagnetism and the valence-bond-solid state. *Physical review letters*, 95(3):036402, 2005.

[376] Nathanan Tantivasadakarn, Ryan Thorngren, Ashvin Vishwanath, and Ruben Verresen. Pivot Hamiltonians as generators of symmetry and entanglement. *SciPost Phys.*, 14(2):012, 2023.

[377] Ryan Thorngren and Dominic V. Else. Gauging Spatial Symmetries and the Classification of Topological Crystalline Phases. *Physical Review X*, 8(1):011040, January 2018.

[378] Ryan Thorngren and Yifan Wang. Fusion Category Symmetry II: Categoriosities at $c = 1$ and Beyond. 6 2021.

[379] Ryan Thorngren and Yifan Wang. Fusion category symmetry. Part I. Anomaly in-flow and gapped phases. *Journal of High Energy Physics*, 2024(4):132, April 2024.

[380] David Tong. Gauge theory. *Lecture notes, DAMTP Cambridge*, 2018.

[381] David Tong. Comments on symmetric mass generation in 2d and 4d. *Journal of High Energy Physics*, 2022(7):1, July 2022.

[382] Matthias Troyer and Uwe-Jens Wiese. Computational Complexity and Fundamental Limitations to Fermionic Quantum Monte Carlo Simulations. *Phys. Rev. Lett.*, 94(17):170201, May 2005.

[383] Ari M. Turner, Frank Pollmann, and Erez Berg. Topological phases of one-dimensional fermions: An entanglement point of view. *Physical Review B*, 83(7):075102, February 2011.

[384] Cumrun Vafa. Quantum Symmetries of String Vacua. *Mod. Phys. Lett. A*, 4:1615, 1989.

[385] Marieke van Beest, Philip Boyle Smith, Diego Delmastro, Zohar Komargodski, and David Tong. Monopoles, Scattering, and Generalized Symmetries. 6 2023.

[386] Erik P. Verlinde. Fusion Rules and Modular Transformations in 2D Conformal Field Theory. *Nucl. Phys. B*, 300:360–376, 1988.

[387] Ruben Verresen, Ryan Thorngren, Nick G. Jones, and Frank Pollmann. Gapless Topological Phases and Symmetry-Enriched Quantum Criticality. *Phys. Rev. X*, 11(4):041059, 2021.

[388] G. E. Volovik. Quantum Phase Transitions from Topology in Momentum Space. In W. G. Unruh and Ralf Schützhold, editors, *Lecture Notes in Physics, Berlin Springer Verlag*,

volume 718, page 31. 2007.

[389] Minoru Wakimoto and Hirofumi Yamada. Irreducible decompositions of fock representations of the virasoro algebra. In *Proceedings of the Symposium on Representation Theory III*, pages 33–38. Publication Society of the Proceedings of the Symposium on Representation Theory, 1983.

[390] Zheyan Wan and Juven Wang. Higher Anomalies, Higher Symmetries, and Cobordisms I: Classification of Higher-Symmetry-Protected Topological States and Their Boundary Fermionic/Bosonic Anomalies via a Generalized Cobordism Theory. *Ann. Math. Sci. Appl.*, 4(2):107–311, 2019.

[391] C. Wang and T. Senthil. Interacting fermionic topological insulators/superconductors in three dimensions. *Physical Review B*, 89(19):195124, May 2014.

[392] Chong Wang, Alexander Hickey, Xuzhe Ying, and A. A. Burkov. Emergent anomalies and generalized Luttinger theorems in metals and semimetals. *Physical Review B*, 104(23):235113, December 2021.

[393] Chong Wang, Adam Nahum, Max A. Metlitski, Cenke Xu, and T. Senthil. Deconfined Quantum Critical Points: Symmetries and Dualities. *Physical Review X*, 7(3):031051, July 2017.

[394] Juven Wang. CT or P Problem and Symmetric Gapped Fermion Solution. *Phys. Rev. D (accepted, in press)*, 7 2022.

[395] Juven Wang, Kantaro Ohmori, Pavel Putrov, Yunqin Zheng, Zheyan Wan, Meng Guo, Hai Lin, Peng Gao, and Shing-Tung Yau. Tunneling topological vacua via extended operators: (Spin-)TQFT spectra and boundary deconfinement in various dimensions. *Progress of Theoretical and Experimental Physics*, 2018(5):053A01, May 2018.

[396] Juven Wang and Xiao-Gang Wen. Non-Perturbative Regularization of 1+1D Anomaly-Free Chiral Fermions and Bosons: On the equivalence of anomaly matching conditions and boundary gapping rules. *arXiv e-prints*, page arXiv:1307.7480, July 2013.

[397] Juven Wang and Xiao-Gang Wen. Solution to the 1 +1 dimensional gauged chiral Fermion problem. *Phys. Rev. D*, 99(11):111501, June 2019.

[398] Juven Wang and Xiao-Gang Wen. Nonperturbative definition of the standard models. *Physical Review Research*, 2(2):023356, June 2020.

[399] Juven Wang, Xiao-Gang Wen, and Edward Witten. Symmetric Gapped Interfaces of SPT and SET States: Systematic Constructions. *Physical Review X*, 8(3):031048, July 2018.

[400] Juven Wang, Xiao-Gang Wen, and Edward Witten. A new su (2) anomaly. *Journal of Mathematical Physics*, 60(5):052301, 2019.

[401] Juven Wang and Yi-Zhuang You. Gauge Enhanced Quantum Criticality Between Grand Unifications: Categorical Higher Symmetry Retraction. 11 2021.

[402] Juven Wang and Yi-Zhuang You. Gauge enhanced quantum criticality beyond the standard model. *Phys. Rev. D*, 106(2):025013, 2022.

[403] Juven Wang and Yi-Zhuang You. Symmetric Mass Generation. *Symmetry*, 14(7):1475, July 2022.

[404] Juven C. Wang, Zheng-Cheng Gu, and Xiao-Gang Wen. Field-Theory Representation of Gauge-Gravity Symmetry-Protected Topological Invariants, Group Cohomology, and Beyond. *Phys. Rev. Lett.*, 114(3):031601, January 2015.

[405] Q.-R. Wang and Z.-C. Gu. Towards a complete classification of fermionic symmetry protected topological phases in 3D and a general group supercohomology theory. *ArXiv e-prints*, March 2017.

[406] Qing-Rui Wang and Zheng-Cheng Gu. Construction and classification of symmetry protected topological phases in interacting fermion systems. *arXiv e-prints*, page arXiv:1811.00536, November 2018.

[407] Wan-Sheng Wang, Yuan-Yuan Xiang, Qiang-Hua Wang, Fa Wang, Fan Yang, and Dung-Hai Lee. Functional renormalization group and variational monte carlo studies of the electronic instabilities in graphene near $\frac{1}{4}$ doping. *Phys. Rev. B*, 85:035414, Jan 2012.

[408] Wei Wang, Da-Chuan Lu, Xiao Yan Xu, Yi-Zhuang You, and Zi Yang Meng. Dynamics of compact quantum electrodynamics at large fermion flavor. *Physical Review B*, 100(8):085123, August 2019.

[409] Xu-Cheng Wang and Yang Qi. Phase fluctuations in two-dimensional superconductors and pseudogap phenomenon. *Physical Review B*, 107(22):224502, June 2023.

[410] Zhenjiu Wang, Michael P Zaletel, Roger SK Mong, and Fakher F Assaad. Phases of the (2+ 1) dimensional so (5) nonlinear sigma model with topological term. *Physical Review Letters*, 126(4):045701, 2021.

[411] Haruki Watanabe. Counting rules of nambu–goldstone modes. *Annual Review of Condensed Matter Physics*, 11:169–187, 2020.

[412] Haruki Watanabe, Hoi Chun Po, Ashvin Vishwanath, and Michael Zaletel. Filling constraints for spin-orbit coupled insulators in symmorphic and nonsymmorphic crystals.

Proceedings of the National Academy of Science, 112(47):14551–14556, November 2015.

[413] Steven Weinberg. *The quantum theory of fields*, volume 2. Cambridge university press, 1995.

[414] X.-G. Wen. A Lattice Non-Perturbative Definition of an SO(10) Chiral Gauge Theory and Its Induced Standard Model. *Chinese Physics Letters*, 30(11):111101, November 2013.

[415] Xiao-Gang Wen. Classifying gauge anomalies through symmetry-protected trivial orders and classifying gravitational anomalies through topological orders. *Phys. Rev. D*, 88(4):045013, August 2013.

[416] Xiao-Gang Wen. Zoo of quantum-topological phases of matter. *Rev. Mod. Phys.*, 89(4):041004, 2017.

[417] Xiao-Gang Wen. Low-energy effective field theories of fermion liquids and the mixed U (1) $\times R^d$ anomaly. *Physical Review B*, 103(16):165126, April 2021.

[418] Christof Wetterich. Exact evolution equation for the effective potential. *Physics Letters B*, 301(1):90–94, 1993.

[419] Steven R. White. Density matrix formulation for quantum renormalization groups. *Phys. Rev. Lett.*, 69:2863–2866, Nov 1992.

[420] E. Witten. The "parity" anomaly on an unorientable manifold. *Physical Review B*, 94(19):195150, November 2016.

[421] Edward Witten. An SU(2) anomaly. *Physics Letters B*, 117(5):324–328, November 1982.

[422] Edward Witten. Current algebra, baryons, and quark confinement. *Nuclear Physics B*, 223(2):433–444, August 1983.

[423] Edward Witten. Global Aspects of Current Algebra. *Nucl. Phys. B*, 223:422–432, 1983.

[424] Edward Witten. On holomorphic factorization of wzw and coset models. *Communications in Mathematical Physics*, 144(1):189–212, 1992.

[425] Edward Witten. SL(2,Z) action on three-dimensional conformal field theories with Abelian symmetry. In *From Fields to Strings: Circumnavigating Theoretical Physics: A Conference in Tribute to Ian Kogan*, pages 1173–1200, 7 2003.

[426] Edward Witten. Fermion Path Integrals And Topological Phases. *Rev. Mod. Phys.*, 88(3):035001, 2016.

[427] Zhengzhi Wu and Linhao Li. Dual topological nonlinear sigma models of *qed* theory by dimensinoal reduction and monopole operators. *arXiv preprint arXiv:2208.10518*, 2022.

[428] Ning Xi and Rong Yu. Emergent o (4) symmetry at an one-dimensional deconfined quantum tricritical point. *Journal of Physics A: Mathematical and Theoretical*, 2022.

[429] Tao Xiang and Congjun Wu. *D-wave Superconductivity*. Cambridge University Press, 2022.

[430] C. Xu. Renormalization group studies on four-fermion interaction instabilities on algebraic spin liquids. *Physical Review B*, 78(5):054432, August 2008.

[431] C. Xu and S. Sachdev. Square-Lattice Algebraic Spin Liquid with SO(5) Symmetry. *Phys. Rev. Lett.*, 100(13):137201, April 2008.

[432] Cenke Xu and Yi-Zhuang You. Self-dual quantum electrodynamics as boundary state of the three-dimensional bosonic topological insulator. *Physical Review B*, 92(22):220416(R), December 2015.

[433] Yichen Xu and Cenke Xu. Green's function Zero and Symmetric Mass Generation. *arXiv e-prints*, page arXiv:2103.15865, March 2021.

[434] Jianwei Yang, Anders W Sandvik, and Ling Wang. Quantum criticality and spin liquid phase in the shastry-sutherland model. *arXiv preprint arXiv:2104.08887*, 2021.

[435] Sheng Yang, Zhiming Pan, Da-Chuan Lu, and Xue-Jia Yu. Emergent self-duality in a long-range critical spin chain: From deconfined criticality to first-order transition. *Physical Review B*, 108(24):245152, December 2023.

[436] H. Yao and S. Ryu. Interaction effect on topological classification of superconductors in two dimensions. *Physical Review B*, 88(6):064507, August 2013.

[437] Yuan Yao and Masaki Oshikawa. Generalized Boundary Condition Applied to Lieb-Schultz-Mattis-Type Ingappabilities and Many-Body Chern Numbers. *Physical Review X*, 10(3):031008, July 2020.

[438] Mengxing Ye and Andrey V. Chubukov. Hubbard model on a triangular lattice: Pseudogap due to spin density wave fluctuations. *Physical Review B*, 100(3):035135, July 2019.

[439] Weicheng Ye, Meng Guo, Yin-Chen He, Chong Wang, and Liujun Zou. Topological characterization of lieb-schultz-mattis constraints and applications to symmetry-enriched quantum criticality. *arXiv preprint arXiv:2111.12097*, 2021.

[440] Kazuya Yonekura. General anomaly matching by Goldstone bosons. *Journal of High*

Energy Physics, 2021(3):57, March 2021.

[441] T. Yoshida and A. Furusaki. Correlation effects on topological crystalline insulators. *Physical Review B*, 92(8):085114, August 2015.

[442] Y.-Z. You, Y. BenTov, and C. Xu. Interacting Topological Superconductors and possible Origin of 16*n* Chiral Fermions in the Standard Model. *ArXiv e-prints*, February 2014.

[443] Y.-Z. You, Z. Wang, J. Oon, and C. Xu. Topological number and fermion Green's function for strongly interacting topological superconductors. *Physical Review B*, 90(6):060502, August 2014.

[444] Y.-Z. You and C. Xu. Interacting topological insulator and emergent grand unified theory. *Physical Review B*, 91(12):125147, March 2015.

[445] Yi-Zhuang You, Zhen Bi, Dan Mao, and Cenke Xu. Quantum phase transitions between bosonic symmetry-protected topological states without sign problem: Nonlinear sigma model with a topological term. *Physical Review B*, 93(12):125101, 2016.

[446] Yi-Zhuang You, Yin-Chen He, Ashvin Vishwanath, and Cenke Xu. From bosonic topological transition to symmetric fermion mass generation. *Physical Review B*, 97(12):125112, March 2018.

[447] Yi-Zhuang You, Yin-Chen He, Cenke Xu, and Ashvin Vishwanath. Symmetric Fermion Mass Generation as Deconfined Quantum Criticality. *Physical Review X*, 8(1):011026, January 2018.

[448] Yi-Zhuang You and Ashvin Vishwanath. Kohn-Luttinger Superconductivity and Inter-Valley Coherence in Rhombohedral Trilayer Graphene. *arXiv e-prints*, page arXiv:2109.04669, September 2021.

[449] Yi-Zhuang You and Juven Wang. Deconfined Quantum Criticality among Grand Unified Theories. *A Festschrift in Honor of the CN Yang Centenary: Scientific Papers*, pages 367–383, 2022.

[450] Yi-Zhuang You, Zhong Wang, Jeremy Oon, and Cenke Xu. Topological number and fermion Green's function for strongly interacting topological superconductors. *Physical Review B*, 90(6):060502, August 2014.

[451] Yi-Zhuang You and Cenke Xu. Symmetry-protected topological states of interacting fermions and bosons. *Physical Review B*, 90(24):245120, December 2014.

[452] Meng Zeng, Zheng Zhu, Juven Wang, and Yi-Zhuang You. Symmetric Mass Generation in the 1 +1 Dimensional Chiral Fermion 3-4-5-0 Model. *Phys. Rev. Lett.*, 128(18):185301,

May 2022.

[453] Hui Zhai, Fa Wang, and Dung-Hai Lee. Antiferromagnetically driven electronic correlations in iron pnictides and cuprates. *Physical Review B*, 80(6):064517, August 2009.

[454] Carolyn Zhang and Clay Córdova. Anomalies of $(1+1)D$ categorical symmetries. 4 2023.

[455] Carolyn Zhang and Michael Levin. Exactly Solvable Model for a Deconfined Quantum Critical Point in 1D. *Phys. Rev. Lett.*, 130(2):026801, 2023.

[456] Jian-Hao Zhang, Yang Qi, and Zhen Bi. Strange Correlation Function for Average Symmetry-Protected Topological Phases. *arXiv e-prints*, page arXiv:2210.17485, October 2022.

[457] Ya-Hui Zhang and Subir Sachdev. Deconfined criticality and ghost Fermi surfaces at the onset of antiferromagnetism in a metal. *Physical Review B*, 102(15):155124, October 2020.

[458] Ya-Hui Zhang and Subir Sachdev. From the pseudogap metal to the Fermi liquid using ancilla qubits. *Physical Review Research*, 2(2):023172, May 2020.

[459] Bowen Zhao, Jun Takahashi, and Anders W Sandvik. Multicritical deconfined quantum criticality and lifshitz point of a helical valence-bond phase. *Phys. Rev. Lett.*, 125(25):257204, 2020.

[460] Bowen Zhao, Jun Takahashi, and Anders W Sandvik. Tunable deconfined quantum criticality and interplay of different valence-bond solid phases. *Chin. Phys. B*, 29(5):057506, 2020.

[461] Jiarui Zhao, Zheng Yan, Meng Cheng, and Zi Yang Meng. Higher-form symmetry breaking at ising transitions. *Physical Review Research*, 3(3):033024, 2021.

[462] Guo-Yi Zhu and Guang-Ming Zhang. Gapless Coulomb state emerging from a self-dual topological tensor-network state. *Phys. Rev. Lett.*, 122(17):176401, 2019.

[463] Liujun Zou and Debanjan Chowdhury. Deconfined metal-insulator transitions in quantum Hall bilayers. *Physical Review Research*, 2(3):032071, September 2020.

[464] Liujun Zou and Debanjan Chowdhury. Deconfined metallic quantum criticality: A U(2) gauge-theoretic approach. *Physical Review Research*, 2(2):023344, June 2020.

[465] Liujun Zou, Yin-Chen He, and Chong Wang. Stiefel liquids: possible non-lagrangian

quantum criticality from intertwined orders. *Physical Review X*, 11(3):031043, 2021.